Unlocking an HDAC Toolbox:

Methods toward understanding isozyme-specific activity

By

Eric D Sullivan

A dissertation submitted in partial fulfillment
of the requirements for degree of
Doctor of Philosophy
(Chemical Biology)
in the University of Michigan
2016

Doctoral Committee:

Professor Carol A. Fierke, Chair
Assistant Professor Tomek Cierpicki
Associate Professor Patrick O'Brien
Professor Stephen W. Ragsdale

Acknowledgements

I want to thank my advisor, Carol Fierke. She is a wonderful mentor and her confidence in the ability of her students is palpable. She gave me room to explore the questions I found interesting, while providing the occasional nudge when I started to lose focus. I could always approach her with some confusing data and we would sit and talk through it together until we developed a hypothesis. I joined this lab in awe of the breadth of her knowledge and I leave it feeling much the same.

I also want to thank my undergraduate advisor, Mark Snider. Mark was the first person to get me genuinely interested in science and to see potential for me in this field. It was his advice that convinced me to continue pursing this interest after Wooster. To this day he is a mentor and a friend. My trajectory would have been very different without him.

The Fierke lab has become a close group of friends. They are a fun and energetic group to work with, especially the HDAC group, past and present including Dr. Lubomir Dostal, Dr. Caleb Joseph, Dr. Noah Wolfson, Dr. Byung Chul Kim, Dr. Ningkun Wang, Dr. Carol Ann Pitcairn, Jeffery Lopez, Katherine Leng, George Murphy III, and Kelsey Diffley. I'm proud to have these colleagues. I would also like to thank Dr. Amit Pithadia for his expertise in synthesis, and Dr. Michael Howard for the philosophical talks over coffee.

Finally, I would like to extend my deepest thanks to my family, my parents John and Diane, my brother David and his fiancée Ashley, my Aunt Mary, and my Uncle David. They have been amazingly supportive of me, and are a continual source of motivation. They possess a passion for learning that I am lucky to have acquired.

Table of contents

List of Tables

List of Figures

List of appendicies

Abstract

Lysine acetylation is a dynamic post-translational modification occurring ubiquitously in cells. Histone deacetylases (HDACs) catalyze the enzymatic hydrolysis of acetyllysine. There are 18 HDACs, tasked with the negative regulation of acetylation of thousands of proteins. It is therefore critical to understand the reactivity and specificity of these enzymes.

To probe the substrate specificity of HDAC isozymes, we developed and optimized a real-time enzyme-coupled assay that measures deacetylation via the formation of acetate and two mass spectrometric assays that measure the mass change associated with deacetylation. These assays were used to measure the reactivity of HDAC8 and HDAC11 with a variety of acetylated peptides and inhibitors, providing insight into the substrate selectivity. To characterize HDAC11, we recombinantly expressed a SUMO-HDAC11 fusion protein in *E. coli* in the presence of the molecular chaperone trigger factor. Interestingly, HDAC11 expressed in bacteria is inactive, in contrast to the catalytically active HDAC11 expressed and purified from eukaryotic cells. HDAC11 purified from insect cells catalyzes deacetylation of unlabeled peptide substrates and demonstrate unique selectivity that differs from HDAC8. To identify protein substrates, we introduced a chip-based proteomics method to screen the reactivity of HDAC isozymes with thousands of full-length human proteins. This work identified 44 and 25 potential HDAC8 and HDAC11 substrates, respectively. These substrates were then validated using peptide mimics with the enzyme-coupled and mass spectrometric assays mentioned above, determining rate constants spanning three orders of magnitude. Based on these results, isocitrate dehydrogenase 1 (IDH1) variants containing single, biologically relevant acetyllysine side chains were expressed and purified. HDAC8 catalyzes the deacetylation of these full-length protein substrates *in vitro* with high efficiency. Furthermore, the acetyllysine modifications decrease the catalytic activity of IDH1. Finally, the first HDAC prodrug, SAHA-TAP, is shown to covalently modify a conserved cysteine residue, Cys153 in HDAC8, leading to irreversible inactivation and simultaneous release of the competitive inhibitor SAHA. Overall, this work provides new methods for the characterization of HDAC reactivity, the identification of novel HDAC8 and HDAC11 substrates, and analysis of HDAC-inhibition. This work provides a foundation for understanding disease states that arise from aberrant acetylation and deacetylation.

Chapter 1

Histone Deacetylases[1,2]

Overview

While the human genome has roughly 20,000 protein coding regions, the complexity of the human proteome is much greater. This is due, in part, to the ability of cells to modify proteins after translation. These post-translational modifications (PTMs) are a diverse set of chemical changes that alter protein structure and function. Many of these modifications are dynamic and reversible. PTMs include methylation, phosphorylation, ubiquitination, acetylation and biotinylation, among others. Some of these PTMs, such as acetylation and methylation, were originally identified as modifications on the tail regions of core histone proteins where they function to regulate access to DNA through alterations to chromatin structure (*1*). Lysine acetylation has garnered increasing interest in recent years, with a trend in publication rate that rivals that of phosphorylation (*2*).

A major advance in the acetylation field has been the transition from analysis of acetylation (hyper- and hypoacetylation) of specific sites in histone tails to defining and understanding the numerous proteins that are modified through acetylation events. Acetylation has been shown to compete and cooperate with other PTMs, such as ubiquitination (*3*), and affect specific protein-protein interactions, protein stability and protein-DNA interactions (*4*). Identifying these interactions will lead to a better

---

[1] Reproduced, in part, from Lopez, J. E., Sullivan, E. D., and Fierke, C. A., (2016) Metal-dependent Deacetylases: Cancer and Epigenetic Regulators. *ACS Chem. Bio. 11*, 706-16.
[2] Original text written by Jeffrey E. Lopez and Eric D. Sullivan. Updated and revised by Eric D. Sullivan.

understanding of the acetylome, the collection of proteins that undergo acetylation/deacetylation, and the role of acetylation in cell regulation, growth and homeostasis (Figure 1).
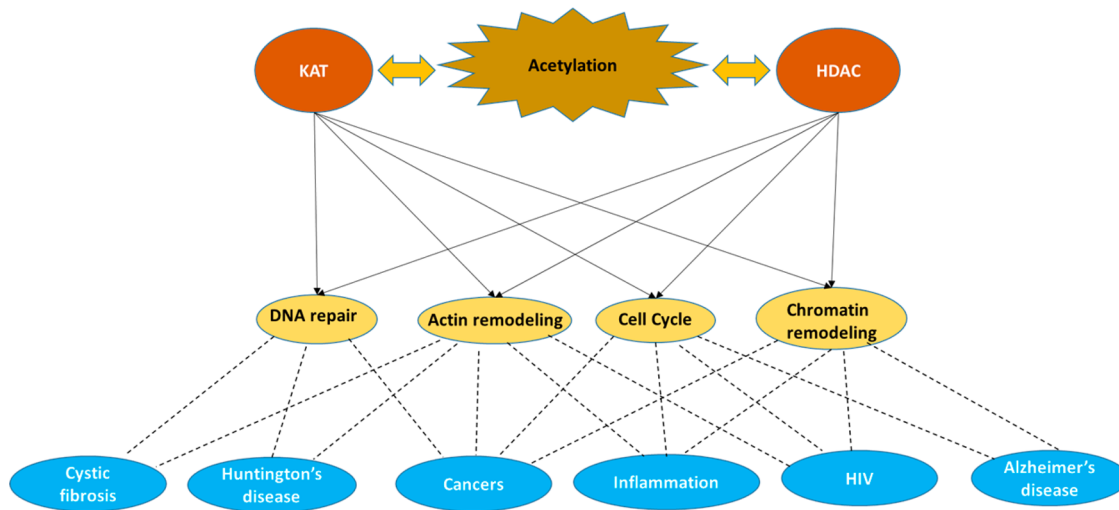
Figure 1.1: Acetylation is critical for regulation and proper cellular function.

Lysine acetyltransferases (KATs) and histone deacetylases (HDACs) maintain acetylation at an optimal level. KATs and HDACs regulate essential processes such as DNA repair, chromatin and actin remodeling, and proteins that serve as checkpoints during the cell cycle.

Acetylation is an enzymatically-catalyzed and reversible PTM in which an acetyl group is added at the N$^\varepsilon$-position of a lysine side chain. This reaction is catalyzed by lysine acetyltransferases (KATs), using acetyl-CoA as a cofactor. The reverse reaction, hydrolysis of acetyllysine, is catalyzed by histone deacetylases (HDACs), and results in regenerated lysine and free acetate. Traditionally, HDACs have been described as transcriptional repressors due to their effect on the recruitment and intramolecular interactions of many proteins, including bromodomain-containing proteins, MEF2-binding proteins and domains, and histone tails. They also aid in local chromatin compaction (*1*). However,

acetylation and deacetylation has now been observed on many non-histone proteins, and is not limited to the nucleus. Currently, over 7000 acetylated proteins have been identified in mammalian cell lines, with more continuing to be discovered through proteomics and computational analyses (*5*, *6*). In light of these many non-histone HDAC targets, a more suitable name for these enzymes is acetyllysine deacetylases, or acKDACs. Aberrant regulation of protein acetylation has been observed in various types of cancers including prostate (*7*), breast (*8*), and colon (*9*), among others, in addition to a variety of diseases, such as Cornelia de Lange Syndrome (CdLS) (*10*), Huntington's disease (*11*), and inflammation (*12*).

The increasingly evident role of HDACs in multiple cancers has made them an interesting anticancer target. Current research shows that there are multiple mechanisms by which HDACs affect cancer development, including inducing growth arrest, differentiation, senescence, and death of cancerous cells (*12*, *13*). Several HDAC inhibitors (HDACi) have been developed to combat these mechanisms, however, the current clinically used compounds do not possess isozyme selectivity. Three pan-HDAC inhibitors – suberoylanilide hydroxamic acid (SAHA) (*14*), Romidepsin (cyclic peptide) (*14*), and belinostat (hydroxamic acid) (*15*) – have been approved by the FDA for the treatment of T-cell lymphomas and a fourth inhibitor, Panobinostat (hydroxamic acid), has recently been approved for multiple myeloma treatment (*16*).

Studies have recently demonstrated that pan-HDACi can also be used to increase the effectiveness of anti-cancer immunotherapy treatments. In one mechanism, T-cell survival is enhanced by HDAC inhibitor treatment through the prevention of activation-induced cell death by lymphocytes (*13*, *17*). However, these effects vary significantly and can produce a

variety of non-desirable side effects as a consequence. Additionally, HDACis have been used to enhance vaccine strategies; namely, mice vaccinated with melanoma cells that have been pre-treated with trichostatin A (TSA) show an increase in immune response towards additional tumors, effectively enhancing their tumor specific immunity mechanisms (*12, 18*).

HDACs are divided into four classes based on their phylogeny and sequence homology to yeast orthologs (*19*). Class I HDACs, which share homology with Rpd3, consist of HDACs 1, 2, 3 and 8. Class II, with homology to Hda1, can be divided into two subclasses – IIa (HDACs 4, 7 and 9) and IIb (HDACs 6 and 10). Class III, with homology to the Sir2 family, is known as the sirtuins and utilizes NAD^+ as a cofactor. Class IV, which shares homology with both class I and class II, consists of HDAC11. Classes I, II and IV are metal-dependent HDACs that use a metal-water as a catalytic nucleophile in a general acid general base mechanism (Figure 2) (*20*). In addition, the catalytic activity of HDACs is sensitive to concentrations of monovalent metal cations, including potassium and sodium (*21*).
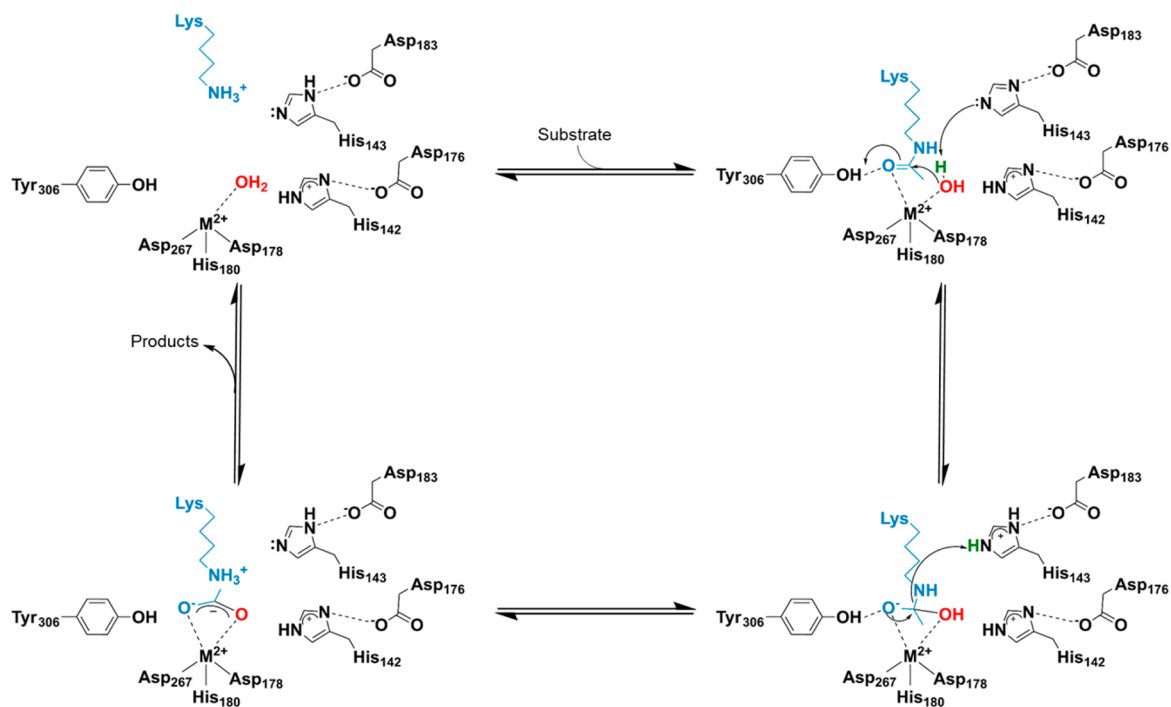
Figure 1.2: General acid general base mechanism of catalysis utilized by metal-dependent deacetylases(20).

The conserved Asp-His-Asp triad coordinates a divalent metal ion that coordinates the metal-water nucleophile. His143 acts as both a general acid and a general base, while Tyr306 and His142 stabilize the oxyanion intermediate.

Metal-dependent HDACs share common sequence motifs (Figure 3), including a deacetylase domain that is comprised of an arginase-deacetylase fold consisting of a multi-strand β-sheet surrounded by α-helices and a divalent metal ion cofactor coordinated by an Asp-His-Asp triad (*22*). Class I HDACs possess a deacetylase domain with little sequence variation and are localized mainly to the nucleus (*19*), with the exception of HDAC8 which has been observed in the cytoplasm of smooth muscle cells (*23*). Class II HDACs are shuttled between the nucleus and the cytoplasm and possess additional domains, such as MEF2 binding domains. HDAC6 has the largest array of domains with two deacetylase domains and a zinc finger protein-binding domain (*19*). Class II HDACs are expressed

ubiquitously through the cell and generally have lower catalytic activity *in vitro* when compared to class I enzymes. Finally, HDAC11, the only class IV metal-dependent deacetylase, possesses characteristics from both class I and II enzymes, and is expressed in higher abundance in specific tissues such as brain, heart and kidney (*24*).

Crystal structures have been solved for HDAC1 (PDB: 4BKX) (*25*), HDAC2 (PDB: 3MAX) (*26*), HDAC3 (PDB: 4A69) (*27*), HDAC4 (PDB: 2VQM) (*28*), HDAC6 (PDB: 3PHD, 5EDU) (*29*, *30*), HDAC7 (PDB: 3C0Y; catalytic domain only) (*31*), HDAC8 (PDB: 2V5W) (*32*), and HDAC9 (PDB: 1TQE) (*33*). The isozymes lacking crystal structures are HDAC5, HDAC10 and HDAC11.

Figure 1.3: Schematic comparison of the metal-dependent deacetylases.

Class I isozymes are highly conserved and small. Class IIa isozymes have specific MEF2-binding domains in addition to their conserved deacetylase domains. Class IIb isozymes contain unique domains unlike the other classes. Only the deacetylase domain has been identified in class IV.

One of the most prevalent questions in the HDAC field is the substrate selectivity of each isozyme. There are thousands of validated mammalian acetylation sites (*5*) and 18 deacetylase isozymes. Thus, defining the substrate pool for each isozyme is essential for understanding the biological functions of acetylation. Additionally, the substrate specificity of HDACs might be regulated by oxidative stress, protein-protein interactions and other

PTMs. Elucidating HDAC substrate specificity and regulation will provide insight into the function and control of acetylation sites in proteins.

Here, we highlight functions of metal-dependent deacetylases with regard to epigenetic regulation and homeostasis, and how these modifications play a role in cell proliferation and growth in various cancers, in addition to other, as of now, unknown roles.

Class I HDACs

The class I HDAC subfamily is disregulated in cancers and is the best-studied subfamily of the metal-dependent deacetylases. Overexpression of this subclass has been observed in a variety of cancers such as gastric (*34*), breast (*8*), prostate (*7*), and colon (*9*), as well as T-cell (*35*) and Hodgkin's lymphoma (*36*).

In the majority of cases, upregulation of HDAC1 is associated with poor cancer prognosis (*37*). Silencing of HDAC1 using siRNA knockouts results in cell cycle arrest, growth inhibition and induction of apoptosis in breast cancer cells (*38*) and induction of a plasminogen activator in neuroblastoma cells, increasing their invasive capacity (*39*). Mass proteomic analyses have revealed additional HDAC1 protein-protein interactions, ranging from short-lived interaction proteins, such as IKF2, HMG box transcription factor BBX, and activity-dependent neuroprotector homeobox protein ADNP, to proteins with methylation-related functions such as ARID5B, to previously uncharacterized zinc-binding proteins and domains, such as C16orf87 (*40*). Additionally, HDAC1 has been demonstrated to interact with the oncogene fusion protein PML-RAR, a protein involved in the pathogenesis of acute promyelocytic lymphoma (APL); in particular, HDAC1 diminishes the tumorigenic activity of PML-RAR by blocking differentiation, impairing genetic stability and increasing the

8

renewal of progenitor cells. However, HDAC1 expression enhances cell survival after differentiation, suggesting a dual role in cancerous tissue (*41*).

Immunodeficient mice have been used to evaluate the role of HDAC1 in tumor formation using teratomas. In these models, HDAC1 deficiency leads to partially undifferentiated carcinomas, upregulation of HDAC2, elevated levels of SNAIL1 expression and delocalization of E-cadherin (*42*). Knockouts of HDAC1 and 2 show dramatic acceleration of leukemogenesis in preleukemic mice. HDAC1 knockouts also led to deletion of p53 and c-myc overexpression (*41*). Additionally, Dovey et al. demonstrated that knockouts of key components of the HDAC1/2 deacetylase complex (Sin3A and Mi2) that decrease HDAC activity in T-cells perturb the differentiation of thymocytes into mature T lymphocytes (*43*). Similarly, mice knockouts of HDAC1/2 demonstrate that the loss of HDAC activity leads to the accumulation of thymocytes in addition to blocking early thymic development (*44*).

The previously described protein-protein interactions have led to the proposal that some HDACs function in large deacetylase complexes. HDAC1 and HDAC2, together with histone binding proteins RBBP4 and RBBP7, DNA/chromatin recognition motifs and transcription factors form the core deacetylase complexes that help localize HDACs 1 and 2 to chromatin (*45*). Expression of HDAC1 and HDAC3 correlate with both estrogen and progesterone receptor expression and have been proposed as prognostic markers in breast cancer tumors (*45*).

HDAC2 is overexpressed in lung cancer tissue and mesenchymal tumors, suggesting that it is an effector for the disease. Silencing of HDAC2 via siRNA leads to an increase in p53 DNA binding activity, Bax activation and Bcl2 suppression (*46*). These changes in Bax

activation and Bcl2 suppression are consistent with suppressed expression of cyclin E2, cyclin D1 and CDK2, blocking cell proliferation and inducing apoptosis (*47*). Truncations of HDAC2 have been detected in a large number of cancers (*48*) and knockouts of both HDAC1 and HDAC2 prompt TRAIL-induced apoptosis in chronic lymphocytic leukemia (CLL), indicating a possible level of cooperativity between these two isozymes (*49*). Recent studies have also shown that both HDAC2 silencing and inhibition induce regression of fibrotic formation in Peyronie's disease models (*50*, *51*). Using mutant fibroblasts that are HDAC2-deficient, Zimmerman *et al.* demonstrated a lack of response to insulin-like growth factors (IGFs) when compared to wild type cells, showing a potential link between HDACs and IGFs (*52*). Mice models lacking HDAC1 and with a single HDAC2 allele develop a lethal pathology within 3 months, likely due to neoplastic transformation of immature T cells (*43*). Additionally, mutant mice with an inactive HDAC2 mutant exhibit a 25 percent decrease in body size and reduced cell number and thickness of intestinal mucosa (*52*).

HDAC3, along with HDAC1 and HDAC2, is often expressed in high levels in renal, colorectal and gastric cancer (*36*, *53*). High expression of HDAC3 has also been observed in eight different pancreatic cancer cell lines and potentially generates a post-induction repression of p53, p27 and Bax genes through deacetylation of K9 of histone H3 (*54*). Knockouts of HDAC3 in promyelocytic leukemia cells restores retinoic acid dependent gene expression, primarily due to loss of the interactions between HDAC3, the nuclear co-repressor NCoR and PML-RARalpha fusion protein. HDAC3 interactions with the nuclear co-repressor NCoR to block transcription are enhanced by PML-RARalpha binding to DNA (*55*). The best understood example of HDAC3 function is repression of retinoic acid and thyroid hormone receptors, which can modulate p53 expression (*54*). Additionally, HDAC3

depletion in mouse liver upregulates lipogenic genes and causes histone hyperacetylation, leading to hepatostaetosis (*56*). However, expression of inactive HDAC3 mutant proteins in these knockout mice almost completely rescues the metabolic and gene transcription alterations, suggesting that HDAC3 plays important non-catalytic roles, such as protein-protein interactions. Consistent with this, mice knockouts of the nuclear co-repressor NcoR, an essential part of the HDAC3 deacetylase complex, exhibit metabolic and transcriptional effects resembling those of mice without hepatic HDAC3, demonstrating that interaction with NcoR is essential for the deacetylase-independent function of HDAC3 (*56*).

HDAC8 is the best biochemically characterized HDAC isozyme to date (*20*, *21*, *57*, *58*). HDAC8 is the only class I isozyme that is localized to both the cytoplasm and the nucleus, and is not observed in large, multi-protein complexes *in vivo* (*59*). HDAC8 is overexpressed in childhood neuroblastoma (*60*) and T-cell lymphoma (*35*). Knockouts of HDAC8 produce skull morphology and growth complications in mice models (*19*) and stop cell proliferation in lung, colon and cervical cancer cells (*60*). Point mutations in HDAC8 have been observed in patients with symptoms similar to the Cornelia de Lange Syndrome (CdLS). Lack of deacetylation of SMC3 in the cohesin complex has been implicated as a contributor to this disease, inhibiting the cell cycle, disrupting proper chromatid separation and causing debilitating mental and physical abnormalities (discussed further below) (*10*). Currently, work on HDAC8 has focused on mass spectrometry and co-immunoprecipitation studies using the HDAC8 specific inhibitor - PCI-34051 – and have provided insight into potential protein substrates and interaction partners (*40*, *61*). Knockouts and inhibition of HDAC8 have been shown to induce apoptosis in T-cell lymphoma and leukemia cell lines

(*35*). Using mice xenograft models of oncogene-amplified neuroblastoma, Rettig *et al.* demonstrated that selective inhibition of HDAC8 shows antineuroblastoma activity without significant toxicity and induces cell cycle arrest and differentiation both *in vivo* and *in vitro* (*62*). Additionally, the combined treatment with HDACi and retinoic acid enhanced cell differentiation, demonstrating that inhibition of HDAC isozymes can be combined with differentiation-inducing agents to target tumors (*62*). Investigations of HDAC8 specificity are poised to provide insight into the role of protein-protein interactions in determining substrate specificity of metal-dependent deacetylases.

Class II HDACs

Class II HDACs were discovered in the early 2000s (*63–65*). These proteins are significantly larger than both class I and class IV HDACs due to N-terminal and C-terminal tails and/or domains attached to the canonical deacetylase domain. This class is subdivided into two subfamilies: Class IIa and IIb. Class IIa consists of HDAC 4, 5, 7 and 9 and class IIb is comprised of HDAC 6, and 10. These isozymes differ from class I HDACs in that the additional N-terminal domains interact with transcription factors and target genes, such as the MEF2 proteins, a family of transcription factors that are key regulators of cellular differentiation (*64*). Recruitment of class II HDACs by MEF2 proteins to protein complexes can heavily alter the protein acetylation landscape due to blocking interactions with acetylation complexes such as p300/CBP in non-Hodgkin lymphoma (*33*, *66*). Class II HDACs are localized to both the cytoplasm and the nucleus. Additionally, both up-regulation and down-regulation of these enzymes have severe repercussions in various types of cancers.

Class IV HDACs

HDAC11, the most recently discovered isozyme, is the sole member of the Class IV HDAC subfamily (*24*). At 39 KDa, HDAC11 is the smallest isozyme. Sequence alignments suggest that HDAC11 is more closely aligned with Class I HDACs (28% sequence identity to HDAC8) than Class II, with retention of highly conserved residues in the active site and in the mono- and divalent metal binding sites seen in other metal-dependent deacetylases. HDAC11 sequence alignments identify one significant sequence change, an aspartate (D101 in HDAC8) to asparagine, a residue located on the flexible L2 loop, near the entrance to the active site tunnel (*32*).

HDAC11 expression is tissue specific, with the greatest expression occurring in the brain, heart, kidneys, skeletal muscle, and testis (*24*). Studies of murine brain development suggest a role for HDAC11 in the formation of mature oligodendrocytes (*67*). Overexpression of HDAC11 in RAW264.7 cells is associated with a decrease in mRNA levels of the anti-inflammatory cytokine interleukin-10, indicating a possible role for HDAC11 in inflammatory and autoimmune diseases (*68*). Furthermore, mRNA analysis uncovered a link between HDAC11 and cancer; mRNA levels for HDAC11 are in the top 1% of differentially overexpressed genes in ductal breast carcinoma when compared to healthy breast tissue (*69*). In addition, the DNA replication factor Cdt1 is a potential HDAC11 substrate. Cdt1 is integral in recruiting mini-chromosome maintenance (MCM) helicase to DNA, which is required for DNA replication during the cell cycle. To maintain a single copy of DNA per cell, Cdt1 must be inhibited after loading MCM in the G1 phase (*70*). Cdt1 is an

acetylated protein that co-immunoprecipitates with HDAC11 (*71*). Finally, HDAC11 knockout mice are viable, but they exhibit increased cell proliferation and secrete higher levels of IL-2, TNF, and IFN-y than WT mice (*72*).

HDACs: mechanism and inhibition

While class I, II, and IV HDACs (HDACs 1-11) vary in sequence and size, they are all metal-dependent enzymes that share a common deacetylase domain (Fig. 1.3) (*73*). This domain features a highly conserved pair of histidine residues as well as a tyrosine, all located within the active site tunnel (*74*). Because HDAC8 has more extensive biochemical characterization *in vitro*, all residue numbers will correspond to their placement in HDAC8 unless otherwise specified. While each of the active site mutants have not been studied for all HDAC isozymes, the high degree of conservation of these residues suggests that these enzymes share a common mechanism.

A divalent metal is situated at the bottom of the HDAC active site tunnel. This metal ion, in a pentacoordinate, square-pyramidal geometry, interacts with an Asp178-His180-Asp267 triad and two displaceable water molecules (*58*, *74*). The identity of this metal ion is frequently reported to be zinc, though the enzyme is activated by a number of divalent metals and the potential for Fe-bound HDAC *in vivo* has been raised (*57*).

The mechanism of HDAC-catalyzed deacetylation, a general acid general base process, has been thoroughly investigated (Fig. 1.2) (*20*). Briefly, an acetylated lysine residue enters the active site tunnel. The carbonyl oxygen of the acetate moiety is coordinated by the divalent metal ion and forms a hydrogen bond with Tyr306, properly

orienting the substrate. The metal-bound water is deprotonated by His143, acting as a general base in concert with nucleophilic attack at the carbonyl carbon atom of the acetyl moiety of the substrate. This forms a tetrahedral intermediate where the oxyanion is stabilized by interactions with Tyr306, the divalent metal ion, and the nearby His142. His143, acting as a general acid, donates a proton to the terminal amine of the lysine side chain to facilitate the collapse of this tetrahedral intermediate to form the acetate and lysine products (*20*).

The divalent metal ion is critical to proper substrate orientation and catalysis. It is also the target of most HDAC inhibitors. Of the four FDA-approved HDAC inhibitors, three are hydroxamic acid based (Vorinostat, Panobinostat, and Belinostat) (Fig. 1.4) and one is a cyclic peptide with a reducible disulfide (*14–16*). All four of these pan-HDAC inhibitors function by chelating the active site metal ion. Additional isozyme-specific inhibitors have been, and continue to be, developed. Of particular interest here are two specific inhibitors: PCI-34051 and MGCD0103.

PCI-34051 is an HDAC8-specific inhibitor (Fig. 1.5A). It has a K_i of 10 nM for HDAC8, making it 200-fold more potent toward HDAC8 than any of the other HDACS tested (HDAC1, 2, 3, 6, and 10) (*35*). This inhibitor has been used extensively in studying HDAC8 and has played an important role in identifying HDAC8 substrates (*61*). MGCD0103 is also an isoform-selective inhibitor, though not as specific as PCI-34051 (Fig. 1.5B). This inhibitor has nanomolar IC_{50} values with HDACs 1, 2, and 11, and < 2 μM with HDAC3. However, it is not a potent inhibitor toward HDAC8 or class II HDACs (*75*). These inhibitors were both used in the work presented in this thesis.
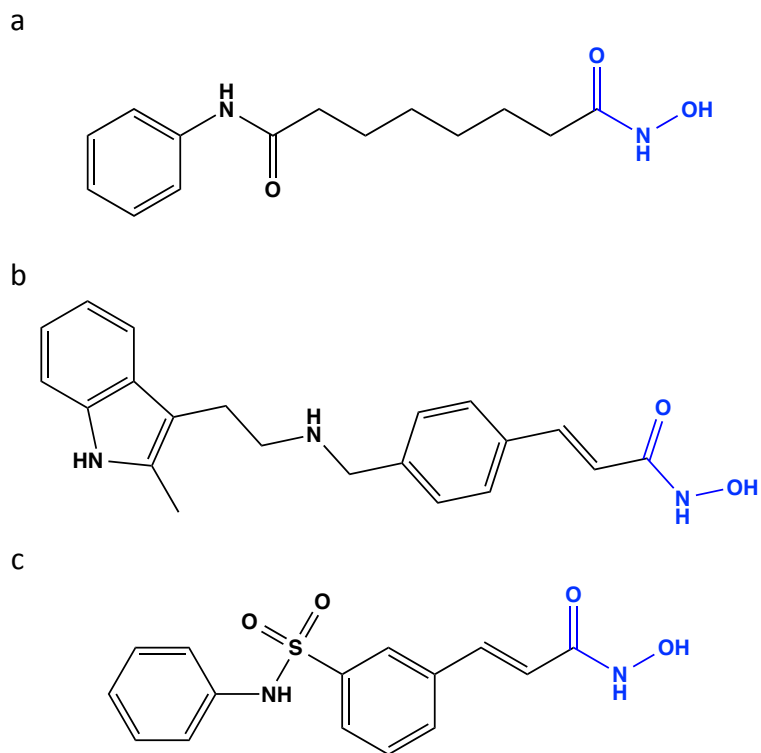
Figure 1.4: Structure of FDA-approved hydroxamic acid HDAC inhibitors

Each inhibitor has a capping group, a linker, and a metal chelator. These FDA-approved inhibitors share a common chelating group, a hydroxamic acid (blue). They differ in the length and composition of their linker regions, and all contain a hydrophobic capping group composed of, at a minimum, a benzene ring. These inhibitors are Vorinostat (A), Panobinostat (B), and Belinostat (C).

a

b
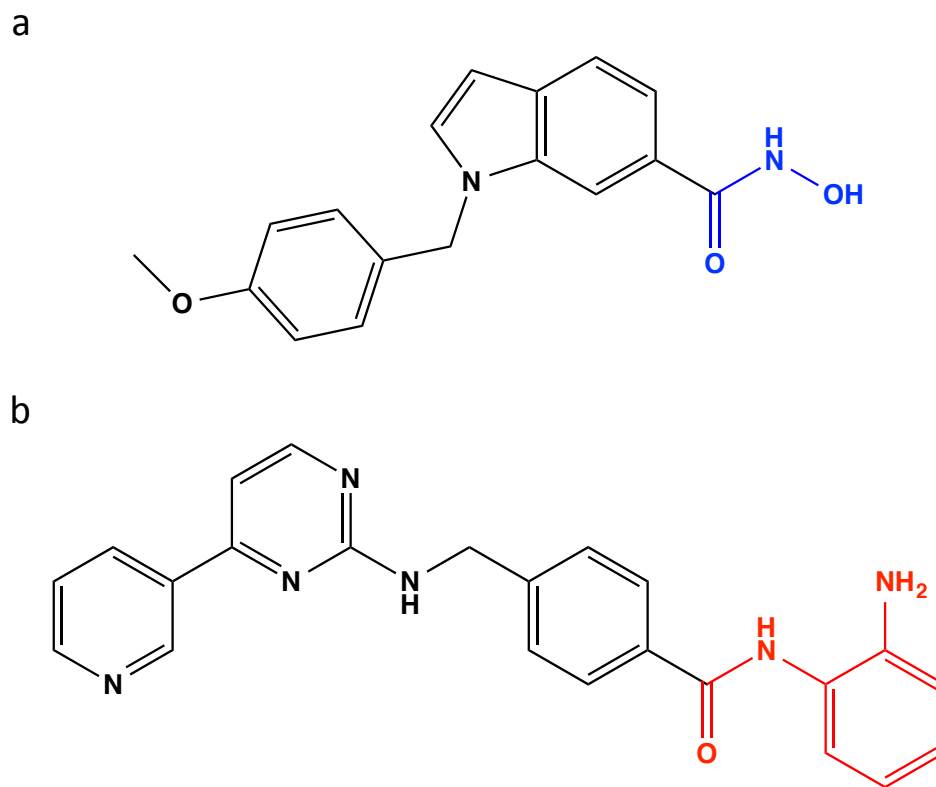
Figure 1.5: Isozyme-selective HDAC inhibitors

(A) An HDAC8-specific inhibitor, PCI-34051, with a hydroxamic acid moiety (blue). This HDACi is > 200 fold more potent toward HDAC8 than other class I HDACs. (B) MGCD0103 is an isozyme-selective inhibitor with sub-micromolar potency toward HDACs 1, 2, and 11. This inhibitor also chelates metal, but the warhead is a benzamide (red) instead of a hydroxamic acid.

Current methods to assay HDAC-catalyzed deacetylation

Methods to accurately determine HDAC catalytic activity are central to studying these enzymes *in vitro* and understanding their cellular roles *in vivo*. HDAC-catalyzed deacetylation has been measured *in vitro* almost exclusively with peptide substrates. The most common assay for determining catalytic activity is the Fluor-de-Lys assay (Enzo Life Sciences) (Fig. 1.6). This assay makes use of short peptides (~ 4 – 6 amino acids), with a C-terminal methyl-coumarin fluorophore. The target acetyllysine residue is positioned adjacent to the fluorophore. Upon HDAC-catalyzed deacetylation of the acetyllysine, the

17

peptide is exposed to a developing reagent, which includes trypsin. Trypsin recognizes and

cleaves at lysine but not acetyllysine. Therefore, only HDAC product peptides are cleaved.

This generates free methyl-coumarin, which can be observed as an increase in fluorescence

(ex. = 340 nm, em. = 450 nm) (Fig. 1.6). This assay is broadly applicable to all HDAC

isozymes, and peptide substrates can differ in their sequence upstream of the acetyllysine.

However, physiological relevance is somewhat limited, as the peptides cannot differ in

sequence downstream of the acetyllysine, where the methyl-coumarin is situated.
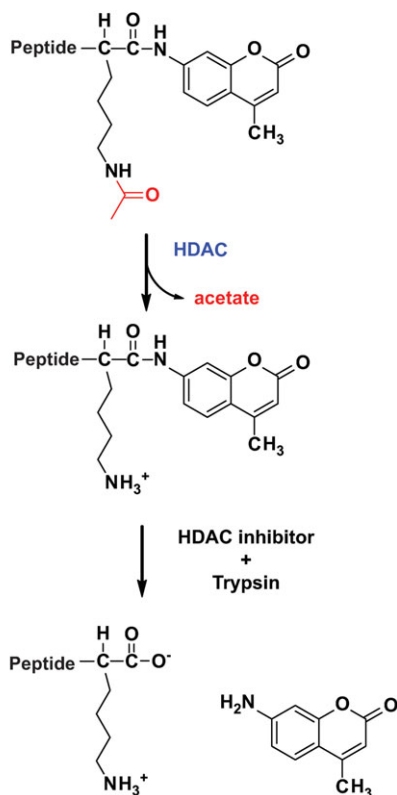
Figure 1.6: The Fluor-de-Lys assay

Methyl-coumarin-labled peptide substrate is deacetylated by HDAC. The free lysine is then recognized and the peptide cleaved by trypsin, releasing free methyl-coumarin. This results in an increase in fluorescence intensity (ex. = 340 nm and em. = 450 nm). Reproduced with permission from Wolfson *et al.*, 2013.

A recent advance in measuring HDAC catalysis *in vitro* is an enzyme-coupled assay developed in our lab (*76*). This assay utilizes free acetate to yield an observable change in equilibrium between NAD^+ and NADH (Fig. 1.7). This assay does not rely on fluorophore-labeled peptides to generate a signal, and therefore, HDAC-catalyzed deacetylation of unlabeled peptides of any sequence can be assayed. The applications and modifications of this assay are discussed further in Chapter 2.
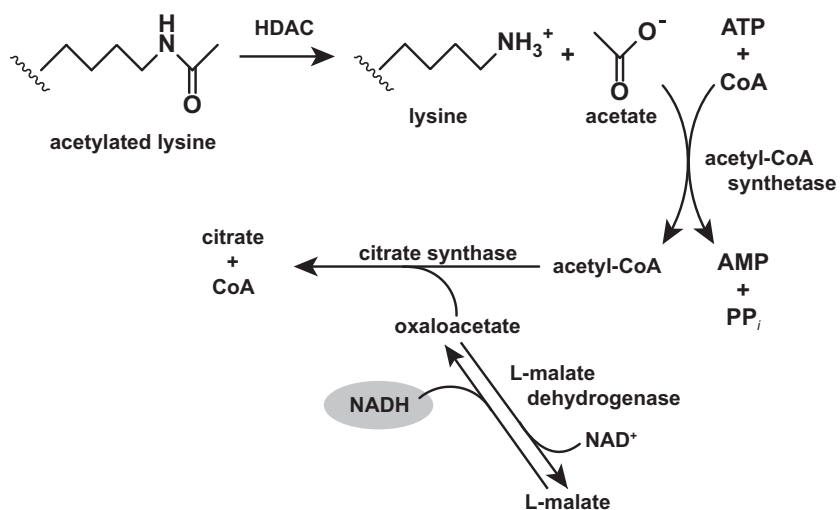
Figure 1.7: Scheme for the enzyme-coupled assay

Briefly, acetate (generated by HDAC activity) is converted into acetyl-CoA by acetyl-CoA synthetase. Citrate synthase then converts oxaloacetate and acetyl-CoA into citrate and regenerates CoA in the process. Oxaloacetate is present as the product of malate dehydrogenase. As citrate is formed, oxaloacetate is depleted. Thus driving the equilibrium of malate and NAD^+ (via malate dehydrogenase) toward oxaloacetate and NADH.

Detecting HDAC-catalyzed deacetylation *in vivo* presents a different set of challenges. Ed Holson's laboratory at the Broad Institute has used stable isotope labeling of amino acids in cell culture (SILAC) to successfully measure changes in protein acetylation upon perturbation of HDAC isozymes. More specifically, they've shown that inhibition of

HDAC8 *in vivo* leads to an increase in acetylation of several proteins, as visualized by mass spectrometry (*61*).

Putative HDAC8 *in vivo* substrates and their biological relevance

Several proteins have been identified as putative HDAC8 substrates, using various techniques, including stable isotope labeling of amino acids in cell culture (SILAC), RNAi knockdowns, and co-immunoprecipitation (*40*, *61*). Perhaps one of the best-validated substrates is SMC3, a protein for which misregulation of acetylation is directly associated with disease.

HDAC8 has recently been identified as a causative agent in the Cornelia de Lange syndrome (CdLS). CdLS is a rare genetic disorder, occurring in about 1 in 10,000 individuals. It is marked by visible, physical deformities, including limb malformations, small hands and feet, and facial deformities. The disorder is also associated with cognitive impairment and low IQ. CdLS results from alterations in the cohesin complex, a protein complex that mediates cohesion of sister chromatids during cell division (*77*, *78*). A core component of the cohesin complex is SMC3, a member of the structural maintenance of chromosome family of ATPases.

SMC3 is an acetylated protein whose acetylation profile changes as the cell cycle progresses. As cells leave anaphase, SMC3 acetylation levels decrease, regenerating a pool of non-acetylated SMC3 to start the next cell cycle (*79*). This deacetylation is attributed to HDAC8 activity *in vivo* based on an RNAi screen and a SILAC experiment in which HDAC8 was specifically inhibited (*10*, *61*). Additionally, in 2012, four unique mutations in HDAC8

were discovered in several CdLS patients who tested negative for traditional genetic markers associated with the disease. When expressed recombinantly in *E. coli*, these mutations (H180R, T311M, G320R, and H334R) result in a significant decrease in HDAC8-catalyzed deacetylation of a Fluor-de-Lys substrate (*10*). Further, we have verified that WT-HDAC8 catalyzes the deacetylation of an SMC3 peptide *in vitro* (*61*).

Additional proposed substrates of HDAC8 include estrogen-related receptor alpha (ERRa) (*80*), cAMP response element-binding protein (CREB) (*81*, *82*), and AT-rich interactive domain-containing protein 1A (ARID1a) (*61*), among others. Of these, perhaps ERRa is the best characterized. This protein, along with other members of the estrogen-related receptor family and additional co-activators, functions to regulate energy metabolism during periods of stress (*83*). Acetylated ERRa has significantly reduced ability to activate a target promoter in Cos1 cells (*80*). HDAC8 and Sirt1 led to the greatest rescue of ERRa activity upon co-transfecting ERRa with a panel of deacetylases, suggesting these two enzymes function as the *in vivo* ERRa deacetylases (*80*).

HDAC11 biological significance and potential *in vivo* substrates

Since its discovery in 2002, a physiological role for HDAC11 has not been well studied. Unlike the Class I HDACs, mRNA levels of HDAC11 are less ubiquitous and more concentrated in specific areas: the heart, brain, kidneys, skeletal muscle, and testis (*24*). In accordance with this tissue specific data from human northern blot analysis, a research group at UNC Chapel Hill found that expression of HDAC11 is elevated in the brains of newborn to 4 week old mice, and expression is abundant in mature oligodendrocytes (*67*). Additionally, these researchers note that postnatal central nervous system development is

correlated with a decrease in core histone acetylation (*84*). Based on this evidence, it has been proposed that HDAC11 is involved in the formation of mature oligodendrocytes through deacetylation of histones 3 and/or 4 (*67*). Evidence for deacetylation of specific side chains in histones is currently limited to the correlation between the observed decreases in histone acetylation in the brain at the same stage in development that HDAC11 expression increases (*84*). Mammalian HDAC11 is highly conserved between mice and humans (92% identity), suggesting that these finding may hold value for human brain development as well.

HDAC11 has also been investigated as a negative regulator of interleukin 10 (IL-10) expression (*68*). IL-10 is an anti-inflammatory cytokine responsible for regulating the magnitude of the immune response and minimizing self-tissue damage. Villagra *et al* demonstrated that overexpression of HDAC11 decreases IL-10 mRNA levels in RAW264.7 mouse cells. They also showed, using a luciferase-based assay, that HDAC11 interacts with the IL-10 promoter region (*68*). These findings suggest that HDAC11, by suppressing the expression of IL-10, plays a pro-inflammatory role. These data highlight a potential use for HDAC11 inhibitors as a therapeutic in autoimmune diseases. Subsequent studies have suggested that HDAC11-mediated regulation of IL-10 may be less straightforward. HDAC inhibitor studies and HDAC knockdowns (RNAi) have demonstrated a link between the loss of HDAC11 and an increase in OX40L, the ligand responsible for activation of the OX40 receptor. The OX40 receptor, once paired with the OX40L, generates a pro-inflammatory immune response. This pathway ultimately leads to a reduction of IL-10 (*85*). These findings demonstrate the complexity of the role HDAC11 plays in regulating the severity of an immune response (Fig. 1.8).

Additionally, a strong link exists between HDAC11 and cancer suppression. Analysis of mRNA expression for HDAC11 revealed that it is in the top 1% of differentially overexpressed genes in ductal breast carcinoma when compared to normal breast tissue. It is also in the top 5% of differentially overexpressed genes for several other cancers, including renal and hepatic (*69*). Deubzer *et al* performed knockdowns of HDAC11 in several cancerous and non-cancerous cell lines using siRNA. They found that lowered levels of HDAC11 led to decreases in the metabolic activity and viability of cancerous cells but had no effect on the viability of non-cancerous cell lines. Additionally, expression of a catalytically impaired HDAC11 variant in cancerous cells produced the same detrimental effects seen with the knockdowns, suggesting that loss of HDAC11 activity is likely responsible for these observations (*69*).

Finally, there is evidence that the DNA replication factor Cdt1, which recruits mini-chromosome maintenance (MCM) helicase to DNA, is a strong candidate to be an HDAC11 substrate. Regulation of Cdt1 is critical, as MCM is required for DNA replication during the cell cycle. After MCM loading onto DNA in the G1 phase, Cdt1 must be inhibited to maintain a single copy of DNA per cell (*70*). Reactivity of Cdt1 with an anti-acetyllysine antibody demonstrated acetylation of this protein, and co-immunoprecipitation experiments have demonstrated an interaction between Cdt1 and HDAC11. Furthermore, this study showed that acetylation of Cdt1 protects it from degradation (*71*).
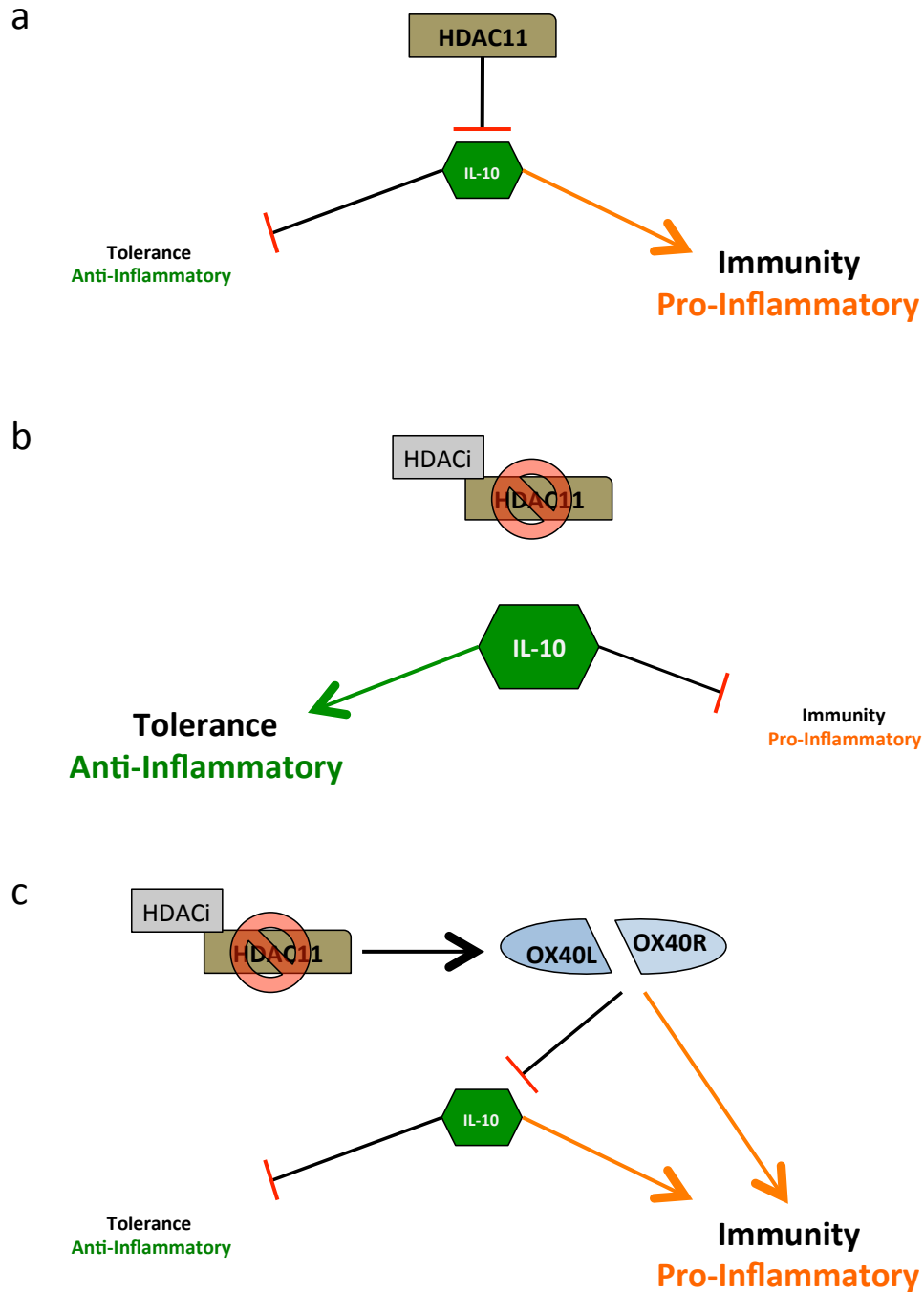
Figure 1.8: Role of HDAC11 in immunity

HDAC11 plays a complex role in cellular immunity, and may be cell-type specific. (A) HDAC11 (in mouse macrophage cells and human antigen presenting cells, APC) suppresses expression of interleukin 10, which in turn generates an increase in immunity and inflammation. (B) Upon inhibition of HDAC11 in these cells IL-10 expression increases, resulting in tolerance and an anti-inflammatory response. (C) However, in three Hodgkin lymphoma-derived cell lines (HL cells), inhibition of HDAC11 resulted in an increase in the OX40 ligand (OX40L). This ligand, when paired with the receptor OX40R, suppressed IL-10 and generates a pro-inflammatory, anti-tumor immune response.

Conclusions

Lysine acetylation/deacetylation is a dynamic, reversible post-translational modification with a defined role in histone modification and a growing pool of non-histone substrates that are critical for epigenetic regulation, DNA repair, cell cycle regulation and cancer growth and proliferation. The HDAC family of enzymes catalyzes deacetylation of both histones and non-histone proteins to maintain acetylation homeostasis that is critical for cell regulation and survival. Changes in acetylation patterns have become a key feature of various types of cancer and many of these changes in acetylation levels are due to increased expression and/or misregulation of HDACs. Due to the link between HDACs and cancer prognosis and survival, these enzymes have become an attractive target for drug development, as shown by the development and FDA approval of pan-HDAC inhibitors and the current development of novel immuno- and oncolytic virus- (OV) therapies. To further our understanding of the cellular function of HDACs, huge strides are currently being made in discovering HDAC specific binding partners and substrates using a variety of methods, from knockouts and mass spectrometric techniques to *in vivo* mammalian cell work. The current body of literature on HDACs has shed light on the multiple roles of these enzymes in both transcriptional regulation and in protein-protein interactions, particularly with respect to their roles in disease, including multiple cancers, Alzheimer's disease, and many others.

We predict that future work will incorporate varied approaches such as mass spectrometry, co-immunoprecipitation, *in vivo* perturbation, *in vitro* functional studies, *etc.*, to advance our understanding of the cellular role of each isozyme. Understanding the

specificity of each HDAC will provide further insight into their individual roles in the regulation of cellular pathways and various diseases states.

Acknowledgements

Chapter 2

Using peptide substrates to measure HDAC-catalyzed deacetylation[3,4]

Introduction

Histone deacetylases (HDACs), or acetyllysine deacetylases, catalyze the hydrolysis of acetate from the side chain of acetylated lysine residues in proteins. This process, occurring at thousands of sites throughout the proteome (*86*), has many different cellular roles. Acetylation of histone proteins can result in changes in chromatin structure and gene transcription. Acetylation of other proteins yields myriad phenotypes, as the post-translational modification has been shown to impact protein function, protein-protein interactions, and protein signaling (*4*).

As the acetylome continues to grow (*6*), so too does the importance of understanding the biochemical relationship between HDACs and their substrates. Current *in vivo* and *in vitro* techniques are uncovering links between specific HDAC isozymes and their substrates. These methods include gene knockdowns, protein co-immunoprecipitation, and mass-spectrometry-based proteomics. These methods are

---

[3] The optimization of the continuous format of the coupled-enzyme assay and the HDAC3/NCOR1 stopped assay data are published in Wolfson *et al.*, 2014. The optimization of the continuous assay was performed by Eric Sullivan and Noah Wolfson. The assaying of HDAC3 was performed by Eric Sullivan. The manuscript was written by Noah Wolfson, Carol Ann Pitcairn, Eric Sullivan, Caleb Joseph, and Carol Fierke. Text, where reproduced, is footnoted.

[4] The validation of peptides from the SILAC experiment is published in Olson *et al.*, 2014. The *in vivo* HDAC8 inhibition and mass spec workup were performed by the Holson group. Peptides representing the protein targets were assayed by Eric Sullivan and Carol Ann Pitcairn, and analyzed by Sullivan, Pitcairn, and Wolfson. Text from this manuscript, reproduced in the methods section, is footnoted.

powerful tools to identify potential protein targets for individual HDACs, however, many of these candidate protein targets lack additional biochemical validation *in vitro.*

Recombinant expression of full-length target proteins is a cumbersome task, and requires proper lysine acetylation. Deacetylation of fluorophore-labeled peptide substrates has been in wide-use for over a decade (*87*), and allows for the rapid analysis of the catalytic activity of HDAC enzymes. However, this method requires a non-physiological substrate, and is of limited use in determining the selectivity differences between isozymes. A reproducible method to assay unlabeled peptides, which can be used to measure reactivity with myriad sequences, has remained a more difficult challenge. Via several interdisciplinary collaborations, we have made strides in advancing the use of unlabeled peptide substrates as a tool to investigate HDAC activity.

Here, we report on current advances in using peptide-based assays *in vitro* to study HDAC specificity and catalysis. We provide recent innovations to a current method using an enzyme-coupled assay and provide a case study in which the ability to assay peptides based on physiological protein sequences provided evidence for the validation of HDAC8 substrates and the extent to which those proteins might be selective toward HDAC8 over other HDAC isozymes. We also discuss the strengths and weaknesses of two mass spectrometry-based peptide assay approaches.

Methods

HDAC8 expression and purification

HDAC8 was expressed and purified as described previously (*57*), with the exception that a 20 mL DEAE Sepharose column was used after the second Chelating Sepharose column. This column used a gradient from low- to high-salt buffer (50 mM HEPES pH 7.8, 10 μM ZnSO$_4$, 1 mM TCEP, 50 mM NaCl, and 5 mM KCl; and 50 mM HEPES pH 7.8, 10 μM ZnSO$_4$, 1 mM TCEP, 1 M NaCl, and 5 mM KCl, respectively).

HDAC8 and HDAC3 activity using the stopped enzyme-coupled assay[5]

To remove contaminating metals from peptide substrates, approximately 6% (v/v) hydrated Chelex 100 was added to the Ac-KGGAKac-NH$_2$ and Ac-KGGAKacW-NH$_2$ peptides and incubated at room temperature for 3 h. The Ac-KGGAKacW-NH$_2$ peptide concentration was determined from the absorbance measurement at 280 nm using an ND-1000 spectrophotometer (NanoDrop) with a calculated extinction coefficient of 5500 M^{-1} cm^{-1} (*88*). In addition, the concentration of peptides containing a free amine (lysine) was measured using the fluorescamine assay described below. Peptide substrates without a fluorophore (0–1600 μM) were pre-incubated in HDAC8 stopped assay buffer (25 mM HEPES pH 8.0, 137 mM NaCl, 3 mM KCl) at 30 °C for 10 min. The reactions were initiated by adding Co(II)-HDAC8 or HDAC3/NCOR1 to a final concentration of 0.5 μM and incubated for 0, 30, 60, and 90 min., and quenched by the addition of 0.37% (v/v) HCl (final concentration). The reactions were flash frozen within 20 min of quenching and stored at -

---

[5] Methods for the coupled-enzyme assay and optimization of a continuous format for this assay are revised from Wolfson et *al.*, 2014.

80°C. On thawing, the reactions were neutralized by the addition of 0.6% (w/v) NaHCO3 (final concentration). The coupler mixture (50 mM HEPES, 400 µM adenosine triphosphate (ATP), 10 µM nicotinamide adenine dinucleotide (NAD$^+$), 30 µM coenzyme A (CoA), 0.07 U/µl citrate synthase (CS), 0.04 U/µl malate dehydrogenase (MDH), 50 µM acetyl CoA synthetase (ACS), 100 mM NaCl, 3 mM KCl, 50 mM MgCl, and 2.5 mM L-malic acid, pH 8.0) was incubated for 20 min at room temperature and added to each quenched reaction (at a ratio of 10 µl coupler mix/65 µl reaction) in a 96-well black plate. The reactions were incubated at room temperature for 40 min, and the NADH fluorescence (Ex = 340 nm, Em = 460 nm) was measured. The steady-state kinetic parameters for the Ac-KGGAKac-COO peptide were determined from fitting the Michaelis–Menten equation (v_0/[HDAC] = (k_{cat}[S]) / (K_M + [S])) to the concentration dependence of HDAC-catalyzed deacetylation.

Optimizing a continuous version of a stopped enzyme-coupled assay to monitor HDAC8 activity

The continuous assay was run according to the same basic method as the stopped enzyme-coupled assay, as described above and in Wolfson *et al.*, with the following differences. The 96-well plates were soaked (>3 hrs) in 100 mM divalent metal free EDTA to strip the plates of contaminating metal. Plates were then rinsed 5 times with divalent metal free ultrapure water. The continuous assay buffer (50 mM HEPES, 400 µM ATP, 10 µM NAD$^+$, 30 µM CoA, 0.07 U/µl CS, 0.04 U/µl MDH, 50 µM ACS, 127 mM NaCl, 2.7 mM KCl, and 2.5 mM L-malic acid, pH 8.0) was incubated with Chelex resin for 1 h at room temperature. The mixture was clarified by centrifugation at 16,800 x g for 2 min, and the supernatant was collected. Then, 6 mM magnesium (MgCl$_2$) was added to the buffer, and

the mixture was incubated for 20 min to allow NAD^+/malate and NADH/OAA (oxaloacetate) to equilibrate. The peptide (100 μM final concentration Ac-KGGAKac-NH_2) in HDAC8 assay buffer was added to this mixture at a ratio of 2:1. The reaction was initiated with the addition of Co(II)–HDAC8 (0.5 – 1 μM final concentration), and deacetylation was measured from the time-dependent increase in NADH fluorescence (Ex = 340 nm, Em = 460 nm).

SILAC target verification by *in vitro* peptide assays[6]

Peptides were purchased from Peptide 2.0 with a purity of > 75% with an acetylated N-terminus and an amidated C-terminus and were resuspended in water. The concentrations of peptides containing an unmodified lysine were measured using the fluorescamine assay as previously described (*76*). All peptide concentrations were within two-fold of the calculated concentration based on weight. The CSRP2BP peptide contains no amine or aromatic amino acids; and therefore, the concentration was calculated based on the mass provided by Peptide 2.0. Recombinant human HDAC8 was either purchased (BPS Bioscience) or purified from E. coli as previously described (*57*), and all other HDAC homologues were purchased from BPS Biosciences. HDAC assays were performed using an enzyme-coupled system to measure acetate production as described above. The reactions were measured under standard HDAC reaction conditions (137 mM NaCl, 2.7 mM KCl, 25 mM HEPES, pH 7.8, 30°C). Reactions measuring deacetylation of acetylated peptides (0 – 1600 μM) were initiated by addition of recombinant Zn(II)-HDAC8 (0.5 – 2.0 μM). The reactions were quenched by the addition of HCl, and the acetate product, as reflected by an

---

[6] Methods for HDAC-assays on SILAC peptides are revised from Olson et *al.*, 2014.

increase in the NADH fluorescence, was measured at 4 time points (up to 50 min). Recombinant HDAC isozymes 1-9 (0.4 μM), prepared by BPS Biosciences from baculovirus expression, were mixed with acetylated peptides (100 μM) and the formation of acetate product was measured as a function of time. The initial velocities (v_0) were calculated from a linear fit of the time-dependent increase in NADH fluorescence. The kinetic parameters were determined from fitting either a line or the Michaelis-Menten equation (v_0/[HDAC8] = (k_{cat}[S]) / (K_M + [S])) to the dependence of the initial velocity on the peptide concentration.

Peptide detection by HPLC-MS

Peptides for HPLC-MS analysis were purchased from Peptide2.0 at ≥ 70% purity. Peptides were ordered with an acetylated N-terminus and an amidated C-terminus. Identical peptides were ordered with and without an acetyllysine residue. Solutions of acetylated and non-acetylated peptide were prepared at various ratios. Formic acid (0.1%) was added to peptide solutions. The samples were injected into an Agilent Q-TOF HPLC-MS instrument at 15 – 20 μL. Samples were run with a flow rate of 0.4 mL/min. Peptide samples were loaded onto an in-line C8 column at 95% buffer A (water with 0.1% formic acid) and 5% buffer B (95% acetonitrile with 0.1% formic acid). Peptides were eluted over a 20-minute gradient of increasing buffer B, up to 100%. Eluant was fed into an electrospray ionization source and analyzed by time of flight. The instrument was operated in positive ion mode, and analysis was performed using the Agilent Qualitative Analysis software. Total ion count traces were integrated to determine area under the curve (AUC) for generating standard curves.

Peptide reactions for HPLC-MS analysis were carried out after a 1-hour reconstitution of 2:1 cobalt to apo-HDAC8. Reactions were run in 1x HDAC assay buffer (25 mM HEPES pH 8.0, 137 mM NaCl, 3 mM KCl) at 34℃ with 100 μM substrate (Ac-KLIS[K_{Ac}]FDKL-NH$_2$). Reactions were initiated by addition of HDAC8 (1 μM final).

Peptide deacetylation detected by MALDI-MS

Peptides for this experiment were purchased from Synthetic Biomolecules and were ordered as 'crude' purity. They ranged from 6-10 amino acids in length, with acetylated N-termini and amidated C-termini. Peptide reactions were carried out in 8 and 6 μL volumes, with 100 and 75 μM peptide concentrations. HDAC8 was reconstituted 1:1 with zinc for one hour on ice. Reaction components were all diluted into HDAC assay buffer, and the final reactions were incubated at 25℃ in 1x HDAC assay buffer. Reactions were initiated by addition of HDAC8 (1 μM final). At time points between 0 and 30 minutes, 2 μL aliquots were removed from the reactions and quenched into 1 μL 10% hydrochloric acid. Quenched time points were then mixed 1:1 (v/v) with an α-Cyano-4-hydroxycinnamic acid (HCCA) matrix solution prepared fresh daily. Single use 1 mg vials of HCCA from Thermo Fisher were dissolved to 10 mg/mL in 70/30 acetonitrile/water with 0.1% TFA. The reaction time points were mixed with matrix, immediately spotted on a 96-spot ground steel MALDI target (Bruker), and allowed to dry completely. Five peptides of higher purity (>75%) were also mixed with matrix solution and spotted on the MALDI target. These peptides were used to calibrate the mass spectrometer.

Results and Discussion

HDAC8 activity can be monitored continuously by an enzyme-coupled assay

[7]A previous lab member, Dr. Noah Wolfson, optimized a stopped coupled-enzyme assay for determining HDAC8-catalyzed deacetylation of unlabeled protein and peptide substrates (*76*). After optimizing this stopped assay, we next evaluated whether this same assay could be carried out as a continuous real-time assay to measure HDAC8 activity. HDAC8 is sensitive to inhibition by metals (*57*) and monovalent cations (*21*), thus the acetate coupling solutions for the continuous assay were reformulated with concentrations of NaCl and KCl typically used to assay HDAC8 activity (BIOMOL, unpublished; see also (*21*)) and were treated with Chelex resin prior to the addition of magnesium. The concentration of magnesium was decreased to 2 mM to minimize inhibition of HDAC8 activity (~2-fold inhibition under these conditions). To counteract the loss in activity of the coupling enzymes due to the lower concentration of magnesium, the concentration of these enzymes was increased by 2.3-fold to yield a final rate for the coupling reactions of 0.046 μM•s^{-1}. These assay conditions were used to measure HDAC8-catalyzed deacetylation of the 100 μM Ac-KGGAK$_{ac}$-NH$_2$ peptide. We repeated this assay with multiple concentrations of HDAC8, yielding rates from 0.006 to 0.024 μM•s^{-1} (Fig. 2.1A). The linear dependence on the HDAC8 concentration demonstrates that the assay rate is not limited by the coupling reactions (Fig. 2.1B). Furthermore, the HDAC8 activity measured using the stopped assay (0.5 μM HDAC8 and 100 μM Ac-KGGAK$_{ac}$-NH$_2$) is 0.033 ± 0.0034 μM•s^{-1}, which is within 2-fold of the rate measured using the continuous assay and is consistent with the expected inhibition of Co-HDAC8 by magnesium.

---

[7] This paragraph revised from Wolfson et *al.,* 2014.

By monitoring HDAC8 activity continuously, we were able to significantly reduce both the time needed to complete an assay and the amount of material required. The time course for the HDAC-catalyzed reaction did not change during continuous assay, but the lengthy work up after the reaction was quenched was eliminated. This also meant assay time points did not need to be thawed, neutralized, or aliquoted into plates with coupled solution; all steps that had the potential to introduce error into the discontinuous method. Additionally, instead of a stopped assay that required 60 μL per each time point, with the continuous method only the equivalent of one time point was required. By doing so we saved HDAC, substrate peptides, and the enzyme mixture used in the coupled reaction. Additionally, the increased number of data points collected during the continuous assay increases its precision. Table 2.1 summarizes the differences between the stopped and continuous versions of this assay.

Table 2.1 Two methods for running our enzyme-coupled assay

	Stopped Assay	Continuous Assay
Assay Time	Prepare coupled enzyme solution (1 hour), HDAC-reaction time (0 - 2 hours), Freeze/thaw/neutralize (1 hour - overnight), Plate time points/coupled-enzyme reaction (1-2 hours), Total Time = 1 - 1.5 days	Prepare copuled enzyme solution (1 hour), HDAC-reaction time (0 - 2 hours), N/A, N/A, Total Time = half day
Material required (5 time points)	HDAC (0.5 μM) - > 300 μL Coupled solution - > 50 μL HCl (10%) - 12.5 μL NaHCO3 (6%) - 37.5 μL Plate wells required - 5	HDAC (0.5 μM) - 60 μL Coupled solution - 10 μL N/A N/A Plate wells required - 1
HDAC Activity	Full activity (100%)	Reduced activity (40-60%)
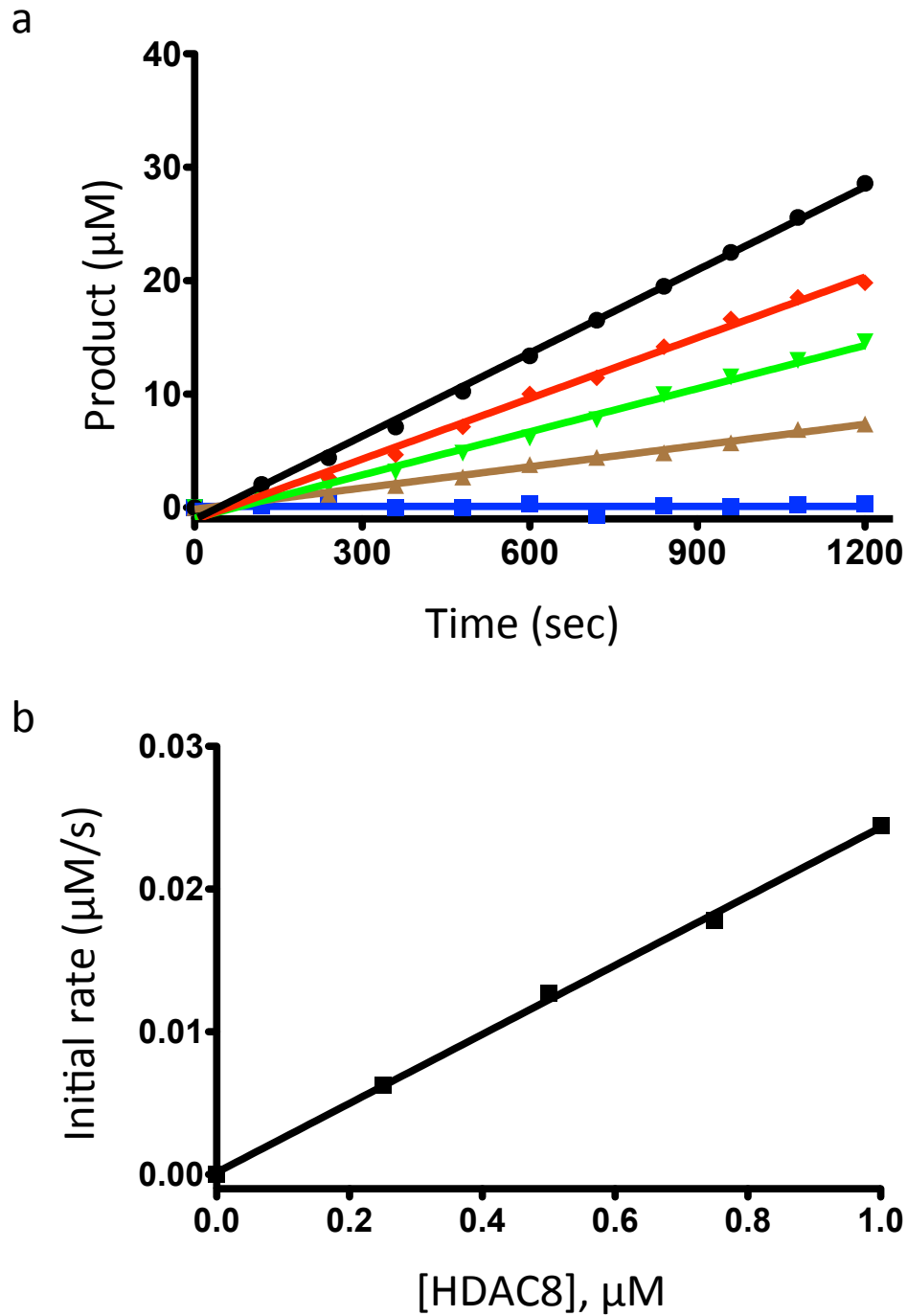
Figure 2.1 Continuous measurement of HDAC8 activity

(A) Continuous measurement of HDAC8 activity. Activity was assayed at 0 μM (blue), 0.25 μM (brown), 0.5 μM (green), 0.75 μM (red), and 1 μM (black). (B) Dependence of the continuously measured HDAC8 initial rates on enzyme concentration. The linear correlation here indicates that HDAC8-catalyzed deacetylation is rate-limiting, not the coupled-enzyme reactions.

Measuring deacetylation catalyzed by other HDAC-isozymes using the coupled-enzyme assay

We optimized this enzyme-coupled assay using HDAC8. We next sought to demonstrate that this assay that detects low micromolar concentrations of acetate was broadly capable of measuring activity for any HDAC isozyme. Using the same peptide that we used to characterize HDAC8 with this assay, we measured the activity of HDAC3 (in complex with NCOR1) using the stopped assay format as proof of principle (Fig. 2.2). The ratio of HDAC3-catalyzed deacetylation of this peptide was about half of that seen with HDAC8 at comparable substrate concentrations.
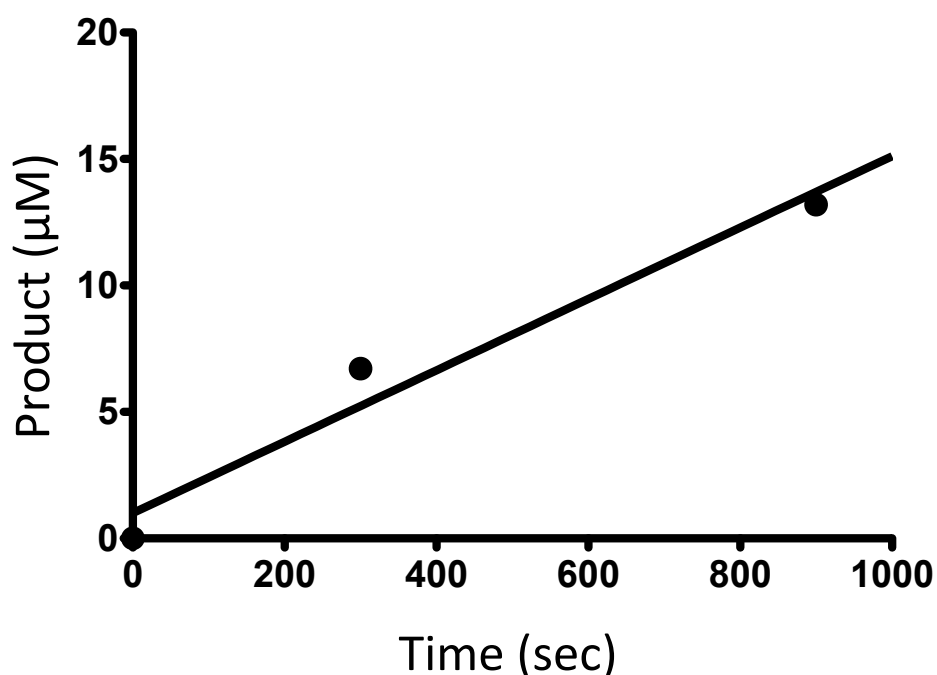
Figure 2.2 HDAC3-catalyzed deacetylation

HDAC3/NCOR1 was assayed with the stopped version of the coupled-enzyme assay to validate that this method is useful for assaying multiple HDAC-isozymes. HDAC3 (0.5 µM) was incubated with 100 µM Ac-KGGAK$_{ac}$-NH$_2$ in 1x HDAC assay buffer at 30℃. Time points were quenched into HCl and the reaction progress was measured by NADH fluorescence, as described.

We next used this assay to validate putative HDAC8 substrates identified by our collaborator Ed Holson at the Broad Institute (*61*). Briefly, the Holson group grew three cell cultures, each with a unique stable isotope label. They treated cultures with a DMSO vehicle control, a pan-HDAC inhibitor, or an HDAC8 specific inhibitor. After treatment, cells were lysed, enriched for acetyllysine, and analyzed by mass spectrometry. Importantly, they identified a small set of proteins whose acetylation profile increased upon addition of the HDAC8-specific inhibitor but not upon addition of DMSO only. We used our enzyme-coupled assay to examine reactivity of acetylated peptides from these proteins with HDAC8, identify which acetyllysine sites were most likely to be deacetylated by HDAC8, and probe the degree to which these substrates might be specific to HDAC8 vs other HDAC isozymes (*61*).

To answer the first two questions, we used the stopped version of the coupled assay to measure kinetic rate constants for peptides corresponding to acetyllysine residues in the identified proteins. We found that our *in vitro* assay showed good agreement with the hypothesis that these proteins could be deacetylated *in vivo* by HDAC8. All acetylated peptides tested were deacetylated by HDAC8 *in vitro*. The measured rate constant, k_{cat}/K_M, which is also known as the specificity constant, varied over three orders of magnitude from less than 5 M^{-1}s^{-1} for the slowest substrate to over 700 M^{-1}s^{-1} for the fastest (Table 2.2).

To determine which peptides are specifically deacetylated by HDAC8 compared to other HDAC isozymes, we used commercially available recombinant HDACs 1-9 to generate apparent k_{cat}/K_M values for each isozyme with each substrate. We found that none of the tested peptides were deacetylated only by HDAC8. Interestingly, the fastest peptide with

HDAC8 was also rapidly deacetylated by HDAC3, the closest homologue to HDAC8 (Table 2.3).

The ability to quickly assay unlabeled peptide substrate *in vitro*, with either a single HDAC isozyme or a panel of HDACs, is a powerful new technique in the acetylation field. This approach has furthered our ability to use biochemical approaches to further test *in vivo* data suggesting HDAC substrates from perturbation of cellular deacetylation. The *in vitro* assay provides evidence to support or refute direct interactions between HDACs and substrates, and can be used to evaluate if phenotypic changes in acetylation are primary or downstream effects.

Table 2.2 Specificity constants for HDAC8-catalyzed deacetylation of SILAC-based

peptides

Peptides were all N-terminally acetylated and C-terminally amidated. Deacetylation was measured with Zn-HDAC8 expressed and purified in-house using the stopped form of the enzyme-coupled assay.

Protein	Peptide Sequence	k_{cat}/K_M (M^{-1}s^{-1})
RAI1	KLGGK$_{ac}$QRAA	11 ± 1
ZRANB2	TEIGK$_{ac}$TLAEK	4.1 ± 0.3
THRAP3	LGDGK$_{ac}$MKS	4.6 ± 0.1
NCOA3	KRILHK$_{ac}$LLQN	50 ± 5
SRSF5	KLSGK$_{ac}$EING	9.8 ± 2
ARID1A	KLISK$_{ac}$FDKL	740 ± 40
CSRP2BP	STPVK$_{ac}$FISR	160 ± 30
MLL2	SKIQK$_{ac}$QLDQ	32 ± 6
SMC3	RVIGAKK$_{ac}$DQY	63 ± 11

Table 2.3 Results from screening HDAC-isozymes against peptide substrates[8]

HDACs in these experiments were commercially purchased recombinant enzymes expressed in insect cells (BPS Bioscience). If an isozyme-substrate pair was not tested, it is marked with a dashed line (-). HDAC-catalyzed deacetylation was measured using the stopped form of the coupled-enzyme assay. All substrates were deacetylated by at least two isozymes. Values shown are $k_{cat}/K_{M, app}$ in $M^{-1}s^{-1}$.

Protein	HDAC1	HDAC2	HDAC3	HDAC4	HDAC6	HDAC7	HDAC8	HDAC9
RAI1	50	< 20	1700	-	-	-	< 20	< 20
ZRANB2	< 20	< 20	50	< 20	270	< 20	< 20	< 20
THRAP3	< 20	30	1600	-	-	-	< 20	< 20
NCOA3	70	< 20	2200	< 20	70	140	-	< 20
SRSF5	< 20	< 20	60	70	820	-	< 20	< 20
ARID1A	50	< 20	2500	< 20	1200	< 20	2400	< 20
CSRP2BP	50	< 20	1500	< 20	210	-	740	< 20
MLL2	< 20	30	220	-	-	-	-	< 20

HDAC8-catalyzed deacetylation of peptides can be quantified by LC-MS

In addition to an enzyme-coupled assay, we are also interested in identifying methods to directly measure HDAC activity. To this effect we have shown that HDAC catalysis of peptides in solution can be visualized as a stopped assay by mass spectrometry. We first demonstrated that an acetylated peptide could be discriminated from a deacetylated peptide by coupling an HPLC with a reversed phase C8 column to an ESI source time-of-flight mass spectrometer. As expected, the acetylated substrate peptide elutes more slowly from a C8 column than the deacetylated, more hydrophilic product

---

[8] Data in table reproduced from Olson *et al.*, 2014.

peptide (Fig. 2.3). By injecting various ratios of 'substrate' and 'product' peptide, we generated a standard curve based on integrating the area under the curve (AUC) created from the total ion counts from each peptide (Fig. 2.4). A linear relationship between fraction product and AUC is observed up to ~50% product. This range is sufficient for monitoring the first 10-20% of a reaction to determine an initial rate. Finally, we demonstrated that this approach could be used to measure HDAC8-catalyzed deacetylation, with minimal sample preparation. We incubated HDAC with an acetylated peptide (Ac-KLISK$_{ac}$FDKL-NH$_2$) and quenched HDAC8 activity at various time points by diluting samples of the reaction into 10% hydrochloric acid. Fractionation using an on-line C8 column provides sufficient separation of substrate, product, and HDAC8 (Fig. 2.5).

This technique is advantageous in its straightforward measurement of peptide deacetylation. This method does not require preparation of coupling reagents and enzymes, and because an exact mass is determined for substrate and product peaks, there is no ambiguity in whether or not deacetylation of the peptide has occurred. This method is best suited to studying HDAC activity on a single substrate. A calibration curve must be prepared for each substrate because acquisition times and the separation between substrate and product peaks are variable and depend on the peptide being analyzed.
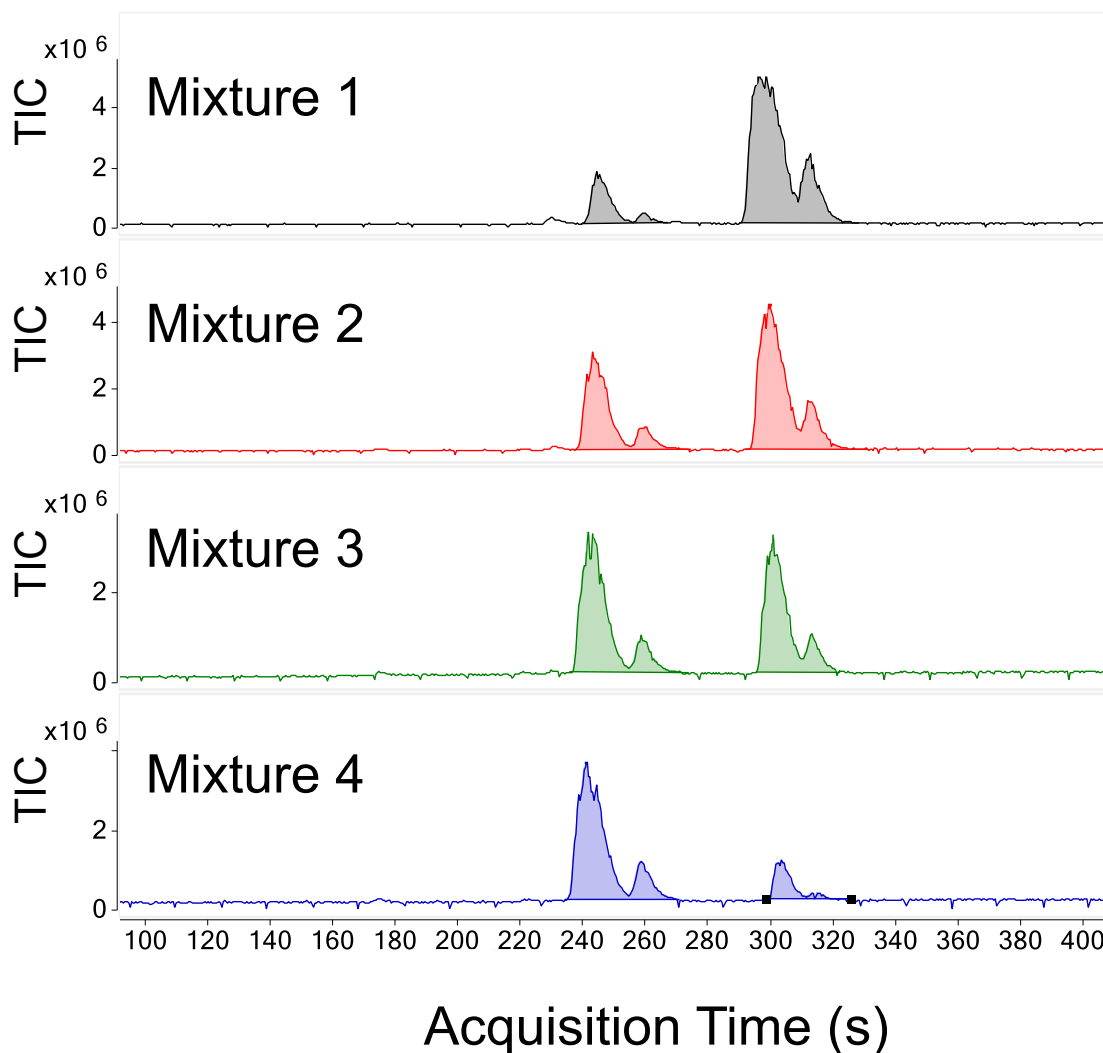
Figure 2.3 Separation of acetylated and non-acetylated peptide mixtures

To determine the effectiveness of HPLC-MS in the separation and quantification of acetylated (substrate) and non-acetylated (product) peptides, a series of samples were run with varying concentrations of substrate and product. The graphs shown are total ion count (TIC) vs. peptide acquisition time from the mass spectrometer. These peptides (based on ARID1A, Table 2.2) were purchased, at >75% purity, with (substrate) and without (product) an acetyllysine reside. The substrate:product peptide ratios included are Mixture 1 = 80:20, Mixture 2 = 50:50, Mixture 3 = 30:70, and Mixture 4 = 10:90. Each major peak is rapidly followed by a less intense peak, which corresponds to a different protonation state. Both the major and minor peaks for each peptide were included in the analysis.
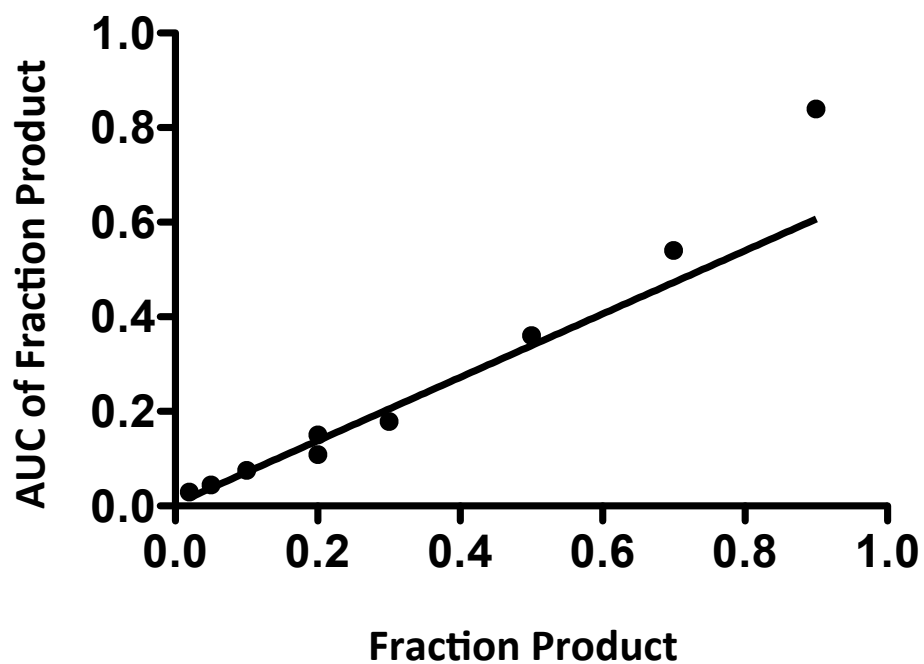
Figure 2.4 HPLC-MS peptide standard curve

Acetylated and non-acetylated peptides (sequence based on ARID1A in table 2.2) were injected into an Agilent Q-TOF HPLC-MS in various substrate and product ratios. The resulting ion count vs acquisition time data, shown in Fig. 2.3, was quantified according to AUC. These data were used to generate a standard curve. This curve is linear through 50% product.
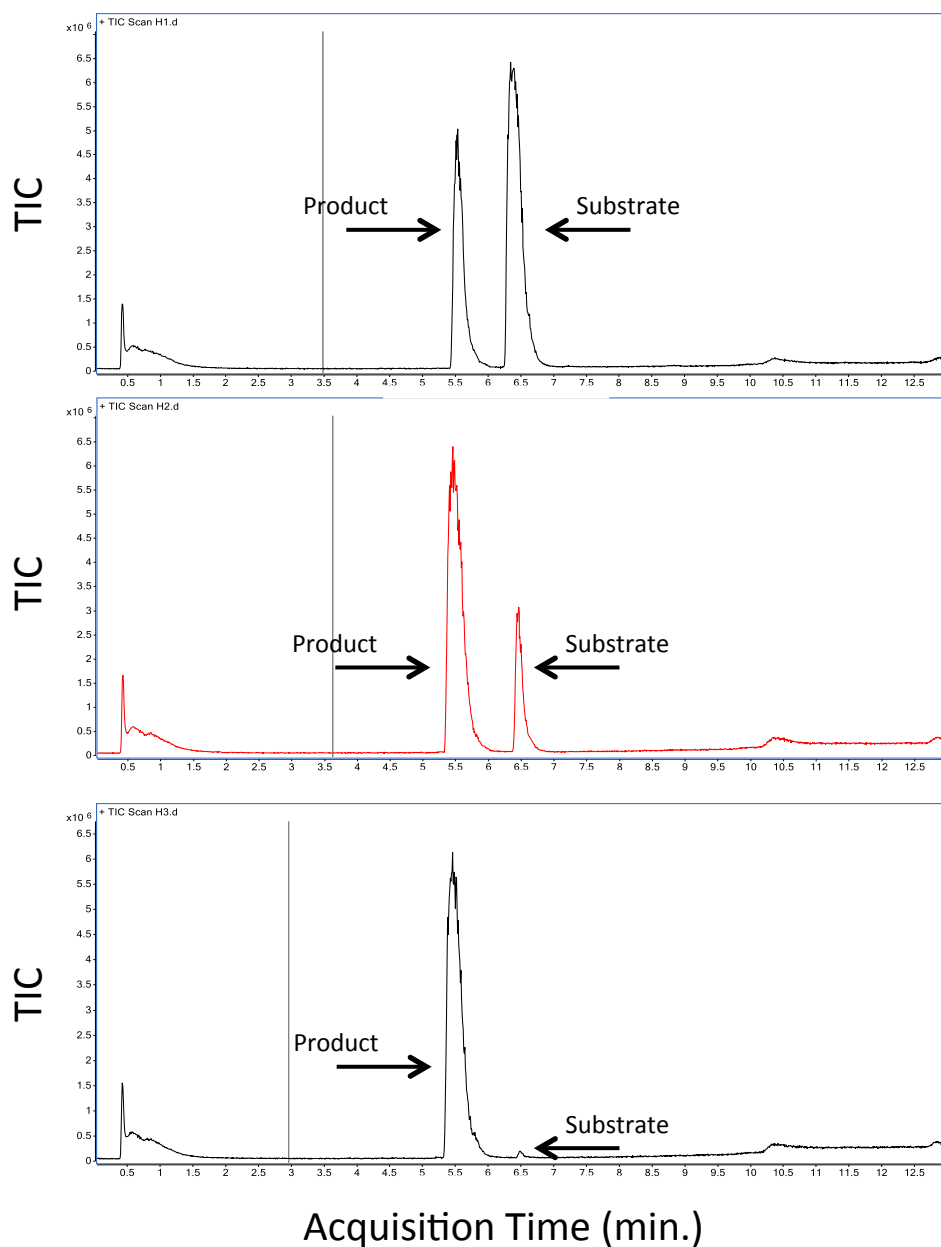
Figure 2.5 HPLC-MS measurement of HDAC8-catalyzed deacetylation

Good separation between substrate and product peaks was observed following HDAC8-catalyze deacetylation. Reactions were run with 1 μM Co-HDAC8 and 100 μM substrate in 1x HDAC assay buffer. Reaction time points (35 μL), from top to bottom (1 min., 5 min., 10 min.), were quenched in 10 μL of 10% hydrochloric acid and 15 μL were injected into the mass spectrometer. The peptide substrate was based on ARID1A (table 2.2).

Peptide substrate libraries can be screened by MALDI-TOF mass spectroscopy

With the HPLC-MS peptide method optimized for quantitative analysis of single substrates, we next looked to find a qualitative mass spectrometry method suitable for assaying multiple substrates. Using a 96-well MALDI target, we were able to detect deacetylation of peptide substrates in a method that is both rapid and consumes a minimal amount of material. Using a small volume of 75 µM peptide, we measured time dependence of deacetylation catalyzed by HDAC8 (Fig. 2.6). We initially developed this assay using four peptide substrates that had not previously been tested with HDAC8 but scored well in an algorithm designed to predict HDAC8 substrates (*89*). Ultimately, we used this technique to evaluate a larger peptide library, finding a mix of substrate and non-substrate peptides. We then used the enzyme-coupled assay to corroborate these results. We found good agreement between the predicted substrates, the MALDI results, and the activity measured using our coupled assay. The biological significance and rational behind the peptides chosen for this experiment, as well as a more detailed explanation of results, is discussed further in Chapter 4 (Proteome chips).

Unlike our HPLC-MS method, this technique using a MALDI source does not provide quantitative kinetic data. This is an inherent limitation of MALDI, where replication of ionization by laser is frequently variable. We are instead able to determine, qualitatively, whether or not a peptide is deacetylated to some extent over a given time course. With this technique, we have eliminated the need for a new calibration curve for each peptide, and can instead use a small set of known molecular weight peptides to calibrate the instrument in a general manner for all peptides to be tested. This method requires only small volumes for each point to be measured, allowing reactions to be run at volumes under 10 µL. This

assay therefore represents a rapid method to qualitatively scan a peptide library using 30-50 fold less material than would be required for the enzyme-coupled assay. Positive hits from a MALDI screen can then be selected and kinetic parameters can be measured using a more resource-intensive method.

We have described various techniques, which differ in their set-up times, material requirements, and detection methods. The advantages and disadvantages of each of these techniques are summarized in Table 2.4. The MALDI assay can be combined with the coupled-enzyme assay to first screen and then quantify HDAC-catalyzed deacetylation of a peptide library. The Q-TOF HPLC-MS method is best suited for experiments that require only one substrate. This could be investigating the effects of site-directed mutagenesis on enzyme activity, environmental variations like divalent metals, salts, and pH, effect of inhibitors, etc. This method is also a useful tool for the validation of indirect assay measurements. The development and optimization of these methods has expanded the available techniques by which HDAC activity and selectivity can be assayed.

Table 2.4 Summary of peptide-based HDAC assay methods

	Advantages	Disadvantages
Coupled-enzyme assay (stopped)	Sensitive detection of acetate (low µM), HDAC-reaction not dependent on speed of coupled enzymes, HDAC-buffer can be altered without affecting coupled enzyme activity	Resource intensive, Time consuming
Coupled-enzyme assay (continuous)	Rapid, no post reaction work-up required, Smaller HDAC and coupled enzyme volumes, No quench solution	HDAC is partially inhibited, Sensitive to activity of coupled enzymes, HDAC deacetylation rate must be slower than coupled reactions
HPLC-MS	Direct measurement of substrate and product, No coupled-reaction enzymes required	Variation between substrates requires multiple standard curves, HPLC-MS instrument cost to own/operate
MALDI-MS	Lowest HDAC and substrate usage, Rapid screen of multiple substrates, No coupled-reaction enzymes required	Requires that peptide ionizes well, Not quantitative, MALDI-MS instrument cost to own/operate, Requires matrix solution
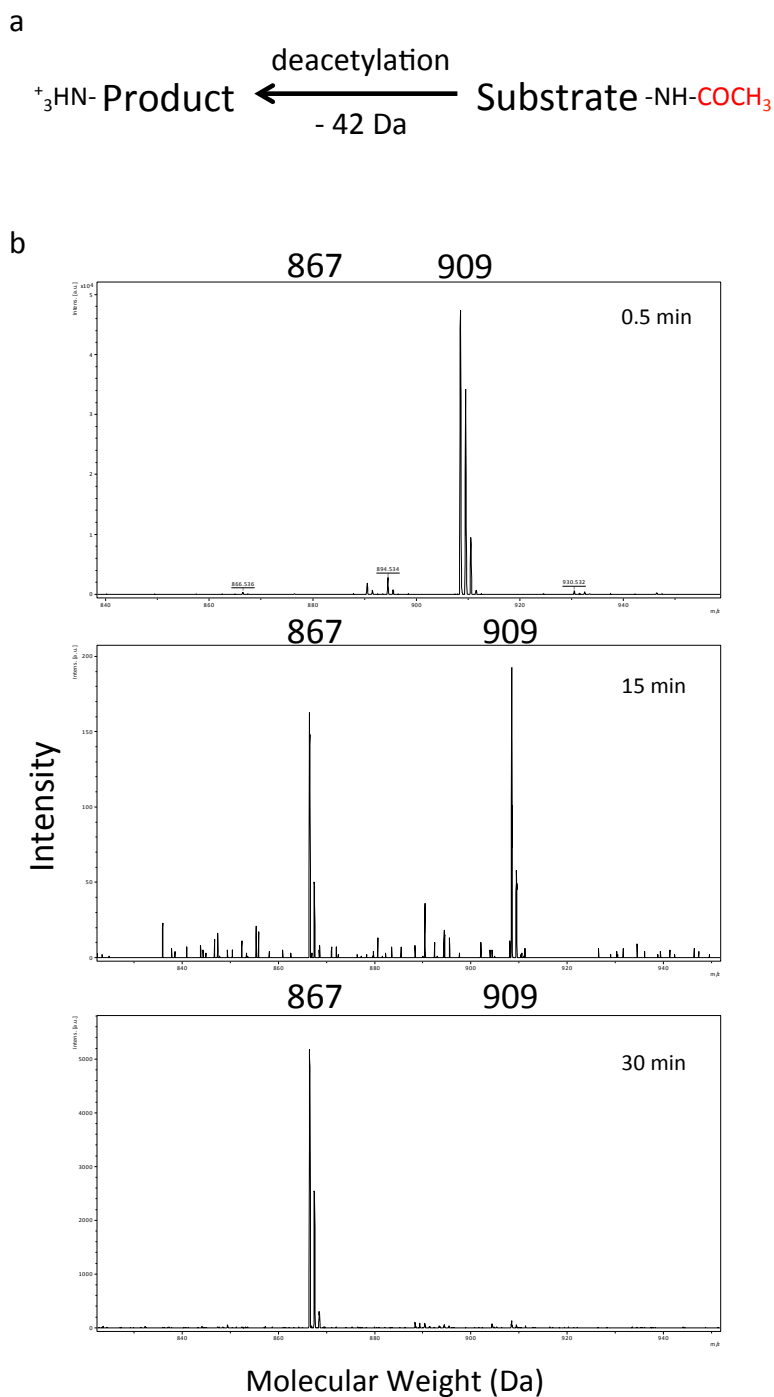
Figure 2.6 MALDI-MS detection HDAC8-catalyzed deacetylation

(A) Deacetylation of peptide substrates results in a 42-dalton shift down in molecular weight. (B) HDAC8 was used at 0.5 μM to catalyze deacetylation of a peptide substrate (75 μM) based on the protein isocitrate dehydrogenase 1. The reaction was quenched at 3 time points (0.5 min., 15 min., 30 min.), shown from top to bottom. The substrate peptide has a molecular weight of 909 Da, and the deacetylated product peptide has a molecular weight of 867 Da, a loss of 42 Da. By 30 min., the substrate peak is no longer visible.

Acknowledgments

I would like to thank the members, past and present, of the HDAC subgroup for collaborating on HDAC8 expressions. I would to thank Noah Wolfson for his guidance, expertise, and insight on the optimization of the enzyme-coupled assay. This was a collaborative endeavor. I would also like to acknowledge Daniel Steyer for his help in running the Q-TOF HPLC MS controls.

Chapter 3

Expression and Characterization of HDAC11[9]

Introduction

N^{ε}-lysine acetylation is a dynamic post-translational modification occurring ubiquitously in eukaryotic cells (*90*, *91*). Recent studies estimate that acetylation occurs on thousands of different proteins (*86*), at over 20,000 lysine residues (*6*). Regulation of lysine acetylation is controlled by the activity of two families of enzymes, the lysine acetyl transferases (KATs) and the histone deacetylases (HDACs). The HDACs are the divided into four classes. Class I (HDACs 1, 2, 3, 8), class II (HDACs 4, 5, 6, 7, 9, 10), class III (sirtuins), and class IV (HDAC11). The class I, II, and IV HDACs are metal-dependent deacetylases that are phylogenetically similar to one another but distinct from the class III sirtuins (*73*).

HDAC11, the only class IV HDAC, is the most recently identified HDAC isozyme (*24*). It is also among the least studied and most poorly understood HDACs. A pubmed search (title/abstract) for the last 10 years shows that HDAC11 was the second least mentioned isozyme, ahead of only HDAC10. HDAC11 was referenced 70 times, while HDAC1, the most highly published isozyme, had 1,666 hits over the same 10-year span.

The bulk of HDAC11 studies are cell based and have uncovered a few potential roles for this enzyme in major pathways and disease states. Changes in HDAC11 expression

---

[9] Lubomir Dostal carried out the expression and purification of HDAC11 from HEK293 cells. HDAC11 was expressed in insect cells by Clay Brown (LSI) and purified by Eric Sullivan. *E. coli* expression and purification of HDAC11 was carried out by Eric Sullivan.

levels have been linked to ductal breast carcinomas, where HDAC11 is in the top 1% of genes that are differentially overexpressed in the disease state (*69*). This same study showed that knockouts of HDAC11 resulted in a selective decrease in cancer cell viability when compared to non-cancerous cells. Additionally, HDAC11 has been implicated in the adaptive immune response, where it influences the expression of interleukin-10 (*68*).

The discovery of disease-related physiological functions for HDAC11 increases the importance of understanding the mechanism by which this enzyme is able to influence these phenotypic results. Here, we sought to develop biochemical methods to characterize the catalytic activity of HDAC11. We successfully expressed HDAC11 in bacterial and eukaryotic cells. HDAC11 expressed in *E. coli* is inactive; HDAC11 from eukaryotic cells is active and mass spectra of the protein expressed in insect sf9 cells has a mass that is 42 Da higher than expected, suggesting a post-translational modification. We used the HDAC11 purified from insect cells to probe the substrate selectivity of HDAC11 by measuring the rate constants for deacetylation of several unique peptide substrates. We show, for the first time, that purified HDAC11 is catalytically active, catalyzing deacetylation of unlabeled and non-fluorinated peptide substrates.

<center>**Methods**</center>

Reagents

      Reagents used to prepare buffers were from Fisher or Sigma, unless otherwise specified. DH10bac cells were a generous gift from Clay Brown at the UM Life Sciences Institute Protein Core.

HDAC11 *E. coli* constructs

      The human HDAC11 gene was used in several different constructs. Our starting gene, based on the human cDNA, was synthesized by GeneScript. We worked with both the cDNA-transcribed human codons, as well as a gene with codon usage optimized for bacterial expression. Our optimization was done through GeneScript. We used standard PCR techniques to clone HDAC11 into pET 21a$^+$ and pET M11 vectors, and add or remove various tags and fusion proteins. A his6-SUMO-HDAC11 construct in a pET 21a$^+$ vector yielded the best results and was the expression construct used for the majority of the work with the bacterially expressed enzyme in this study. We also created WT HDAC11, his6-TEV-HDAC11, his10-TEV-HDAC11, HDAC11-TEV-his6, and his10-TEV-HDAC11-eGFP-TEV-his6. The his10-tagged constructs are codon optimized for bacterial expression.

Bacterial expression of HDAC11 in various cell lines

      Fresh transformations were used for each HDAC11 culture. Transformations were generally done with 75-150 μL of plasmid DNA. Plasmids were transformed into either BL-21, arabinose induced (AI), or Rosetta II competent cells. AI cells have a tighter regulation on protein expression than standard T7 systems. They feature an arabinose-inducible

araBAD promoter upstream of the T7 RNA polymerase gene. Cells were plated on LB-Amp/Kan/combo plates, as appropriate and grown overnight at 37℃. Antibiotic concentrations were 100 μg/mL ampicillin and 50 μg/mL kanamycin. Single colonies were selected and inoculated into 10 mL starter cultures of 2xYT, plus antibiotics (present for the rest of the expression). These were grown, with shaking, at 37℃ until cloudy (~4 hrs). These starter cultures were then used to inoculate 1-liter cultures of terrific broth (TB) media, buffered with potassium phosphate. Cells were grown, in the same manner, to an OD_{600} of 0.6, at which point the temperature was decreased to 18℃. After cooling (~1 hr), the cells were induced as follows; BL-21, Rosetta II, and AI cultures were induced with isopropyl *B*-D-1-thiogalactopyranoside (IPTG) at a final concentration of 0.4 mM. AI cells were also treated with 0.2% (final) arabinose. Cultures were grown for 16 hours. Cells were then pelleted by centrifugation at for 15 minutes at 4,000 x g in a Beckman JLA 8.1000 rotor. Cell pellets were resuspended in HDAC11 *E. coli* lysis buffer 1 (30 mM HEPES pH 8.0, 80 mM NaCl, 1 mM TCEP, 5% glycerol) with a Roche EDTA-free protease inhibitor cocktail tablet and lysed using a microfluidizer (DivTech Equipment). Protein expression, both soluble and insoluble (separated by centrifugation of the lysate at 27,000 x g), was determined by a western blot probing for HDAC11.

Bacterial expression of HDAC11 in various growth mediums

His6-SUMO-HDAC11 was transformed into BL-21 (DE3) cells, plated, and grown in 10 mL starter cultures as described above. Starter cultures were then used to inoculate 1-liter cultures of LB, 2xYT, or TB media with ampicillin present. Cells were grown according to the conditions described above for BL-21 cells (starter cultures at 37℃ and larger

cultures at 34°C, followed by a decrease to 18°C at OD_{600} = 0.6), and all cell lines were induced with 0.5 mM IPTG and grown overnight. Additionally, a second 2xYT culture was induced with only 0.2 mM IPTG. Overnight cultures were pelleted, and lysed via a microfluidizer. Soluble expression of HDAC11 was determined by a western blot using an antibody that recognizes poly-histidine.

Adjusting buffers and addition of alcohol to HDAC11 *E. coli* expressions

SUMO-HDAC11 was transformed into BL-21 cells, plated, and inoculated into starter cultures as described above. Starter cultures were then used to inoculate several 1-liter cultures. The following expressions were performed in parallel to test the effect of added zinc to the media. One set of expressions (3, 1 L cultures) was performed in TB media with ampicillin and a potassium phosphate buffer. The parallel expressions (3, 1 L cultures) were performed in TB media with ampicillin and a tris buffer. These tris cultures were also supplemented with 100 μM zinc sulfate at induction. All cultures were grown according to the procedure above. At induction, one liter of culture from each buffer set was treated with: 1.5% (final) ethanol, 10 mM (final) benzyl alcohol, or no additive. Each culture was then induced with 0.5 mM IPTG. Cells were grown, pelleted, and lysed as described above. Soluble and insoluble expression was determined by western blot using an antibody toward HDAC11.

Preparation of competent cells transformed with plasmids encoding molecular chaperones

Z-competent "mix and go" cells (Zymo Research) were prepared according to the kit. Briefly, BL-21 (DE3) cells (10 mL) were transformed with various molecular chaperone

plasmids (Takara) (Table 3.1) and grown overnight in LB medium with the appropriate

antibiotics. 0.5 mL of these starter cultures was used to inoculate 50 mL cultures of Super

Optimal Broth (S.O.B.) medium. These were grown, with shaking, at 34°C until OD_{600}

reached 0.4. The kit buffers were diluted to 1x concentration ahead of time and chilled on

ice. Once the bacterial cultures had reached the desired OD, they were transferred to ice

for 10 minutes. The cells were then pelleted by centrifugation at 2,000 x g for 10 minutes.

The supernatants were removed and the cell pellets were resuspended in 5 mL 1x wash

buffer. Cells were pelleted again. The supernatants were removed and cells were not

resuspended in 5 mL 1x competent buffer. Cells were immediately aliquoted (200 µL) into

microcentrifuge tubes on ice before being flash frozen in liquid nitrogen and stored at -

80°C.

Table 3.1: Chaperone proteins co-expressed with HDAC11.

Plasmid	Chaperone	Promoter	Inducer	Resistance
pG-KJE8	dnaK-dnaJ-grpE groES-groEL	*araB* *Pzt1*	L-Arabinose Tetracyclin	chloramphenicol
pKJE7	dnaK-dnaJ-grpE	*araB*	L-Arabinose	chloramphenicol
pG-Tf2	groES-groEL-tig	*Pzt1*	Tetracyclin	chloramphenicol
pTf16	tig	*araB*	L-Arabinose	chloramphenicol

Co-expression of molecular chaperones with HDAC11 in *E. coli*

SUMO-HDAC11 was transformed into four different BL-21 competent cell lines, each

with a different expression vector for molecular chaperones (described above). Cells were

plated on LB-Amp/Chloramphenicol (100 µg/mL and 34 µg/mL, respectively) plates and

grown overnight at 37°C. Starter cultures, grown as described above, were inoculated into

1-liter cultures. Cultures 1, 3, and 5 were treated with 1 mg/ml arabinose, and cultures 1

and 4 were treated with 1 ng/ml tetracycline to induce expression of the chaperones. After

cells reached OD_{600} = 0.6, the temperature was decreased to 20°C and HDAC11 was induced

by addition of 0.5 mM IPTG in all culures. Cells were grown and lysed as described above,

with the following exception. The cell pellet was resuspended and lysed in *E. coli* HDAC11

lysis buffer 2 (50 mM HEPES pH 8.0, 300 mM NaCl, 10% glycerol). HDAC11 expression,

both soluble and insoluble, was again determined by a western blot using an antibody to

probe for poly-histidine.

Purification of *E. coli* expressed SUMO-HDAC11

His6-SUMO-HDAC11 was expressed in the presence of trigger factor in TB medium,

as described above. Culture sizes were scaled from 1-liter expressions to up to 4-liter

expressions. Cell pellets were resuspended with 25 mL of lysis buffer per liter of culture.

After lysing the cells using a microfluidizer, lysate was incubated on ice with 2 μL of

benzonase per 25 mL for 15 minutes. Lysate was then cleared via centrifugation at 27,000

x g (Sorvall SS-34 rotor) for 1 hour. Cleared lysate was decanted and added to 5 mL of pre-

charged nickel resin in buffer A (HDAC11 *E. coli* lysis buffer 2 with only 2.5% glycerol).

This slurry was incubated, with mild shaking, at 4°C for four hours. Lysate and resin were

then poured into a gravity-flow bench-top column, and the flow-through was collected.

The resin was then washed with a stepwise elution of increasing buffer B (buffer A plus

500 mM imidazole) (steps at 10 mM, 25 mM, 50 mM, 100 mM, 200 mM and 500 mM

imidazole) and fractions were collected. HDAC11 elution was determined by both

coomassie staining of an acrylamide gel and by western blot probing for HDAC11. Samples

with HDAC11 were pooled, ubiquitin ligase specific protease 1 (Ulp1) was added, and the mixture was dialyzed overnight at 4℃ against buffer A. Protein was then run over a second nickel column to remove His6-Ulp1 and any proteins that bind non-specifically to the nickel resin, and again a stepwise elution was run with buffer B (steps at 10 mM, 50 mM, and 500 mM imidazole). HDAC11-containing fractions from the flow through and low imidazole washes were pooled and concentrated using Amicon Ultra centrifugal filters. Purity was assessed by sodium dodecyl sulfate polyacrylamide gel electrophoresis (SDS-PAGE). If the protein was pure (> 50% purity), it was aliquoted and flash frozen in liquid nitrogen before storage at -80℃. If HDAC11 needed additional purification, the enzyme was further fractionated on either a size exclusion column (SEC) (GE sephacryl S-200 26/60) or a 5 mL mono-Q column. Both columns were run on an FPLC at 4℃. The SEC column was run in nickel column buffer A, with a constant flow rate of 1 mL/min. The Q column was run at 5 ml/min. Additionally, the Q-column was pre-washed with 5 column volumes (CV) of Q-Low Salt buffer (50 mM HEPES pH 8.0, 50 mM NaCl, 2.5% glycerol) and the sample was diluted in Q-Low Salt buffer to bring [NaCl] < 80 mM before the sample was loaded. The sample was eluted using a linear gradient over 20 CV to 100% Q-High Salt buffer (Q-Low Salt buffer with 1 M NaCl). HDAC11 was concentrated after these additional purification steps and flash frozen for storage.

HDAC11 cloning for insect cell expression

The human HDAC11 gene was PCR amplified from His6-SUMO-HDAC11 in a pET 21a+ vector. The forward and reverse primers (Fig. 3.1) add restriction sites (BamHI and EcoRI) to the N- and C-terminal ends, respectively. A pFASTBAC dual vector (courtesy of

59

Clay Brown, UM) and the HDAC11 insert were digested with the appropriate restriction enzymes. The digestion was stopped and fragments separated on a 1% agarose gel. Insert and vector were excised from the gel and purified using a Promega DNA gel purification kit. The HDAC11 gene was ligated to the pFASTBAC vector on ice using Quick Ligase (New England Biolabs) for 5 minutes. The plasmid was then immediately transformed into XL1-Blue competent cells to assess ligation efficiency. Cells transformed with the plasmid were grown on LB-Amp plates at 37°C. Single colonies were selected and used to inoculate 10 mL cultures of 2xYT with ampicillin. These cultures were grown overnight with shaking at 37°C. Cells were then pelleted by centrifugation in falcon tubes. Plasmid DNA was extracted using a Promega Mini-Prep kit. Proper gene insertion was verified by Sanger sequencing at the UM DNA sequencing core.

Forward Primer

5'– GCA CTG GGA TCC GGT ACC ATG CTA CAC ACA ACC 3'

Reverse Primer

5'– CCA GCT GAA TTC TCA GTG GTG GTG GTG GTG GTG CTC 3'

Figure 3.1: Primers for cloning HDAC11 into pFASTBAC

The forward and reverse primers used to clone HDAC11 into pFASTBAC. The restrictions site are colored red (forward: BamHI, reverse: EcoRI). Regions that overlap with the HDAC11 gene are highlighted in yellow.

At this point we gave the pFASTBAC HDAC11 plasmid to the LSI protein core. They transformed the plasmid into DH10bac cells, which produces bacmid DNA. They then isolated the bacmid DNA and transfected it into insect cells (sf9 and HighFive). This method generates recombinant baculovirus, which was amplified and stored as a high titer stock to infect insect cells for large-scale expression of HDAC11.

HDAC11 validation techniques (western blotting and mass spectrometry)

For western blotting, HDAC11, following fractionation by SDS-PAGE, was transferred to a nitrocellulose membrane in a semi-dry transfer cell. Western blots were then run according to one of the two following methods. The first method involves 1 hour of blocking with 5% non-fat milk, followed by 1-2 hours of incubation at room temperature with a primary anti-HDAC11 or anti-polyhistidine antibody in 2% milk. Blots were washed 3x for 5 minutes each with tris-buffered saline (20 mM tris pH 7.6, 150 mM NaCl) and 0.1% tween 20 (TBST). Blots were then incubated with a secondary antibody for 1 hour, and again washed 3x with TBST. In the second method, blots were developed using in a Snap I.D. 2.0 instrument. The nitrocellulose membrane was blocked with 0.5% bovine serum albumin (BSA) in TBST. The blocking solution was then pulled through the membrane by vacuum. Primary antibody, in blocking solution, was incubated with the blots for 10 minutes, and then pulled through with vacuum. With the vacuum running, blots were quickly washed 3x with TBST. Secondary antibody, in blocking solution, was also incubated for 10 minutes, and blots were again washed under vacuum 3x with TBST. The following primary antibodies were used: Sigma anti-HDAC11 polyclonal antibody from rabbit or Sigma monoclonal anti-polyhistidine alkaline phosphatase antibody from mouse.

The following secondary antibodies were used: Life Technologies Alexa Fluor 633 goat anti-rabbit or Cell Signaling anti-rabbit IgG HRP-linked. Antibodies were visualized on an Azure Biosystems C-series imager using either chemiluminescence (HRP) or fluorescent excitation at 628 nm (Alexa Fluor).

Prior to mass spectrometry, HDAC11 samples were desalted using 7 kDa molecular weight cutoff Zeba desalting spin columns. Intact protein was separated on an HPLC through a C18 column before being injected into an electrospray mass spectrometer (Agilent Q-TOF). Protein peaks were deconvoluted and identified based on mass.

Expression and purification of HDAC11 from HEK293

We cloned a wild-type HDAC11 gene (from our bacterial expression vectors) into a pcDNA4 mammalian expression vector with an N-terminal ZZ-tag and a TEV recognition site. The plasmid encodes resistance to puromycin, which was used (at 1 µg/mL) to select for stable incorporation of the HDAC11 expression plasmid after transfection into HEK293 cells. These cells were cultured in 75 cm^2 flasks at 37℃. Before purifying HDAC11, cells were harvested by treatment with trypsin and pelleted by centrifugation in falcon tubes, followed by lysis via freeze-thaw cycles. Lysate was incubated with protein IgG beads (ThermoFisher) to immobilize ZZ-tagged HDAC11. Lysate was decanted and beads were washed three times with pull-down buffer. Cells were then incubated overnight at 4℃ with TEV protease to cleave HDAC11 from the beads. Beads were pelleted and HDAC11 in solution was decanted and flash frozen in liquid nitrogen.

Fluor-de-Lys HDAC11 assays

We measured HDAC11 activity against several substrates using the Fluor-de-Lys assay (Enzo Life Sciences and (*87*)). HDAC11 was reconstituted with cobalt or zinc for 1 hour on ice at a 2:1 cobalt to enzyme or 1:1 zinc to enzyme ratio. All assay components were diluted in 1x HDAC8 assay buffer (25 mM HEPES pH 8.0, 137 mM NaCl, 3 mM KCl). Substrates were used at final concentrations ranging from 20 – 200 μM. Initial rates for HDAC11 catalysis were assayed at final enzyme concentrations from 500 nM – 1 μM. All assays were conducted at 34°C. Time points were quenched in a commercial solution of trypsin developer and trichostatin A (TSA) (Enzo Life Sciences). The fluorescence of the product (ex. 340 nm, em. 450 nm) and substrate (ex. 340 nm, em. 380 nm) were measured using a PolarStar Fluorescent plate reader and Corning 96-well half area black plates. Standard curves were prepared by mixing known concentrations of product and substrate.

HDAC11 activity using a coupled enzyme assay

HDAC11 activity on unlabeled peptides was determined using an enzyme-coupled assay as described in Wolfson *et al.* ((*76*) and Chapter 2). Briefly, hydrolysis of acetyllysine results in the release of free acetate. This is ultimately converted to citrate through the enzymatic activity of acetyl-CoA synthetase, citrate synthetase, and malate dehydrogenase. A byproduct of the malate dehydrogenase reaction is the conversion of NAD+ to NADH, which detected by fluorescent excitation at 340 nm and emission at 460 nm. We used concentrations of substrate ranging from 50 – 200 μM, and enzyme concentrations from 0.2-1.5 μM. Assays were conducted at 34°C. HDAC11 was reconstituted with cobalt (2:1

metal to enzyme) or zinc (1:1 metal to enzyme) for 1 hour on ice prior to usage. All assays were run in HDAC8 assay buffer. Aliquots at various time points (60 µL) were quenched by addition of 2.5 µL of 10% hydrochloric acid and flash frozen in liquid nitrogen. Quenched points were stored for up to 2 days at -20℃ or longer at -80℃. Immediately before being mixed with the coupled enzymes, reaction aliquots were thawed and neutralized by the addition of 7.5 µL of 6% sodium bicarbonate. In a black Corning 3868 plate, 10 µL of coupling solution (as described in (*76*)) was added to 60 µL of reaction. NADH formation was monitored in a PolarStar fluorescent plate reader every 1 – 2 minutes until reactions reached completion (less than 2 hours). Results were compared to a standard curve generated by addition of known concentrations of acetate to the coupled solution and monitoring NADH formation.

HDAC11 inhibition by SAHA and MGCD0103

Inhibition of HDAC11 was measured using the Fluor-de-Lys assay, as described above, with the BOC-Lys substrate (shown in Fig. 3.11). Briefly, 10 mM SAHA in 100% DMSO was serially diluted into HDAC8 assay buffer. HDAC11 was reconstituted on ice for 1 hour at a 2:1 cobalt:enzyme ratio. Substrate was diluted into HDAC assay buffer and used at final concentrations of 50 and 100 µM and SAHA concentrations varied (up to 10 µM). SAHA and BOC-Lys were pre-incubated in buffer at 34℃ before initiation of the reaction by addition of HDAC11. HDAC concentration was 0.15 – 0.55 µM. Reaction time points were quenched into a mixture of trypsin developer and TSA. After a 15-minute incubation with the developer solution, time points were read in a PolarStar fluorescence plate reader, as described above.

MGCD0103 inhibition was performed as described for SAHA, with 0.2 μM HDAC11 and up to 10 μM MGCD (structure shown in Fig. 3.11).

Results

Optimization of expression of recombinant human HDAC11 in *E. coli*.

We originally expressed a His6-tagged HDAC11 in a pET vector. After induction with IPTG of BL-21 (DE3) cells containing this HDAC11 plasmid, a prominent band appeared at the correct molecular weight after coomassie staining an SDS-PAGE gel. However, mass spectrometry of this protein showed that it was about 3 kDa heavier than expected from the HDAC11 sequence. The molecular weight was consistent with the bacterial elongation factor Ef-Tu, suggested by our collaborator, David Christianson. We determined the protein was likely the bacterial elongation factor Ef-Tu. We confirmed that this protein was Ef-Tu by probing a western blot with a primary anti-Ef-Tu antibody. Therefore, we tried alternative methods to express and purify HDAC11.

To better separate HDAC11 from Ef-Tu by SDS-PAGE, we fused the sequence for SUMO protein to the 5' end of the HDAC11 gene behind a T7 promoter. This fusion increased the molecular weight by 12 kDa. We next optimized expression conditions to increase the yield of soluble HDAC11. We examined three different cell lines, BL-21 (DE3), Rosetta II, and arabinose induced (AI) cells, and found that after induction with IPTG at 18°C in TB media, the soluble yield of HDAC11 was highest in the BL-21 (DE3) cells (Fig. 3.2). However, only a small percent of the total HDAC11 was in the soluble fraction. To evaluate whether the expression of HDAC11 was dependent on the media, we tested expression levels in 2xYT, LB, and TB medias. We also tested two concentrations of IPTG (0.2 mM and 0.5 mM) in 2xYT. We found that the total yield of HDAC11 was significantly higher in TB media (Fig. 3.3). LB and 2xYT (with 0.5 mM IPTG) yielded similar levels of HDAC11, and the 2xYT sample with 0.2 mM IPTG yielded the least amount of protein.

Figure 3.2: HDAC11 expression trials in various cell lines

His6-SUMO-HDAC11 expression after induction with IPTG of 1 liter cultures in arabinose inducible (AI) cells, standard BL21 (DE3) cells, or Novagen Rosetta II (Rose) cells grown overnight at 18°C. Lysates were centrifuged to separate soluble and insoluble cellular components. HDAC11 expression levels (at 52 kDa) were determined by a western blot probed with an anti-HDAC11 primary antibody. Soluble yield was greatest using the BL21 cell line, and lowest using the Rosetta II cells.
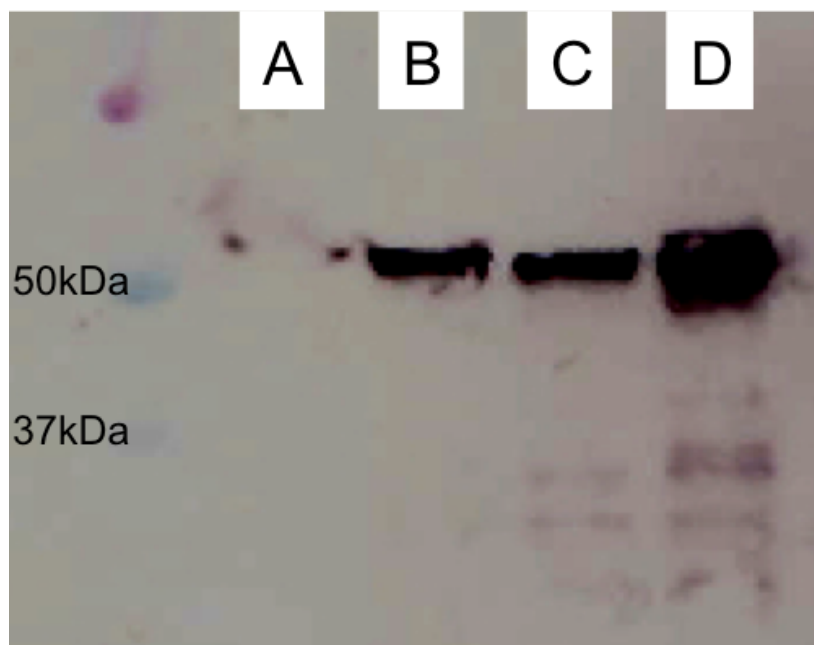
Figure 3.3: HDAC11 expression trials in various medias

Western blot of lysate from BL-21 (DE3) cells containing the His-SUMO-HDAC11 plasmid. Cells were induced with IPTG and grown overnight in 2xYT (A and B), LB (C), or TB (D) media. Total HDAC11 expression was determined here by a western blot probed against poly-histidine. The cells in lane A were induced with 0.2 mM IPTG, while cells in lanes B-D were induced with 0.5 mM IPTG. The greatest expression of HDAC11 was observed in TB-grown cells, and 0.5 mM IPTG yielded more protein than 0.2 mM IPTG.

We had successfully increased expression, using TB media with 0.5 mM IPTG induction, of total expression of HDAC11 in BL-21 (DE3) cells using the His6-SUMO-HDAC11 plasmid. Further more, the SUMO fusion separated HDAC11 from Ef-Tu by mass for easier identification and purification. However, the majority of His6-SUMO-HDAC11 was insoluble. We decided to try increasing soluble expression through additives to the media, including alcohols and metals, as well as coexpressing molecular chaperones. We found that including 1.5% ethanol at induction had little effect on protein solubility, while 10 mM benzyl alcohol modestly increased soluble expression (Fig. 3.4). Interestingly, this effect was only observed in media buffered with phosphate. In a tris-buffered culture with added zinc, we observed that neither alcohol improved solubility. Finally, we assessed the

impact on soluble expression of HDAC11 of co-transformation with four different plasmids expressing molecular chaperones. These plasmids encoded: 1) dnaK-dnaJ-grpE and groES-groEL; 2) dnaK-dnaJ-grpE; 3) groES-groEL-trigger factor; and 4) trigger factor. We found that co-expression with trigger factor (Tig) alone had a significant impact on SUMO-HDAC11 solubility.

Based on these, we used the following method for optimal HDAC11 expression: The HDAC11 construct contained both a His6-tag and a SUMO tag on the N-terminus (Fig. 3.5). We created a stock of BL-21 (DE3) competent cells that contained the expression vector for Tig, and transformed these cells with the HDAC11 plasmid prior to each expression. Using this combination, a 1 L culture of HDAC11 grown at 18°C in TB media with 0.5 mM IPTG added at induction yielded > 5 mg of soluble enzyme.
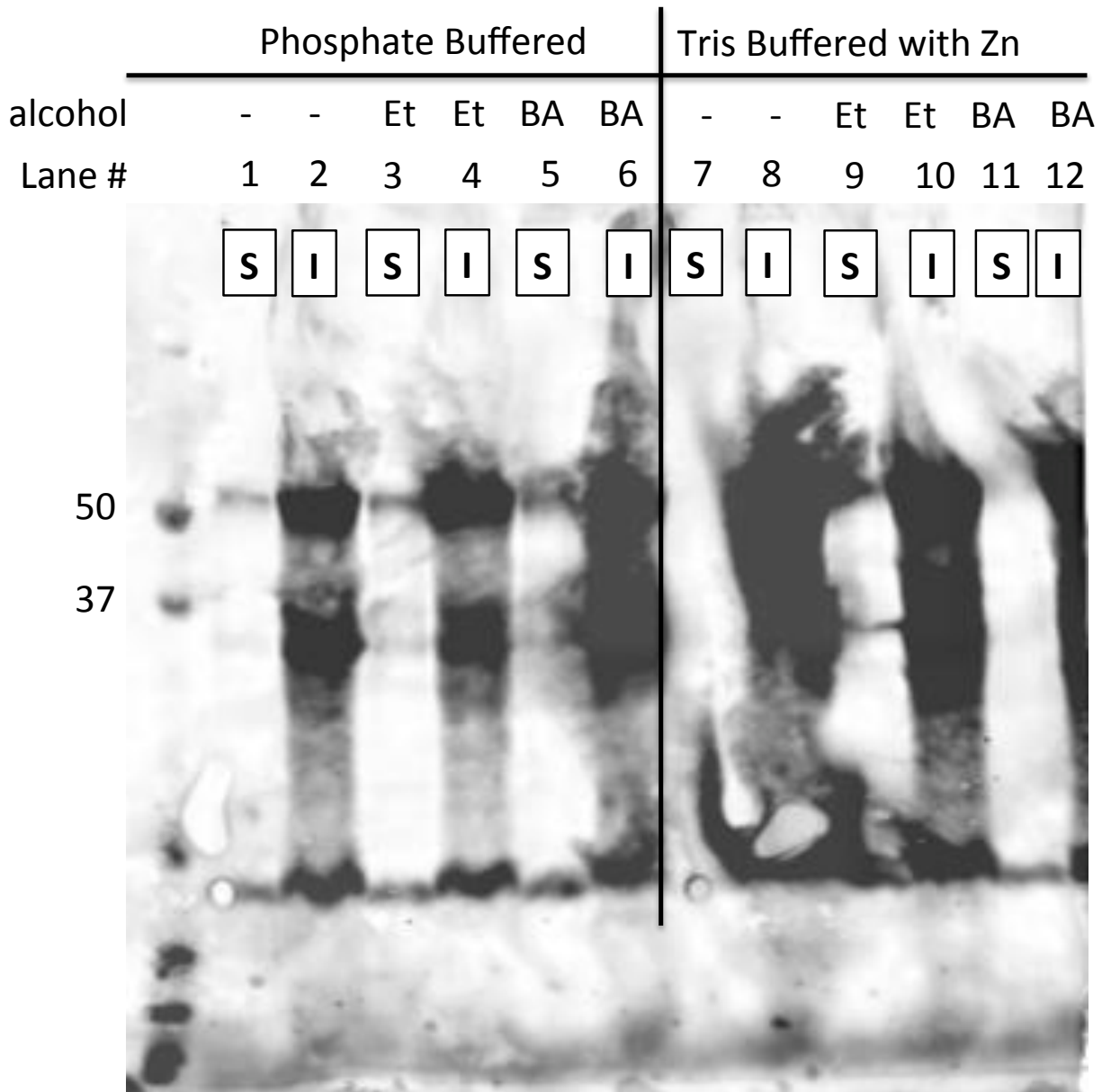
Figure 3.4: HDAC11 solubility with added alcohols visualized on a western blot

The effects of adding alcohol to expression media were tested. Labels S (soluble) and I (insoluble) denote which portion of the lysate was run in each lane. Lanes 1-6 represent bacteria grown in media buffered with potassium phosphate. Lanes 7-12 represent bacteria grown in tris-buffered media, supplemented with zinc (200 μM). Additionally, lanes 1, 2, 7, and 8 are from expressions with no added alcohols. Lanes 3, 4, 9, and 10 are from expressions with 1.5% ethanol (Et). Lanes 5, 6, 11, and 12 are from expressions with 10 mM benzyl alcohol (BA). HDAC11 (52 kDa) expression is determined here by a western blot probed with an anti-HDAC11 primary antibody. Soluble yield of HDAC11 is greater using a potassium phosphate buffer, and greatest in the presence of benzyl alcohol.
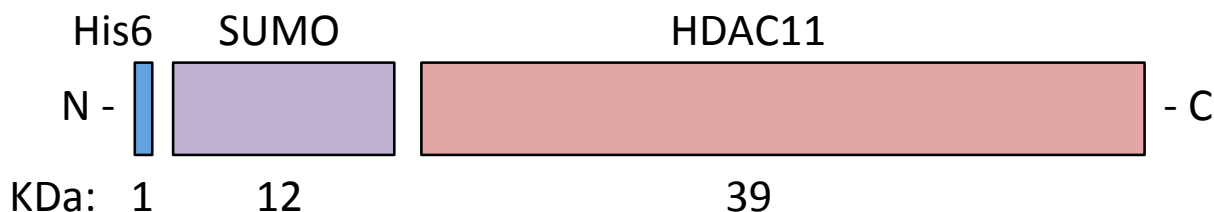
Figure 3.5: HDAC11 *E. coli* construct

The His6-SUMO-HDAC11 construct used for our *E. coli* growths. The construct is sufficiently heavier than the bacterial elongation factor Ef-Tu, and has a higher expression of soluble protein than non-SUMO tagged HDAC11.

Expression and purification of active HDAC11 from insect sf9 cells

Concurrent with our work on expressing HDAC11 in *E. coli*, we also prepared HDAC11 for expression in sf9 cells. We cloned a His-tagged human HDAC11 gene into a pET 21a+ vector using PCR and transformed this plasmid into DH10 alpha cells for transfection. We looked at His6-HDAC11 expression in two insect cell lines: sf9 and HighFive. We found expression to be similar, though slightly higher in HighFive cells (Fig. 3.6). However, the lysate from the HighFive cells was more difficult to clear and contained a greater percentage of insoluble His6-HDAC11. For this reason, we chose to move forward expressing HDAC11 in sf9 cells.

Purification of HDAC11 from these cells proved to be challenging. Our initial attempts to purify the protein using a Ni-column demonstrated that the his-tagged protein did not bind to the Ni-resin. We varied the incubation time for batch loading the Ni-resin, from 30-minutes to 16 hours. We found that a 4 – 5 hour incubation at 4°C was optimal. Longer incubation times led to a modest increase in HDAC11 recovery, but non-specific binding of host proteins also increased significantly. We purified His6-HDAC11 from insect cells using His6-TEV protease to cleave the His-tag from HDAC11 after the first nickel

column. His6-TEV protease was then removed on a second nickel column. This purification scheme yields protein that is > 60% pure. Approaches to further purify HDAC11 are addressed in the discussion.
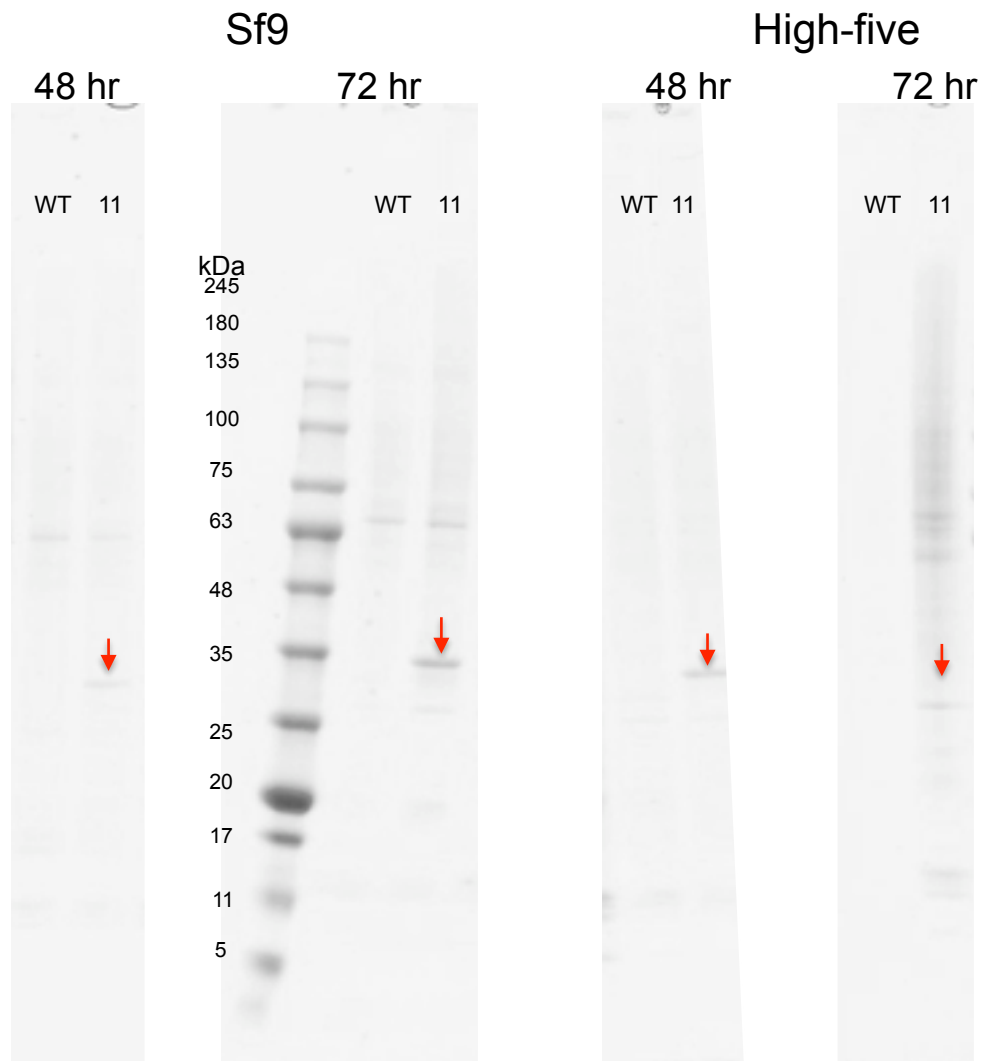
Figure 3.6: HDAC11 expression in insect cells

An SDS-PAGE gel comparing expression of HDAC11 in two insect cell lines, sf9 and HighFive. Small scale expressions were stopped after 48 or 72 hours, lysed, and passed over a nickel column. HDAC11 (lane 11) is highlighted with a red arrow. Expression is similar in both cell lines.

Validation of HDAC11 from sf9 expression

To validate the identity of the purified HDAC11, we first fractionated the protein by SDS-PAGE stained with coomassie, followed by a western blot probed with anti-HDAC11 antibodies (Fig. 3.7). The gels confirmed that the purified protein is HDAC11. We also used liquid-chromatography mass spectrometry of the intact protein to determine the molecular weight of the purified protein (Fig. 3.8). The intact-protein MS data gave an interesting result, the mass of HDAC11 purified from insect cells is 42 daltons heavier than predicted from the amino acid sequence for the wild-type enzyme. This is based on the assumption that the purified protein has no remaining tags and the N-terminal methionine remains. We hypothesize that this increase in mass is due to a post-translational modification; the 42 dalton increase in the molecular weight is consistent with the addition of an acetyl group or tri-methylation, among others. Possible PTMs are discussed in more detail in the discussion section.
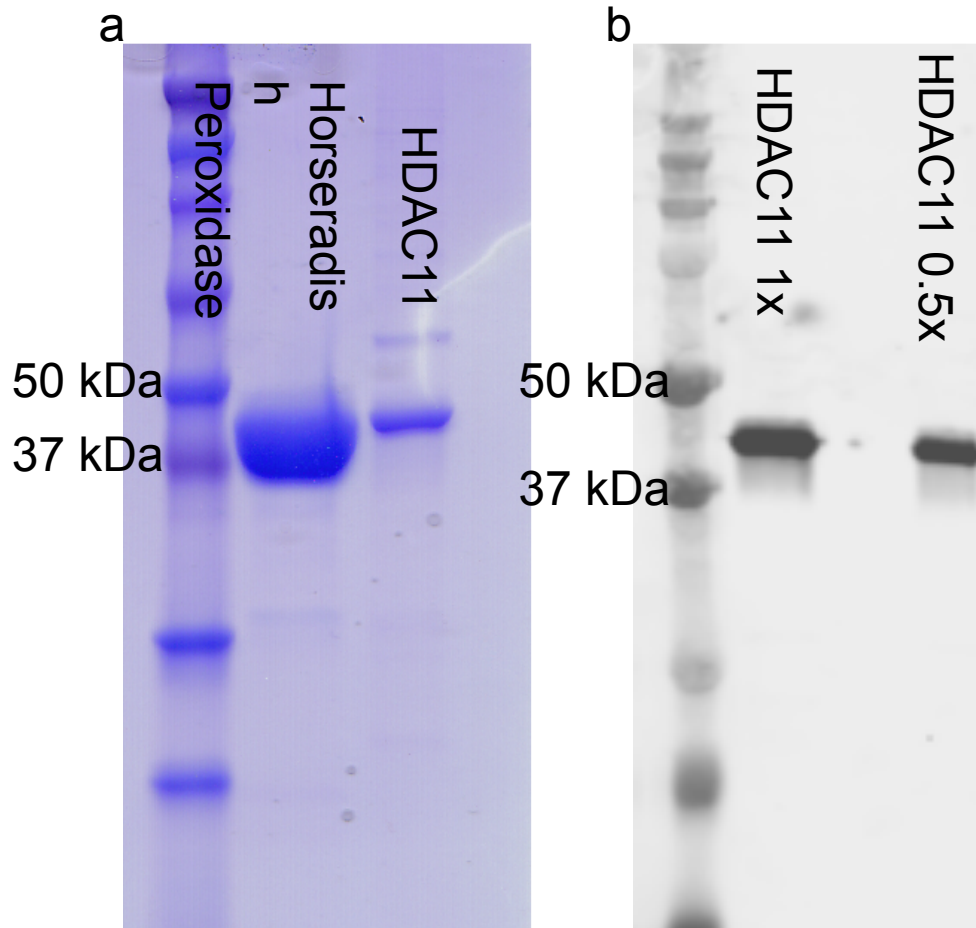
Figure 3.7: SDS-PAGE gel and western blot of HDAC11 from sf9

Validation of HDAC11 expressed and purified from sf9 cells. In both gels lane 1 is molecular weight ladder. A. SDS-PAGE stained with coomassie blue. HDAC11 ($\sim$ 40 kDa) was run along with a horseradish peroxidase control ($\sim$ 40 kDa). B. Western blot probed with an anti-HDAC11 primary antibody (Sigma). HDAC11 (exact concentration unknown) was loaded at 1x and 0.5x concentration.

a

b
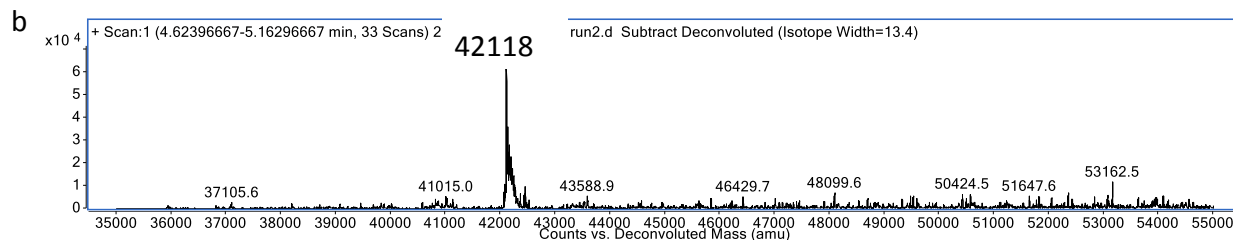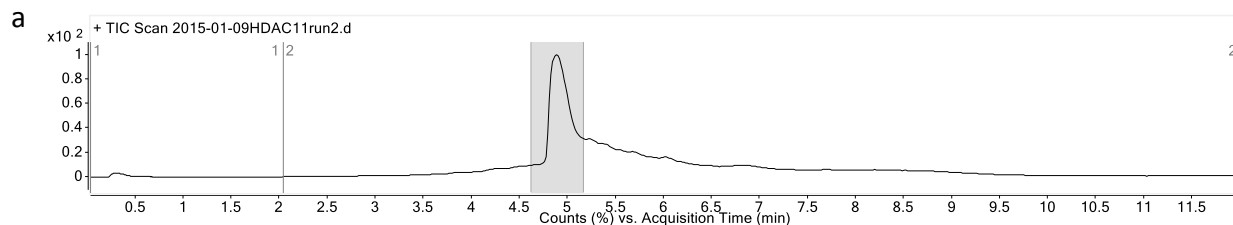
c

MLHTTQLYQHVPETRWPIVYSPRYNITFMGLEKLHPFDAGKWGKVINFLKEEKLLSDSMLVEAREASEE
DLLVVHTRRYLNELKWSFAVATITEIPPVIFLPNFLVQRKVLRPLRTQTGGTIMAGKLAVERGWAINVGG
GFHHCSSDRGGGFCAYADITLAIKFLFERVEGISRATIIDLDAHQGNGHERDFMDDKRVYIMDVYNRHIY
PGDRFAKQAIRRKVELEWGTEDDEYLDKVERNIKKSLQEHLPDVVVYNAGTDILEGDRLGGLSISPAGIVK
RDELVFRMVRGRRVPILMVTSGGYQKRTARIIADSILNLFGLGLIGPESPSVSAQNSDTPLLPPAVPGLENL
YFQGDYDIPTTLEHHHHHH

Native sequence: 42,076 Da
Observed sequence: 42,118 Da

Figure 3.8: Mass Spectra of HDAC11 from sf9

Intact HDAC11 from an sf9 expression was desalted on a zeba spin column. The protein solution (~15 μM) was injected into an HPLC-MS and run across a C8 reverse phase column before being shot into the Q-TOF. (A) Raw trace of ion count vs. acquisition time. (B) The deconvoluted mass of the highlighted region from the ion counts in A. (C) HDAC11 gene sequence used in insect cell expression. The mass of the wild-type protein, with an intact N-terminal methionine, is expected to be 42,076 Da. This is 42 daltons lower than we observed, consistent with a post-translational modification.

HDAC11 exhibits different activity depending on the host expression system

HDAC11 was expressed in HEK293 cells transfected with a plasmid encoding HDAC11 with an N-terminal ZZ tag. This allowed for purification of the protein using protein A beads. We were only able to recover a small portion of the enzyme by simply cleaving the tag, perhaps suggesting that HDAC11 itself was bound to either protein A or the sepharose beads. In an effort to disrupt the S-S bonds between ZZ-tagged HDAC11 and IgG sepharose beads, we added molar concentrations of DTT.

We assayed HDAC11 expressed and purified from *E. coli*, sf9, and HEK293 cells. Activity was determined using a peptide with a tri-fluorinated acetyllysine, followed by a methyl-coumarin moiety. Deacetylation is observed from a change in fluorescence caused by cleavage of the methyl-coumarin moiety from the deacetylated product, catalyzed by trypsin(*87*). This substrate, BPS Bioscience's HDAC Substrate 2a (Fig. 3.11), is a highly reactive peptide. We observed little change in the fluorescence signal over background when HDAC11 expressed and purified from *E. coli* was incubated with HDAC substrate 2a, with enzyme concentrations from 500 nM to 2 μM tested. HDAC11 expressed in and purified from eukaryotic sf9 cells, however, does catalyze deacetylation of the trifluoro-substrate 2a (Fig. 3.9). Additionally, HDAC11 expressed and purified from HEK293 cells also catalyzes deacetylation of substrate 2a. However, HDAC11 recovered from protein A beads after addition of high concentrations of DTT was no longer active (Fig. 3.10). The significance and potential cause of these differences is discussed below.
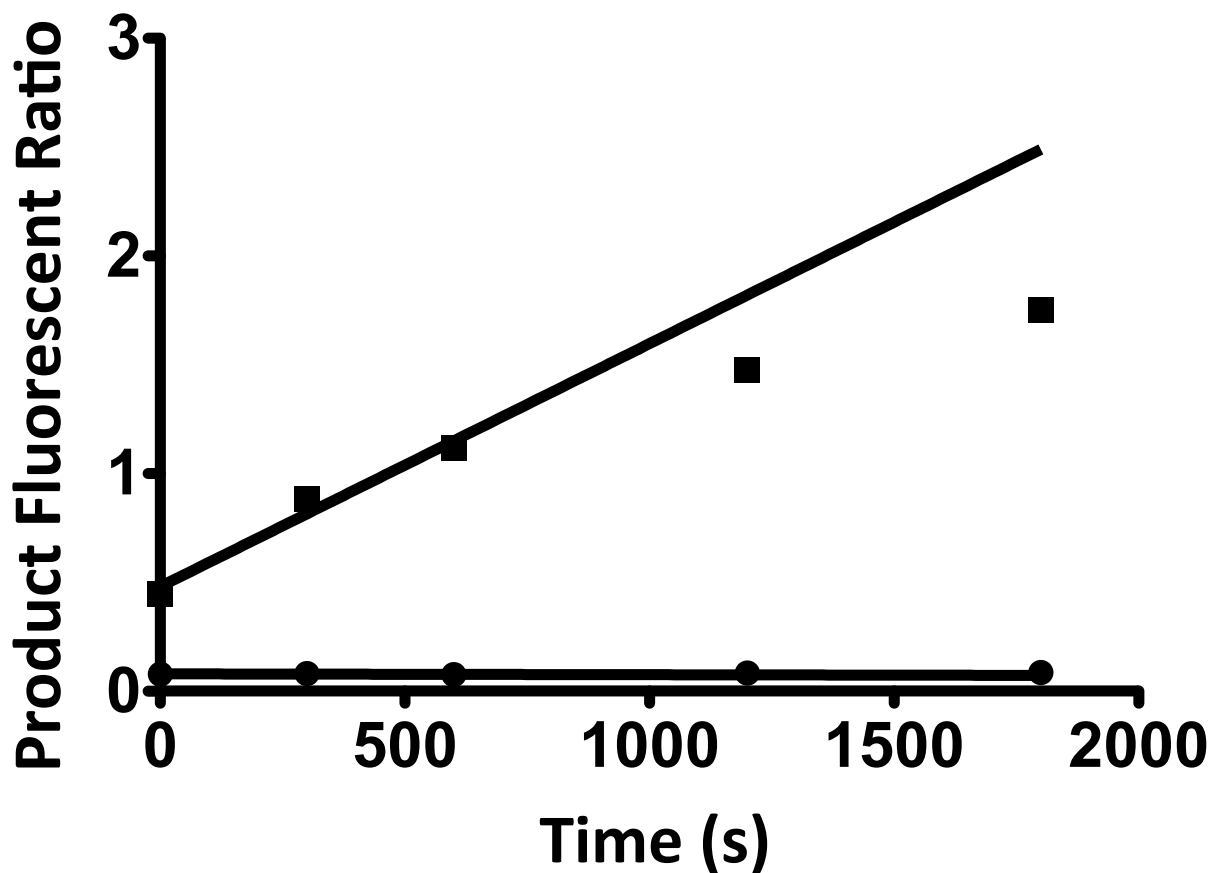
Figure 3.9: HDAC11 from bacterial and insect expression systems[10]

Progress curves for HDAC11-catalyzed deacetylation of HDAC substrate 2a (BPS Bioscience). HDAC11 (0.5 µM, purchased from BPS Biosciences) from an sf9 expression (■) showed significantly higher activity than HDAC11 (1 µM) from a bacterial expression (●). The rate/[HDAC11] from sf9-expressed HDAC11 is 0.0022 fluorescence units • s^{-1} • μM^{-1} enzyme and for the bacterial HDAC11 it is < 0.0001 fluorescence units • s^{-1} • μM^{-1} enzyme, a decrease of more than 20-fold.

---

[10] This graph depicts HDAC11 activity based on a recombinant enzyme purchased from BPS Biosciences, expressed in sf9 cells. All other HDAC11 activity in this chapter is from HDAC11 expressed in house.
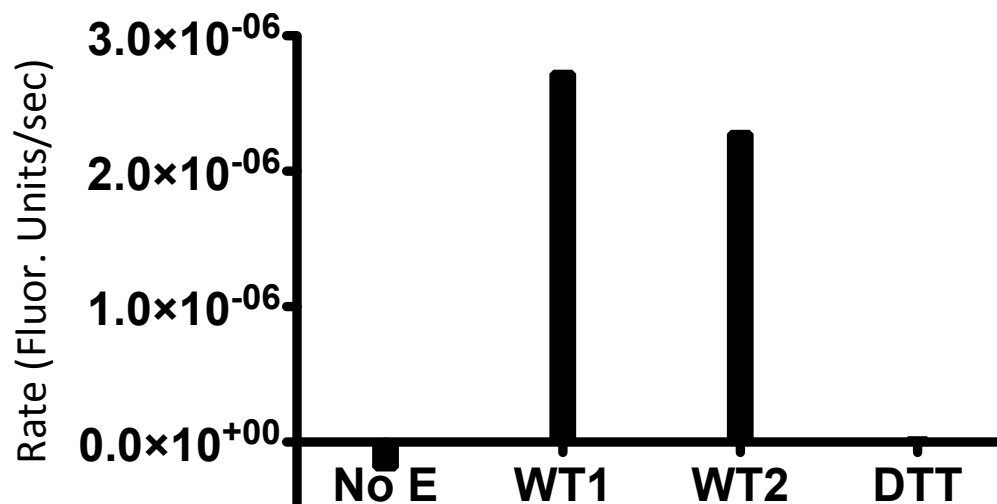
Figure 3.10: HDAC11 from HEK cells is active and sensitive to DTT

HDAC11 was overexpressed in HEK cells transfected with a plasmid encoding ZZ-tagged HDAC11. Protein was purified by affinity to sepharose beads labeled with protein A and cleaved with TEV protease. HDAC11 catalyzed deacetylation of HDAC substrate 2a was determined by fluorescence of the product (ex. = 340 nm and em. = 450 nm) of a trypsin digest of the deacetylated peptide. HDAC11 was overexpressed and purified twice and both preparations had similar activity (WT1 and WT2). However, a sample that was subjected to 1 – 2 M DTT, to free residual HDAC11 from protein A beads, showed no measurable activity.

HDAC11 catalyzes deacetylation of several FdL-style peptides

Using human HDAC11 expressed and purified from sf9 cells, we measured deacetylase activity using a variety of coumarin-labeled peptide substrates. These included Substrate 2a (BPS Bioscience), BOC-Lys substrate (Bachem), HDAC8 FdL substrate (Enzo), and Sirt1 FdL substrate (Enzo) (Fig. 3.11). The BOC-Lys substrate was used previously by Fournel *et al.*, (*75*) to screen their isozyme selective inhibitor MGCD0103. Interestingly, HDAC11 does not show catalytic activity toward Enzo's HDAC8 substrate (at the concentration and time range tested) but does catalyze deacetylation of the other three substrates. Between the two non-fluorinated substrates, both assayed at 100 μM, HDAC11 catalyzes deacetylation of the Sirt1 substrate more rapidly than the BOC-Lys substrate

(Table 3.2). We measured the dependence of activity on the concentration of the BOC-Lys

substrate to calculate k_{cat}/K_M = 250 ± 100 M^{-1}s^{-1} (Fig. 3.12).

BPS substrate 2a

BOC-Lys substrate

Enzo HDAC8 substrate

Enzo Sirt1 substrate
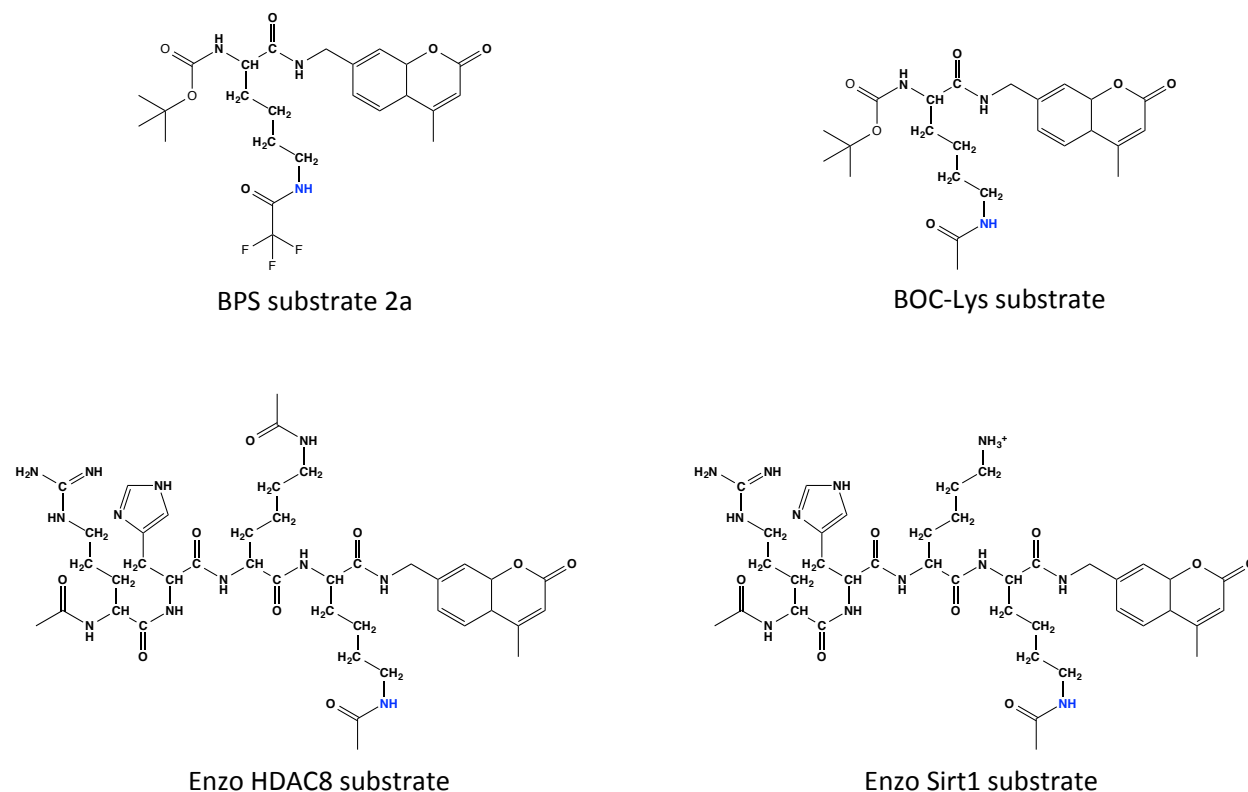
Figure 3.11: Tested HDAC11 FdL-style substrates

Structures for the commercially available coumarin labeled substrates used to test HDAC11 activity. HDAC11 showed measurable deacetylase activity toward substrate 2a, BOC-Lys, and the Sirt1 substrate. HDAC11 did not show activity toward Enzo's HDAC8 substrate, which differs from the Sirt1 substrate in just one place: an additional acetyl moiety on the lysine residue just upstream of the target acetyllysine. The N$^\varepsilon$ position of the lysine that is deacetylated is highlighted in blue in each structure. All structures were prepared using ChemDraw.

Table 3.2: HDAC11 specific activity on coumarin-labeled peptides

Substrate	Activity at 100 µM substrate (initial rate / µM HDAC11)
BOC-Lys	0.00011
Enzo HDAC8	< 0.00001
Enzo Sirt1	0.00069

a

b
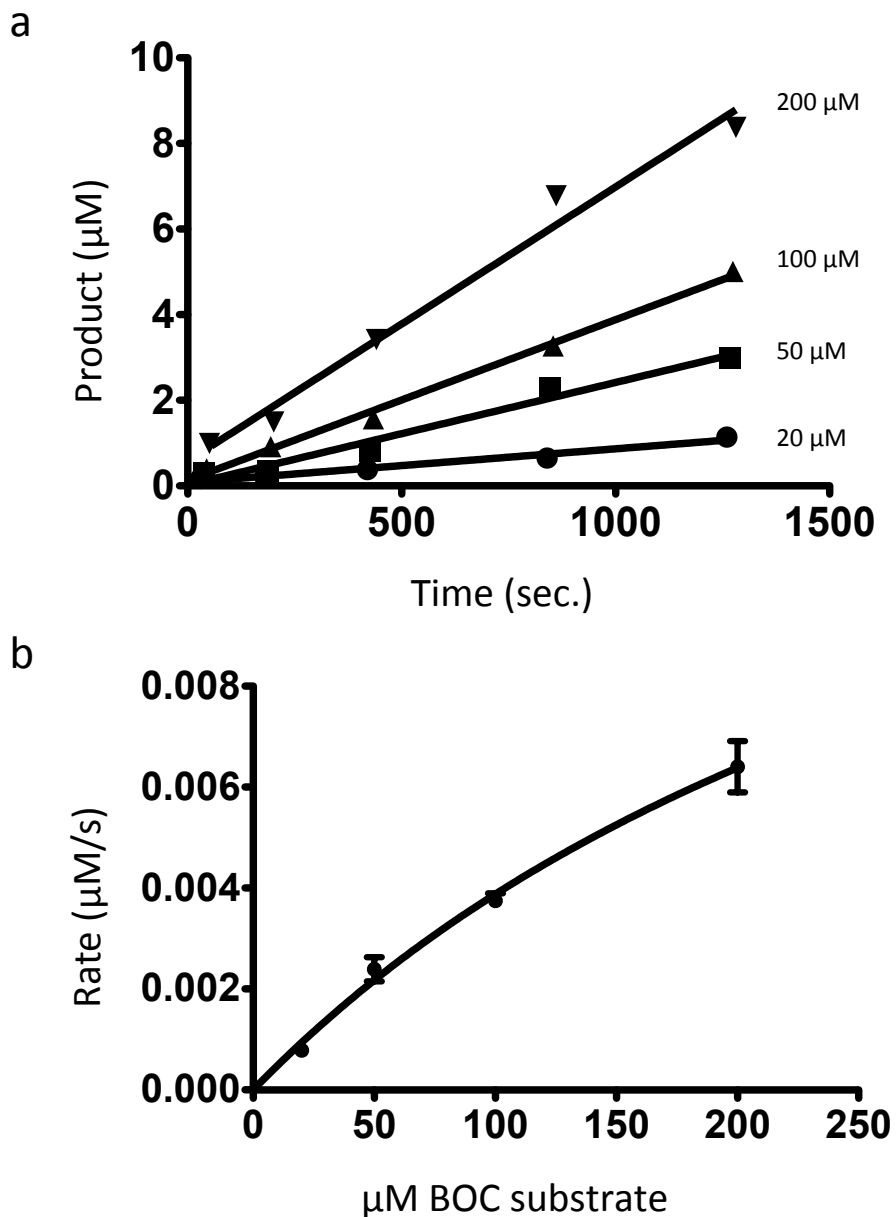
Figure 3.12: HDAC11 activity toward BOC-Lys substrate

(A) Progress curves for HDAC11 (0.2 μM) catalyzed deacetylation of varying concentrations of the BOC-Lys substrate (Bachem). Deacetylation was measured from a change in fluorescence (ex. = 340 nm and em. = 450 nm.) after quenching the reaction mixture with trypsin and TSA. Product concentrations were calculated from standard curves. (B) Plot of HDAC11-catalyzed initial rates vs. BOC-Lys concentration. The Michaelis–Menten equation is fit to the data to yield k_{cat}/K_M = 250 ± 100 $M^{-1}s^{-1}$, k_{cat} = 0.09 ± 0.02 s^{-1}, and K_M = 0.00037 ± 0.0001 M.

HDAC11 catalyzes deacetylation of unlabeled peptides

We next examined whether HDAC11 catalyzed deacetylation of peptides that do not contain a coumarin moiety. We initially measured HDAC11 activity using non-fluorinated peptides that had been chosen as likely HDAC8 substrates. While the majority of these peptides showed little to no activity with HDAC11 ($k_{cat}/K_{M, app}$ < 0.5 M^{-1}s^{-1}), a couple of peptides showed measurable deacetylation. The best HDAC8-based peptide was deacetylated by HDAC11 with a $k_{cat}/K_{M, app}$ = 7 M^{-1}s^{-1} (Fig. 3.13A). We also measured activity against one peptide from Cdt1, a protein associated with HDAC11 in literature (*71*), and a histone H4 K16 peptide. These two peptides were the best substrates for HDAC11 identified yet, with $k_{cat}/K_{M, app}$ values of 30 and 50 M^{-1}s^{-1}, respectively (Fig. 3.13B).

The Cdt1 and H4 K16 peptides have similarities in both sequence and charge (Table 3.3). Both peptides have an arginine residue immediately downstream of the acetyllysine. Additionally, both peptides have an abundance of positively charged residues. This is a potentially important pattern, and one that may be useful for predicting additional HDAC11 substrates.

Table 3.3: Sequences of unlabeled peptides with the highest k_{cat}/K_M values

The final protein, nMBP, is representative of the average non-membrane bound protein. The average nMBP is comprised of 24% charged residues. The % charged residues column has two values; the value in parentheses assumes histidine residues are charged.

Protein	Peptide Sequence	% charged residues	k_{cat}/K_M (M^{-1}s^{-1})
H4 K16	Ac-KGGA(Kac)RHR-NH$_2$	38 (50)	50
Cdt1 K49	Ac-GSR(Kac)RAR-NH$_2$	43 (43)	30
IDH1	Ac-KLKQMW(Kac)SPN-NH$_2$	20 (20)	7
nMBP	-	24 (26)	-
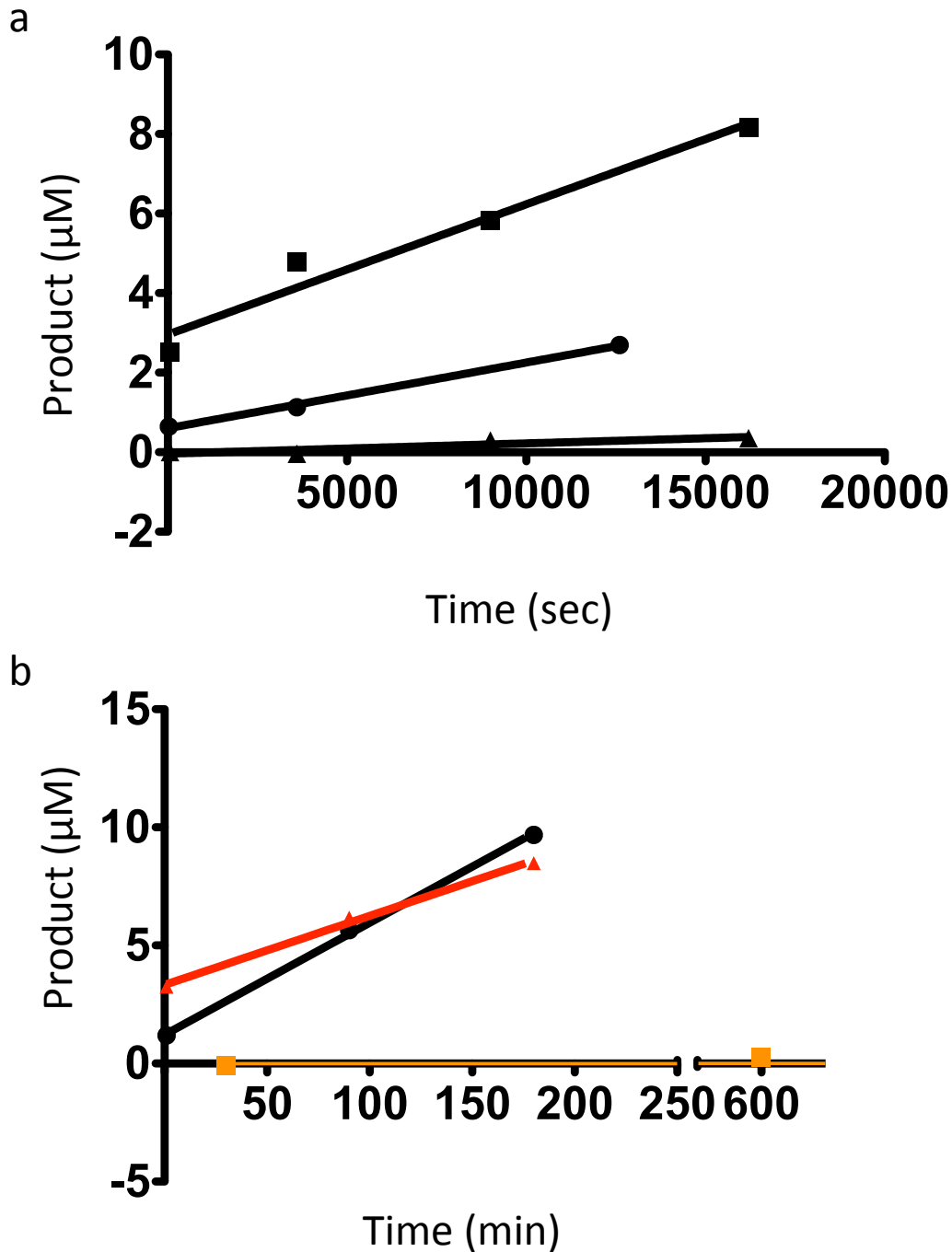
Figure 3.13: HDAC11 activity toward unlabeled peptides

Progress curves for HDAC11 deacetylase activity toward unlabeled peptide substrates. Deacetylation of these peptides was measured using an enzyme-coupled assay, described in chapter 2 and (*76*). (A) Deacetylation of an HDAC8-substrate peptide (from isocitrate dehydrogenase 1, see Table 3.3) by HDAC11. The reaction was run at two concentrations of HDAC11, 0.24 µM and 0.48 µM. Both experiments were consistent with a $k_{cat}/K_{M, app}$ = 7 $M^{-1}s^{-1}$, with the assumption that the [S] < K_M. (B) HDAC11 (0.15 µM) catalyzed deacetylation of peptides (100 µM) from Cdt1 (red) and Histone H4 K16 (black), along with a no-enzyme control (orange). These assays were performed without replicates.

HDAC11 is inhibited by SAHA and MGCD

We measured HDAC11 inhibition by both the pan-HDAC inhibitor SAHA and an isozyme-selective inhibitor MGCD0103 (Fig. 3.14). The isozyme selective inhibitor has a reported IC_{50} of 600 nM against HDAC11 (*75*). It is also reported to have sub-micromolar IC_{50} values against HDACs 1 and 2. We pre-incubated the coumarin-labeled BOC-Lys substrate with SAHA or MGCD0103 at various concentrations, and initiated reactions by addition of HDAC11. The SAHA-treated HDAC11 (0.55 µM) reaction showed complete inhibition at stoichiometric concentrations of inhibitor (Fig. 3.15AB). We repeated this SAHA titration with 150 nM HDAC11. This titration also showed complete inhibition by stoichiometric SAHA (Fig. 3.15C), suggesting that the IC_{50} value is below 150 nM. The MGCD0103-treated HDAC11, however, showed a maximum of ~50% loss of enzyme activity at all concentrations of inhibitor (Fig. 3.16). These data are consistent with MGCD0103 being an allosteric inhibitor that does not cause complete loss of activity. Alternatively, the lack of complete inhibition could be caused by the MGCD0103 solubility.

a
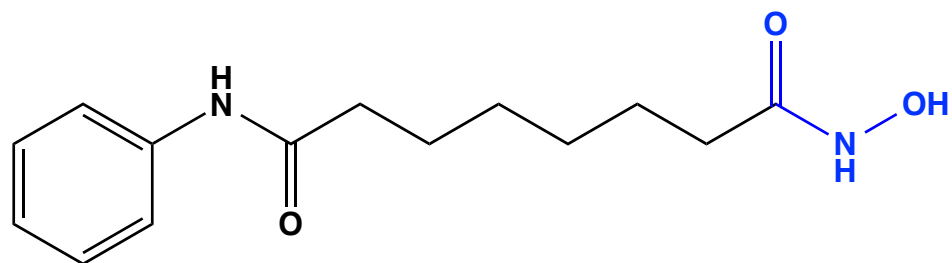
b
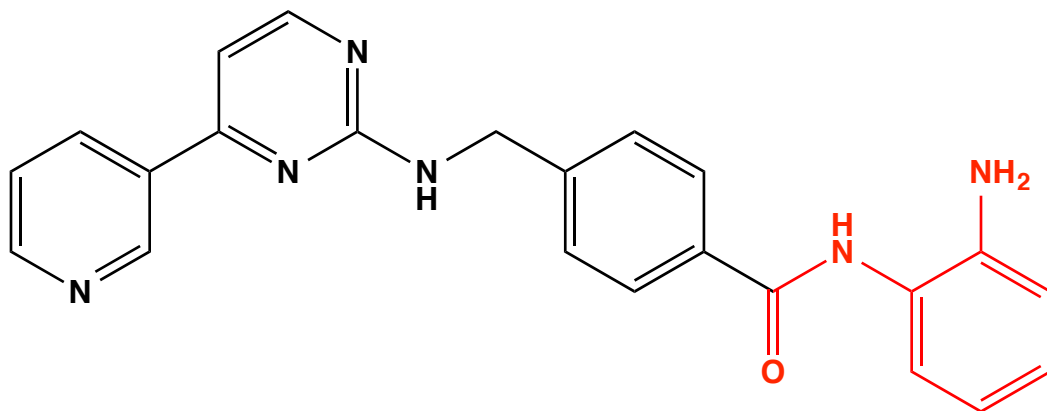
Figure 3.14: Structures of SAHA and MGCD0103.

Chemical structures of the pan-HDAC inhibitor SAHA (A) and the isozyme selective inhibitor MGCH0103 (B). Metal chelating groups are colored (hydroxamic acid, blue and benzamide red).
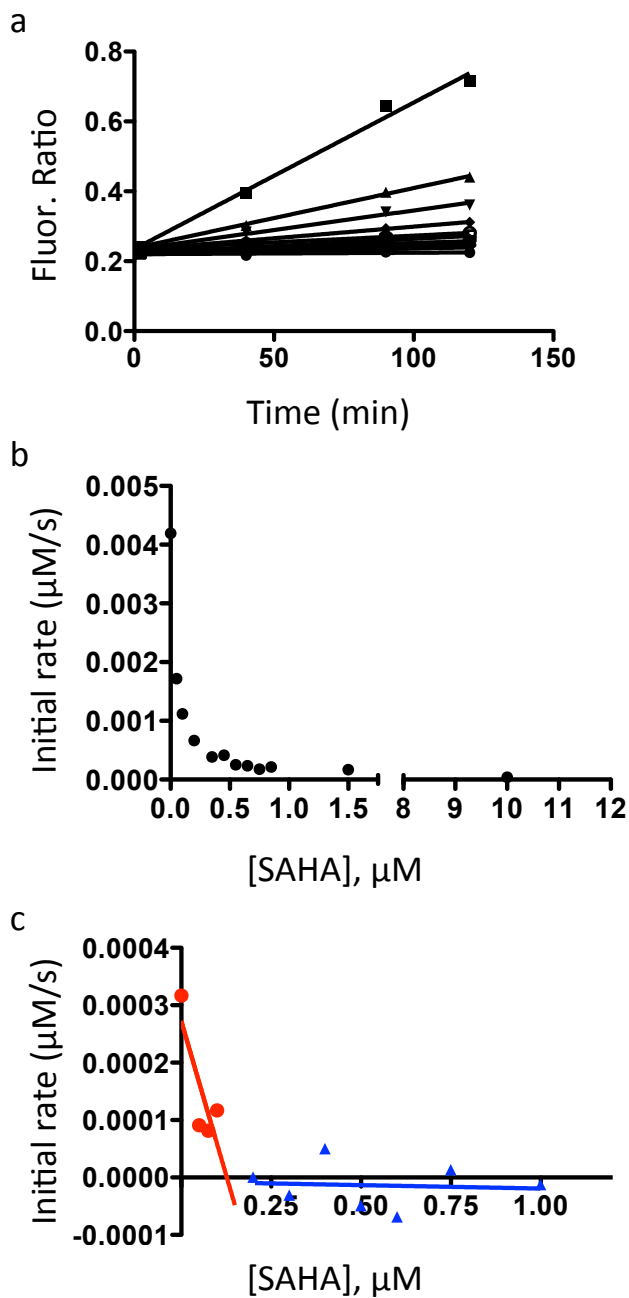
Figure 3.15: HDAC11 is inhibited by SAHA

(A) Progress curves for HDAC11 (0.55 μM) inhibition of deacetylation by increasing concentrations of SAHA. The BOC-Lys coumarin labeled substrate (50 μM) was assayed as described in Figure 3.12. (B) HDAC11 initial rates plotted against SAHA concentrations. This curve indicates a nearly complete loss of activity at equimolar concentrations of HDAC11 and SAHA, suggesting that the $IC_{50} < 0.5$ μM. (C) HDAC11 inhibition by SAHA was assayed at a lower enzyme concentration (0.15 μM). This curve shows stoichiometric inhibition, suggesting that the IC_{50} for HDAC11 inhibition by SAHA is below 150 nM.
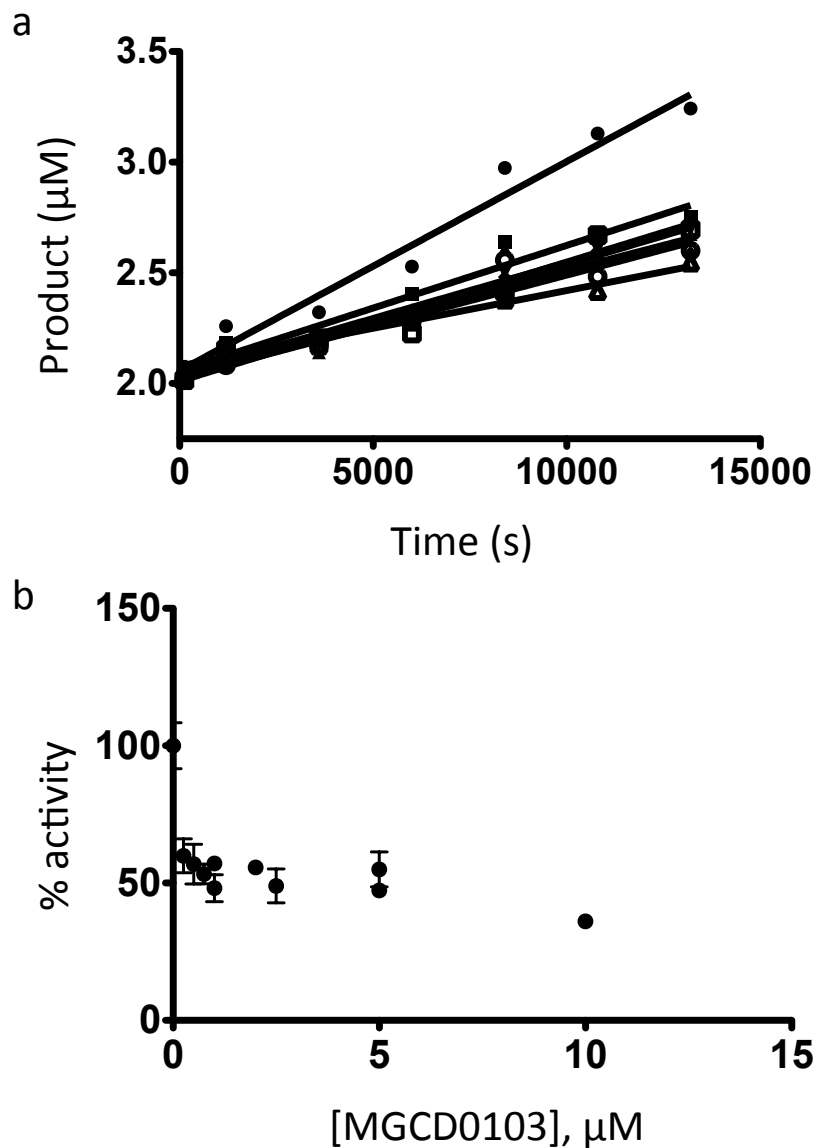
Figure 3.16: HDAC11 is partially inhibited by MGCD0103

(A) Progress curves for HDAC11 (0.55 μM) measured as in the figure legend of Fig. 3.12, with increasing concentrations of the isozyme-selective inhibitor MGCD0103. (B) Percent of HDAC11 activity as a function of the concentration of MGCD0103. This curve shows that 40% of activity is lost at 25 μM inhibitor, suggesting a high affinity interaction. MGCD0103 appears to bind HDAC11 tightly, but inhibition hovers at about 50%. These data raise the possibility that MGCD0103 is an allosteric, rather than competitive, HDAC11 inhibitor.

Discussion

HDAC11 is the most recently discovered isozyme in this family of enzymes, and it is the sole member of the class IV deacetylases. Cell-based assays have demonstrated the importance of HDAC11 to immune function and inflammation control (*68*, *85*), brain formation (*67*), and breast cancer (*69*). To date, however, *in vitro* biochemical characterization of HDAC11 has been difficult. Here we have, for the first time, directly compared the activity of recombinant HDAC11 expressed in *E. coli*, bacmid infection of insect cells, and HEK293 cell cultures. We have also begun a basic characterization of the enzymology of HDAC11, including an analysis of substrate selectivity and inhibition by pan and proposed HDAC11-selective inhibitors.

To date, there is no published data on the reactivity of HDAC11 expressed and purified from bacteria, a limiting factor in the biochemical characterization of this enzyme. Our initial attempts to express recombinant HDAC11 in bacteria unveiled two issues: soluble expression of HDAC11 was low and one of the most abundantly expressed bacterial proteins, Ef-Tu, displayed similar properties to HDAC11 (*92*). The two proteins are within a couple kDa in molecular weight, and due to parallels in pI, also run similarly on ion exchange columns. Additionally, native Ef-Tu binds to nickel resin, and is such a common contaminant that there is an effort to develop a strain of BL-21 cells with mutant forms of this protein (*93*). By altering our expression methodology and HDAC11 construct, we developed a scheme for the efficient expression of HDAC11 in *E. coli*.

Interestingly, we demonstrated that soluble expression of HDAC11 was not improved by optimizing codon usage for bacterial expression, or by expression of the enzyme in Rosetta II cells. We hypothesize that increasing the rate of translation of mRNA

to amino acids is unbeneficial, leading to increased aggregation of HDAC11, resulting in the low yield of soluble protein. The fusion of HDAC11 with SUMO both slightly increases soluble protein expression and shifts the molecular weight to a higher value than Ef-Tu (39 kDa vs. 52 kDa).

We successfully increased soluble expression of HDAC11 by co-expression of the molecular chaperon trigger factor (tig). Soluble expression was not increased by co-expression of several other chaperones, including GroEL-GroES. Tig was unique among the chaperones we examined (and among all known bacterial chaperones for that matter) in that it is a ribosome-associated chaperone (*94*). Most bacterial chaperones catalyze the folding of proteins in the cytosol to their final, native tertiary structure. Tig, in contrast, binds to and traps small regions of the nascent polypeptide at the ribosome, preventing aggregation of potentially 'sticky' stretches of amino acids as they are being translated (*95*).

We were surprised to find that prokaryotic expression of HDAC11 yields enzyme that, in our *in vitro* assays, does not display catalytic activity. However, HDAC11 expressed in and purified from two eukaryotic cells, HEK293 cells and sf9 insect cells, is catalytically activity. The reason for this discrepancy in activity is not yet understood; however, the 42-dalton increase in molecular mass for HDAC11 expressed in sf9 insect cells compared to *E. coli* expression suggests that a post–translational modification of HDAC11 occurs in eukaryotic but not prokaryotic expression, and this PTM may activate the enzyme. We hypothesize that this modification is acetylation of a lysine residue. This PTM is consistent with the observed shift in molecular mass. Additionally, proteolysis of HDAC11 expressed in sf9 and *E. coli*, prior to mass spectroscopy demonstrates acetylated peptides unique to the eukaryotic expression. This hypothesis is explored in greater detail in chapter 6.

Using HDAC11 expressed in sf9 cells, we sought to understand HDAC11 specificity by performing the first screen of this isozyme against a small library of peptide substrates. We began this process using non-fluorinated coumarin-labeled peptides. We tested three of these fluorescently labeled peptides and found that two of the three showed measurable deacetylation over the time course and enzyme concentrations used. The first that reacted with HDAC11 was a very simple substrate, an acetyllysine residue with an N-terminal BOC protecting group and a C-terminal methyl-coumarin. The second two peptides sequences were based on p53; the inactive Enzo HDAC8 substrate contains two acetyllysine residues adjacent to one another, while the active substrate (Enzo's Sirt1) is only acetylated at one of these lysines (Fig. 3.11). HDAC11 reacted with the Sirt1 substrate at least 10-fold faster than the HDAC8 substrate. These results suggest that HDAC11 may have a preference for substrates with charged residues near the acetyllysine.

We also demonstrated that HDAC11 catalyzes deacetylation of several unlabeled peptides. These were peptides originally designed as potential HDAC8 substrates, with the exception of one peptide from the DNA replication factor Cdt1. Cdt1 has previously been shown to co-immunoprecipitate with Flag-tagged and GST-tagged HDAC11 (*71*), suggesting that it might be an *in vivo* substrate. Additionally, a Histone H4 lysine 16 (H4 K16) peptide was tested. This peptide has been used to assay HDAC8 activity, but there is also evidence that HDAC11 interacts with histone H4 (*68*), making this a candidate for an *in vivo* substrate as well. While HDAC11 showed little catalytic activity with most of these peptides (less than 10 $M^{-1}s^{-1}$), the top two candidates proposed from the *in vivo* pulldowns, the Cdt1 and H4 K16 peptides, were deacetylated. In accordance with our hypothesis that HDAC11 favors substrates with charged amino acids, both of these peptides have an

abundance of polar residues, with all of them being basic (Arg, Lys, and His). We showed with the Sirt1 substrate than an upstream positive charge was beneficial for HDAC11 catalysis. With these peptides, we see a distribution of these charged residues, occurring both upstream and downstream of the acetyllysine. This trend is the first information we have on how HDAC11 recognizes substrates, and how that recognition differs from the well-characterized isozyme HDAC8.

While the majority of catalytic residues are conserved between HDAC8 and HDAC11, a key residue involved in substrate binding at the L2 loop of HDAC8 (Asp101), and all class I HDACs, is not conserved in HDAC11 (*58*); sequence alignments show that this residue is an asparagine in HDAC11. It is not yet understood what change the loss of this positive charge would have, though one possibility is that this mutation eliminates one point in the loop-substrate interaction, allowing the substrate to bind in a different orientation. It is possible that this residue, along with small changes in the residues responsible for forming the active site tunnel (*96*), are responsible for HDAC11 specificity. Of the six residues that form the HDAC8 tunnel, 5 are conserved in HDAC11 (based on sequence alignment). The variable residue is Met274, which is a Leu in HDAC11. This single amino acid change contributes to the wider active site tunnel (based on modeling) in HDAC11 (*96*). This modeling also predicts that His142, which is 0.49 Å from the active site divalent metal in HDAC8, is 0.7 Å away in HDAC11. When the tunnel Leu in HDAC11 is mutated to methionine, that distance shrinks to 0.44 Å, suggesting this single residue may play a large role in the geometry of the catalytic pocket of HDAC11 (*96*). Consistent with our current hypothesis that HDAC11 is selective toward substrates with localized charged residues, a subsequent peptide library of putative HDAC11 substrates (Chapter 4) showed

that several of the fastest peptide substrates had an above average abundance of polar residues.

We have demonstrated here, for the first time, that purified HDAC11 catalyzes the deacetylation of unlabeled (non-fluorinated) peptide substrates. HDAC11 also shows selectivity between these substrates. This work demonstrates that the *in vitro* catalytic activity for deacetylation of peptides by HDAC11 is comparable to that of HDAC8 where the deacetylation of a peptide from SMC3, a generally *in vivo* HDAC8 substrate (*10*), has a rate constant of about 60 $M^{-1}s^{-1}$ (*61*). The *in vitro* deacetylase activity of HDAC11 with a peptide from the DNA replication factor Cdt1 supports the pull down data suggesting that this is an *in vivo* substrate of HDAC11.

Chapter 4

Development of an on-chip proteomics method for identifying full-length HDAC substrates

Introduction

Lysine acetyltransferases (KATs) and histone deacetylases (HDACs) are two families of enzymes that catalyze the addition and hydrolysis, respectively, of acetyl moieties attached to the N^ε-position of lysine residues, respectively (*97*). The 18 histone deacetylases are organized into four classes, based on both similarity to yeast homologs and phylogeny (*73*). Class I, II, and IV HDACs are metal-dependent enzymes, all with a conserved deacetylase catalytic domain. Contrary to their name, HDACs are involved in the deacetylation and regulation of thousands of proteins, both nuclear and cytoplasmic (*4, 73, 98*).

In 2009, a landmark global mass spectrometry approach was used to assess the broad impact of lysine acetylation on virtually every cellular process. This study identified roughly 3,600 acetylation sites on nearly 2,000 proteins (*86*). Today, the most recent statistics in the phosphosite database (June, 2016) show over 20,000 lysine acetylation sites in humans, coming from over 7,000 proteins (*6*). As the acetylome continues to expand, the importance of the function and specificity of individual HDAC isozymes similarly grows. With 11 metal-dependent HDACs, deacetylation must be a combination of specificity and promiscuity.

To date, very little direct evidence has been produced linking specific HDAC isozymes to substrate proteins. Perhaps the strongest case for an HDAC-substrate pair is HDAC1 and the tumor suppressor p53, as evidenced by immunoprecipitation, *in vitro* peptide analysis, and co-expression (*99*). Additional studies have used similar techniques, identifying proteins that pull-down with specific HDAC isozymes. This approach has yielded dozens of proteins, and has been applied to each of the 11 HDACs (*40*). Additionally, Ed Holson's group at the Broad Institute has recently used a SILAC mass spectrometry-based approach to look for changes in protein acetylation after HDAC8-specific inhibition in cell culture (*61*). These are both powerful approaches that have provided the field with new avenues of research. They do, however, have limitations in their ability to identify isozyme-specific substrates. The pull-down experiments require that proteins have a long lasting, stable interaction with HDACs. This is likely to increase the identification of protein partners relative to substrates in these results. Additionally, while *in vivo* changes in protein acetylation upon HDAC-specific inhibition are strong and important pieces of evidence, they do not differentiate between a direct substrate and a downstream effect. Furthermore, this strategy is reliant upon a protein's relative abundance, and ionizability in a mass spectrometer.

Here, we present a novel and orthogonal method toward identifying HDAC substrates. We have chosen to use both HDAC8 (Class I) and HDAC11 (Class IV) to demonstrate the broader abilities of this approach to the HDAC field as a whole. Using a chip-based proteomics approach, we report the identification of over 40 putative HDAC8 substrates and over 25 putative HDAC11 substrates. In collaboration with Phil Cole at Johns Hopkins University, we used a recombinantly expressed, truncated construct of the

lysine acetyltransferase p300 to acetylate proteins immobilized on a glass slide. We then exposed these slides to individual HDAC isozymes and monitored changes in acetylation by immunochemistry. The immobilized proteins, roughly 20,000, represent the majority of the human proteome. The HDAC protein substrates identified using this method are largely novel targets, but several proteins that overlap with the results of previous experimental approaches were also identified. As validation, we demonstrated that HDAC catalyzes deacetylation of peptides corresponding to these proteins. We also use unnatural amino acid incorporation to show that HDAC8 catalyzes deacetylation, *in vitro,* of singly acetylated, full-length isocitrate dehydrogenase 1 (IDH1), marking the first time this approach has been used successfully on a non-histone protein. Taken together, these data demonstrate that IDH1 is an HDAC8 substrate and provide validation of the usefulness of this method in identifying HDAC-substrate pairs.

Reagents

Reagents used to prepare buffers were from Fisher or Sigma, unless otherwise specified. The p300 plasmid was a generous gift from Phil Cole. The 14mer peptide for expressed protein ligation was synthesized in the Cole laboratory. HuProt chips were generated by Heng Zhu's laboratory and CDI laboratories (*100*). The pEVOL plasmid encoding a tRNA/tRNA synthetase pair for the incorporation of acetyllysine was a generous gift from Wenshe Lui.

HDAC expression and purification

HDAC8 and HDAC11 were expressed and purified as described previously in chapters 2 and 3, respectively. The HDAC11 expression was in sf9 insect cells.

p300 expression and purification

A plasmid encoding the catalytic domain of p300 was provided by Phil Cole (*101*). This pTYB2 plasmid encodes truncated p300 including residues 1287 – 1652, with two mutations (M1652G and K1637R) and deletion of the loop comprised of residues 1523-1554. The gene encoded is 5' - p300 - Sce VMA Intein - Factor X_a - chitin binding domain (CBD) under control of a T7 promoter. The plasmid was transformed into z-competent BL-21 DE3 cells (competency achieved using Zymo Mix and Go kit) and grown on an LB-ampicillin plate overnight at 37℃. The following morning, two single colonies were

---

[11] Purification of p300 for EPL, EPL, p300 activity, and HDAC catalyzed deacetylation on proteome chips were carried out in Phil Cole's laboratory.

[12] Purification of p300 (and EPL) and on-chip enzyme assays were performed by Eric Sullivan and Beth Zucconi. Verification of p300 activity using a radiolabeled substrate was performed by Beth Zucconi.

selected and inoculated into 2, 10 mL tubes of 2xYT (MP Biomedical) containing 100 µg/mL ampicillin. Starter cultures were grown at 37°C with shaking (225 rpm) for approximately 4 hours, until cultures were visibly cloudy. Each culture was then diluted into 1 L of freshly autoclaved 2xYT media containing ampicillin and grown at 34°C with shaking (180 rpm). At O.D.$_{600}$ = 0.4 the cultures were induced by addition of 1 mL of 500 mM Isopropyl β-D-1-thiogalactopyranoside (IPTG) per liter of culture (final concentration = 0. 5 mM). Cultures were grown at 34°C with shaking (180 rpm) for 5 hours. Following growth, the cultures were pelleted by centrifugation for 20 minutes at 6,000 x g (Beckman JLA 8.1000). Cell pellets were kept on ice, and resuspended into p300 lysis buffer (25 mM HEPES pH 8.0, 500 mM NaCl, 10% glycerol). Resuspended cells were frozen and stored at -80°C.

Purification of p300 test expression (no ligation)

Resuspended cells from 1 L of p300 expression were thawed on ice. The cell suspension was lysed by two passes through a microfluidizer (DivTech Equipment). Cell lysate was loaded onto a 5 mL chitin column and washed with 20 column volumes (CV) of chitin binding buffer (25 mM HEPES pH 8.0, 500 mM NaCl). Cleavage of p300 from the chitin-binding domain was catalyzed by addition of 3 CV of chitin cleavage buffer (25 mM HEPES pH 8.0, 500 mM NaCl, 50 mM dithiothreitol (DTT)). The column flow was then stopped and the cleavage was allowed to progress for 16 hours at 4°C. The free protein was then eluted with 5 CV of chitin binding buffer. Cleavage efficiency was determined using a coomassie-stained polyacrylamide gel following sodium dodecyl sulfate polyacrylamide gel electrophoresis (SDS-PAGE) (Fig. 4.1).
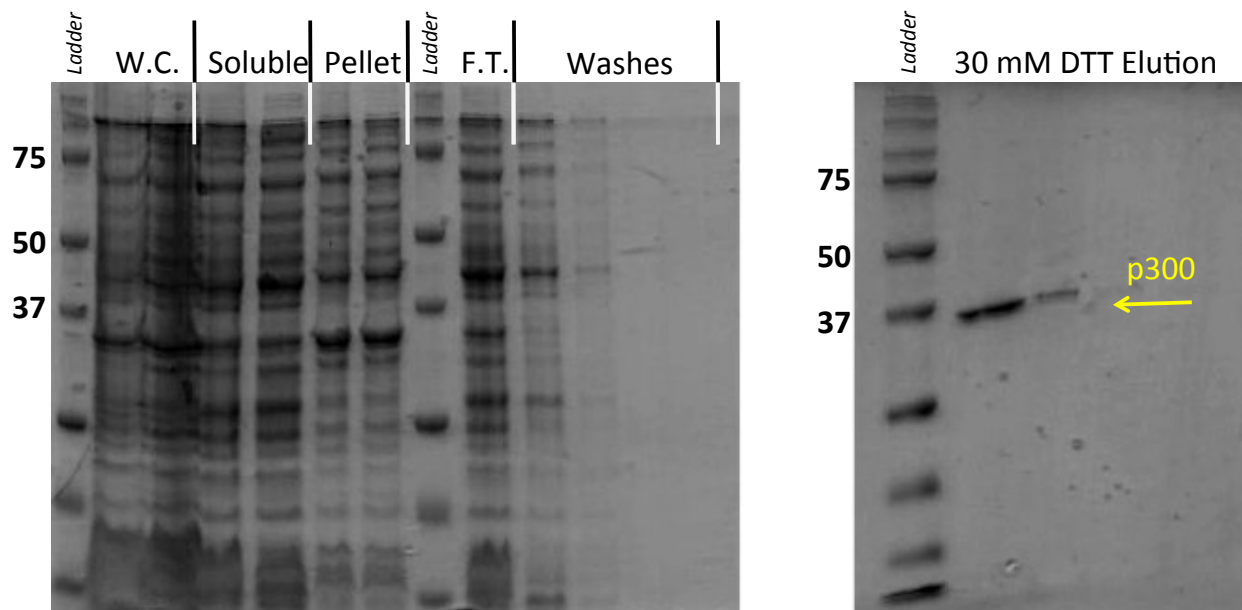
Figure 4.1: Purification of unligated p300

A 1 L expression of p300 was lysed and purified on a 5 mL chitin column. The p300-CBD construct is 76 kDa before cleavage. Based on the degree of total protein in the pellet lanes, lysis may have been incomplete. The wash steps appear to have efficiently removed unbound protein from the column. The thiol-cleavage product, on right, is a pure protein corresponding to the correct molecular weight for our p300 construct (38 kDa).

p300 Expressed Protein Ligation and purification

The p300 cell pellets from 2 L of culture were thawed on ice and resuspended in 60 mL of p300 EPL lysis buffer (25 mM HEPES pH 7.9, 500 mM NaCl, 10% glycerol, 1 mM phenylmethylsulfonyl fluoride (PMSF), 1 mM $MgSO_4$). Cells were lysed by 1 pass through a French Press. The lysate was cleared by centrifugation at 27,000 x g for 30 minutes in a J20 rotor. Cleared lysate was loaded onto a 15 mL chitin resin bed, in a 4°C cold room. The loaded resin was washed with 5 CV of chitin EPL binding buffer (25 mM HEPES pH 7.9, 250 mM NaCl, 1 mM EDTA), 3 CV of chitin EPL buffer B (25 mM HEPES pH 7.9, 500 mM NaCl, 1 mM EDTA), 2 CV chitin binding buffer, and 2 CV of ligation buffer (25 mM HEPES pH 7.4, 250 mM NaCl, 1 mM EDTA, 200 mM 2-mercaptoethanesulfonic acid (mesna)).

The C-terminal 14mer peptide (29 mg) (sequence: CMLVELHTQSQDRF) was dissolved in 4 mL ligation buffer. This solution was applied to the top of the column, followed by a 1 mL ligation buffer stacker. Cleavage and ligation were allowed to occur for 3 hours at 4°C, followed by 16 hours at room temperature.

After the 16-hour reaction, the column was returned to 4°C. The ligation product was eluted with 4 CV chitin buffer. The eluent (35 mL) was added to a dialysis cassette (20,000 Da MWCO) and dialyzed at 4°C for 2 hours against p300 dialysis buffer 1 (20 mM HEPES pH 7.9, 500 mM NaCl, 10 mM DTT), 2 hours against p300 dialysis buffer 2 (20 mM HEPES pH 7.9, 100 mM NaCl, 5 mM DTT), and 2 hours against p300 dialysis buffer 3 (20 mM HEPES pH 7.9, 50 mM NaCl, 1 mM DTT). The protein was then loaded onto an SP-strong cation exchange column and eluted via fast protein liquid chromatography (FPLC) using an AKTA pure (GE Healthcare). The column was equilibrated with 10 CV S-Buffer A (20 mM Tris pH 8.0, 50 mM NaCl, 2 mM DTT) and the protein sample was applied using a

superloop. The elution gradient was as follows: 0-30% S-Buffer B (20 mM Tris pH 8.0, 1 M NaCl) over 25 CV, followed by 30-60% gradient over 10 CV, and then 60-100% gradient over 10 CV. Protein elution and purity was confirmed by polyacrylamide gel electrophoresis. Fractions containing pure p300 were pooled and concentrated from 4.5 mL to <1 mL via Amicon centrifugation tubes. Sample was then dialyzed for 2 hours against 20 mM HEPES pH 7.9, 50 mM NaCl, 1 mM DTT, 10% glycerol. Following dialysis, protein concentration was determined by the micro BCA assay (Pierce) using bovine serum albumin (BSA) as the standard, as well as by comparison to BSA on a denaturing polyacrylamide gel .

Proteome Chip Assays

The proteome chip experiments varied in amount of p300, HDAC8, and HDAC11 used on each chip. However, the general protocol was consistent for each chip and details for each assay are described below. In all cases, chips were removed from -80℃ storage and immediately placed in 5 mL blocking solution (5% BSA in phosphate-buffered saline with 0.5% tween 20 (PBST)).

p300 Reaction

Chips were blocked for 1 hour with rocking at room temperature. Blocking buffer was then removed and the chips were washed twice for 5 minutes each with 5 mL p300 reaction buffer (50 mM HEPES pH 7.9, 50 mM NaCl, 1 mM TCEP). During washes, the p300 reaction solution was prepared on ice as follows, 1x p300 reaction buffer, 8 μM p300, and 200 μM acetyl-CoA added immediately prior to using the reaction. 120 μL of reaction was

pipetted onto the appropriate chips and coverslips were carefully applied using tweezers to avoid creating air pockets beneath them. The tray containing the chips was wrapped in a paper towel moistened with water and clear plastic wrap to prevent the reactions from drying. The reactions were incubated at 30°C for 2 hours. As this reaction progressed, HDAC was reconstituted 1:1 with zinc. HDAC8 was used at 2 and 7.5 µM final concentrations and HDAC11 at 1 and 1.5 µM final concentrations. The p300 reactions were quenched by two 10-minute washes with 5 mL sodium bicarbonate wash buffer (50 mM $NaHCO_3$-Na_2CO_3 pH 9.3).

HDAC reaction

After blocking, the chips were washed once with 5 mL of 20 µM EDTA in 0.5x HDAC reaction buffer (12.5 mM HEPES pH 8.0, 68.5 mM NaCl, 1.5 mM KCl) for 5 minutes, followed by two washes with 5 mL 0.5x HDAC reaction buffer for 10 minutes each, and a final wash of 5 mL 0.75x HDAC reaction buffer for 10 minutes. HDAC reaction solutions were added: in round 1 experiments 120 µL of HDAC reaction solution was added to each chip, in round 2 experiments 3 mL of HDAC reaction solution was added to each chip, enough to submerge the chips completely. The chip trays were again wrapped in moist paper towels and plastic wrap and returned to 30°C for 2.5 hours. Following the reaction, the HDAC solution was removed and the chips were washed twice with p300 reaction buffer for 10 minutes each.

Antibody treatment of chips

Chips were washed three times with 1% SDS in tris-buffered saline with 0.5% tween 20 (TBST) for 10 minutes each. They were then washed four times with tris-buffered saline (TBS) for 15 minutes each. Primary antibody (anti-acetyllysine from rabbit, ThermoFisher) was diluted 1:5,000 in TBST with 5% BSA and 3.5 mL were added to each chip and incubated at 4°C overnight. The primary antibody was then removed and the chips were washed four times with TBST for 10 minutes each. Secondary antibody (anti-rabbit Alexa Fluor 647, ThermoFisher) was diluted 1:10,000 in TBST with 5% BSA and 3.5 mL were added to each chip and incubated for 1.5 hours at room temperature. This solution was poured off and chips were washed three times with ultrapure water (Milli-Q, Millipore) for 10 minutes each. The chips were then dried by centrifugation for 2 minutes at 1,000 rpm and stored for 1 hour away from light at room temperature to complete drying.

Chip Readout

Dry chips were protected from light until ready to be scanned. Chips were read one at a time in a GenePix 4000B Microarray Scanner (Molecular Devices). This dual laser scanner visualizes the acetyllysine secondary fluorophore at 635 nm and the GST secondary fluorophore at 532 nm. The Pixel diameter was fixed at 5 μM and the fluorescence scans were always performed using the same instrument parameters (power and gain).

Cloning of IDH1

Human IDH1 cDNA (Dharmacon) was cloned into a pET-M11 bacterial expression vector. Primers were designed to amplify the IDH1 cDNA and generate an N-terminal NcoI and C-terminal NotI cleavage sites (Fig. 4.2A).

Polymerase chain reaction (PCR) amplification was performed in a thermocycler using Q5 HotStart DNA polymerase (New England Biolabs). The PCR products were separated on a 1% agarose gel. DNA was stained using Sybr Safe DNA stain (Thermo Fisher) and the band corresponding to the correct size for the desired insert was excised from the gel and cleaned using a DNA Gel Purification Kit. Insert and vector were both digested with NcoI and NotI (New England Biolabs) for 4 hours at 37°C to generate the appropriate sticky ends. The restriction digest reactions were quenched and the products separated using a second agarose gel, followed by an additional DNA Gel Purification step. The fragments, at a 3:1 insert to vector ratio, were treated with Quick T4 DNA Ligase and Quick Ligation Buffer and Mix (New England Biolabs) on ice to prepare the new circular plasmid. The final construct was His6 – TEV – IDH1 in a pET M11 vector encoding kanamycin resistance (Fig. 4.2B). This plasmid was transformed into XL1-Blue super competent cells and plated on LB-Kan plates. The cells were grown overnight at 37°C. Single colonies were then picked and 10 mL cultures were grown and treated with a Promega Wizard Plus SV Miniprep DNA Purification kit. DNA was sequenced to confirm the correct gene sequence.

A)
```
Forward primer:
5'- GCG TCC ATG GGT TCC AAA AAA ATC AGT GGC GGT TCT GTG GTA GAG

Reverse primer:
5'- CGC GCG GCC GCT TAA AGT TTG GCC TGA GCT AGT TTG ATC TT
```

B)
ATGAAACATCACCATCACCATCACCCCATGAGCGATTACGACATCCCCACTACTGAGAATCTTT
ATTTTCAGGGCGCCATGGGTTCCAAAAAAATCAGTGGCGGTTCTGTGGTAGAGATGCAAGGAGA
TGAAATGACACGAATCATTTGGGAATTGATTAAAGAGAAACTCATTTTTCCCTACGTGGAATTG
GATCTACATAGCTATGATTTAGGCATAGAGAATCGTGATGCCACCAACGACCAAGTCACCAAGG
ATGCTGCAGAAGCTATAAAGAAGCATAATGTTGGCGTCAAATGTGCCACTATCACTCCTGATGA
G<mark>AAG</mark>AGGGTTGAGGAGTTCAAGTTGAAACAAATGTGG<mark>AAA</mark>TCACCAAATGGCACCATACGAAAT
ATTCTGGGTGGCACGGTCTTCAGAGAAGCCATTATCTGCAAAAATATCCCCCGGCTTGTGAGTG
GATGGGTAAAACCTATCATCATAGGTCGTCATGCTTATGGGGATCAATACAGAGCAACTGATTT
TGTTGTTCCTGGGCCTGGAAAAGTAGAGATAACCTACACACCAAGTGACGGAACCCAAAAGGTG
ACATACCTGGTACATAACTTTGAAGAAGGTGGTGGTGTTGCAATGGGGATGTATAATCAAGATA
AGTCAATTGAAGATTTTGCACACAGTTCCTTCCAAATGGCTCTGTCTAAGGGTTGGCCTTTGTA
TCTGAGCACCAAAAACACTATTCTGAAGAAATATGATGGGCGTTTT<mark>AAA</mark>GACATCTTTCAGGAG
ATATATGACAAGCAGTACAAGTCCCAGTTTGAAGCTCAAAAGATCTGGTATGAGCATAGGCTCA
TCGACGACATGGTGGCCCAAGCTATGAAATCAGAGGGAGGCTTCATCTGGGCCTGTAAAAACTA
TGATGGTGACGTGCAGTCGGACTCTGTGGCCCAAGGGTATGGCTCTCTCGGCATGATGACCAGC
GTGCTGGTTTGTCCAGATGGCAAGACAGTAGAAGCAGAGGCTGCCCACGGGACTGTAACCCGTC
ACTACCGCATGTACCAG<mark>AAA</mark>GGACAGGAGACGTCCACCAATCCCATTGCTTCCATTTTTGCCTG
GACCAGAGGGTTAGCCCACAGAGCAAAGCTTGATAACAATAAAGAGCTTGCCTTCTTTGCAAAT
GCTTTGGAAGAAGTCTCTATTGAGACAATTGAGGCTGGCTTCATGACCAAGGACTTGGCTGCTT
GCATTAAAGGTTTACCCAATGTGCAACGTTCTGACTACTTGAATACATTTGAGTTCATGGATAA
ACTTGGAGAAAACTTGAAGATCAAACTAGCTCAGGCCAAACTTTAA

Figure 4.2: Sequences for cloning IDH1 cDNA

(A) Human wild-type IDH1 cDNA (Dharmacon) was amplified using the listed forward and reverse primers. These primers were used in a PCR reaction to prepare an IDH1 gene with an N-terminal NcoI site and a C-terminal NotI site. (B) DNA sequence coding for His6-TEV-IDH1 in a pET M11 vector. The labeled regions are polyhistidine (blue), TEV recognition site (red), start of IDH1 sequence (orange), and lysine residues that will be mutated for incorporation of acetyllysine (highlighted yellow).

Expression of WT-IDH1

The plasmid encoding his-tagged IDH1 was transformed into Rosetta 2 (DE3) competent cells (Novagen), per the manufacturer's protocol. Briefly, cells (50 μL) were thawed on ice before ~100 ng of plasmid DNA was added. Cells were incubated on ice for 5

minutes before 30 seconds of heat shock in a 42°C water bath and finally 2 minutes on ice. Following this, 250 µL of room temperature Super Optimal broth with Catabolite repression (S.O.C.) medium was added to the cells and incubated for 1 hour at 37°C with shaking. This solution was then plated on LB-Kanamycin/Chloramphenicol (50 µg/mL and 34 µg/mL, respectively) plates and grown overnight at 37°C. The following day colonies were picked and used to inoculate 10 mL of 2xYT media with kanamycin and chloramphenicol present (at the above concentrations). These starter cultures were grown for ~4 hours before being diluted to 1 L (1:100 dilution) in 2xYT with fresh antibiotics present. Cultures were grown with shaking (175 rpm) at 34°C until an O.D.$_{600}$ of 0.5. Then the cultures were cooled to 18°C and induced by addition of IPTG to a final concentration of 0.5 mM. The cultures were grown for another 16 hours. Following growth, the cells were pelleted by centrifugation at 6,000 x g for 20 minutes in a Beckman JA 8.1000 fixed angle rotor. Cells were then frozen and stored at -80°C.

Purification of WT-IDH1

The IDH1 cell pellet was thawed on ice and resuspended in 30 mL IDH1 Lysis buffer (50 mM HEPES pH 8.0, 150 mM NaCl, 10% glycerol) with 1 Roche Complete protease inhibitor tablet per liter of cell growth. The cell solution was lysed via two passes through a chilled micro-fluidizer. Cell lysate was then treated with 1 µL of DNase I and incubated on ice for 30 minutes. Lysate was then cleared via centrifugation at 27,000 x g for 1 hour (Sorvall SS-34 rotor). The cleared supernatant was decanted and passed through a 5 mL nickel affinity column (HisPur Ni-NTA resin, Thermo) using gravity-flow. The column was then washed with 5 CV of IDH1 buffer A (50 mM HEPES pH 8.0, 150 mM NaCl), followed by

104

elution through a step-wise gradient of increasing imidazole buffers, from 0 mM imidazole to 250 mM imidazole (steps at 0 mM, 50 mM, and 250 mM). Fractions containing IDH1 (determined by coomassie staining of an SDS-PAGE gel) were pooled and treated with of TEV protease (1.5 mg total). The protein was transferred to a Slide-A-Lyzer dialysis cassette and dialyzed overnight at 4°C against 4 L of IDH1 buffer A. The following day, the protein was removed from dialysis and again passed over a 5 mL nickel affinity column, run in the same fashion as the first Ni-column (Fig. 4.3). Fractions containing TEV-cleaved IDH1 were pooled and concentrated using Amicon Ultra centrifugal filters. Final protein concentration was determined to be 145 µM by absorbance at A_{280} using a nano-drop spectrophotometer. IDH1 was aliquoted and flash frozen in liquid nitrogen, then stored at -80°C.
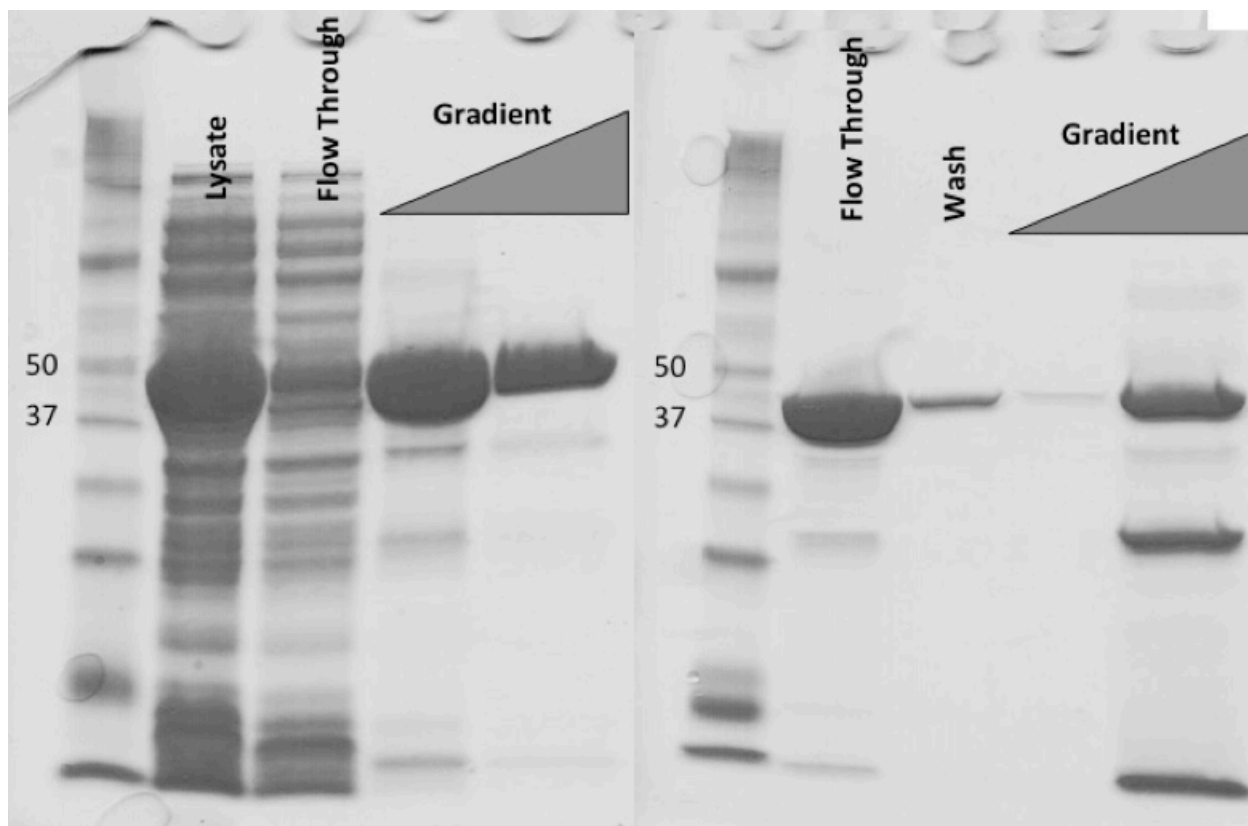
Figure 4.3: Purification of wild-type IDH1

A 1-L IDH1 expression was purified over two nickel columns. The first nickel column is shown on the left. IDH1 (46 kDa) overexpression is seen in the lysate and in the imidazole gradient with protein eluting at both steps (50 mM and 250 mM imidazole). After a TEV protease cleavage step, a second nickel column (right) was run. Here, untagged IDH1 elutes in the column flow through. The presence of an IDH1 band in the imidazole gradient suggests that TEV-cleavage was incomplete.

Generation of amber stop IDH1 mutants

Primers were designed for site-directed mutagenesis of IDH1. Four lysine residues were mutated, individually, to amber stop codons, to generate four new IDH1 constructs. PCR was run following a basic QuikChange II (Agilent) site-directed mutagenesis protocol, using Q5 HotStart DNA polymerase. PCR mutagenesis products, still in pET M11 plasmids, were incubated for 1 hour with DpnI, followed by transformation into XL1 Blue super competent cells. Cells were plated on LB-Kanamycin plates and single colonies were picked and sequenced to verify incorporation of the desired mutants.

Expression of truncated IDH1

To verify that the mutant IDH1 would express and terminate translation at the desired amber stop codons, each construct was transformed into Z-competent BL21-DE3 and grown overnight on LB-Kan plates. Colonies were picked and inoculated into 10 mL 2xYT starter cultures and grown with shaking at 37°C. These cultures were diluted into fresh 2xYT at 1:100 and grown at 34°C until an O.D.$_{600}$ of 0.5. Cultures were then cooled to 18°C and induced with IPTG at a final concentration of 0.5 mM. Cultures were grown overnight with shaking. Cells were pelleted using the same centrifugation protocol outlined above. A small portion of each cell pellet was lysed with B-PER II bacterial extraction reagent (Thermo Fisher), as per the manufacturer's protocol. Briefly, cells were resuspended in 10 mL B-PER reagent and shaken at room temperature for 10 minutes. Insoluble protein was then pelleted by centrifugation at 27,000 x g (Sorvall SS-34 rotor) for 15 minutes. Soluble and insoluble fractions were fractionated using SDS-PAGE and analyzed on a western blot probed with anti-Poly Histidine AP primary antibody and

visualized by colorimetric change upon addition of 5-bromo-4-chloro-3-indolyl-phospahte (BCIP) and nitro blue tetrazolium (NBT) from an alkaline phosphatase reagent detection kit (EMD Millipore).

Preparation of a pEVOL Kac plasmid competent cell line

BL-21 DE3 z-competent cells were transformed with the pEVOL Kac plasmid generously provided by Wenshie Lui, similar to that used in(*102*, *103*). These cells were plated on LB-Chloramphenicol and grown overnight at 37°C. Single colonies were selected and inoculated into 10 mL of LB culture with chloramphenicol present. These starter cultures were allowed to grow overnight at 37°C. The following day, 1 mL of starter culture was used to inoculate 100 mL of LB-chloramphenicol medium. This culture was grown at 34°C until it reached an OD_{600} of 0.4. The cells were immediately incubated on ice for about 30 minutes. The following procedure to prepare calcium competent cells was performed on ice, using pre-chilled buffers and chilled centrifuge rotors. The cell culture was pelleted by centrifugation at 3,000 x g for 15 minutes, and the supernatant was decanted and disposed of. The cell pellet was resuspended in 20 mL $MgCl_2$ buffer (100 mM $MgCl_2$, sterilized by autoclave). The cells were pelleted again by centrifugation at 2,000 x g for 15 minutes and the supernatant was again decanted. Cells were resuspended in 50 mL $CaCl_2$ buffer A (100 mM $CaCl_2$, sterilized by autoclave). The cell suspension was again pelleted by centrifugation at 2,000 x g for 15 minutes and the supernatant decanted. Cells were resuspended in 10 mL $CaCl_2$ buffer B (100 mM $CaCl_2$, 15% glycerol, sterilized by autoclave). The cells were pelleted by centrifugation at 1,000 x g for 15 minutes and the supernatant was decanted. The cell pellet was resuspended in 0.5 mL $CaCl_2$ buffer B. The cell

108

suspension was aliquoted (50 µL) and flash frozen in liquid nitrogen. Cells were stored at -80°C.

Expression and purification of singly acetylated IDH1

The Lysine to amber stop mutants of IDH1 (K81ac, K93ac, K224ac, and K321ac) were transformed into calcium competent cells containing a pEVOL Kac plasmid that encodes a tRNA/tRNA synthetase pair for acetyllysine incorporation. Briefly, roughly 100 ng of plasmid DNA for each lysine mutant was added to 50 µL of competent cells. Cells were incubated on ice for 5 minutes, followed by a 30 second heat shock in 42°C water, and placed back on ice for 2 minutes. S.O.C. medium was then added to each aliquot of cells (200 µL of S.O.C.) and the cells were incubated for 1 hour with shaking at 37°C. Cells were then plated on LB-Kan/Chlor plates and grown overnight at 37°C. The expression of mutant IDH1 was carried out using a similar method to WT-IDH1 expression, with minor differences. Culture sizes were limited to <500 mL total. After cooling the cells when the OD_{600} reached 0.5, the cells were treated with nicotinamide (final 20 mM) and then continued shaking for 10 minutes. Cells were then treated with acetyllysine (final 10 mM) and the pEVOL plasmid was induced by addition of arabinose (final 0.2%). After 30 minutes, IDH1 was induced by addition of IPTG (final 0.5 mM).

Following expression, mutant IDH1 was purified over two nickel columns, according to the same method used for WT-IDH1. Acetylation was verified by western blot probed with an anti-acetyllysine primary antibody.

HDAC8-catalyzed deacetylation of full-length IDH1

HDAC8 catalyzed deacetylation was measured for all four IDH1 acetylation mutants. Reactions were done under single turnover conditions ([E] > [S]), and all components were diluted in HDAC reaction buffer (25 mM HEPES pH 8.0, 137 mM NaCl, 3 mM KCl). HDAC8 was in excess of the acetylated IDH1 substrate, which was assayed in the low- to sub-micromolar range. An internal standard, BSA, was used in all reactions. Reactions were carried out at 30°C in microcentrifuge tubes. Reaction aliquots were quenched into SDS, 10% HCl, or SAHA. Each time point was then fractionated on a polyacrylamide gel and transferred to a nitrocellulose membrane. Western blots were probed with primary anti-acetyllysine antibody (rabbit, from Abcam) at a 1:1000 dilution for 2 hours at room temperature. Horseradish peroxidase (HRP) - conjugated secondary antibody was used, followed by addition of SuperSignal West Pico Chemiluminescent substrate (Thermo).

Preparation of peptide substrates from chip-based hits

Acetylated peptides ranging from 6-12 amino acids were ordered from Synthetic Biomolecules. Lyophilized peptides were resuspended in ultrapure water (Milli-Q, Millipore). Those that would not dissolve in pure water were resuspended in water containing DMSO, acetonitrile, sodium bicarbonate, or formic acid. To reduce metal contamination in the peptides, 50 – 100 μL of a pre-washed Chelex-100 resin (BioRad) slurry in Milli-Q water was added to each peptide. The peptides were incubated on ice, with agitation once every 5 minutes for an hour. Chelex was then pelleted by centrifugation at 3000 x g and supernatant was collected and transferred to clean, metal-free microcentrifuge tubes. Peptide concentrations were determined using a micro-BCA kit

with 8 BSA standards and 3 concentrations of each peptide. Additionally, select peptide concentrations were also measured by a fluorescamine-based assay as described in Wolfson *et al.* (*76*) and by absorbance measurements at A_{280}.

Measuring turnover of acetylated peptides from chip-hits

The turnover of acetylated peptides was measured using an enzyme-coupled assay, as described in Wolfson *et al.*, (*76*). In summary, peptides, when possible, were measured at 100 μM. If peptide stocks did not allow this, then 50 μM peptide substrate was used. HDAC8 was reconstituted with cobalt or zinc at a 1:1 ratio at concentrations ranging from 0.5 – 1 μM. HDAC11 was reconstituted with zinc at a 1:1 ratio, with concentrations ranging from 0.2 – 0.5 μM. Both enzymes were assayed at 34°C. Time points ranged from 0 – 4 hours, and reactions from both enzymes were quenched into 10% HCl. Acidified solutions were neutralized by addition of 6% sodium bicarbonate immediately before analysis. In Corning 3868 black plates, 60 μL of neutralized reactions were added to 10 μL of a coupled-enzyme solution to catalyze the conversion of NAD+ to NADH using acetate as a starting material (as previously described). Reaction fluorescence was read (ex. 340 nm and em. 460 nm) at short time intervals (1-2 minutes) until the coupled enzyme reactions reached completion, in less than 2 hours.

IDH1 activity

IDH1 was assayed with 75 μM NADP+ and 200 μM isocitrate. Assays were run in 50 – 100 μL volumes in a black Corning 3686 96-well half-area plate. Progress curves were measured by fluorescence with excitation at 340 nm and emission at 460 nm (PolarStar

Fluorescence plate reader). IDH1 WT was assayed at 5 – 50 nM, and IDH1 acetylated mutants were assayed at 10 nM – 1 µM.

Results

Expressed Protein Ligation of p300 generates active enzyme and results in acetylation of proteins 'on-chip.'

HuProt chips, developed by Zhu and coworkers at Johns Hopkins and manufactured by CDI Laboratories, were used for our studies. These chips contain approximately 20,000 human proteins, each printed in duplicate in defined locations. The proteins printed on these chips all contain a GST-tag, used both in their purification as well for verification of protein density at each discrete spot on the chips. Lysine acetyltransferase p300 was used to generate a pool of acetylated proteins on the chips. To acetylate a broader range of proteins, a truncated form of p300 was used, containing the catalytic domain but lacking the specificity domain. The truncated gene encodes amino acids 1287-1652, with the deletion of an auto-acetylation loop region (1523-1554) and point mutations at M1652G and K1637R (*101*). This construct yields a hypoacetylated, inactive p300, allowing recombinant expression of the protein in *E. coli* without toxicity to the cells. The protein is then activated via an expressed protein ligation protocol to extend the C-terminus by 14 amino acids, which are necessary for catalysis. The M1652G mutation increases efficiency of the ligation reaction.

P300 was expressed with a C-terminal *Saccharomyces cerevisiae* Vacuolar Membrane ATPase (Sce VMA) intein region followed by a chitin-binding domain (Fig. 4.4). We verified expression of the protein in BL-21 DE3 cells via a one-column purification on chitin resin, followed by thiol-induced splicing at the intein. Protein expression and purity were determined by Coomassie staining of a polyacrylamide gel. We observed a yield of 25 mg of p300 from a 1-liter expression in 2xYT media.

113

To generate active p300 protein, expressed protein ligation (EPL) was used to append a 14mer peptide to the C-terminus of the p300 construct. EPL was carried out after p300 was bound to chitin resin. Instead of initiating intein cleavage by DTT thiol addition, MESNA reagent was used. Cleaved and ligated protein was further purified on an S-cation exchange column. Activity of our p300 enzyme was verified by Beth Zucconni, a post-doctoral research fellow in Phil Cole's group, with experience assaying histone acetyltransferase activity.

To acetylate proteins on the HuProt chips, p300 (8 – 10 µM) and acetyl-CoA (200 µM) were applied to the chips and allowed to react for up to 2 hours at 30℃. A limitation to this type of experiment is that the pool of potential substrate proteins is 'pre-determined' by the activity of the KAT enzyme. Therefore, our objective was to maximize acetylation of chip-based proteins by using concentrations of enzyme and acetyl-CoA that were intentionally above the range typically used for kinetic studies of p300. After reacting, p300 was quenched with an ammonium bicarbonate buffer and the chips were thoroughly washed.
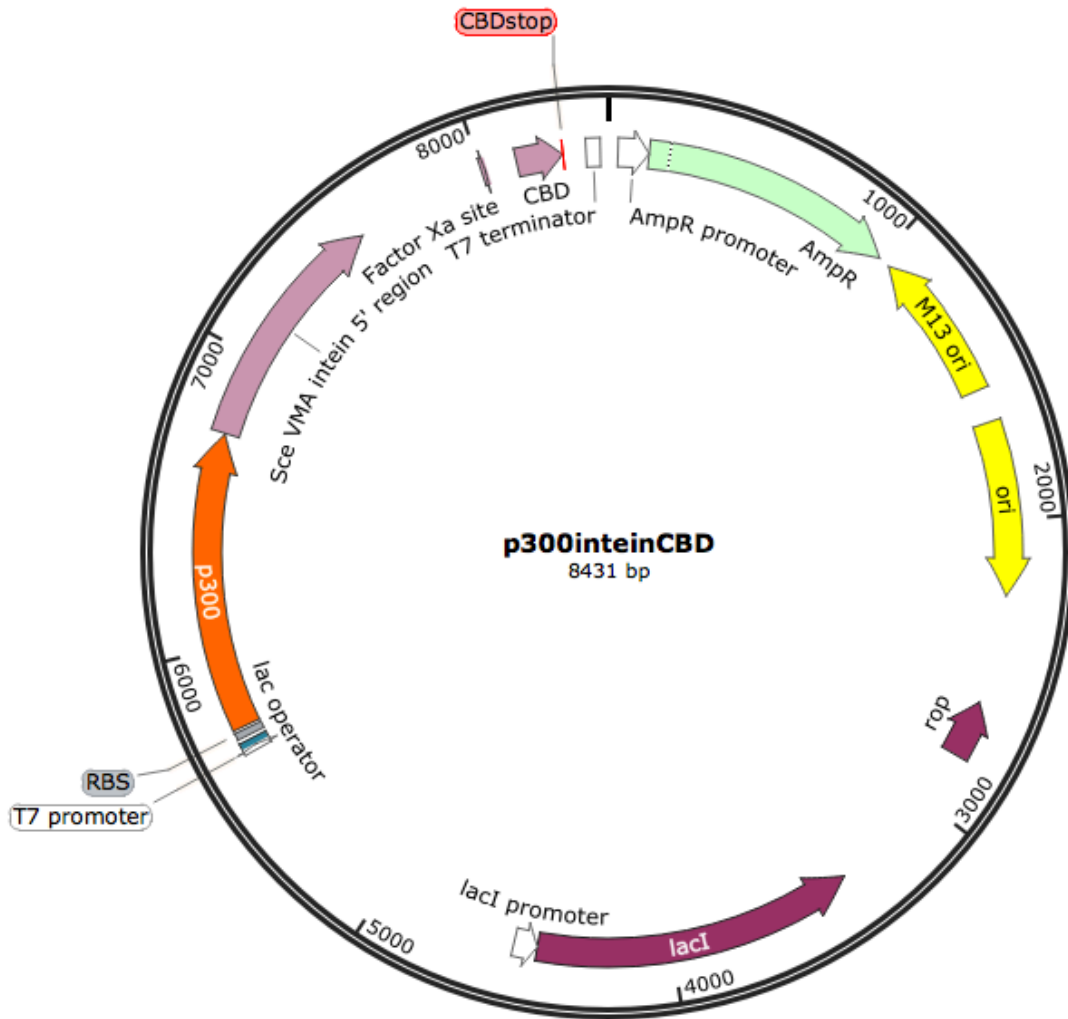
Figure 4.4: p300 expression vector

p300 construct in pTYB2 vector from New England Biolabs, with c-terminal intein and chitin binding domain (CBD). This p300 construct encodes amino acids 1287-1652, M1652G, K1637R, with a deletion of the loop from 1523-1554 (Created using SnapGene).

Developing a method for assaying p300 and HDAC activity on proteome chips

For our pilot round of chip-based assays, only HDAC8 was used. Briefly, these assays utilize chip-based libraries of 20,000 immobilized human proteins. Chips were treated with differing combinations of KAT and HDAC, and differences in protein acetylation were visualized. HDAC8 was reconstituted with cobalt and used at a range of 2.5 – 7.5 µM. We also examined the role EDTA treatment of the chips, to remove excess divalent metals, on HDAC activity by washing a subset of the chips with an EDTA containing buffer after acetylation and a second subset of chips with an identical buffer lacking EDTA. Both sets of chips were then washed with HDAC reaction buffer to remove any residual EDTA. HDAC8 was applied to the surface of the chips (120 µL) and a cover slip was applied. The HDAC reaction was allowed to proceed for 2 hours at 30℃. The acetylation state of individual proteins was determined by anti-acetyllysine immunofluorescence with excitation at 635 nm (Fig. 4.5A).

A second round of chip-based assays was run, looking at the activity of both Zn-HDAC8 and Zn-HDAC11 (Fig. 4.5B). The chips were handled in a similar manner, but some adjustments were made based on observations from the pilot experiment. HDAC8 was used at a final assay concentration of 2 µM, and HDAC11 was used at 1 and 1.5 µM. For these chips, HDAC reaction solutions were made in a greater volume. Instead of applying a microliter volume of enzyme to each chip, followed by a coverslip, we added 3 mL of HDAC solution, enough to submerge the HuProt chips and negate the need for a coverslip. In doing so, we sought to reduce background noise and increase HDAC-chip interaction by avoiding the formation of air pockets beneath a coverslip.
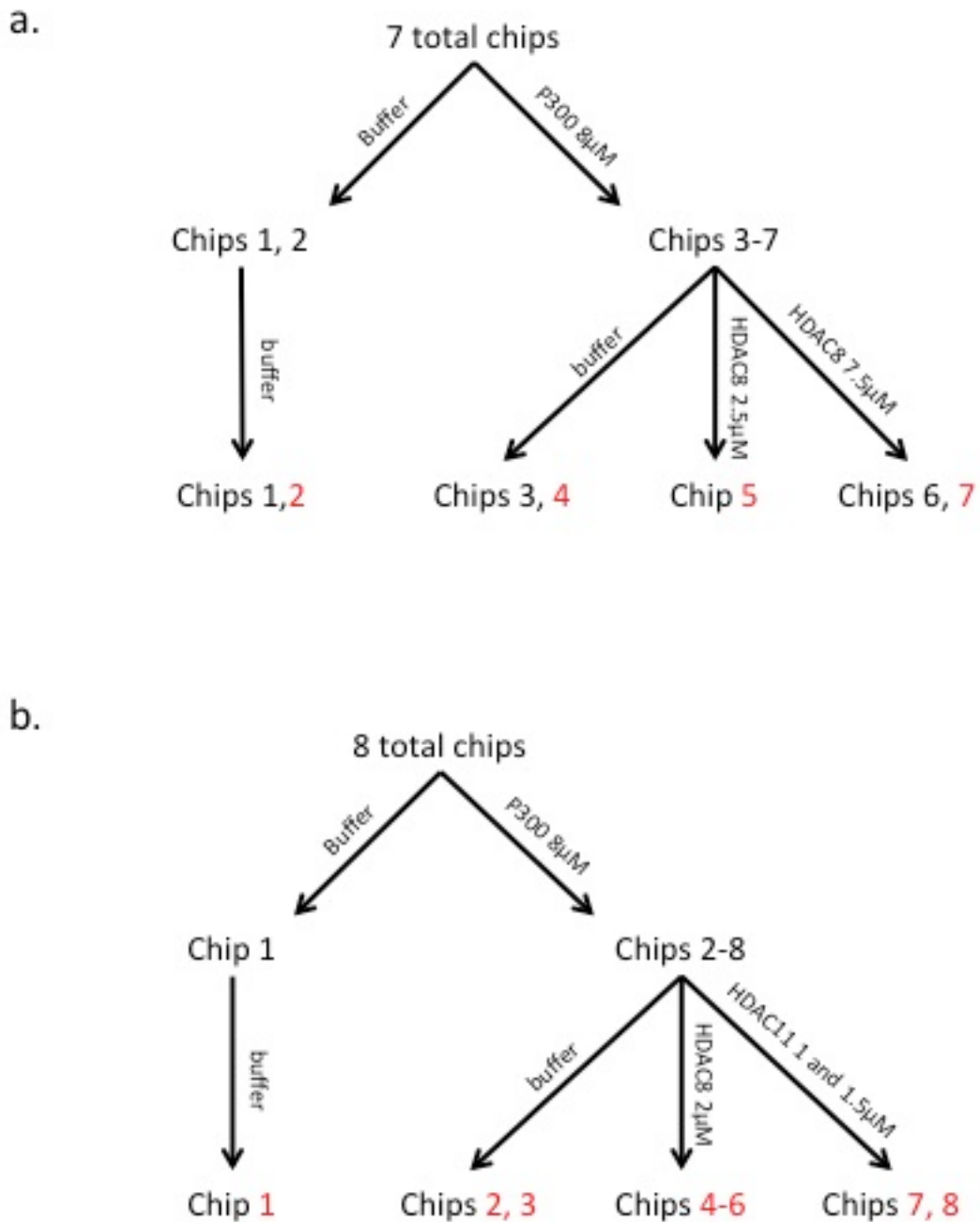
Figure 4.5: Proteome chip assay scheme

Proteome chips in both round 1 experiments (A) and round 2 experiments (B) that are labeled red were washed with EDTA to remove divalent metals before HDAC application. A. The first round of proteome chip experiments utilized a total of 7 HuProt chips. p300 was applied to chips 3-7, as shown. HDAC8, at various concentrations, was then incubated with select chips. B. The second round of proteome chip experiments utilized 8 HuProt chips and measured deacetylation by either HDAC8 or HDAC11. p300 was applied to chips 2-8, as shown. Individual HDAC isozymes were then applied to select chips, as labeled.

HDAC8 catalyzes deacetylation of proteins on HuProt chips

To measure HDAC-catalyzed deacetylation of protein on the chips, we first determined which proteins were acetylated upon incubation with the p300 construct. For both rounds of experiments, we first manually flagged and removed artificial spots where the antibody precipitated, which causes 'firework' patterns. We then identified and verified that control proteins were successful (landmarks, rabbit-IgG, etc.). These control proteins were then removed before analysis of acetylation and deacetylation of chip-based substrates. For our pilot chips, identification of the acetylated proteins was determined using an anti-acetyllysine antibody and visualized via a fluorescent secondary antibody. These data were then analyzed as histograms of foreground to background fluorescent intensity (f/b), indicative of acetylated lysines. We then considered proteins with f/b more than three standard deviations higher than the median value to be acetylated. Furthermore, we required both copies of a given protein on the chip to be scored as acetylated. Using this method, the pilot round of chips identified 164 acetylated proteins. For our second round of chip-based experiments, we introduced a more stringent method for determining acetylation. Here we first determined the average f/b ratio for all proteins on the chip. If no acetylation occurred, a plot of these averages would yield a symmetrical bell curve. Acetylation increases the high values of f/b on this curve. To correct for this skew when determining a standard deviation, we used the low f/b side of the curve to recreate a symmetrical bell, which we refer to as our mirror method. From this modified graph we calculated standard deviation values. Here, we used two standard deviations above average to determine KAT hits. Proteins had to meet these criteria in all four replicates (two spots, on two KAT only chips) to be considered acetylated. In this round of

experiments, we found 506 proteins that were acetylated twice on both KAT control chips. While there was some overlap in acetylated proteins between the two rounds of experiments, we did see differences (discussed further below).

Using these data to identify acetylated proteins, we then looked for a loss of acetylation in the HDAC-treated chips. For our pilot experiment, we used the difference in f/b of the KAT-only chips compared to the KAT-HDAC chips. Proteins with a greater than average difference between these conditions were considered hits. Analysis of these chips showed that 43 of the 164 acetylated proteins were deacetylated upon incubation with HDAC8. Further evaluation of these 43 hits by visually inspecting the raw fluorescent images suggested that 8 were false positives (i.e. should have been flagged and removed as antibody precipitate spots), 9 appeared mediocre, and 26 looked to be good hits (Appendix 1, Table S1). These hits represented proteins from a diverse set of biological functions, including protein folding pathways, metabolism, and the cell cycle.

For our second round of chip-based assays we used a more stringent methodology to identify proteins that were deacetylated by HDAC8. We used three separate methods to identify hits from these chips. The first, similar to the pilot experiment, was to look for the largest f/b differences between KAT-only and KAT-HDAC chips. We then repeated our methodology for determining p300 hits, where a mirror image of a bell curve was used to determine standard deviation. Again, proteins two standard deviations at high f/b values were considered acetylated. We compared KAT-only and KAT-HDAC chips using this method, and looked for proteins that no longer met the acetylation threshold upon treatment with an HDAC. Finally, we ran t-tests to analyze the significance of f/b changes

seen between each occurrence for a given protein on the chips. For HDAC8 treated chips, this test analyzed a total of 10 spots per substrate protein.

Using the mirror method of analysis, we identified 228 proteins that fit the criteria for deacetylation by HDAC8. These proteins showed loss of f/b for the duplicate spots on one of the three HDAC8-treated chips. Of those 228 proteins, about half (109) were identified on only one of the HDAC8-treated chips, 67 of them were identified on two of the three HDAC8-treated chips, and 52 were identified on all three HDAC8-treated chips. Only proteins that showed loss of signal on all three chips were analyzed further. Using the t-test statistical method, we identified 347 proteins that met a $p<0.05$ cutoff and were acetylated on the KAT-only chips. We compared these results and identified 19 proteins that met the criteria for at least two of the three methods of determining HDAC activity (Appendix 1, Tables S2 and S3).

We next analyzed the literature to determine which of these proteins have documented acetyllysine sites, and found that 11 of the 26 hits from the pilot experiment and 11 of the 19 hits from the second round experiment were known to be acetylated. Using the FlexPepBind algorithm developed by our collaborator Ora Furman (*89*), we scored each known acetyllysine on these 22 proteins to perform as a first round of validation. The FlexPepBind algorithm outputs an i_score, a prediction of the likelihood of an amino acid sequence with an acetyllysine being an HDAC8 substrate. The more negative a score, the higher the chance that the peptide is a substrate. Peptides with score's below -17 are considered strong candidates, and -16 to -17 are considered good candidates, but with a greater chance of false positives. Our hits ranged from >0 to <-20, suggesting a

number of the sites on these proteins were good to strong candidates to be deacetylated by HDAC8.

HDAC11 deacetylates an overlapping and distinct set of proteins on the HuProt chips

Chips treated with HDAC11 (second round experiment only) were analyzed according to the same method as the HDAC8-treated chips. Using the mirror method, we identified 259 proteins that met the criteria for deacetylation on both HDAC11-treated chips (4 spots total). Of these proteins, 96 were also identified in two of the three HDAC8-treated chips when analyzed using this same method. Additionally, using the t-tests as described above, 364 proteins met a $p<0.05$ and were previously identified as acetylated. Of the 364 proteins that passed our t-test threshold, 70 also had f/b intensity differences between that KAT-only and KAT-HDAC11 chips of 0.5 or greater (f/b intensity of acetylated chip minus f/b intensity of deacetylated chip $\geq$ 0.5). When combined, we identified 22 proteins that passed all three of our criteria and 3 additional proteins that scored highly in 2 of our 3 criteria. Of these 25 total proteins, 14 are known to be acetylated (Appendix 1, Table S4). Unlike HDAC8, we have no computational substrate recognition algorithm to triage our peptide library prior to in-solution HDAC11 assays.

MALDI-MS makes an efficient method for screening large batches of peptides

Based on our FlexPepBind scores, we ordered a library of short peptides (6 – 10 amino acids) based on the local sequences surrounding acetyllysines on the HDAC8 chip hits. In total, we tested 16 peptides from our pilot round of chip experiments. Before using the peptides in our enzyme-coupled assay, we ran small-scale reactions (20 – 60-fold less

volume than the enzyme-coupled assay) where each peptide was incubated with HDAC8 and spotted time points on a polished steel MALDI-target. We looked at 2 – 3 time points for each peptide, from a zero point to a 30-minute point. At time point zero, the exact mass of the peptide substrate is observable. At later time points, a peptide that is a substrate should show a new peak corresponding to the peptide minus an acetyl group (M-42 Da). This approach provided a good indication of which peptides would be highly reactive (Fig. 4.6). There were a few peptides, however, for which no peak corresponding to the expected parent mass was observable. While there were some outliers, this MALDI-based pre-screen of HDAC8 activity followed the same general trend predicted by the FlexPepBind algorithm. The most reactive peptide substrates following this screen were peptides #136 and #138, corresponding to acetyllysine residues on isocitrate dehydrogenase (IDH1) and retinol dehydrogenase (RDH16); at 30 minutes only a product peak was observable in the mass spectrum. Peptide #137 (IDH1) was the next best peptide as evaluated by MALDI, where the substrate and product peaks were about equal at 30 minutes. Peptide #135, from Aldo-keto reductase (AKR1C2), also gave a strong, clean peak of correct mass. However, no product peak appeared over the time course tested. As we moved from the best-scored to lowest-scored peptides, we found no other peptides that went to completion, but several that showed a product peak. The data from the MALDI assay was largely consistent with the chip and FlexPepBind data, and informed our selection of peptides for more detailed kinetic analysis.
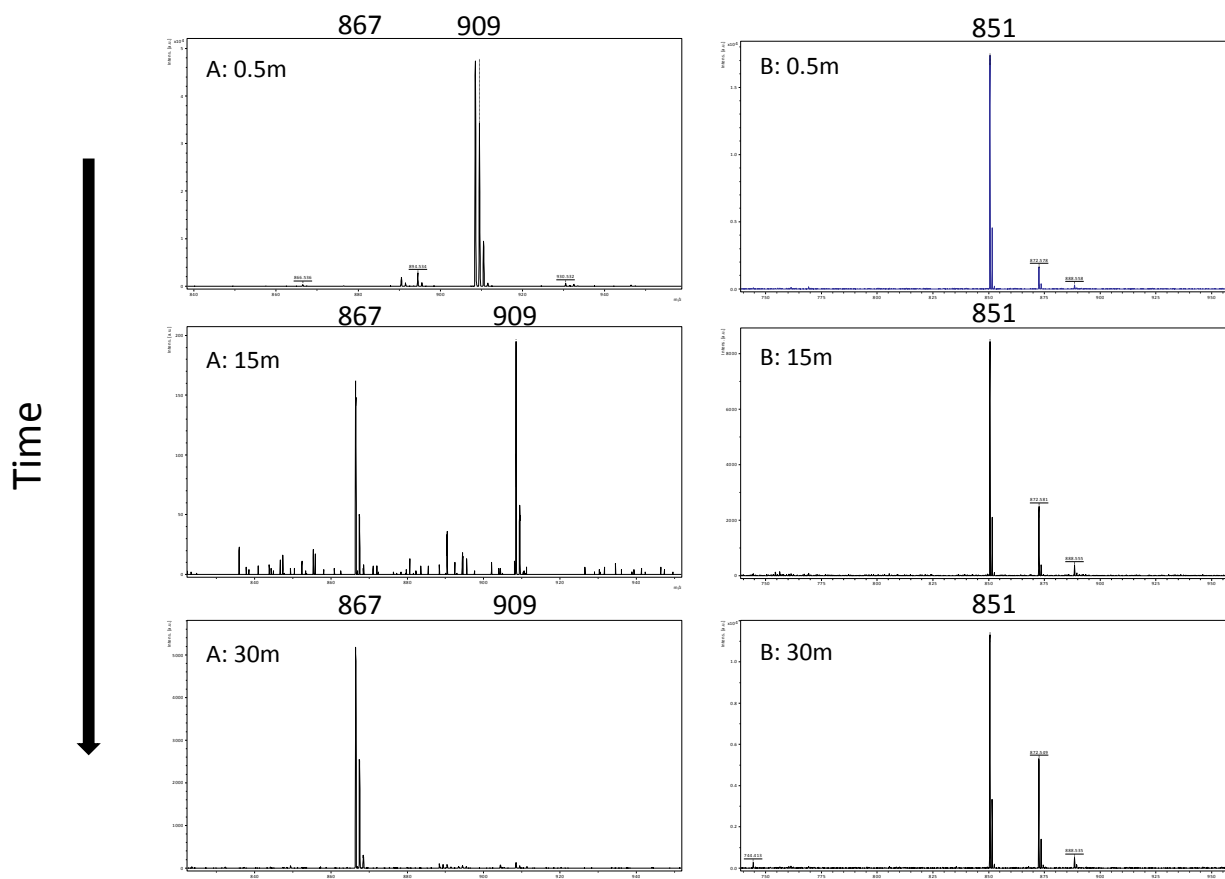
Figure 4.6: Determination of HDAC8 activity by MALDI-MS

Peptides (100 µM) were incubated for 30 minutes with 0.5 µM HDAC8. During this time, a total of three time points were quenched into 10% HCl. The first time point (t=0 min.) is at the top of each figure. Moving down, t=15 min. is the middle frame, and t=30 min. is the bottom frame. A. Peptide 136 (Ac-RF(K_{Ac})DIF-NH2) is a positive hit by MALDI analysis, where the parent peptide (909 Da) decreases by 42 Da to a product peak (867 Da) over the time course. B. Peptide 135 (Ac-AK(K_{Ac})HKR-NH2) is a negative hit, where the parent peptide (851 Da) does not give way to an observable product peak over the time course.

Peptide assays in solution are consistent with HDAC kinetic trends observed in MALDI assay.

To determine the rate constants for HDAC8-catalyzed deacetylation of these peptides, we used an enzyme-coupled assay in which acetate production is coupled to the formation of NADH and visualized by fluorescence with ex. = 340 nm and em. = 460 nm(*76*). We measured activity at 50 or 100 μM peptide concentrations and calculated the specificity constant, $k_{cat}/K_{M, app}$, for HDAC8 catalysis of these peptides. This calculation was done under the assumption that our substrate concentration was below K_M. The measured values for $k_{cat}/K_{M, app}$ ranged over three orders of magnitude, from $10^0 – 10^2$ M^{-1}s^{-1} (Table 4.1). The largest k_{cat}/K_M value was observed for HDAC-catalyzed deacetylation of peptide #137, corresponding to IDH1. This was followed by peptide #136, also from IDH1, and peptide #138 from RDH16 (Fig. 4.7). These are the same three peptides that were identified as the best substrates in the MALDI screen. Not only did IDH1 provide the fastest peptide tested from this round of chip experiments, but three of the four sites we tested from IDH1 showed a $k_{cat}/K_M > 20$ M^{-1}s^{-1}.

Table 4.1: Kinetics of HDAC8-catalyzed deacetylation of peptides from Chip set 1 hits[13],[14]

Table arranged by peptide # and I_score

Peptide #	Protein	Ac-Sequence-NH2	I_score(*89*)	k_{cat}/K_M (M^{-1}s^{-1})
135	AKR1C2	AK(K–Ac)HKR	-19.2	<10
136	IDH1	RF(K–Ac)DIF	-18.3	90
137	IDH1	KLKQMW(K–Ac)SPN	-18	160
138	RDH16	ERFL(K–Ac)SFLE	-17.4	54
139	PTEN	HC(K–Ac)AGK	-17.2	<10
140	HSPA1L	VE(K–Ac)ALR	-17.1	<10
141	AKR1C2	LA(K–Ac)KHK	-16.8	20
142	IDH1	YQ(K–Ac)GQE	-16.3	<10
143	AKR1C2	YQ(K–Ac)GQE	-16	<10
144	CRIP1	SLG(K–Ac)DWHR	-15.8	46
145	PTEN	II(K–Ac)EIVSR	-15.4	<10
146	AKR1C2	SV(K–Ac)RED	-15.2	12
147	RFK	TK(K–Ac)SME	-15.1	34
148	RABL3	EE(K–Ac)TYY	-15.1	<10
149	IDH1	DE(K–Ac)RVE	-15	38
150	PTEN	DK(K–Ac)GVT	-14.6	<10

---

[13] I_score is a substrate prediction value based on an algorithm developed by Alam *et al.*, 2016

[14] Peptides were assayed with 0.5 – 1 µM zn-HDAC8 and 100 µM substrate. Assay time points were quenched into 10% HCl and developed using a coupled-enzyme assay. The listed specificity constant, k_{cat}/K_M is an apparent value, calculated on the assumption that [S] < K_M.
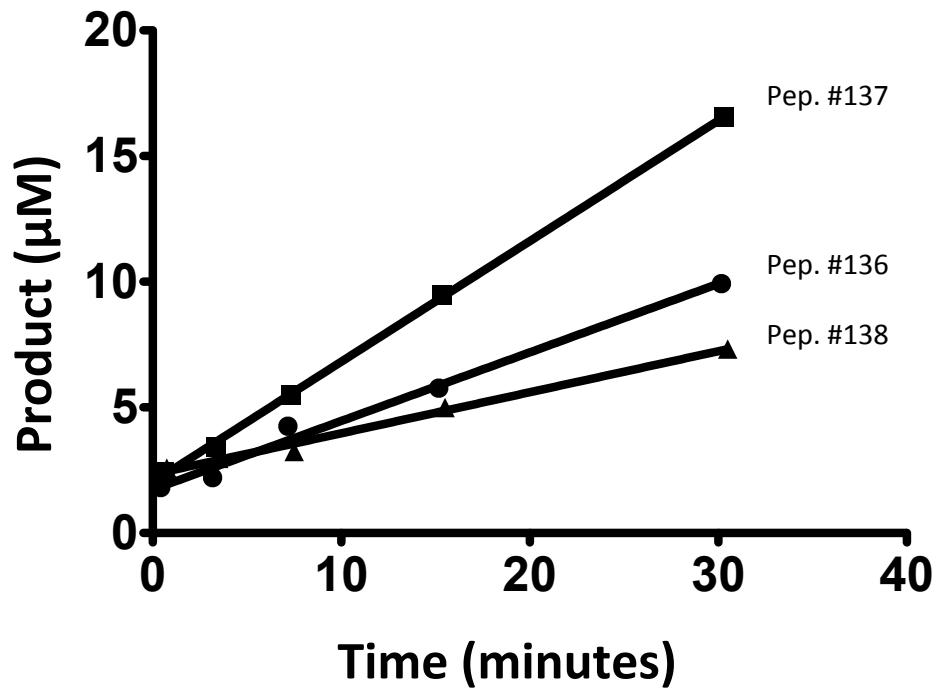
Figure 4.7: HDAC8-catalyzed deacetylation of chip-based peptides from round 1

Progress curves for peptides identified in the first round of the HDAC8 proteome chip experiments. Peptides are representative of IDH1 (peptides 136 and 137) and RDH16 (peptide 138). HDAC8 was assayed at 1 µM, with substrates at 100 µM. We measured activity using a coupled-enzyme assay.

HDAC8 and HDAC11 both deacetylate peptides from the second round of chip experiments.

Using the same enzyme-coupled assay, we measured deacetylation of peptides based on protein hits identified in the second round of chip-based experiments. HDAC8 and HDAC11 were both catalytically active against peptide substrates. In total, we measured HDAC8 deacetylation toward 32 peptides (from 16 proteins) and HDAC11 deacetylation toward 18 peptides (from 9 proteins). Both enzymes displayed apparent k_{cat}/K_M values ranging from $10^0 - 10^2$ M^{-1}s^{-1} (Tables 4.2 and 4.3). The top HDAC8 hit from this screen was a peptide corresponding to protein disulfide isomerase (P4HB), with a $k_{cat}/K_{M, app}$ = 300 M^{-1}s^{-1} (Fig. 4.8). This was one of three peptides tested from P4HB, but the only one that showed activity greater than 10 M^{-1}s^{-1}.

The HDAC11 set of peptides is the first library of HDAC11-specific peptides tested to date. Without the benefit of a predictive algorithm for HDAC11, peptides were chosen based on trends we observed. Based on previous HDAC11-catalyzed deacetylation of peptides (Chapter 3), we hypothesized this isozyme might display a preference for acetyllysines surrounded by charged residues. Phosphosite data on proteins deacetylated by HDAC11 on our chips showed several acetyllysine residues flanked by charged sequences. When proteins had multiple acetylation sites, we preferentially included those found in charged regions. The top scoring HDAC11 substrate was peptide was #215, which corresponds to an acetyllysine site from treacle protein (TCOF1), with a k_{cat}/K_M = 175 M^{-1}s^{-1} (Fig. 4.9).

TABLE 4.2: HDAC8 Chip set 2

Table arranged by peptide # and corresponding protein

peptide #	Protein	Ac-Sequence-NH2	I_score(*89*)	k_{cat}/K_M (M^{-1}s^{-1})
169	PFKP	TY(K-Ac)RLAIK	-17.4	<5
171	PFKP	EL(K-Ac)KQT	-16.6	5
172	PFKP	HRIP(K-Ac)EQW	-18.3	30
175	BOLL	NY(K-Ac)DKK	-17.0	<5
176	ASAP2	IR(K-Ac)VWQK	-16.7	<5
177	ASAP2	WQ(K-Ac)RKC	-18.3	13
178	EIF4B	ENPAS(K-Ac)FSSASK	-17.4	35
179	KLC2	YL(K-Ac)QGKYQD	-18.3	<5
181	P4HB	FK(K-Ac)FDE	-18.2	300
182	P4HB	GL(K-Ac)KEE	-17.4	<5
183	P4HB	WD(K-Ac)LGE	-17.8	<5
184	PRDX4	EF(K-Ac)ELK	-17.4	15
186	TCOF1	QA(K-Ac)KTR	-18.3	<5
187	TCOF1	SG(K-Ac)SPR	-16.7	<5
188	TCOF1	SR(K-Ac)RKL	-17.5	<5
189	TCOF1	RS(K-Ac)KKK	-18.2	32

TABLE 4.3: HDAC11 Chip set 2

Table arranged by peptide # and corresponding protein. Charged residues are highlighted in red (acidic) or blue (basic).

peptide #	Protein	Ac-Sequence-NH2	k_{cat}/K_M (M^{-1}s^{-1})
211	TCOF1	SM(K-Ac)EKA	<5
212	TCOF1	TG(K-Ac)TVA	60
213	TCOF1	PG(K-Ac)VGD	<5
215	TCOF1	QV(K-Ac)AEK	175
216	TCOF1	PG(K-Ac)TGPAVAK	8
217	TCOF1	SAPG(K-Ac)VVT	33
218	TCOF1	PA(K-Ac)ESP	<5
219	TCOF1	GA(K-Ac)DEP	9
221	EIF5	EG(K-Ac)GNG	47
222	EIF5	EGKGNGI(K-Ac)TVI	16
225	NIF3L1	RPM(K-Ac)RIT	31
226	NIF3L1	NTW(K-Ac)ER	10
228	GOT1	DAE(K-Ac)RGLD	60
229	LUC7L	EEIG(K-Ac)LLA	18
230	ZBTB21	LAL(K-Ac)RPR	<5
231	CNP	DDL(K-Ac)KLK	31
232	CEBPZ	KGGKQLN(K-Ac)YDPFSRN	51
233	C2orf47	KEVLHAL(K-Ac)EKVTSLP	35
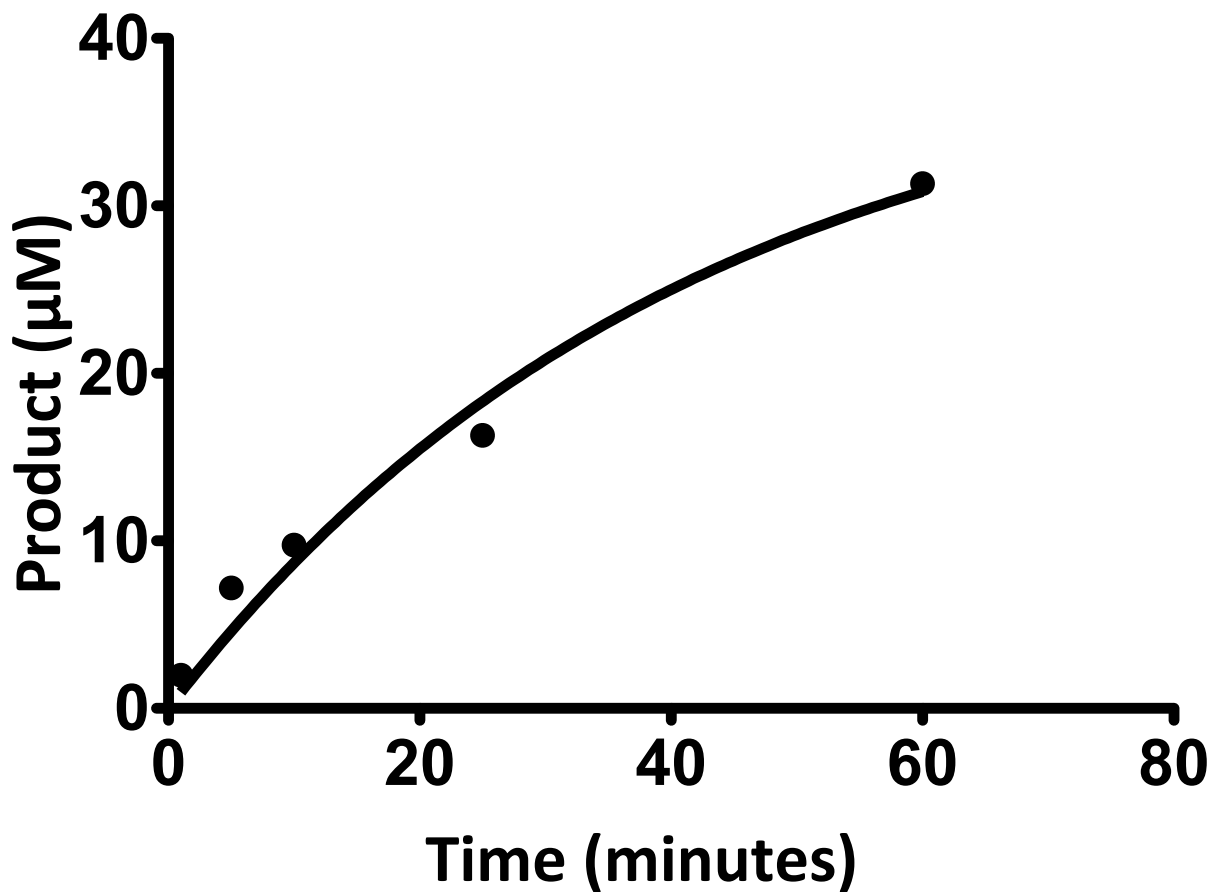
Figure 4.8: HDAC8-catalyzed deacetylation of chip-based peptide 181

Progress curve for deacetylation of peptide 181 (100 μM), corresponding to protein P4HB, catalyzed by 0.5 μM HDAC8. Data is fit with a single exponential equation, and k_{cat}/K_M was calculated to be 300 M^{-1}s^{-1} based on the assumption that [S] < [K_M]. This progress curve and the measured apparent rate constant are based on a single substrate concentration.
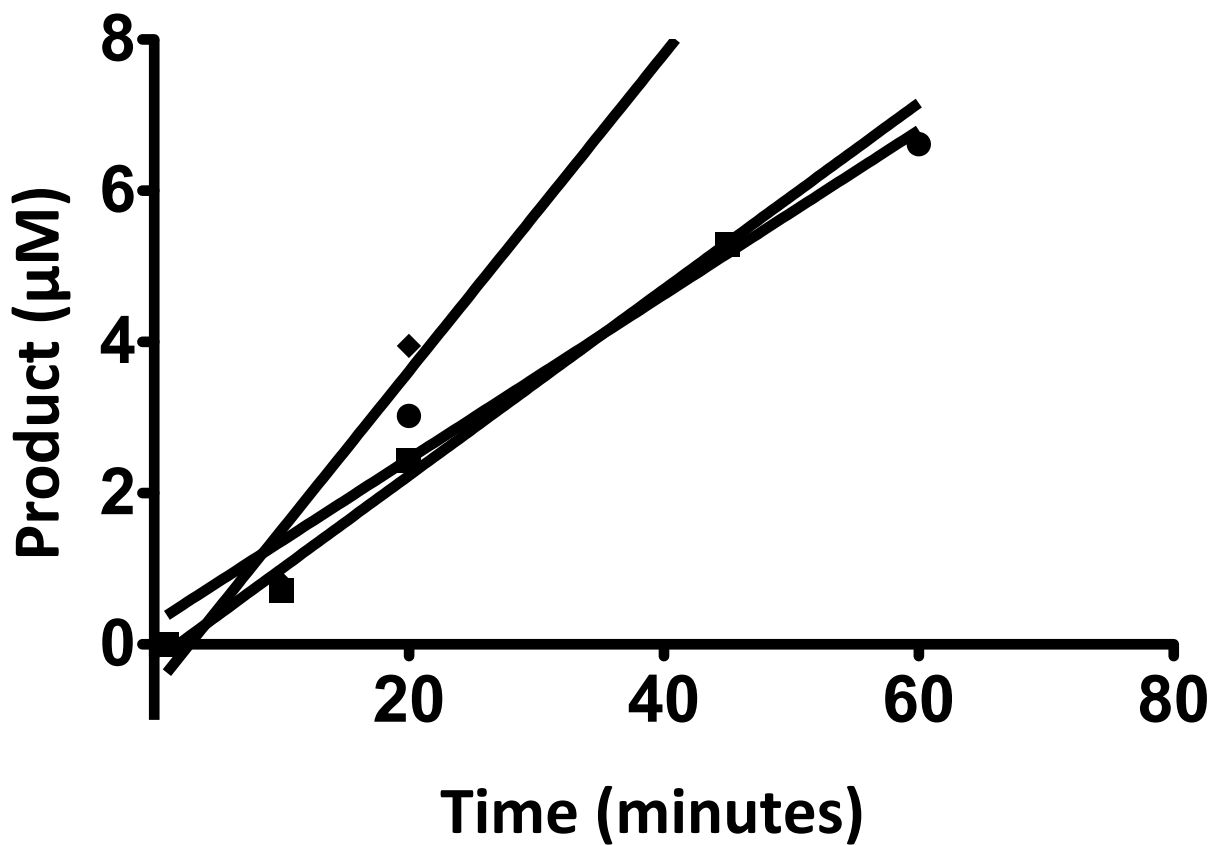
Figure 4.9: HDAC11-catalyzed deacetylation of chip-based peptides

Progress curves for the deacetylation of peptides 212 (■) and 215 (♦), corresponding to protein TCOF1 and peptide 228 (●), corresponding to protein GOT1. These peptides were deacetylated with some of the highest observed k_{cat}/K_M values for HDAC11. These assays were run at a single concentration of peptide.

Cloning and expression of WT IDH1 and amber stop mutants

After measuring deacetylation of peptides from our first HDAC8 chips, we decided to further examine reactivity of HDAC8 with the top substrate, IDH1. We were interested in HDAC8-catalyzed deacetylation of the full-length protein. While there are a variety of methods to generate acetylated protein substrates, it seemed that a method that allows for the controlled insertion of single acetylation sites would provide the most reproducible and reliable results. For this reason, we chose to express singly acetylated proteins by incorporating acetyllysine as an unnatural amino acid. We acquired a pEVOL plasmid from Wenshe Liu at Texas A&M encoding the required tRNA/tRNA synthetase pair for acetyllysine incorporation. We cloned the cDNA for human IDH1 into a pET expression vector with an N-terminal His6 tag (Fig. 4.10), and expressed the WT enzyme in Rosetta cells. WT-IDH1 expressed well and was easily purified on nickel-affinity resin (Fig. 4.3), resulting in a yield of about 25 mg/L. We used QuikChange site-directed mutagenesis to create four additional clones, each with an amber stop mutation at one of the four lysine residues identified as acetylated *in vivo* (K81 [pept. #149], K93 [pept. #137], K224 [pept. #136], K321 [pept. #142]) (*6*). We transformed the pEVOL plasmid into z-competent BL-21 DE3 cells and grew a 100 mL culture. This culture was used to create a stock of chemically competent cells. We then transformed the plasmids encoding the amber stop IDH1 mutants into this cell line, avoiding the need to perform a simultaneous dual transformation. We observed significantly lower yields for these mutant proteins (<1 mg/mL), and found that they showed greatest expression in culture sizes below 500 mL. Regardless, we were able to express and purify acetylated forms of IDH1, as verified by anti-IDH1 and anti-acetyllysine western blots.
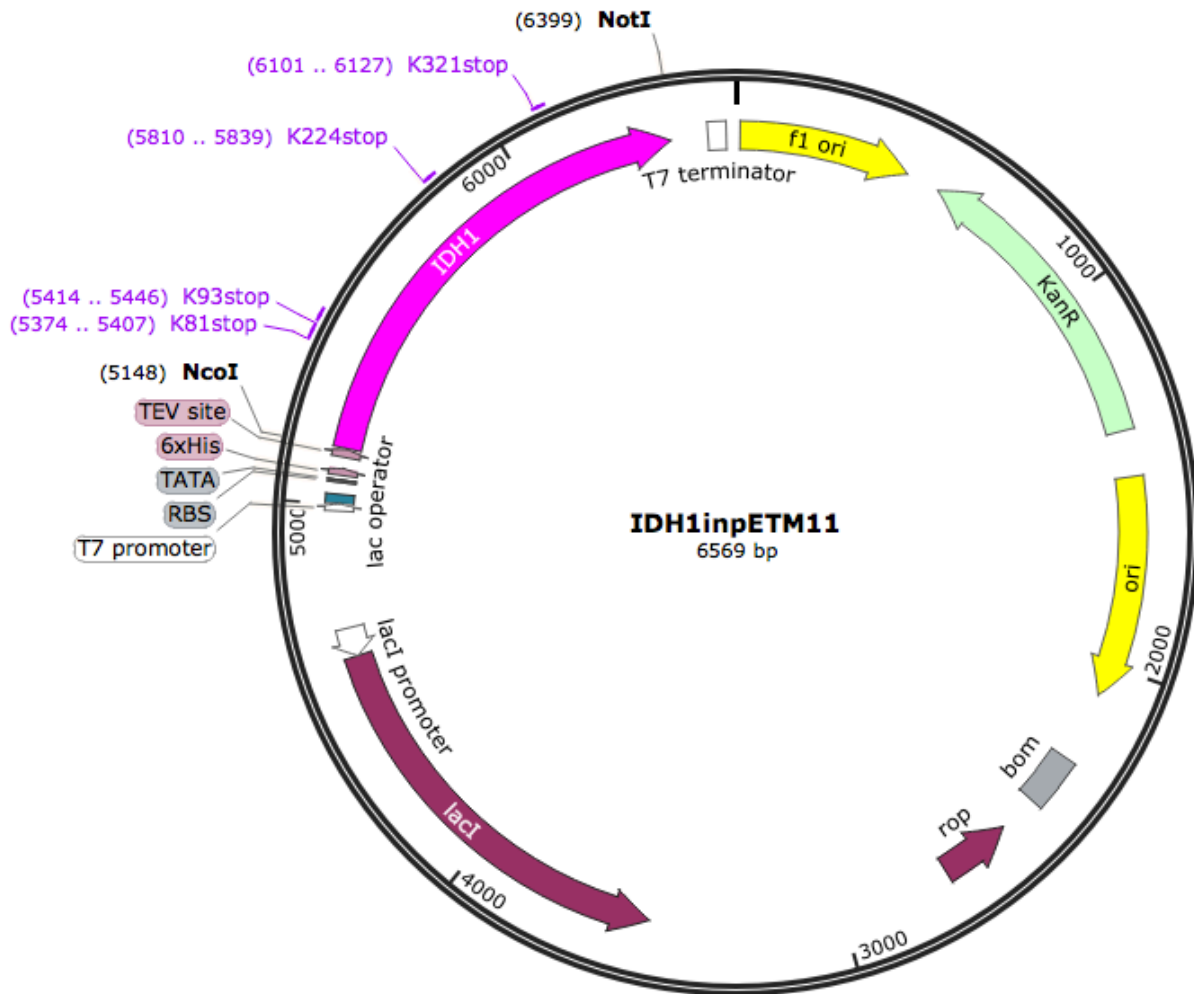
Figure 4.10: IDH1 WT and acetylation mutant constructs

pET-M11 vector with an IDH1 gene insert. Construct has an N-terminal His6 – TEV site. Also highlighted are the four lysine residues that were selected for unnatural amino acid incorporation (Constructed using SnapGene).

IDH1 is the first non-histone full-length protein to be deacetylated by HDAC8 *in vitro*

To assess the deacetylation of purified IDH1 by HDAC8, we ran kinetic assays under single turnover conditions ([E] > [S]). The assays were stopped reactions, in which time points were quenched into either SAHA or 5x SDS gel loading dye and moved onto ice. To visualize changes in acetylation, we ran each time point on an SDS-PAGE gel and transferred them to a nitrocellulose membrane. We then probed blots with an anti-acetyllysine antibody and visualized using an HRP-conjugated secondary antibody and chemiluminescence. To account for possible differences in loading of samples, transformation efficiency, etc., BSA was included in our reaction tubes. This BSA standard was also probed for on our blots and was used to calibrate our analysis of acetylation changes. In our initial experiment, we used the 5x SDS gel loading dye as our quench. Using this assay, we found that all four IDH1 mutants (K81, K93, K224, and K321) are deacetylated by HDAC8, but to differing amounts (Fig. 4.11a). From this experiment, we saw changes in acetylation ranging from 85% deacetylation (K321) to less than 20% deacetylation (K81) over the course of three hours (Fig. 4.11b). While K81 showed the smallest change over the time course, it also had the lowest starting intensity. This suggested that deacetylation could be occurring rapidly under these conditions. For this reason, we carried out additional assays to measure deacetylation of the singly acetylated IDH1 proteins.

A more rigorous assay was run with IDH1 acetylated at either K81 or K93, in which we took a total of six time points. Again, we used BSA as our loading control and 5x SDS as our quench solution. Analysis of the western blots showed that K93 was 80% deacetylated after the 60-minute time course, with a k_{obs} of 0.35 min^{-1} (Fig. 4.12A and Fig. 4.13).

Analysis of K81 was not as simple. There was no visible signal corresponding to acetyllysine in any of the K81 time points (Fig. 4.12BC). However, in a no-HDAC8 control there was a clear acetyllysine signal in all time points. These data suggested that the quench (5x SDS) might not inactivate HDAC8 sufficiently, and that K81 may have been completely deacetylated. To address this issue, K81 was re-assayed using 50 µM (final) SAHA as the quench for each time point. Over the 15-minute time course, we saw greater than 50% deacetylation in 15 minutes (Fig. 4.14). However, even with the SAHA-quench method, the zero-time point has only 60% of the signal generated by the no-HDAC8 control points. This suggests that even inactivation with SAHA may not be a sufficiently rapid quench method.
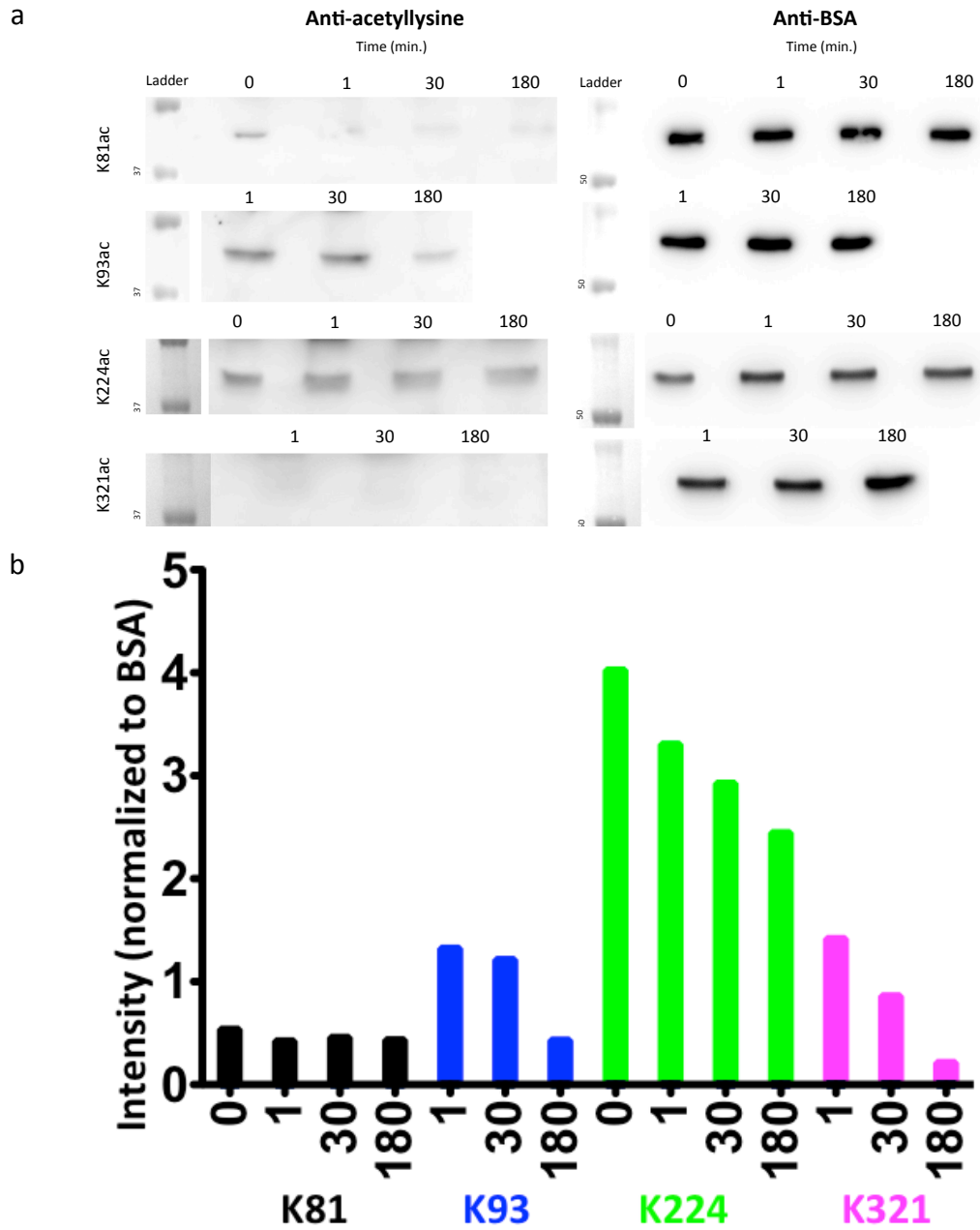
Figure 4.11: HDAC8-catazlyed deacetylation of all IDH1 acetyllysine constructs

Singly-acetylated IDH1 (0.3 µM K81ac, 0.8 µM K93ac, 4.7 µM K224ac, and 2.7 µM K321ac) was incubated with HDAC8 (7.5 µM) in 1x HDAC8 assay buffer at 34°C for a time course of three hours. Assays were run at single-turn over concentrations ([E] > [S]), with three to four time points for each IDH1 variant. A. Western blots for each acetylated IDH1 substrate over the given time course. Blots were probed with anti-acetyllysine (left) and anti-BSA (right) primary antibodies. Blots were separately treated with secondary antibody conjugated to HRP and visualized by chemiluminescence. B. Quantification of the western blot band intensities for acetylated IDH1, normalized to BSA internal standards. Quantification of band intensity was performed using ImageJ. Loss of acetylation, shown as a decrease in intensity, corresponds to HDAC8-catalyzed deacetylation of the target protein.

136
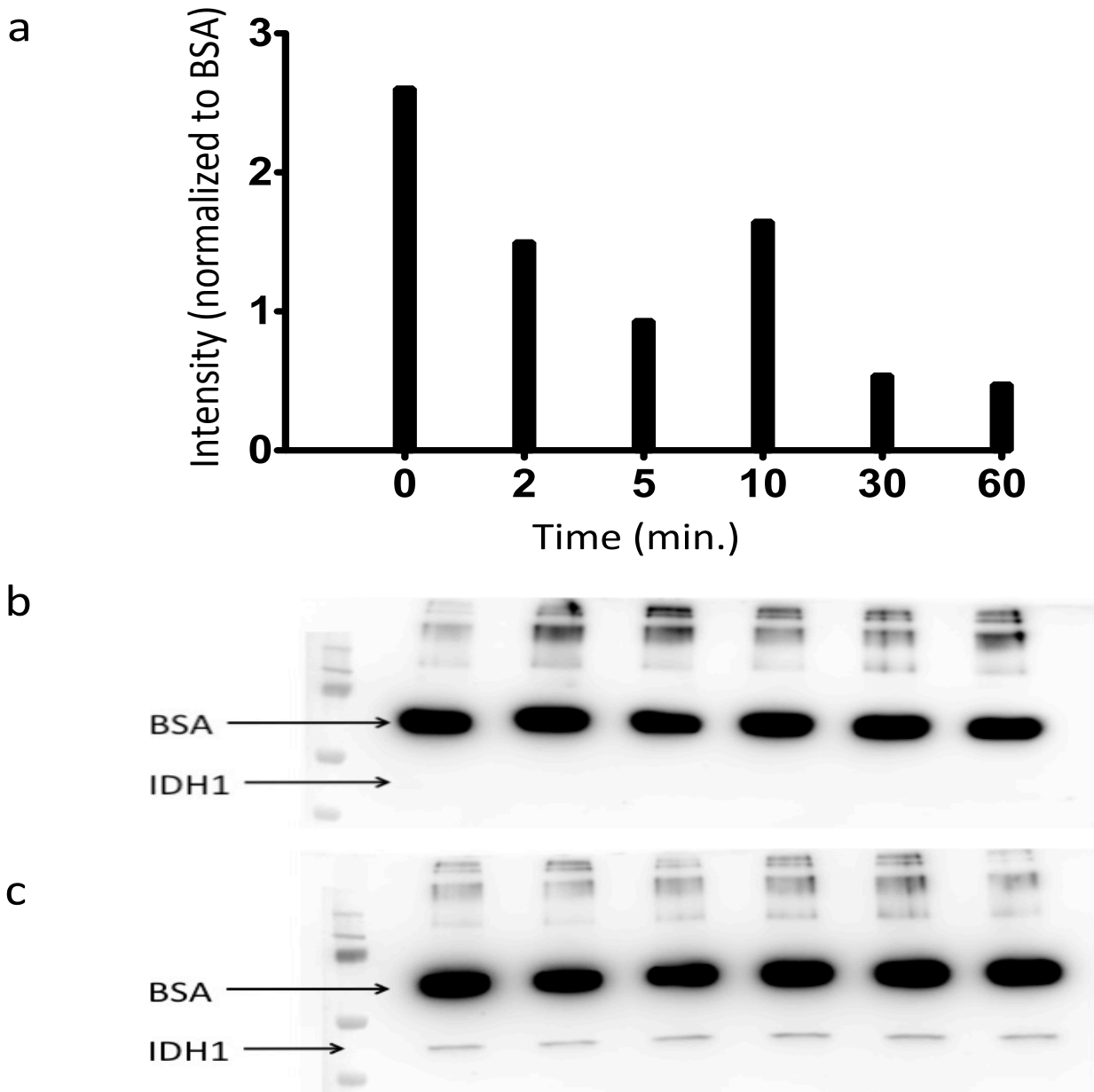
Figure 4.12: Time course of HDAC8-catalyzed deacetylation of IDH1 acetylated at either K81 or K93

A. Quantification of IDH1 K93ac (2.5 µM) deacetylation by HDAC8 (10 µM) over a one hour time course (quantified using ImageJ). Time points were quenched in 5x SDS and visualized by western blot. BSA was used as an internal standard, and all quantification was normalized to BSA. By one hour, IDH1 K93ac was more than 80% deacetylated. B. IDH1 K81ac incubated with HDAC8 (15 µM) for one hour. The western blot was probed with anti-acetyllysine and anti-BSA antibodies. IDH1 and BSA bands are separated and labeled on the blot. No IDH1 K81ac is seen at any time point, including the zero time. This is in contrast to a no-HDAC control reaction (C) with IDH1 K81ac that does show acetylated IDH1 through all time points. This result is consistent with some level of HDAC8 catalytic activity remaining in our 5x SDS quenches.

137
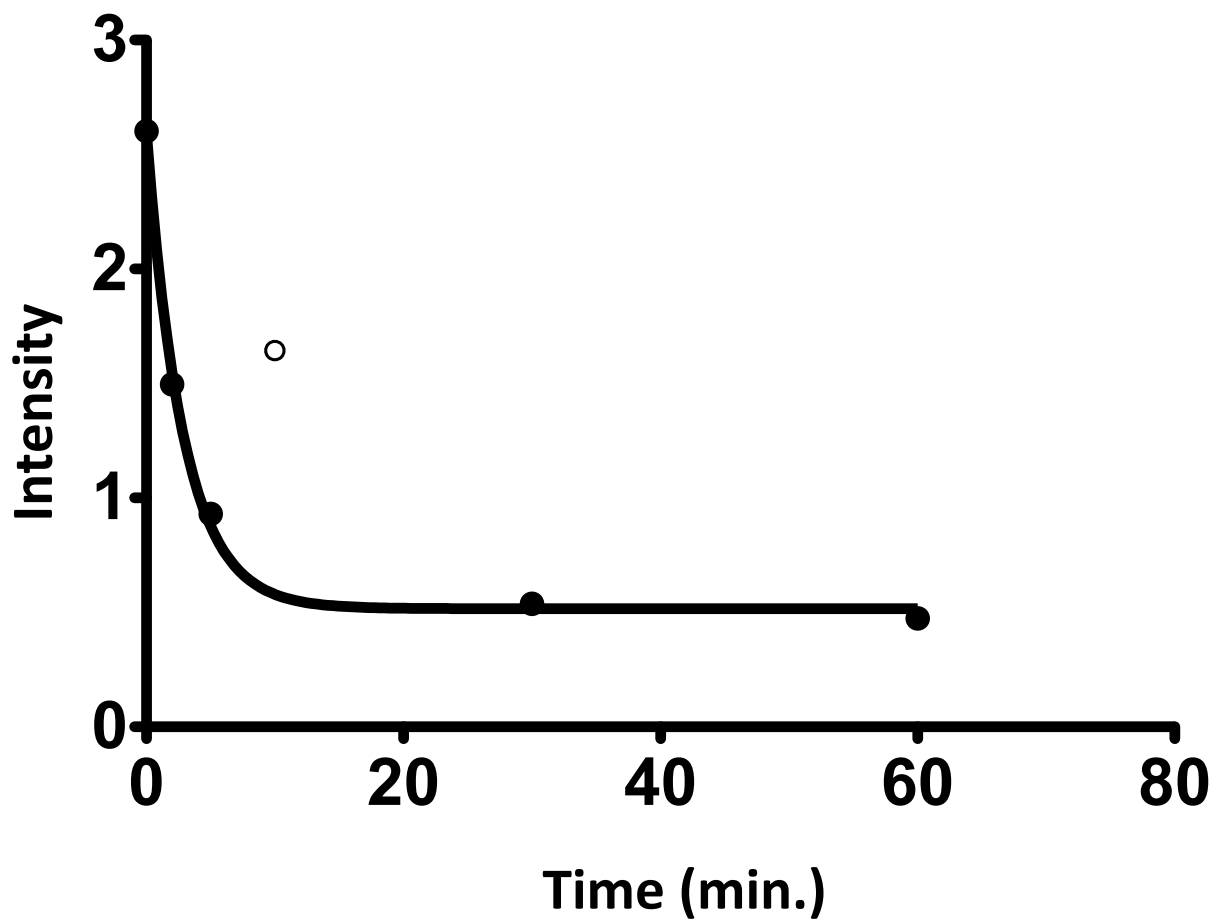
Figure 4.13: Analysis of HDAC8 deacetylation of IDH1 K93ac

HDAC8 (10 μM) catalyzed deacetylation of IDH1 K93ac (2.5 μM), as described in Figure 4.12A legend. The loss of substrate (Y axis) over time is shown here, fit with a single exponential. We determined the k_{obs} = 0.35 min^{-1}. One point (10 minutes, open circle) was determined to be an outlier to this data, based on a Grubb's test with a p < 0.05 cutoff.
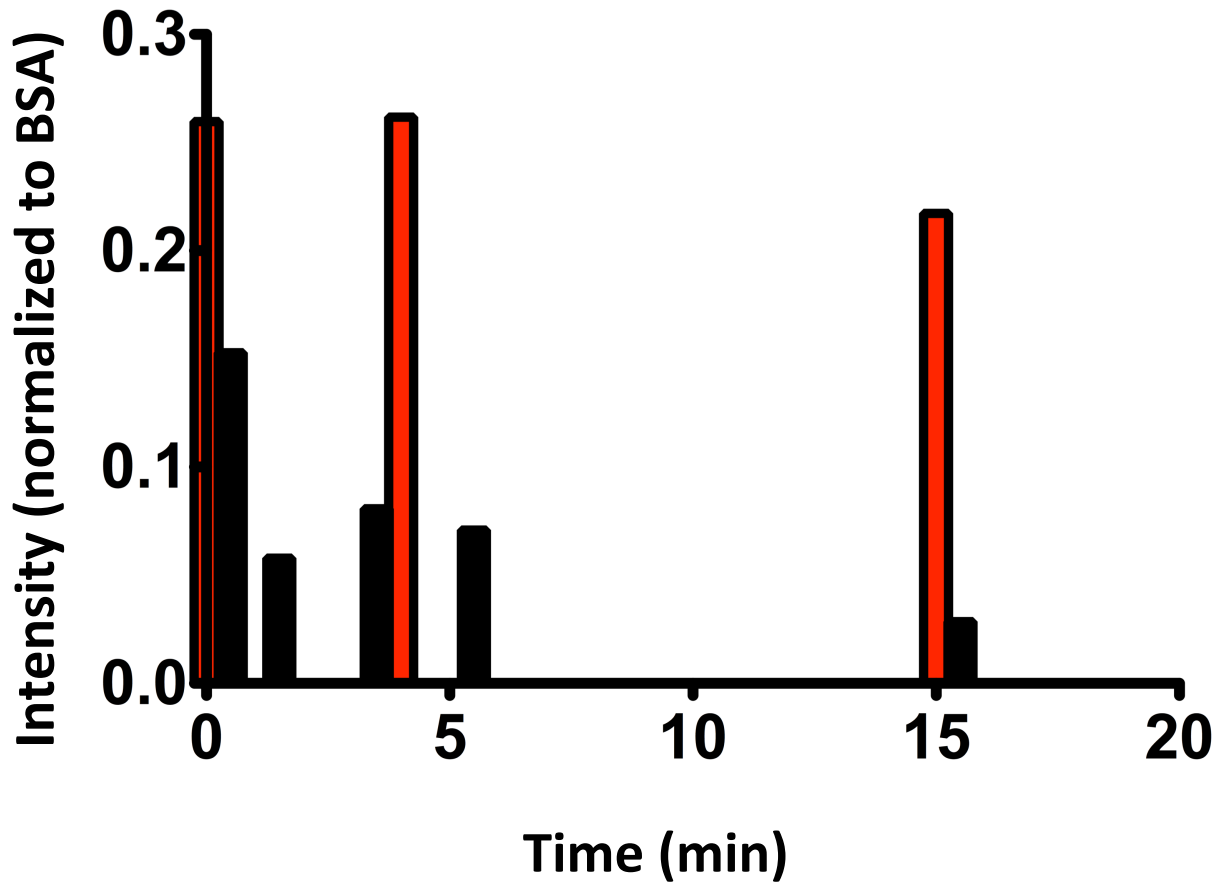
Figure 4.14: Quenching HDAC8 deacetylase activity toward IDH1 K81ac with SAHA

Quantification of IDH1 K81ac after incubation with single-turn over concentrations of HDAC8 (black bars) or with 1x buffer control (red bars). Quantification is normalized to an internal BSA standard. Acetylation of IDH1 K81 decreased to less than 20% of the starting value over 15 minutes, while the no-HDAC control reaction remained above 80% of the starting value over the same time course.

Acetylation inhibits IDH1 activity

To investigate the potential biological effects of acetylation on IDH1 activity, we assayed WT and mutant IDH1 (Table 4.4). Briefly, we used assay conditions of 75 µM NADP$^+$ and 200 µM isocitrate, both above their published K_M values([104]). We found that IDH1 K81ac showed no activity at the concentration tested, and was at least 25-fold less active than wild-type enzyme (Fig. 4.15). Due to limitations in the amount of IDH1 K81 we had available, we were unable to test higher concentrations to get a more accurate sense of the inactivation caused by acetylation at this site. IDH1 K93 and K321 both showed no activity at the concentrations tested (Fig 4.15 and Fig 4.16). IDH1 K224 is the only acetylation mutant to show activity (Fig. 4.16). It is reduced about 650-fold from wild-type IDH1 under the circumstances tested.

Table 4.4: IDH1 catalytic activity change with acetylation

IDH1 mutant	Fold decrease from WT
K81ac	> 25
K93ac	> 5000
K224ac	650
K321ac	> 2500
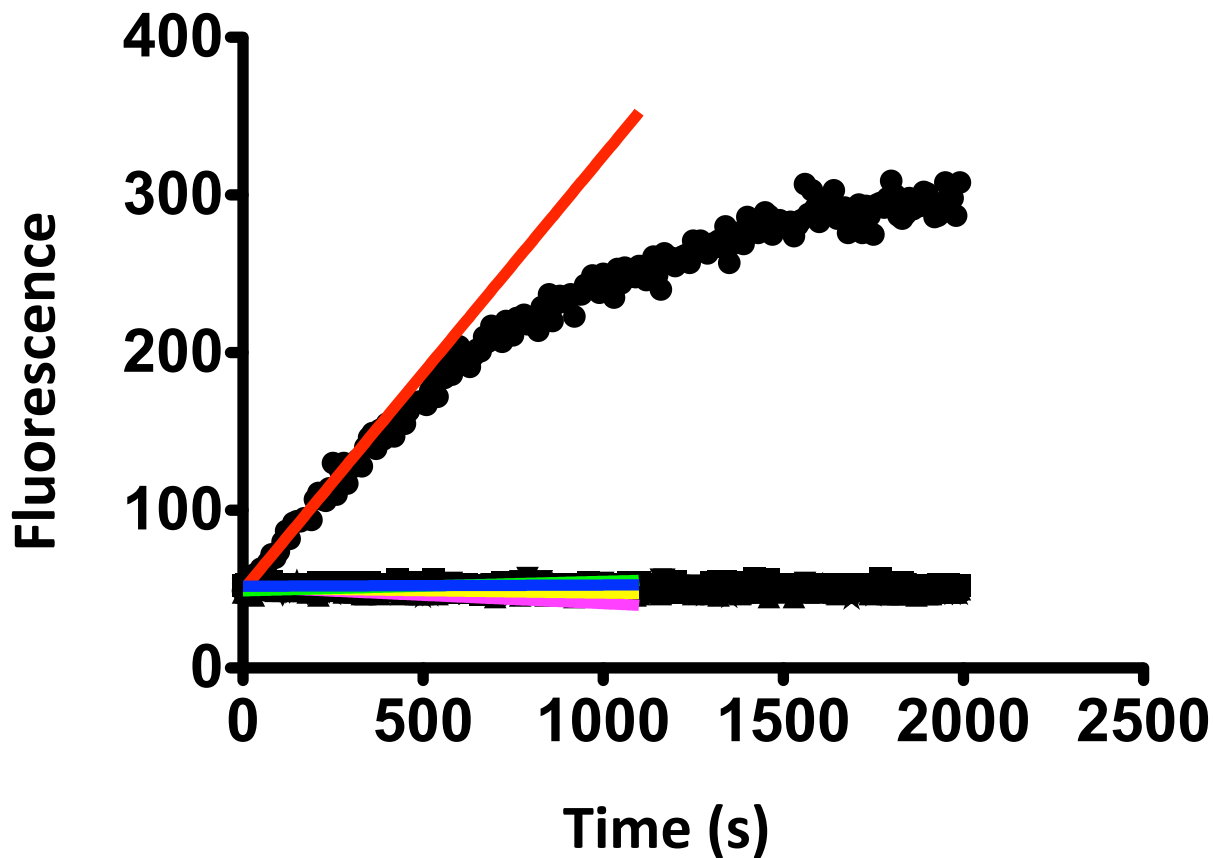
Figure 4.15: Progress curves for WT and Acetylated IDH1

IDH1 was assayed using 75 µM NADPH and 200 µM isocitrate. Progress was determined by measuring fluorescence of the NADP+ reaction product. IDH1 variants were assayed at the following concentrations: Wild-type (red) at 20 nM, K81ac (blue) at 40 nM, K93ac (green) at 20 nM, K224ac (purple) at 20 nM, and K321ac (yellow) at 20 nM. No activity was observed for acetylated IDH1 at the concentrations tested.
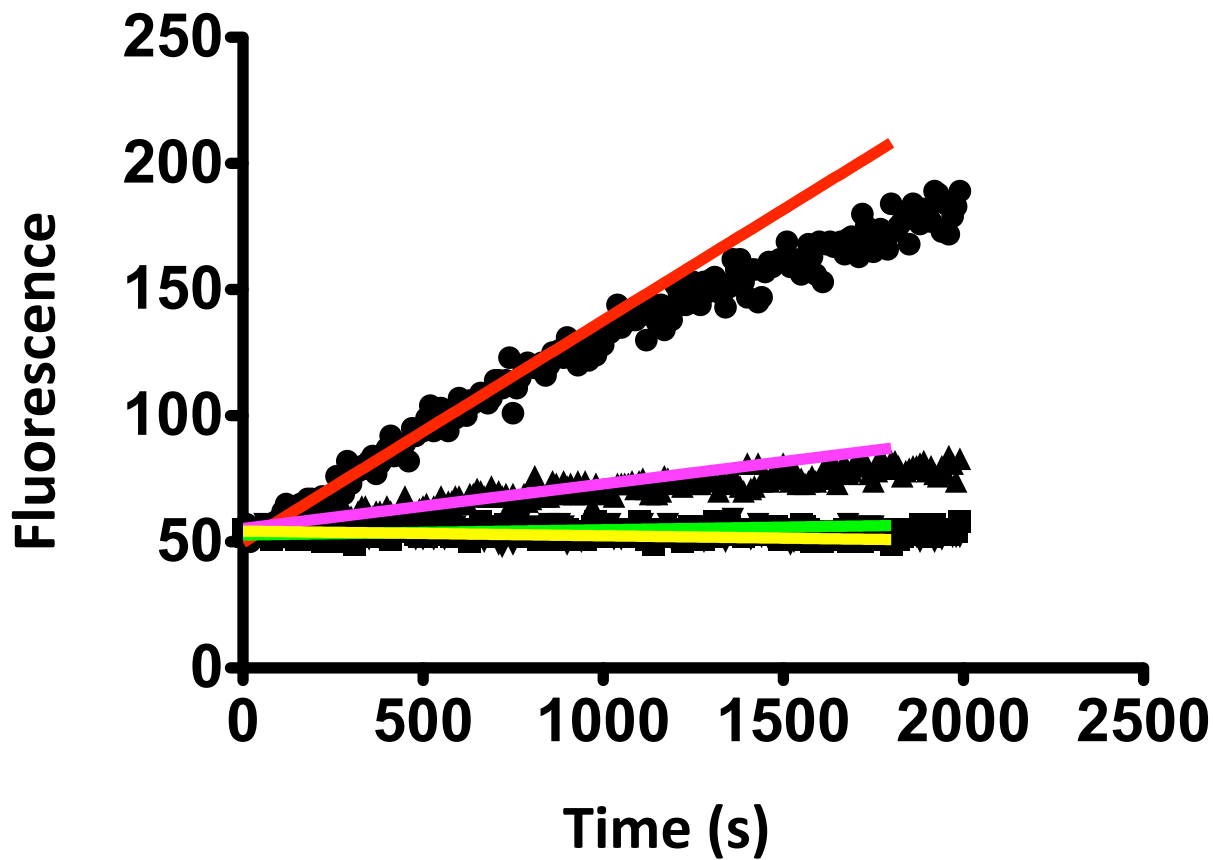
Figure 4.16: Progress curves for acetylated IDH1 at elevated concentrations

Acetylated IDH1 activity was assayed at the higher concentrations. Concentrations of NADPH and isocitrate remained 75 µM and 200 µM, respectively. IDH1 WT (red) was lowered to 10 nM. K93ac (green) was assayed at 150 nM, K224ac (purple) at 1 µM, and K321ac (yellow) at 500 nM. Only K224ac had measurable activity.

Discussion

Using a chip-based proteomics method, we have identified 44 proteins that were deacetylated by HDAC8 on the chips and 25 that were deacetylated by HDAC11. Of the 44 proteins deacetylated by HDAC8, 22 have documented acetyllysine sites in literature. Likewise, for the 25 HDAC11 hits, 14 have documented acetyllysine sites. Based on these findings, we measured HDAC8 and HDAC11 catalyzed deacetylation of peptides corresponding these proteins and found that the rate constant k_{cat}/K_M ranged from 10^0 – 10^2 $M^{-1}s^{-1}$ for both HDAC isozymes.

Of the novel HDAC8 hits that we continued to test *in vitro*, IDH1 was among the most interesting putative substrates. IDH1 has 4 known acetylation sites, one of which corresponded to one of our best HDAC8 peptide substrates. HDAC8-catalyzed deacetylation of peptides corresponding to these sites had k_{cat}/K_M values ranging from < 10 $M^{-1}s^{-1}$ to > 150 $M^{-1}s^{-1}$. IDH is a family of proteins, (IDH1, 2, and 3) involved in the decarboxylation of citric acid. These enzymes require either NADP+ (IDH1, IDH2) or NAD+ (IDH3) as a cofactor (*105*, *106*). Additionally, IDH2 and IDH3 are mitochondrial proteins (*106*), while IDH1 is cytosolic (*105*). IDH1 mutations have been linked to gliobastomas (*104*), with more than 80% of secondary glioblastoma patients testing positive for these mutations (*107*).

We continued investigating the role of HDAC8 catalysis on the deacetylation of IDH1 by expressing four different singly acetylated mutants. Our data is consistent with the hypothesis that HDAC8 does catalyze deacetylation of this protein, from a substrate prediction algorithm to *in vitro* activity with peptides to activity with purified, singly acetylated full-length IDH1. Additionally, we show that deacetylation is not uniform across

all four acetyllysine mutants; HDAC8 has specificity for select sites on the protein. This marks the first time a singly acetylated non-histone protein has been deacetylated by HDAC8 *in vitro*.

While IDH1-acetylation has been documented, the functional role of this modification is not yet understood. We sought to address this question by assaying acetylated IDH1 mutants in comparison to WT-enzyme. Interestingly, we found that acetylation significantly decreases IDH1 activity, with some acetylation sites having greater than 10^3 fold loss of activity. The only IDH1 variant with measurable activity was acetylated at K224, but activity loss was in the range of 650-fold. These observations are in agreement with the observed inactivation of acetylated IDH2 (*108*). Upon addition of HDAC8 to IDH1-K224ac, we did not see an increase in IDH1 activity. We hypothesized that this could be due to a protein-protein interaction between IDH1 and HDAC8. Upon addition of saturating SAHA, we observe a moderate recovery of IDH1 activity. Addition of HDAC8 to WT-IDH1 also yields a decrease in IDH1 activity, consistent with our protein-protein interaction hypothesis.

Understanding the role of each HDAC isozyme is crucial for understanding and developing potent and selective therapeutics, and the acetylation field has developed methods identify putative HDAC-substrate pairs. The majority of data on this topic comes from pull-down experiments or analysis of proteins after treating cells with an HDAC inhibitor. A recent study identifying protein-protein interactions, established via immunoaffinity purification of eGFP tagged HDACs, identified dozens of proteins that interact with specific HDAC isozymes (*40*). These included 15 proteins that pulled down with HDAC8 and 124 proteins that pulled down with HDAC11. These HDAC8 proteins

included members of the structural maintenance of chromosomes (SMC) family, among others. The HDAC11 hits represented proteins from a large diversity of both function and localization, highlighting possible roles in chromatin modification and gene expression, as well as RNA editing. It is of note, though, that this method looks for stable protein-protein interactions. It does not bias the result toward substrate proteins, and there is no requirement that the proteins identified must undergo any change in acetylation. Indeed, one could imagine that potentially transient interactions between HDAC8 and its substrates might not be seen.

A subsequent study, from Ed Holson at the Broad Institute, utilized a mass spectrometric approach to identify putative HDAC8 substrates (*61*). Here, researchers treated cells with an HDAC8-specific inhibitor and utilized a SILAC approach to identify changes in protein acetylation. This approach identified several additional putative HDAC8 substrates, as well as a few proteins that were very near the arbitrary cutoffs used. The only overlapping protein between this method and the immunoaffinity purification was SMC3. This technique requires that identified proteins must undergo a change in acetylation between control and treated cells, that the acetylated peptides pulldown with anti-acetyllysine antibodies, and that they are in sufficient concentration to be identified by mass spectrometric analysis. It does not, however, require that acetylation changes are a direct effect of HDAC8 inhibition. Downstream effects would likely have introduced false positives into the results. Subsequent *in vitro* analysis of peptides based on these hits showed that ARID1A and CSRP2BP were the strongest substrate candidates (*61*).

The method outlined here is based on the HDAC-catalyzed deacetylation of purified full-length human proteins. These proteins are immobilized, in duplicate, in a microarray

format on a functionalized glass surface. We incubated this proteome library with a KAT protein, p300, to acetylate chip-based proteins. This introduces perhaps the most significant limitation of this assay. Acetylation by p300 is required for a protein in our assay to then be deacetylated by an HDAC. To reduce the impact of this limitation, we chose to use a p300 construct containing the acetyltransferase domain but lacking the specificity domain, and supplied excess acetyl-CoA to the acetyltransferase reaction.

This setup allows for the *in vitro* assaying of thousands of proteins simultaneously. Any HDAC isozyme can be incubated with the acetylated chips to measured deacetylase activity. Visualization of acetylation and deacetylation is based on reactivity of protein acetyllysine sites with an anti-acetyllysine antibody. This, as was also the case with the SILAC method, requires that the antibody recognizes these sites. This technique does not select for proteins based on their tendency to complex or pull down with HDACs, nor does it identify downstream effects of HDAC catalysis.

Of the 15 proteins identified via eGFP-HDAC8 immunoprecipitation, only one of these proteins was marked as acetylated on our proteome chips. This protein, gamma-adducin (ADD3), is involved in cytoskeleton assembly (*109*). It was identified as deacetylated by HDAC8 in one of the three methods used to evaluate HDAC8 hits on the chips, but failed to meet the criteria in our other analysis methodology. It was a requirement in choosing our top HDAC8 hits that they be identified by at least two methods. For this reason, it was not marked as an HDAC8 hit. Additionally, at the time of this document, ADD3 had no acetylation sites scored by FlexPepBind. However, due to its appearance in multiple approaches, ADD3 should be kept in mind as a potential HDAC8 substrate.

From the handful of proteins identified by the SILAC method, only one of the targets was acetylated on the proteome chips, CSRP2BP. Additionally, treacle protein (TCOF1), which met the thresholds for acetylation change in their study but was considered insignificant (p = 0.05 instead of p < 0.05), was acetylated on our proteome chips. CSRP2BP is a member of the acetyltransferase complex ATAC, and has weak acetyltransferase activity itself (*110*). Like ADD3, CSRP2BP was identified in only one of the three methods used to select HDAC8 hits from our proteome experiment. A scan of known acetylation sites through FlexPepBind does show that CSRP2BP has three acetylation sites that score < -16.5, suggesting that they may be good substrates *in vitro*. The second protein, TCOF1, is known for its role as the host gene for mutations leading to Treacher Collins Syndrome. TCOF1 is believed to undergo extensive post-translational modification (*111*), and is involved in ribosomal biogenesis (*112*). TOCF1 was deacetylated on HDAC8 proteome chips, and was identified as a top-scoring hit. This protein also has several acetylation sites, some of which are predicted by FlexPepBind to be good HDAC8 substrates. A peptide from this protein (peptide #189 in Table 4.2) was among the top scoring peptides from the proteome chip experiments.

As mentioned, the immunoaffinity purification method was also used to identify proteins that associate with HDAC11 (*40*). Of the 124 proteins identified, 4 were acetylated on the proteome chips. Of those four, 3 were identified as deacetylated on our HDAC11-treated proteome chips. These were CCAAT/enhancer-binding protein zeta (CEBPZ), DnaJ homolog subfamily B member 2 (DNAJB2), and an uncharacterized protein (C2orf47). Two of these three proteins had known acetylation sites, CEBPZ and C2orf47. CEBPZ stimulates a transcriptional promoter for HSP70 (*113*). While acetylation of CEBPZ has been seen

across multiple studies (*86*, *114*), the role of this modification is not yet understood. C2orf47 is an uncharacterized protein. While it is expressed in the cytoplasm, according to the Human Protein Atlas, it appears to localize to the mitochondria. Analysis by TargetP's prediction server also suggests the presence of a mitochondrial localization peptide. This distinction, between expressed in the mitochondria vs. localized in the mitochondria, is important. Evidence suggests HDAC11 is present in both the nucleus and the cytoplasm (*24*, *40*, *115*), but there is no record of HDAC11 in the mitochondria. So while C2orf47 may localize to the mitochondria, the potential for modification exists before this protein reaches that final location.

Taken together, there were three proteins that were acetylated on the proteome chips and also identified as potential HDAC8 substrates in published literature. All three of these proteins were identified as deacetylated in at least one of the analysis methods used on our chips. One of the three was identified by multiple analysis methods, and upon *in vitro* peptide testing it was shown that a peptide representing an acetyllysine from this protein, TCOF1, was turned over by HDAC8. Additionally, of the 4 proteins that were acetylated on our chips and previously identified as interacting partners with HDAC11, three were also deacetylated by HDAC11 in our chip experiments. Two of these had known acetylation sites, and we found that peptides from both proteins were turned over by HDAC11 in subsequent *in vitro* testing. These results bolstered our confidence in the multitude of novel protein targets identified using this new on-chip proteomics method.

In summary, we have shown that HDAC deacetylase activity from multiple isozymes can be observed with proteins immobilized on a proteome chip microarray. This data set has led to the identification of several new putative substrates for both HDACs 8 and 11.

Using an *in vitro* enzyme-coupled assay, we have verified HDAC activity against several peptides corresponding to these proteins. Finally, we have shown that HDAC8 can deacetylate recombinantly expressed and purified singly-acetylated IDH1 *in vitro*, marking a first for the HDAC field. We hope the techniques presented here will continue to be applied, in conjunction with current methods, to additional HDAC isozymes to further our understanding of this family of enzymes.

Chapter 5

Dual-Mode HDAC Prodrug for Covalent Modification and Subsequent Inhibitor

Release[15,16]

Introduction

Transcription is a tightly regulated biological process that is the first step in gene expression (*19*, *116*, *117*). In eukaryotic cells, sequence- specific DNA binding factors control the flow of genetic information from DNA to RNA, thereby regulating transcription. In cells, DNA is tightly compacted into chromatin, a highly organized and dynamic complex between DNA and proteins. When gene transcription is activated, the DNA is made accessible to transcription factors via nucleosome modification (*19*, *116*) The local architecture of chromatin, which is influenced by post-translational modifications of histones, can regulate gene expression. These modifications include methylation, phosphorylation, and acetylation of core histones. Histone acetylation occurs at the ε-amino groups of conserved lysine residues near the N-termini. Acetylation levels of core histones are a result of the balance between histone acetyltransferases (HATs) and histone deacetylases (HDACs) (*19*, *116–118*) Increased levels of histone acetylation are generally

associated with transcriptional activity, whereas decreased levels of histone acetylation are associated with repression of transcription. Additionally, acetylation of specific lysines on histone tails facilitates the recruitment of bromodomain-containing chromatin remodeling factors (*119*, *120*) Furthermore, acetylated lysines have been observed in many cellular proteins, indicating that HATs and HDACs do not function solely to modify histones (*86*) Histone deacetylase inhibitors (HDACi) have been developed as a class of therapeutic agents intended to target aberrant epigenetic states associated with a variety of pathologies, most notably cancer (*121*) Recent findings have shown that the relief of oncogenic transcriptional repressors by HDACi can lead to cell cycle arrest and apoptosis (*19*, *116–118*) This is because many cancers have evolved such that pro-apoptotic pathways are transcriptionally repressed via histone deacetylation. HDACi prevent deacetylation of the lysine residues of the histone tails, which, in turn, leads to transcriptional activation, gene expression, and cell death (*19*, *121*)

The development of HDACi has been ongoing, and >10 candidates have progressed to clinical trials (*117*) HDACi can be subdivided into structural classes including hydroxamic acids, cyclic peptides, aliphatic acids, and benzamides (*122*) The HDACi Vorinostat (suberoylanilide hydroxamic acid, SAHA) received approval by the United States Food and Drug Administration (FDA) in 2006 for the treatment of cutaneous T-cell lymphoma (CTCL) (*123*) Crystallization of SAHA with HDAC8 supported a model involving the linkage of a metal-binding pharmacophore (MBP) to a capping group designed to form favorable interactions with amino acid residues at the entrance to the active site tunnel (Figure 5.1a) (*124*) Three other HDACi have been approved by the FDA, including Panobinostat and Belinostat, both broad-spectrum, hydroxamate-based HDACi for the

treatment of multiple myeloma or relapsed/refractory peripheral T-cell lymphoma, respectively (Figure 5.1a) (*125*, *126*) Romidepsin (FK228), a cyclic peptide HDACi that uses a thiol group to coordinate the active site metal ion, is approved for CTCL treatment (Figure 5.1a) (*123*)

SAHA, Romidepsin, and Panobinostat act to inhibit most isoforms of the metal-dependent HDAC family and are regarded as broad-spectrum HDAC inhibitors. Despite promising clinical results for HDACi, these drugs have not been effective in clinical trials involving solid tumors. In fact, these FDA-approved drugs have been associated with the onset of serious side effects, including fatigue, gastrointestinal issues (diarrhea, nausea, vomiting), and hematologic complications (thrombocytopenia, anemia, neutropenia) (*121*, *123*) Both SAHA and Romidepsin have also been associated with cardiotoxicity(*121*) Clinical studies in humans determined the major metabolic pathways of SAHA degradation involve glucoronidation by UDP-glucoronosyltransferases (UGTs) to generate inactive 1 (Figure 5.1b). Alternatively, hydrolysis of SAHA to the carboxylic acid analogue (2) followed by β-oxidation generates the inactive metabolite 4-anilino-4-oxobutanoic acid (3, Figure 5.1b) (*123*, *127*) Clinical studies determined that the mean steady-state serum exposures of 1 and 2 were 4- and 13-fold higher than SAHA, respectively. Additionally, the apparent $t_{1/2}$ of SAHA in human serum was ~1.5 h for patients receiving single doses of 400 mg of SAHA (*121*, *123*, *127*) The poor pharmacokinetic (PK) properties of SAHA are similar for other hydroxamic acid-based compounds and involve chemical instability and rapid elimination (*121*, *128*) In fact, the FDA has approved SAHA for CTCL only in patients with persistent or recurrent disease who have already followed two systemic therapies (*121*) Similarly, the FDA has only approved Romidepsin for CTCL treatment in patients who have

received at least one prior systemic therapy, and Panobinostat is administered only after two prior standard therapies have failed (*129*) The onset of these deleterious side effects is proposed to originate, in part, from the lack of selectivity of these drugs for a specific HDAC isozyme (*121*)
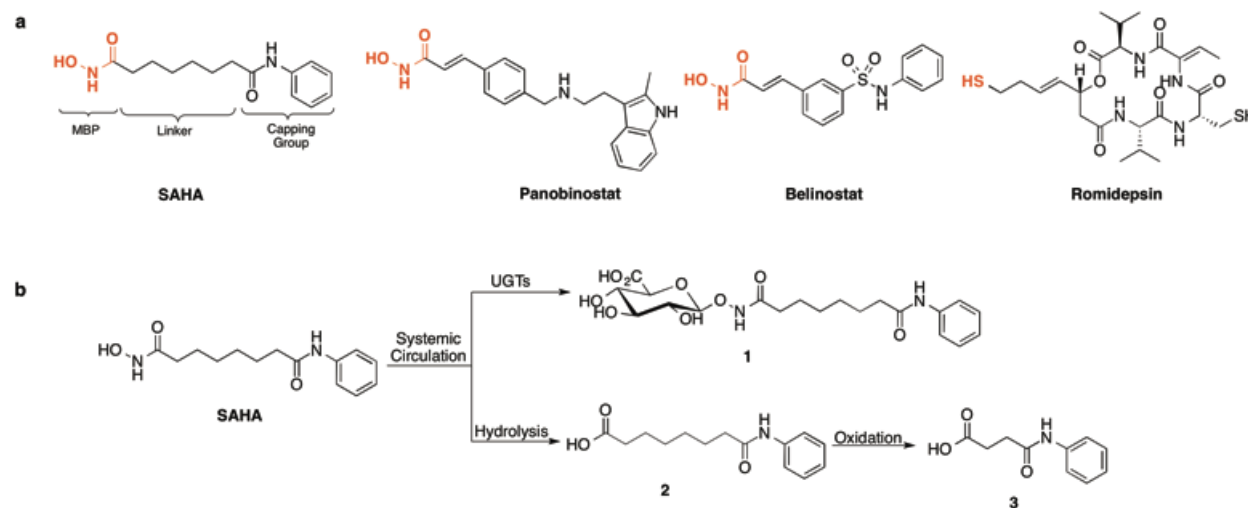
Figure 5.1: FDA-approved HDAC inhibitors.

(A) The hydroaxamic acid and sulfhydryl MBP donor atoms of SAHA, Panobinostat, and Romidepsin are shown in red. (B) Metabolism of SAHA. Upon systemic circulatin, UGT enzymes localized in the liver can convert SAHA to a SAHA b-D-glucuronide (1), rendering the drug inactive. A different pathway involves initial hydrolysis of SAHA to the corresponding carboxylic acid (2), followed by oxidation to 3.

Chemically modified versions of active drugs have been developed in an effort to overcome barriers to drug formulation and delivery. The modified, latent version of the drug, termed the prodrug, undergoes a transformation in the presence of a desired chemical or enzymatic stimulus *in vivo* to generate the active agent (*130*, *131*) The chemical group appended to the active drug rendering it inactive is termed the promoiety. Only a handful of reports have investigated HDAC prodrugs, with most studies focused on developing acyl derivatives of SAHA or similar hydroxamic acid-based HDACi to enhance

cell permeability and hydrolytic stability (*132*). As expected, these prodrugs showed little activity as HDAC inhibitors, and biochemical assays suggest that the acylated prodrugs are more cell-permeable than the hydroxamic acid parent drugs. A similar report investigated a carbamate prodrug concept for hydroxamate HDACi (including SAHA) to improve drug-like properties, including cellular permeability (*133*). However, both of these strategies rely on hydrolysis *in vivo* to release the active drug and do not improve drug–target specificity for selected disease states or sites of disease.

Initially, we sought to develop new HDAC inhibitor prodrugs (proinhibitors) that become activated in the presence of thiols such as glutathione in its reduced form (GSH), which is frequently more abundant at the site of disease (e.g., cancer) (*134*). Previously, Huang and co-workers reported the development of a long-wavelength fluorescent probe involving a quinone-methide reaction that can detect physiologically relevant thiols including GSH (*135*). Although the quinone promoiety functions as an electrophilic Michael acceptor, it was determined that other biologically relevant nucleophiles, including serine and lysine, were unreactive with this functionality. Our prodrug approach considered the covalent appendage of this quinone promoiety to the hydroxamate of an HDACi, since the alkylation of hydroxamates has been shown to be effective in improving PK properties including hydrolytic stability, cellular permeability, and glucoronidation (*132*, *136*, *137*).

As described below, even in the absence of nucleophilic thiols, we observed activation of our prodrug (SAHA-TAP); sequence homology analysis revealed that a single cysteine (Cys) residue is conserved in all metal-dependent HDAC isoforms, which we found was reactive with our prodrug (Appendix 2, Figure S1) (*138*). The crystal structure of HDAC8 complexed with SAHA reveals that the conserved Cys (Cys153 for HDAC8) is

located in the catalytic active site pocket ~5.6 Å away from the hydroxamic acid moiety of

SAHA (Figure 5.2). Thus, we have concluded that our prodrug is cleaved by the sulfhydryl

moiety of the conserved Cys of HDAC, leading to drug activation and a dual mode of

inhibition: covalent modification of the conserved Cys leading to the formation of an

inactive, covalently modified enzyme and release of the competitive inhibitor SAHA.
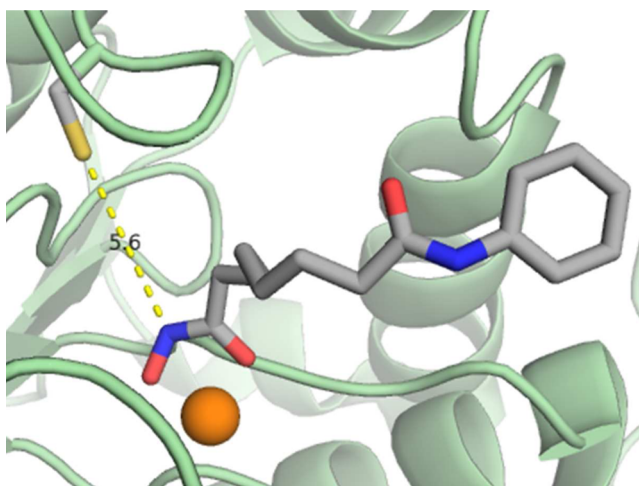
Figure 5.2: Protein crystal structure of HDAC8 complexed with SAHA.

The distance between the sulfhydryl moiety of Cys153 and the nitrogen atom of the MBP of SAHA was determined to be 5.6 Å. SAHA and Cys153 are shown as sticks in color code (carbon, gray; nitrogen, blue; oxygen, red; sulfur, yellow), and the Zn^{2+} ion is shown as an orange sphere (PDB: 1T69).

Results and Discussion

Development of a Unique HDACi Prodrug.

SAHA was chosen as the drug of interest because it is FDA-approved for the treatment of CTCL and has been well-studied. A prodrug of SAHA containing a quinone-based, thiol-sensitive promoiety was designed, termed SAHA-TAP (TAP, thiol activated prodrug) (Figure 5.3). To develop SAHA-TAP, the promoiety was first synthesized using a modified literature procedure (*135*). The promoiety was appended to SAHA under basic conditions to generate SAHA-TAP. The activation of SAHA-TAP by reaction with GSH is summarized in Figure 5.3a. A control compound, SAHA-OBn, was synthesized in a similar manner. This compound contains a benzyl moiety appended to SAHA via the N-hydroxyl functionality. SAHA-OBn was designed to have a similar structure as that of SAHA-TAP but to be unreactive toward nucleophilic thiols.

Assessment of SAHA-TAP Reactivity with GSH.

To evaluate the reactivity of SAHA-TAP and SAHA-OBn with nucelophilic thiols, analytical HPLC was utilized under simulated physiological conditions (50 mM HEPES, pH 7.4). SAHA-TAP was treated with GSH (2 mM, 2 equiv) to confirm that the prodrug is indeed reactive with thiols. After incubation of SAHA-TAP with GSH, three distinct peaks were apparent in the HPLC chromatogram (Figure 5.3b). Liquid chromatography–mass spectrometry (LC-MS) confirms that the identity of the first peak (t_R = 10.5 min) is the quinone-methide side product, the second peak is SAHA (t_R = 10.7 min), and the third peak is unreacted SAHA-TAP (t_R = 14.7 min). Treatment of SAHA-OBn with GSH under the same conditions resulted in no change in the HPLC chromatogram, indicative of the expected lack

of reactivity (Figure 5.3c). Having shown that SAHA-TAP reacts rapidly with GSH, the aqueous stability of SAHA-TAP was evaluated under simulated physiological conditions (50 mM HEPES, pH 7.4). An HPLC chromatogram was obtained immediately after preparation in aqueous buffer, and a second trace was collected after incubation at 37 °C for 24 h. SAHA-TAP was determined to be >97% stable to hydrolysis in the absence of thiols (Appendix 2, Figure S2).
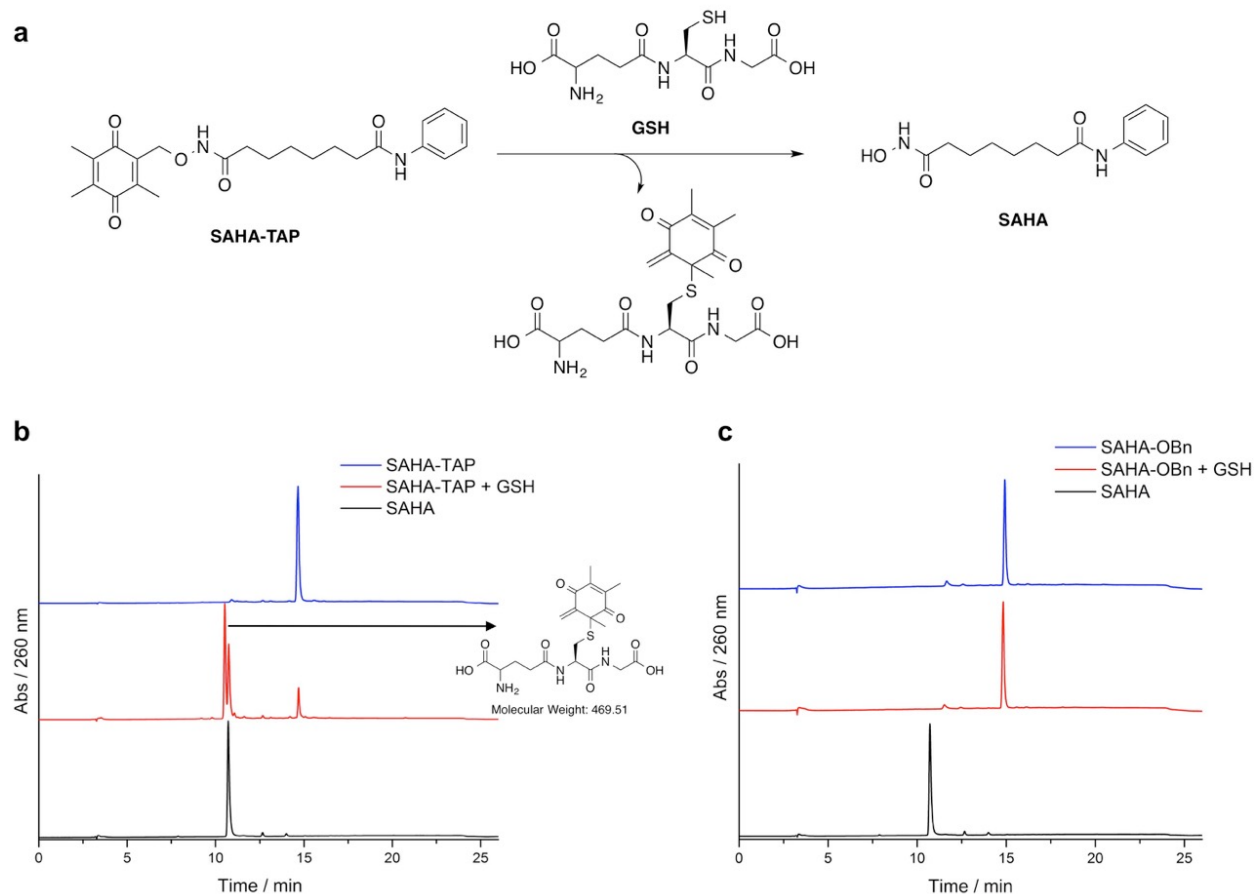
Figure 5.3: Treatment of SAHA-TAP with GSH

(A) Activation of SAHA-TAP by GSH. In the presence of GSH, the sulfhydryl moiety can attack the electrophilic quinone moiety. Subsequent rearrangement releases SAHA along with the quinone-methide adduct. (B) HPLC trace of SAHA (black), SAHA-TAP (blue), and SAHA-TAP after treatment with GSH (2 mM, 2 equiv.) for 2 h at 37°C (red). Retention times are 10.7 min. for SAHA and 14.7 min. for SAHA-TAP, and 10.5 min. for the quinone-methide GSH adduct generated from the reaction. (C) HPLC trace of SAHA (black), SAHA-OBn (blue), and SAHA-OBn after incubation in HEPES (50 mM, pH 7.4) for 24 h at 37°C (red). Retention times are 10.7 min. for SAHA and 14.9 min. for SAHA-OBn.

HDAC Inhibition by SAHA-TAP.

To determine the efficacy of the SAHA-TAP prodrug strategy, the ability of SAHA-TAP and SAHA-OBn to inhibit HDAC-1, -2, -3, -6, and -8 was evaluated using an optimized homogeneous fluorescence-based assay (BPS Bioscience). Surprisingly, even in the absence of exogenous thiols, SAHA-TAP was an effective inhibitor of all HDACs tested, with

an apparent IC$_{50}$ value that is slightly less potent (2- to 50-fold) than that of the parent

inhibitor, SAHA (Table S1). This result was unexpected because the metal-binding ability

of the hydroxamic acid MBP of SAHA-TAP is blocked by the promoiety, which should

render the drug nearly inactive. Recent studies indicate that the metal-free form of HDAC8

has a low affinity for SAHA analogues, further demonstrating the importance of metal

binding for HDAC inhibition(*139*). To determine if a component of the biochemical assay

resulted in SAHA-TAP activation, analytical HPLC was utilized. SAHA-TAP was incubated

with either BSA (5 mg/mL) or trypsin (5 mg/mL) at 37 °C for 2 h; however, SAHA-TAP was

found to be >95% stable in the presence of either of these assay components (data not

shown).

Because SAHA-TAP is a larger molecule than SAHA and the metal-binding

hydroxamate group is blocked, it is feasible that the promoiety may be positioned very

close to Cys153 when bound to HDAC8. This positioning could be ideal for nucleophilic

attack by the sulfhydryl moiety, leading to covalent modification and SAHA release. We

hypothesized that the Cys153 residue of HDAC8 reacts with bound SAHA-TAP, resulting in

a covalent modification of the protein and subsequent release of SAHA, a competitive

inhibitor (Appendix 2, Figure S3). It is important to note that there are many other Cys

residues in the metal-dependent HDAC isoforms (e.g., 10 Cys residues in HDAC8), and

activation of SAHA-TAP by these residues may also be responsible, in part, for the release

of SAHA that we observe (vide supra).

Mass Spectrometry Analysis.

To investigate whether the active site Cys153 is covalently modified by the SAHA-

TAP promoiety, mass spectrometry (MS) techniques were utilized. Digestion of wild-type (WT) HDAC8 with trypsin yields an 18 amino acid peptide containing Cys153, which can be used to monitor the modification via mass spectrometry (Figure 5.4a). If a covalent modification occurs at this position after treatment of WT HDAC8 with SAHA-TAP, then the expected MS ion for this peptide fragment will be different from the unmodified parent ion.

HDAC8 (WT, with or without incubation with a 12-fold excess of SAHA-TAP for 60 min at 37 °C) was digested with trypsin, and the resulting peptides were analyzed by LC-MS. The expected parent ion for the WT HDAC8 Cys153 peptide was consistent with a peak at t_R = 84.5 min (Figure 5.4b). Similarly, a peak at t_R = 88.5 min corresponds to the expected parent ion for the covalently modified Cys153 HDAC8 peptide after SAHA-TAP treatment (Figure 5.4c). To eliminate other digestion products that could account for this ion, further MS techniques were applied to verify that these ion peaks correspond to the peptide sequence of interest.

Tandem mass spectrometry (MS^2 or MS/MS) is routinely used in proteomics to characterize amino acid sequences of proteins, where peptides undergo further fragmentation to amino acid aggregates (*140*). The fragmentation patterns observed in the MS/MS spectra of tryptic peptides for WT HDAC8 and SAHA-TAP treated HDAC8 were investigated to obtain additional insight into the possibility of covalent modification of Cys153. The expected monoisotopic masses for the y ion series in both WT HDAC8 and the SAHA-TAP treated sample are summarized in Table S2. The expected y fragment ions for both peptides align until Cys153 (y_{12}), where this ion and each subsequent ion have different masses. Indeed, the MS/MS fragmentation spectrum for the WT HDAC8 tryptic peptide (parent ion m/z = 1006.98, $[M + 2H]^{2+}$) shows many of the expected y ions

(Appendix 2, Figure S4). Similarly, the MS/MS fragmentation spectrum for the SAHA-TAP treated HDAC8 tryptic peptide (parent ion m/z = 1059.53 [M + 2H]$^{2+}$) shows many y ions, including the characteristic peak of m/z = 1511.82 (Appendix 2, Figure S5). This peak is indicative of a covalent modification of m/z = 162.1 for the HDAC8 tryptic fragment at Cys153. These data prove that the covalent modification of Cys153 is occurring to form an adduct containing the SAHA-TAP promoiety, as shown in Appendix 2, Figure S3.

MS analysis also indicated that Cys102, Cys244, and Cys314 could be modified by the TAP moiety from SAHA-TAP. Importantly, the peptides containing surface cysteines (Cys275 and Cys352) were not modified with TAP, suggesting that activation is not nonspecific. Nonetheless, the hypothesized mechanism of activation involving a covalent modification of Cys residues in HDAC8, including Cys153, was observed, which can aid in explaining the inhibition of HDACs by SAHA- TAP even in the absence of exogenous nucleophilic thiols, as observed in the *in vitro* assays.

DEASGF**C**YLNDAVLGILR

Fragment Type	Expected Ion [M+2H]$^{2+}$
WT HDAC8	1006.98 *m/z*
SAHA-TAP treated HDAC8	1060.16 *m/z*
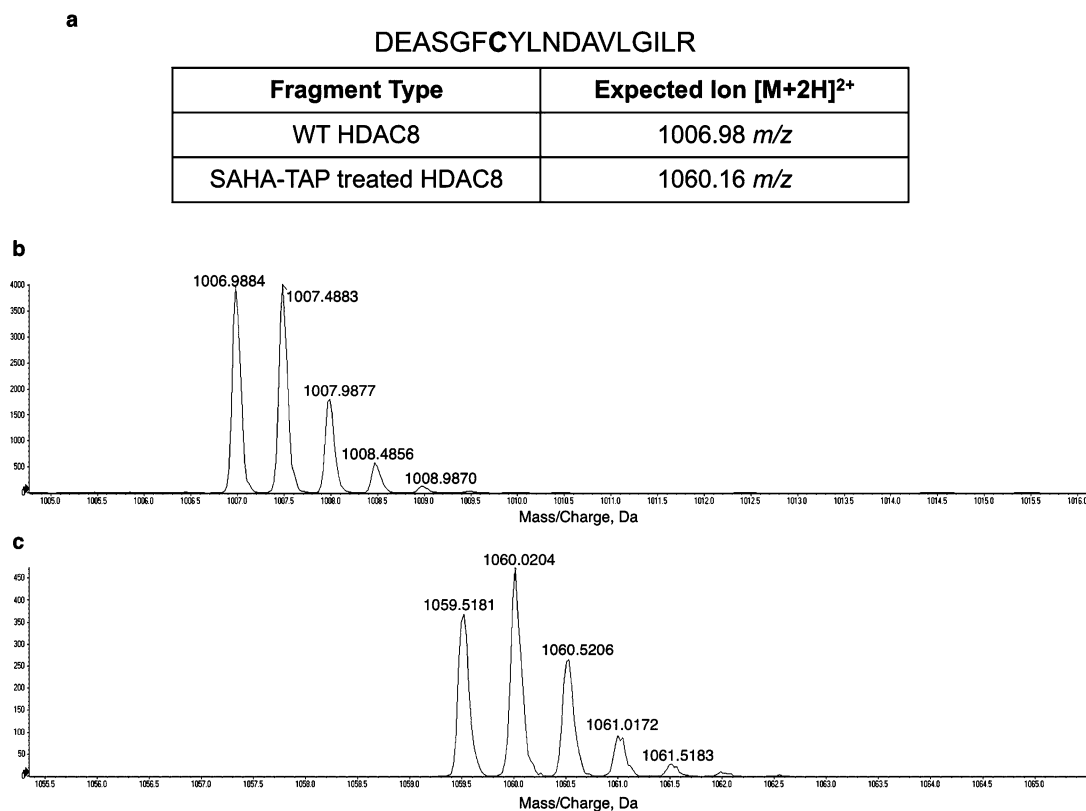
Figure 5.4: HDAC8 tryptic fragment MS data.

(A) Expected HDAC8 Cys153 peptide upon digestion with trypsin (Cys153 in bold). The expected MS ion for the WT protein is shown along with the expected ion for the peptide including the covalent addition of the TAP promoiety on Cys153. (B) The tryptic fragment of WT HDAC8 (t_R = 84.5 min) is consistent with the expected [M + 2H]$^{2+}$ ion. (C) After treatment of HDAC8 with SAHA- TAP (12 equiv) and digestion with trypsin, a peak aligning with the expected [M + 2H]$^{2+}$ ion is observed (t_R = 88.5 min).

In vitro Time Dependence of SAHA-TAP HDAC Inhibition.

With the MS data in hand confirming covalent modification of Cys residues in HDAC8, we sought to investigate the kinetics of inhibition of HDAC8 by SAHA-TAP using the Fluor-de-Lys activity assay (Enzo Life Sciences). A previous study determined that the catalytic activity and thus inhibition of HDAC8 is dependent on the identity of the active site metal ion (e.g., Co^{2+}, Fe^{2+}, Zn^{2+}, and Ni^{2+}) (*57*). To obtain the most accurate results, apo-

HDAC8 (human, recombinant) was initially prepared before the addition of Zn^{2+} in a 1:1 stoichiometry. An initial test of HDAC8 inhibition by preincubation of the enzyme with SAHA-TAP demonstrated that activity loss occurred within the first 0.5 h (data not shown). To determine the kinetics for the time-dependent inhibition by SAHA-TAP, HDAC8 progress curves were measured through a range of inhibitor concentrations (Figure 5.5). For these reactions, the Fluor-de-Lys HDAC8 substrate (150 µM) and SAHA-TAP (0−20 µM) were added to each assay prior to initiating the reactions with WT HDAC8 (0.5 µM). Over a time course, aliquots of the reactions were stopped by dilution into a solution of trichostatin A and trypsin, and product formation was analyzed from the resulting change in fluorescence. Analysis of the HDAC8 progress curves in the presence of increasing concentrations of SAHA-TAP demonstrates a nonlinear formation of product with respect to time. Equation 5.1, which describes the time-dependent decrease in initial velocity under steady-state turnover conditions ($141, 142$), was fit to the progress curves

$$P = \frac{(v_s * t) + (v_0 - v_s) * [1 - \exp(-k_{obs} * t)]}{k_{obs} + C}$$

(Equation 5.1)

where P represents production formation, v_s and v_0 represent final and initial velocities, respectively, t is time, C is the initial fluorescent ratio, and k_{obs} is the rate constant describing the transition from the initial velocity to the final steady-state velocity, reflecting the time-dependent enzyme inactivation.

This fit reveals that both the initial velocity and the rate constant for inactivation, k_{obs}, have a hyperbolic dependence on the concentration of SAHA-TAP (Figures 5.5b,c). The initial velocity decreases with an apparent $K_i = 7 \pm 4$ µM, and the rate constant for

inactivation increases with a $k_{1/2}$ = 8 ± 2 μM to a maximal rate constant of 0.0013 s^{-1} at saturating SAHA-TAP. This type of inhibition is characteristic of a two-step mechanism (Scheme 5.1) in which a rapid reversible step, such as binding of SAHA-TAP to HDAC8, is followed by a time-dependent step, consistent with irreversible inactivation (*141*, *142*). These data demonstrate that the prodrug, SAHA-TAP, is capable of binding to and inhibiting HDAC8. The time-dependent decrease in activity is consistent with the MS data demonstrating the formation of a covalent enzyme adduct.

$$\textbf{E + I} \underset{}{\overset{K_I}{\rightleftharpoons}} \textbf{E·I} \xrightarrow{k_{obs}} \textbf{E-I}$$ (Scheme 5.1)

For comparison, progress curves for inhibition of HDAC8 with the competitive inhibitor SAHA and a negative control, SAHA-OBn, were evaluated. These assays were performed in the same manner as the SAHA-TAP progress curves, where substrate and inhibitor were added to the assay prior to the addition of HDAC8 to initiate the reaction. In contrast to the data with SAHA-TAP, these progress curves are linear with no observable curvature for all concentrations of SAHA (Appendix 2, Figure S6a) and SAHA-OBn (Appendix 2, Figure S6b). As expected, HDAC8 (0.5 μM) is inhibited >90% by SAHA in the concentration range tested (2–8 μM), which is in agreement with the 250 nM K_i reported for Zn^{2+}-HDAC8. SAHA-OBn (2–10 μM) does not inhibit the activity of HDAC8. The lack of inhibition by SAHA- OBn is consistent with previous IC$_{50}$ data (Table S1). Taken together, these data show that SAHA-TAP has a unique mode of inhibition for HDAC8 when compared to SAHA. This inhibitor functions both as a competitive inhibitor and as a time-dependent inactivator, in contrast to the linear, time- independent inhibition observed for SAHA.

To determine the role of Cys153 in the time-dependent inhibition of HDAC8, a Cys153Ala (C153A) HDAC8 mutant was prepared and purified. *In vitro* assays for the mutant were conducted under the same conditions used for WT HDAC8. Progress curves for these assays reveal dose-responsive inhibition with K_i = 8 ± 4 μM for SAHA-TAP (Figures 5.5d and Appendix 2, Figure S7). Furthermore, these progress curves are linear for all concentrations of inhibitor, showing a loss of the time-dependent inhibition observed with WT HDAC8. This data suggests that SAHA-TAP, containing the same linker spacer and capping group as SAHA, can bind HDAC8 in a noncovalent manner, inhibiting the enzyme (Scheme 5.1). The linear progress curves also demonstrate that Cys153 is important for the time-dependent inactivation, eliminating an alternate explanation that the time-dependent inhibition is due to the slow formation of SAHA from SAHA-TAP. Progress curves with C153A HDAC8 measured with SAHA and SAHA-OBn data reveal that the HDAC8 mutant remains susceptible to inhibition by SAHA and not SAHA-OBn (Appendix 2, Figure S8).

Collectively, these data indicate both that SAHA-TAP binds noncovalently to HDAC8 to inhibit the activity and that the time-dependence mainly reflects the reaction of SAHA-TAP with Cys153. Although the MS data suggests that SAHA-TAP can react with other Cys residues in HDAC8, leading to SAHA release, C153A HDAC8 is not inactivated in a time-dependent manner, demonstrating the importance of this particular Cys in the mechanism of inhibition for the WT enzyme. The combination of the enzyme kinetics and MS data provides evidence that the inactivation of HDAC8 by SAHA-TAP involves two steps: noncovalent binding of SAHA-TAP to HDAC8 followed by covalent modification of Cys153.
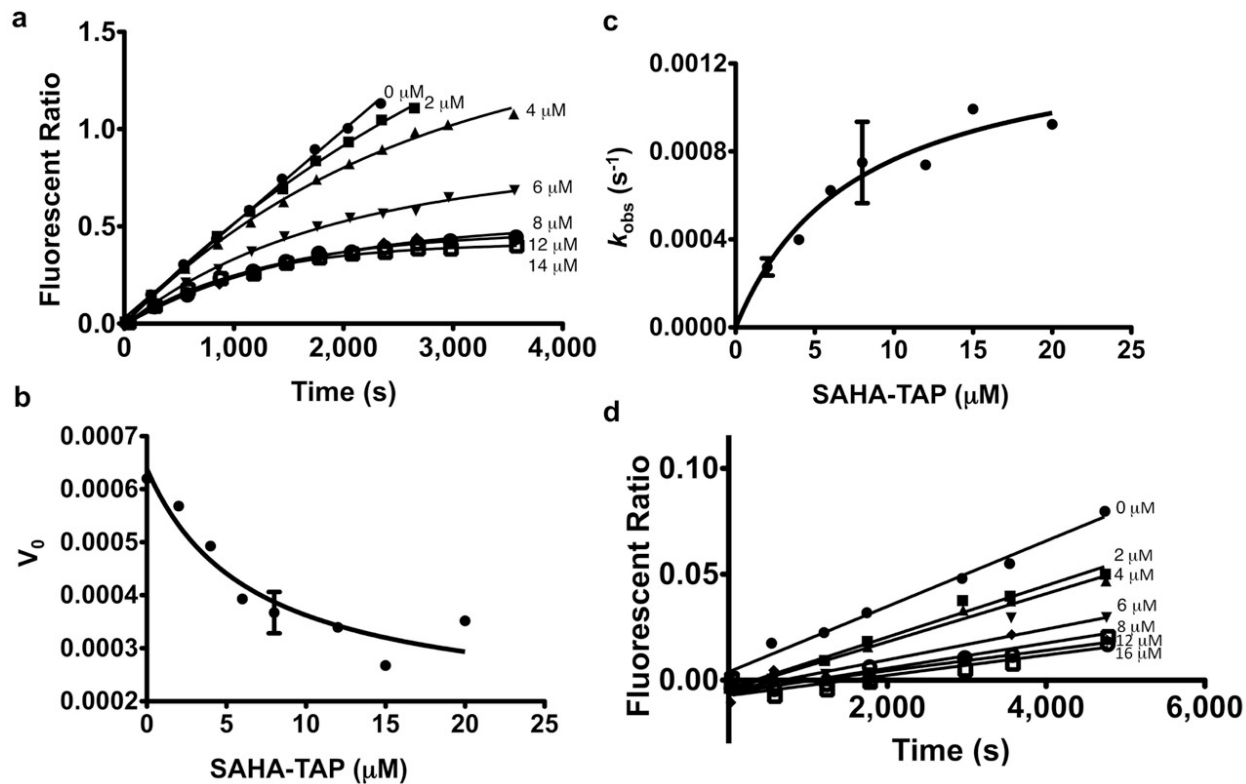
Figure 5.5: Time dependence of HDAC8 inhibition.

(A) WT HDAC8 (0.5 µM) progress curves at varying concentrations (0−20 µM) of SAHA-TAP. Dependence of both the (B) initial rate, v_0, and (C) k_{obs} on the concentration of SAHA-TAP. (d) C153A HDAC8 (2 µM) progress curves at varying concentrations (0−20 µM) of SAHA-TAP.

Plasma Stability.

As mentioned earlier, SAHA suffers from poor PK properties, including hydrolytic instability with t ~1/2 1.5 h. To determine the stability of SAHA-TAP in a biologically relevant model, human plasma stability studies were conducted as previously reported (*143*). After incubating SAHA or SAHA-TAP in human plasma, aliquots were withdrawn at various time points (0, 15, 30, 60, and 120 min), quenched with acetonitrile, filtered, and evaluated via analytical HPLC. The percent parent compound remaining was determined by integrating the area under the curve and comparing this number with the initial sample

166

of parent compound at an incubation time of 0 min. Approximately 72% of SAHA-TAP remained after 1 h incubation at 37 °C, whereas only ~60% of SAHA remained under identical conditions. Only ~50% of either parent compound remained after a 2 h incubation at 37 °C (Figure 5.6a). After 2 h incubation at 37 °C, the HPLC trace of SAHA-TAP showed that the major degradation peak (~23%) corresponds to SAHA, with ~52% SAHA-TAP remaining and ~25% other products. This suggests that hydrolysis of SAHA-TAP to SAHA is a major component of the degradation process in human plasma (Appendix 2, Figure S9). For comparison, after a 2 h incubation in human plasma under identical conditions, the HPLC chromatogram for SAHA shows the emergence of a series of new unidentifiable peaks (~45%), with ~55% SAHA remaining (Appendix 2, Figure S9). Even though SAHA-TAP gradually degrades over this 2 h period, it is relatively slow and results in the release of the active drug SAHA. Efforts to identify other product peaks via LC-MS were inconclusive. Overall, this study indicates that SAHA-TAP has a moderately improved stability profile than SAHA in human plasma.

Cell Proliferation Studies.

With the kinetics of activation and plasma stability of SAHA-TAP elucidated, we then studied the effect of SAHA-TAP on the proliferation of a variety of cell lines. Because SAHA is FDA-approved for CTCL, we selected HH (CTCL) and Jurkat (T-cell leukemia) cell lines for analysis. The viability of NIH/3T3 (mouse embryo fibroblast) was also tested to determine the toxicity of each compound for a noncancer cell line. The EC_{50} values of SAHA, SAHA-TAP, and SAHA-OBn are shown in Figure 5.6b for each cell line. The observed EC_{50} values of SAHA for HH and for Jurkat cell lines were 1.03 ± 0.21 μM and 1.66 ± 0.14 μM,

respectively, consistent with previously reported data (*144*, *145*). SAHA-TAP is ~3–4-fold less potent than SAHA, but it is still an active compound, with calculated EC_{50} values of 3.38 ± 0.30 μM and 6.05 ± 0.14 μM for HH and Jurkat cells, respectively. This difference in potency may be attributed to the alkylated Cys affecting the binding of SAHA to HDAC8; further structural studies are needed to confirm this hypothesis. Interestingly, SAHA also is toxic for NIH/3T3 cell lines, with a calculated EC_{50} of 4.80 ± 0.99 μM. Other studies also report cytotoxicity of healthy kidney cells (Vero) after treatment with SAHA (EC_{50} = 5.20 ± 0.96 μM) (*57*). Unfortunately, cell proliferation studies indicate that SAHA-TAP is also slightly toxic for NIH/ 3T3 cells with an apparent EC_{50} value of 9.37 ± 1.21 μM. As expected, cell proliferation is unaffected by the addition of SAHA-OBn for all cells studied.

Intracellular Target Validation.

With the cell proliferation data in hand for both Jurkat and HH cells, we sought to validate the intracellular target of SAHA-TAP using western blotting techniques. Broad-spectrum HDACi are known to increase the steady-state accumulation of tubulin, an endogenous HDAC substrate and a common marker for intracellular HDAC6 activity (*146*, *147*). For these experiments, SAHA was used as a positive control, since it has been shown to dramatically increase tubulin acetylation in a variety of cells (*145*, *148*). Indeed, we observed that SAHA-TAP increased tubulin acetylation in both Jurkat and HH cells without disturbing actin levels (Figure 5.6c), suggesting that the antiproliferative mechanism of action for SAHA-TAP, like SAHA, involves nonspecific HDAC inhibition.

a

b

Compound	HH	Jurkat	NIH/3T3
SAHA	1.03±0.21 μM	1.66±0.14 μM	4.80±0.99 μM
SAHA-TAP	3.38±0.30 μM	6.05±0.14 μM	9.37±1.21 μM
SAHA-OBn	NI	NI	NI

c
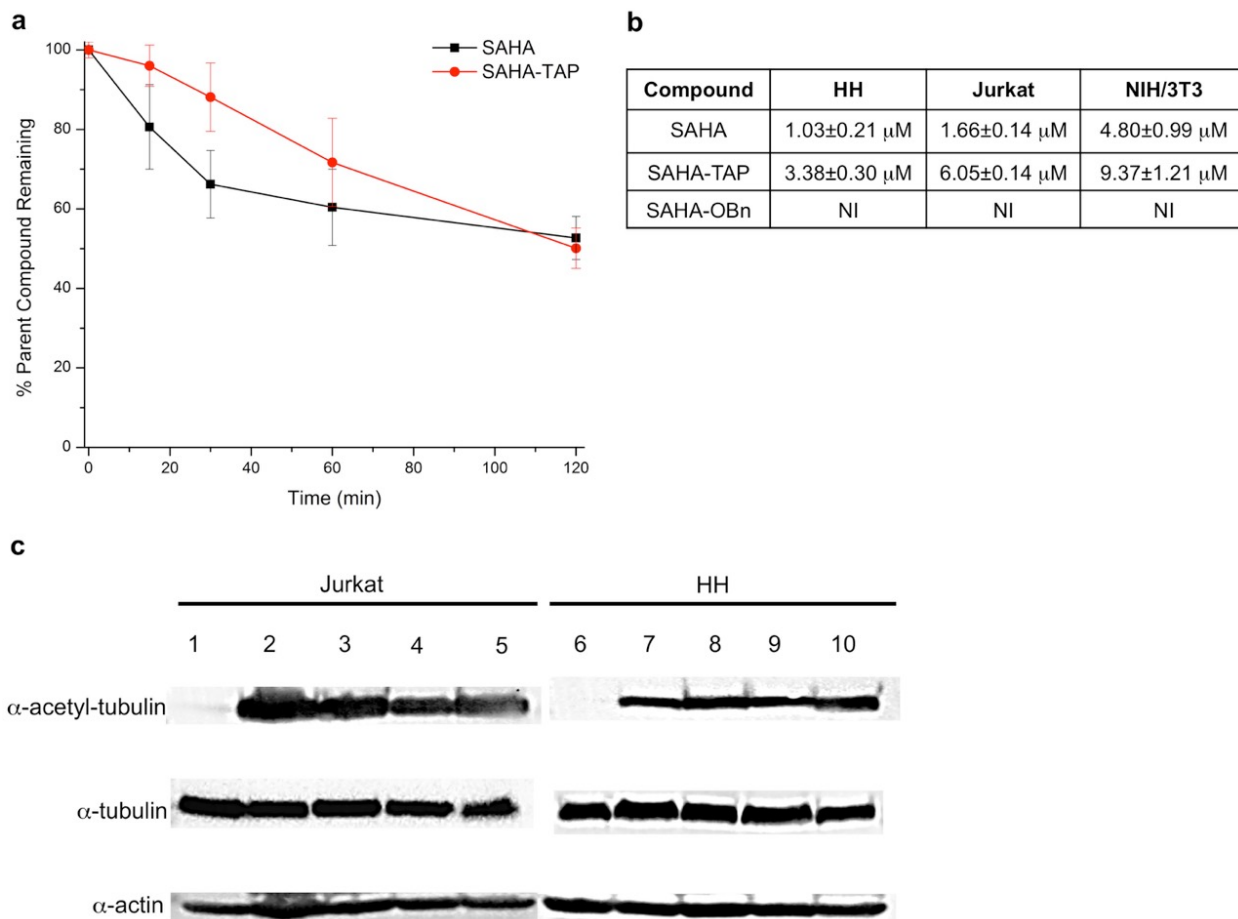
Figure 5.6: SAHA-TAP cell proliferation and potency

(a) Plasma stability for SAHA (red circles) and SAHA-TAP (black squares) over time (mean ± SD). (b) Cellular EC$_{50}$ values (μM) obtained from the MTS cell proliferation assay. NI, no inhibition at 50 μM. (c) Western blot analysis of tubulin acetylation for Jurkat (lanes 1–5) and HH (lanes 6–10) cells. Lane 1, control (no treatment); lane 2, SAHA (1.5 μM); lane 3, SAHA (20 μM); lane 4, SAHA-TAP (6 μM); lane 5, SAHA-TAP (20 μM); lane 6, control (no treatment); lane 7, SAHA (1.5 μM); lane 8, SAHA (20 μM); lane 9, SAHA-TAP (6 μM); lane 10, SAHA- TAP (20 μM).

Conclusions

A thiol-sensitive prodrug of the FDA-approved HDACi SAHA has been developed that displays a time-dependent inhibition of HDAC8. SAHA-TAP functions as a dual-mode HDAC inhibitor with both a covalent modification and a noncovalent, conventional mode of action. SAHA-TAP is susceptible to nucleophilic attack by Cys residues on the target HDAC, particularly the conserved Cys153 residue in the catalytic domain of HDAC8. These Cys residues are covalently modified with the promoiety, inactivating the enzyme, followed by the release of the competitive inhibitor SAHA. Proteomic MS confirms that this modification occurs at Cys153, and the kinetics of inhibition show unambiguous time-dependent inhibition of HDAC8 by SAHA-TAP, indicative of a covalent modification with release of SAHA. The HDAC8 C153A mutant retains the noncovalent mode of inhibition by SAHA-TAP (Scheme 5.1), whereas the time-dependent mode of inhibition disappears. This result demonstrates the importance of the active site Cys in the inactivation of HDAC8 by SAHA-TAP. The stability of SAHA-TAP in human plasma is slightly improved, with slow conversion to SAHA observed. In contrast, SAHA is rapidly degraded to several products under identical conditions, consistent with previous literature studies. Finally, cellular proliferation studies show a clear dose–response relationship with SAHA-TAP for two distinct cancer cell lines, with only moderately inferior EC_{50} values compared to SAHA; immunoblotting confirms that the antiproliferative mechanism of action of SAHA-TAP involves HDAC inhibition. To the best of our knowledge, SAHA-TAP is the first dual-mode HDAC proinhibitor that exploits the modification of endogenous, conserved Cys residues, namely, the catalytic site Cys153 residue in HDAC8, to generate a covalent adduct in addition to releasing a competitive inhibitor.

Experimental Section

Enzyme Inhibition Assays.

HDAC-1, -2, -3, -6, and -8 activity was determined *in vitro* with an optimized homogeneous assay performed in a 384-well plate. Recombinant, full-length HDAC protein (BPS Biosciences) was incubated with fluorophore-conjugated substrate, MAZ1600 and MAZ1675, at [substrate] = K_m (MAZ1600; 11 μM for HDAC1, 18 μM for HDAC2, 9 μM for HDAC3, 4 μM for HDAC6; MAZ1675; 263 μM for HDAC8). Reactions were performed in assay buffer (50 mM HEPES, 100 mM KCl, 0.001% Tween-20, 0.05% BSA, pH 7.4, and additional 200 μM TCEP was added for HDAC6) and followed by fluorogenic release of 7-amino-4- methylcoumarin from substrate upon deacetylase and trypsin enzymatic activity. Flourescence measurements were obtained every 5 min using a multilabel plate reader and plate stacker (Envision; PerkinElmer). Each plate was analyzed by plate repeat, and the first derivative within the linear range was imported into analytical software (Spotfire DecisionSite). Replicate experimental data from incubations with inhibitor were normalized to DMSO controls ([DMSO] < 0.5%). IC_{50} values are determined by logistic regression with unconstrained maximum and minimum values.

Mass Spectrometry Experiments.

Preparation. An aliquot of HDAC8 (1.7 μM) was incubated with SAHA-TAP (12 equiv, 20 μM) at 37 °C for 1 h. The protein was purified by SDS-PAGE followed by Coomassie staining prior to analysis.

In Gel Digest.

The gel slices of interest were cut to 1 mm cubes and destained three times by first washing with 100 mM ammonium bicarbonate (100 µL) for 15 min followed by the addition of ACN (100 µL) for 15 min. The supernatant was collected, and samples were dried in a SpeedVac. The samples were then reduced by the addition of 100 µM ammonium bicarbonate/10 mM DTT (200 µL) and incubated at 56 °C for 30 min. The liquid was removed, and 100 mM ammonium bicarbonate/55 mM iodoacetamide (200 µL) was added to gel pieces and incubated at RT in the dark for 20 min. After the removal of the supernatant and one wash with 100 mM ammonium bicarbonate for 15 min, the same volume of ACN was added to dehydrate the gel pieces. The solution was then removed, and the samples were dried in a SpeedVac. For digestion, enough solution of ice-cold trypsin (0.01 µg/mL) in 50 mM ammonium bicarbonate was added to cover the gel pieces, which were then incubated on ice for 30 min. After complete rehydration, the excess trypsin solution was removed, replaced with fresh 50 mM ammonium bicarbonate, and incubated overnight at 37 °C. The peptides were extracted twice by the addition of 0.2% formic acid and 5% ACN (50 µL) and vortex mixing at RT for 30 min. The supernatant was removed and saved. A total of 50 µL of 50% ACN/0.2% formic acid was added to the sample, which was vortexed again at RT for 30 min. The supernatant was removed and combined with the supernatant from the first extraction. The combined extractions were analyzed directly by LC-MS.

LC-MS/MS.

Trypsin-digested peptides were analyzed by HPLC coupled with tandem mass spectrometry (LC-MS/MS) using nanospray ionization. The nanospray ionization experiments were performed using a TripleTOF 5600 hybrid mass spectrometer (SCIEX) interfaced with nanoscale reversed-phase HPLC (Tempo) using a 10 cm × 100 μm i.d. glass capillary packed with 5 mm C18 Zorbax beads (Agilent Technologies). Peptides were eluted from the C18 column into the mass spectrometer using a linear gradient (5– 60%) of ACN at a flow rate of 250 μL/min for 1 h. The buffers used to create the ACN gradient are buffer A (98% H_2O, 2% ACN, 0.2% formic acid, and 0.005% TFA) and buffer B (0.2% formic acid and 0.005% TFA in ACN). MS/MS data were acquired in a data- dependent manner in which the MS1 data was acquired for 250 ms at m/z of 400 to1250 Da and the MS/MS data was acquired from m/z of 50 to 2000 Da. Independent data acquisition (IDA) parameters were MS1-TOF 250 ms followed by 50 MS2 events of 25 ms each. The IDA criteria were as follows: over 200 counts threshold, charge state +2−4, with 4 s exclusion. Finally, the collected data were analyzed using MASCOT (Matrix Sciences).

Protein Expression and Purification.

Recombinant human HDAC8 in a pET-20b-derived plasmid with an added C-terminal TEV protease cleavage site and His_6 tag (termed pHD) was expressed and purified in Escherichia coli BL21(DE3) according to Gantt and co-workers (*57*), with the following modification: elution from the nickel columns was performed using a linear gradient (10−250 mM imidazole). In the preparation of apo-enzyme, HDAC8 was dialyzed twice at 4

°C against 4 L of 25 mM MOPS, 1 mM EDTA, 5 mM KCl, 1 mM TCEP, pH 7.5, followed by four times against 2 L of 25 mM MOPS, 5 mM KCl, 1 mM TCEP, pH 7.5. All components were free of transition metals, and dialysis occurred in plasticware that had been washed with EDTA and rinsed with Milli-Q ddH$_2$O. Apo- enzyme was stored at −80 °C in the same metal-free buffer. The Cys153Ala HDAC8 mutant was constructed in a pHD4 TEV-His plasmid, using the QuikChange site-directed mutagenesis protocol and kit, and the mutation was confirmed by the UM DNA sequencing facility. This construct was expressed and purified in the same manner as wild-type enzyme.

HDAC8 Time-Course Inhibition Experiments.

Recombinant WT or C153A mutant human HDAC8 was reconstituted for 1 h on ice at a 1:1 stoichiometry (at 10 µM) with Zn^{2+} in 1× HDAC assay buffer (25 mM HEPES, 3 mM KCl, 137 mM NaCl, pH 8.0). The 5 and 50 mM SAHA-TAP, SAHA-OBn, and SAHA stocks were serially diluted into decreasing concentrations of DMSO to maintain solubility of the compounds. Reaction mixtures of 1× HDAC assay buffer, 150 µM Fluor-de-Lys peptide substrate (R−H−K(Ac)−K(Ac)−fluoro- phore) (Enzo Life Sciences), and various concentrations of inhibitors (SAHA-TAP, SAHA-OBn, or SAHA) were prepared and allowed to equilibrate at 30 °C. The final DMSO content was <1%. Assays were initiated by addition of wild-type (0.5 µM) or Cys153Ala mutant (2 µM) HDAC8. At various time points, a reaction aliquot (5 µL) was diluted into a Fluor-de-Lys quench solution (45 µL) containing trypsin and trichostatin A (TSA). Assays were read in 96-well plates (Corning 3686) using a PolarStar fluorescent plate reader. The fluorescence corresponding to product formation (λ_{ex} = 340 nm, λ_{em} = 450 nm) and remaining substrate (λ_{ex} = 340 nm, λ_{em} = 380 nm) was

174

measured, and the ratio of product formed/remaining substrate is reported. Standard curves demonstrate that this fluorescent ratio linearly reflects product under these conditions.

Cell Proliferation Studies.

HH and Jurkat cell lines were obtained from ATCC (Manassas, VA, USA) and grown in RPMI 1640 medium supplemented with 10% fetal bovine serum (Gibco, Grand Island, NY, USA). The NIH/3T3 cell line was kindly donated by Dr. Richard Klemke and grown in DMEM medium supplemented with 10% fetal bovine serum (Gibco, Grand Island, NY, USA) at 37 °C in an incubator with 5% CO_2. The CellTiter 96 aqueous one solution cell proliferation assay (MTS) kit was purchased from Promega (Madison, WI, USA). Cell viability was measured using the MTS assay according to the manufacturer's protocol. To start the assay, cells were counted with a hemocytometer, diluted with fresh medium to the proper concentration, and seeded in 96-well plates (5000 cells/well for NIH/ 3T3 and 20 000 cells/well for HH and Jurkat). Jurkat and HH cells were then directly incubated in media containing the various concentrations of drugs for 70 h (ranging from 0.5 to 128 µM). NIH/3T3 cells were first incubated at 37 °C with 5% CO_2 for 16 h prior to the drug treatment for cell attachment. The cells were then treated with various concentrations of drugs for 70 h. The CellTiter 96 aqueous one solution was added (20 µL per well), and the plate was incubated at 37 °C for 2 h (NIH 3T3) or 4 h (HH and Jurkat). The absorbance was recorded at 490 nm using the BioTek Synergy HT microplate reader. Each concentration of drug treatment was conducted in triplicate for each trail, with 2−3 trials conducted.

Plasma Stability.

The plasma stability of SAHA and SAHA-TAP was investigated with pooled normal human plasma (Innovative Research, Novi, MI). In duplicate, plasma (1.0 mL) was preincubated for 2 min at 37°C followed by the addition of 20 μL of a 5.0 mM stock solution (DMSO). Aliquots (100 μL) were withdrawn at 0, 15, 30, 60, and 120 min and immediately quenched with 100 μL of ACN to precipitate the proteins. The samples were vortexed thoroughly and centrifuged for 2 min at 13 000 rpm. The supernatant was collected and centrifuged through 0.2 μm spin filters (Corning) for 5 min at 8000 rpm. Samples were then frozen until analyzed by HPLC with the following method: analytical HPLC was performed on a HP Series 1050 system equipped with a Poroshell 120 reverse-phase column (EC-C18, 4.6 × 100 mm, 2.7 μm). Separation was achieved with a flow rate of 1 mL min^{-1} and the following mobile phase: 2.5% ACN + 0.1% formic acid in H$_2$O (A) and 0.1% formic acid in ACN (B). Starting with 95% A and 5% B, a linear gradient was run for 15 min to a final solvent mixture of 5% A and 95% B, which was held for 5 min before ramping back down to 95% A and 5% B over the course of 2 min, with constant holding at this level for 4 additional min.

Western Blot Analysis.

Log phase growing HH and Jurkat cell lines were cultured until 70% percent confluent and treated with specified concentrations of compounds for 4 h prior to harvesting. Cells were spun at 250g and washed with DPBS buffer (Life Technologies) before lysis using RIPA buffer (50 mM Tris-HCl (pH 7.5), 150 mM Na$_2$EDTA, 1% Nonidet P-40, 1% sodium deoxycholate, 0.1% sodium dodecyl sulfate) supplemented with complete

protease inhibitor cocktail (Roche) for 30 min on ice. Samples were then spun at 12 000g

before quantification of total protein concentration using a BCA assay (Thermo). Dilutions

were made to normalize total protein concentration for each gel sample. Diluted samples

were then run on a 10% SDS-PAGE gel at 100 V for 2 h before transfer onto Immobilon-P

PVDF Membrane (EMD Millipore) at 100 V for 45 min before blocking in 5% (v/v) Casein-

TBST (Tris-buffered saline Tween-20; 0.05% Tween-20 v/v) at 4 °C. Blots were then

incubated with monoclonal mouse anti-acetylated tubulin (Life Technologies), polyclonal

rabbit anti-tubulin (Sigma), or anti-actin–HRP (Santa Cruz) in 5% (v/v) BSA-TBST at

dilutions according to manufacturer's instructions overnight at 4 °C. Blots were then

washed by three 5 min washes in TBST (0.05% v/v); anti-acetylated tubulin and anti-

tubulin antibodies were then incubated with HRP-conjugated anti-mouse (Santa Cruz) or

anti-rabbit (Pierce) antibodies. Detection was performed using SuperSignal West pico

substrate (Pierce) with 10% (v/v) SuperSignal West femto substrate (Pierce) and imaged

on ChemiDoc XRS+ System with Image Lab Software (Bio-Rad).

Chapter 6

Conclusions and Future Directions

Overview

The acetylome has grown from histone tails at its discovery in the early 1960's to almost 2,000 proteins in 2009 (*86*, *149*, *150*). In the 7 years since, that number has continued to grow, and acetylation has now been documented on over 7,000 proteins (*6*). Acetylation is known to affect proteins in virtually every cellular process, including cell cycle, metabolism, and gene expression (*86*). With the acetylome expanding, research has also increased into understanding the regulation of this dynamic post-translational modification. The catalysts of lysine acetylation and deacetylation are the lysine acetyltransferases and histone deacetylases, respectively. The first human HDAC, HDAC1, was annotated more than 30 years after the discovery of histone acetylation (*151*). Today, there are 18 deacetylases capable of the negative regulation of lysine acetylation. Of these, there are 11 metal-dependent enzymes, the Class I, II, and IV HDACs (*73*).

While research is rapidly expanding the knowledge on the function of HDACs, the field is complex and still evolving. In this thesis I have presented a body of work that not only improves upon the understanding of HDAC8 and HDAC11, but perhaps equally importantly, also describes a set of methods and techniques that can be applied to any of the HDAC isozymes.

Deacetylase activity on peptides

Deacetylation of peptide substrates has been, and remains, a rapid and effective method of assaying HDAC catalysis. Peptide-based HDAC assays are useful methods when addressing a variety of questions, including isozyme-specificity of inhibitors (*35*), substrate selectivity of a single isozyme (*152*), and selectivity of multiple HDAC isozymes against individual substrates (*61*). HDAC catalysis on peptides has historically involved methyl-coumarin labeled peptides (*87*). Here we reported on the advancement of several peptide substrate-based methods that do not require fluorophore-labeled peptide, allowing more freedom in peptide length and sequence. These various techniques differ in their advantages and disadvantages, making some more useful for specific applications than others.

Previous work in the Fierke laboratory developed an enzyme-coupled assay for HDAC activity that measures acetate production in a stopped format (76). I optimized this assay so that it can be run as a continuous assay. In doing so, the amount of time and materials required was reduced. However, this assay is now sensitive to the activity of the coupling enzymes and requires that HDAC deacetylation be the rate-limiting step of the coupled reactions. This continuous assay is well suited for quantifying the function of HDAC inhibitors in a high-throughput manner, since the maximum rate of the HDAC reaction is predetermined. I also demonstrated that two mass spectrometry approaches, Q-TOF HPLC-MS and MALDI-TOF, could be used to assay HDAC deacetylation. Both methods provide direct evidence for HDAC-catalyzed deacetylation of peptide substrates by determining the exact mass of the substrate and product. Q-TOF HPLC-MS provides

quantifiable deacetylation data, but due to variation in elution times and the differing ionizability of peptides, multiple standard curves are needed. The MALDI-TOF approach, while not easily quantitative, only requires a calibration curve of known molecular weight standards. This technique is rapid and suitable for small-volume reactions. This makes the MALDI-TOF approach best suited for preliminary screening of large substrate libraries.

The ability to quickly and accurately measure HDAC catalysis on unlabeled peptide substrates was instrumental to the initial biochemical characterization of HDAC11 (Chapter 2) and to the validation of substrates identified for both HDAC8 and HDAC11 (Chapter 3). These methods should continue to be useful tools for understanding HDAC catalysis and specificity.

Expression and characterization of HDAC11

HDAC11 is the most recently identified and one of the most poorly understood HDACs (*24*). I successfully expressed and purified HDAC11 from *E. coli*, insect cells (sf9), and human HEK293 cells. To achieve sufficient expression levels and soluble yields of HDAC11 from bacteria, I fused the gene encoding HDAC11 to SUMO. I also tested a panel of molecular chaperones and observed that co-expression of SUMO-HDAC11 with trigger factor significantly improved soluble yield of HDAC11. Interestingly, and perhaps a factor in the limited understanding of this isozyme, HDAC11 expressed in bacteria is inactive, while HDAC11 expressed in insect cells and HEK293 cells is catalytically active.

Using HDAC11 expressed and purified from insect cells, I demonstrated that HDAC11 catalyzes the deacetylation of both methyl-coumarin-labeled peptides as well as unlabeled peptides. I measured activity with multiple unlabeled peptides and found that

two peptides proposed in literature as substrates through pull-down methods had among the most rapid rates of deacetylation of those tested. These peptides correspond to sequences from the DNA replication factor Cdt1 and histone H4 K16. We also observed that the best HDAC11 substrates from this initial screen were positively charged. After measuring additional peptides, based on proteins identified on the proteome chips (Chapter 4), the data suggest that the charge at the +1 position downstream of the acetyllysine may have an impact of the reactivity of the peptide with HDAC11 (Table 6.1). The total charge of the peptide and the charge at the -1 positions do not demonstrate a trend. These data, based on rate constants determined for HDAC11-catalyzed deacetylation of 21 peptides, refined our hypothesis from HDAC11 favors substrates with a positive charge to HDAC11 favors substrates with a positive charge immediately downstream of the acetyllysine. A fit of the dependence of Log (k_{cat}/K_M) on the charge at the +1 position shows a trend toward increasing peptide reactivity with positive charges, but the R-factor is not significant. The data suggest that positive charges at the +1 position enhance reactivity, but there are clearly more determinants in HDAC11 specificity. Measuring HDAC11-catalyzed deacetylation of a peptide library with variability at the +1 and -1 positions, as has been done with HDAC8, will help to elucidate the role of local charges on HDAC11 substrate selectivity.

Table 6.1: Peptide substrates used to assay HDAC11 catalytic activity

Peptides all contain an acetylated N-terminus and an amidated C-terminus. Charged residues are shown in red (acidic) or blue (basic). Table is sorted by charge of the amino acid at the +1 position, immediately downstream of the acetyllysine. Proteins with multiple acetylation sites tested are labeled with a suffix (*a, b, c, etc.*)

Protein	Peptide Sequence	k_{cat}/K_M (M^{-1}s^{-1})	+1 Position Charge
GOT1	DAE(K-Ac)RGLD	60	1
H4 K16	KGGA(Kac)RHR	50	1
NIF3L1*a*	RPM(K-Ac)RIT	31	1
CNP	DDL(K-Ac)KLK	31	1
Cdt1 K49	GSR(Kac)RAR	30	1
ZBTB21	LAL(K-Ac)RPR	5	1
TCOF1*a*	QV(K-Ac)AEK	175	0
TCOF1*b*	TG(K-Ac)TVA	60	0
CEBPZ	KGGKQLN(K-Ac)YDPFSRN	51	0
EIF5*a*	EG(K-Ac)GNG	47	0
TCOF1*c*	SAPG(K-Ac)VVT	33	0
LUC7L	EEIG(K-Ac)LLA	18	0
EIF5*b*	EGKGNGI(K-Ac)TVI	16	0
TCOF1*d*	PG(K-Ac)TGPAVAK	8	0
IDH1	KLKQMW(Kac)SPN	7	0
TCOF1*e*	PG(K-Ac)VGD	5	0
C2orf47	KEVLHAL(K-Ac)EKVTSLP	35	-1
NIF3L1*b*	NTW(K-Ac)ER	10	-1
TCOF1*f*	GA(K-Ac)DEP	9	-1
TCOF1*g*	SM(K-Ac)EKA	5	-1
TCOF1*h*	PA(K-Ac)ESP	5	-1

Using intact protein mass spectra, we observed that the molecular weight of HDAC11 expressed and purified from insect cells was 42 daltons heavier than the predicted mass based on amino acid sequence. We hypothesize that a post-translational modification, occurring in eukaryotic expression of HDAC11 but not in prokaryotic expression, is activating the enzyme. A mass gain of 42 daltons is consistent with both an acetyl moiety and trimethylation, among others. Post-translational modifications have

been identified on other HDAC isozymes, including lysine acetylation and lysine methylation of HDAC1 (*86*, *153*).

We collaborated with the Martin laboratory to use a bottom-up mass spectrometry approach to evaluate differential modifications on HDAC11 expressed in *E. coli* and HDAC11 expressed in insect cells. We digested purified HDAC11 from bacterial and insect cells with Asp-N and Trypsin, separately. We identified multiple sites of acetylation (lysine) and methylation (lysine, arginine, glutamine, glutamate, and histidine) present on HDAC11 expressed and purified from insect cells that were not present on HDAC11 expressed and purified from bacteria. We also observed two sites of methylation unique to *E. coli* (Table 6.2). It is difficult to quantify the fraction of HDAC11 that is modified in each sample. Based on our intact protein spectra, we predicted one main modification but have not yet observed this using the bottom-up approach. Additionally, neither the Asp-N digest nor the trypsin digest achieved 100% sequence coverage of HDAC11 (45% and 80%, respectively, with a combined 85%). The effect of post-translational modifications at these positions is not yet understood; we hypothesize that one or more of these modifications may activate HDAC11.

Table 6.2: Unique PTMs identified on HDAC11 expressed and purified from sf9 insect cells and *E. coli* bacterial cells.

HDAC11 expressed and purified from sf9 insect cells and *E. coli* bacterial cells was digested with Asp-N and trypsin. This table includes only modifications unique to one expression system. The modified residues are highlighted (red).

protease	modification	sf9	*E. coli*
Asp-N	acetylation (K)	DKVERNIKKSLQEHLP	-
Asp-N	acetylation (K)	DRLGGLSISPAGIVKR	-
trypsin	acetylation (K)	VINFLKEEK	-
trypsin	mono-methylation (K)	VINFLKEEK	-
Asp-N	di-methylation (K)	-	DKVERNIKKSLQEHLP
Asp-N	di-methylation (K)	-	DKVERNIKKSLQEHLP
trypsin	tri-methylation (K)	ATIIDLDAHQGNGHERDFMDDK	-
trypsin	mono-methylation (E)	FLFERVEGISR	-
trypsin	mono-methylation (R)	FLFERVEGISR	-
trypsin	mono-methylation (R)	MLHTTQLYQHVPETRWPIVYSPR	-
trypsin	mono-methylation (R)	LLSDSMLVEAR	-
trypsin	di-methylation (R)	LLSDSMLVEAR	-
trypsin	di-methylation (QH)	MLHTTQLYQHVPETRWPIVYSPR	-

To completely elucidate the role of these post-translational modifications, the modifications should be inserted into HDAC11 expressed and purified from *E. coli*, followed by measurement of the changes in HDAC11 catalytic activity for comparison with the activity and specificity of HDAC11 expressed in sf9 or HEK293 cells. Insertion of the modifications at specific positions could be accomplished through the incorporation of unnatural amino acids representing these modifications into the primary sequence of HDAC11. To this end, we have used site-directed mutagenesis to replace one lysine, based on those identified in table 6.2, in HDAC11 with an amber stop codon, and are currently in the process of using a modified tRNA^acK/tRNA^acK synthetase pair to incorporate acetyllysine at that site. We plan to use this method to determine the effects of modifications at multiple sites. Identification of an activating modification on HDAC11 would provide

insight into the *in vivo* regulation of this enzyme. It would also provide a method by which active HDAC11 could be expressed and purified from *E. coli*, allowing for more rapid expression of HDAC11 than from insect cells, and point mutations can be more easily prepared and expressed without the need to create baculovirus stocks for each HDAC11 construct.

Chip-based substrate identification

Using a chip-based format, we observed HDAC catalyzed deacetylation on a library of full-length human proteins in collaboration with the Cole laboratory. This method is an advance in the field for identification of substrate; it does not rely upon stable protein-protein interactions (pulldowns) or the ability to immunoprecipitate peptides with an anti-acetyllysine antibody. Instead, it is an assay based on changes in protein acetylation upon incubation with an HDAC isozyme, visualized by fluorescence of an anti-acetyllysine antibody. Using this method we identified 44 putative substrates of HDAC8 and 25 putative substrates of HDAC11. We identified proteins involved in various cellular pathways, including metabolism and gene transcription. These putative substrates were predominantly novel HDAC targets, though some have been identified previously (*40*, *61*). We found that CSRP2BP and TCOF1, both identified as likely HDAC8 substrates in a SILAC-based method (*61*), were also deacetylated by HDAC8 on the proteome chips.

One of the most promising HDAC8 substrates identified through the chip-based screen is isocitrate dehydrogenase 1 (IDH1). I measured HDAC8-catalyzed deacetylation of 4 peptides from this protein, and found rate constants varying from less than 10 to greater than 150 $M^{-1}s^{-1}$. To further validate IDH1 as an HDAC8 substrate, I expressed and purified

five constructs of recombinant IDH1, using non-natural amino acids to incorporate single acetyllysine residues into the protein (IDH1 WT, K81ac, K93ac, K224ac, and K321ac). I incubated acetylated IDH1 with HDAC8 and observed changes in acetylation with time by visualizing IDH1 acetylation with an anti-acetyllysine antibody. IDH1 is now the first singly-acetylated full-length non-histone protein demonstrated to be deacetylated *in vitro* by HDAC8.

To further validate IDH1 as an HDAC8 substrate, I would like to see *in vivo* evidence demonstrating an increase in IDH1 acetylation upon specific inhibition of HDAC8 in cells. IDH1 acetylation could be verified by mass spectrometry, as was used in the SILAC experiments, or, if protein concentration is high enough, it could be pulled-down and verified by probing a western blot with an anti-acetyllysine antibody.

The effect of acetylation on IDH1 is not currently known. To address this question we assayed IDH1 catalytic activity with isocitrate. We found that acetylation significantly reduces the activity of IDH1, with some acetylation sites causing a decrease of over 10^3-fold in activity. These data suggest that IDH1 activity is negatively regulated by acetylation *in vivo*, and that HDAC8 may function as the deacetylase that restores IDH1 activity through site-specific deacetylation. I attempted to rescue activity of acetylated IDH1 *in vitro* by addition of HDAC8 (Fig. 6.1). Unexpectedly, I found that addition of HDAC8 did not increase the activity of acetylated IDH1. One possible explanation is that HDAC8 and IDH1 undergo a protein-protein interaction that prevents IDH1 catalysis. In agreement with this hypothesis, adding HDAC8 to WT IDH1 decreases IDH1 catalytic activity. Furthermore, I found that adding saturating concentrations of SAHA after adding HDAC8 to an acetylated IDH1 reaction resulted in an increase in IDH1 activity. It is worth noting that these data are

a preliminary finding. To continue exploring this hypothesis, these reactions should be repeated with additional controls. For example, longer time-course controls need to be run simultaneously with the HDAC8 rescue experiment. Additionally, pulldown experiments may provide evidence for an IDH1-HDAC8 protein complex.

Finally, the chip-based assay requires that proteins are acetylated by the catalytic domain of p300 in order to be considered as an HDAC substrate. This will, inherently, limit the pool of potential substrates. To determine a more complete picture of isozyme-specific HDAC-catalyzed deacetylation of the proteome chips, additional lysine acetyltransferases such as GCN5 may need to be used in addition to, or in place of, p300.
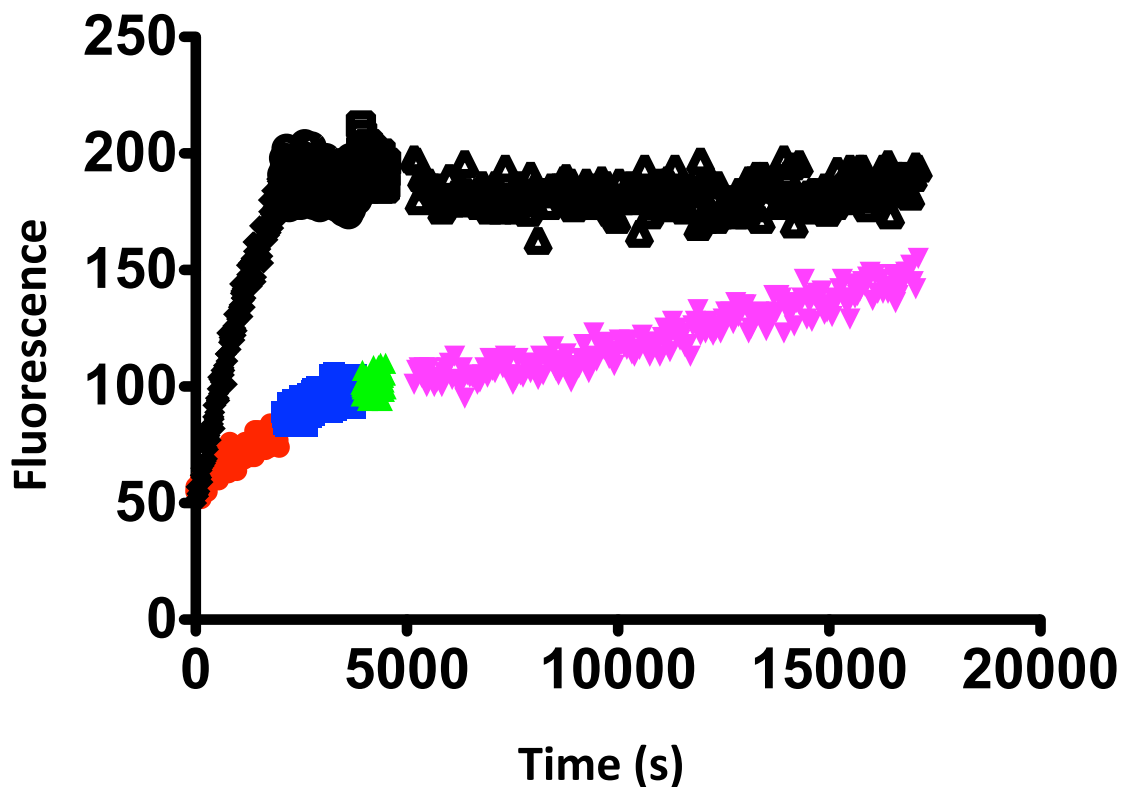
Figure 6.1: Effect of HDAC8 on acetylated IDH1 activity

Progress curves for IDH1 WT (0.01 μM) and K224ac (1 μM) variant were measured by monitoring the change in fluorescence (ex. = 350 nm, em = 450 nm) of the cofactor being reduced from NADP$^+$ to NADPH. Isocitrate and NADP$^+$ were at starting concentrations of 200 μM and 75 μM, respectively. IDH1 WT (black) progressed at a rate of 0.077 F.U./sec, reaching completion in less than 2000 seconds and had a steady NADPH fluorescent signal through the remaining time course. IDH1 K224ac (red) progressed at a slower rate (0.012 F.U./sec). At 2000 seconds, 5 μM HDAC8 was added to this reaction (blue). We had expected to see that addition of HDAC8 rescued IDH1 activity, but in contrast we observed that by 3000 seconds, the rate of IDH1 catalysis had plateaued. At 4000 and 5000 seconds, 5 μM and 50 μM SAHA were added to the reaction, respectively (green and pink). After the addition of SAHA, the fluorescence begins to increase, consistent with restored IDH1 activity.

Covalent inhibition of HDAC8

HDAC inhibitors play important roles both as therapeutics in clinical settings and as biochemical tools in basic research. Here we have introduced the first dual-mode HDAC proinhibitor, SAHA-TAP. In collaboration with the Cohen lab, we demonstrated that this molecule covalently modifies the active site of HDAC8 at Cys153 with its TAP moiety,

188

inactivating the enzyme. Additionally, upon thiol-induced cleavage of the TAP moiety, the competitive inhibitor SAHA is released. We have demonstrated that SAHA-TAP inhibits HDAC8 in a time dependent manner, via a two-step mechanism. We hypothesize that the first step is the rapid binding of SAHA-TAP to HDAC8, followed by slow, irreversible inactivation through the covalent linkage at Cys153. We also demonstrate that SAHA-TAP shows an improvement in plasma stability over its parent compound, SAHA.

These results are encouraging for the development of additional covalent HDAC inhibitors. SAHA-TAP is, like SAHA, a pan-HDAC inhibitor. The covalently modified residue, Cys153, is highly conserved among HDAC isozymes. The synthesis of SAHA-TAP does not require modifications to the cap or linker regions of SAHA, and upon cleavage of the TAP moiety, the parent compound SAHA is released. It would be exciting to see this synthetic approach used on other hydroxamate-based HDAC inhibitors, like the HDAC8-specific inhibitor PCI-34051 (Fig. 6.2).
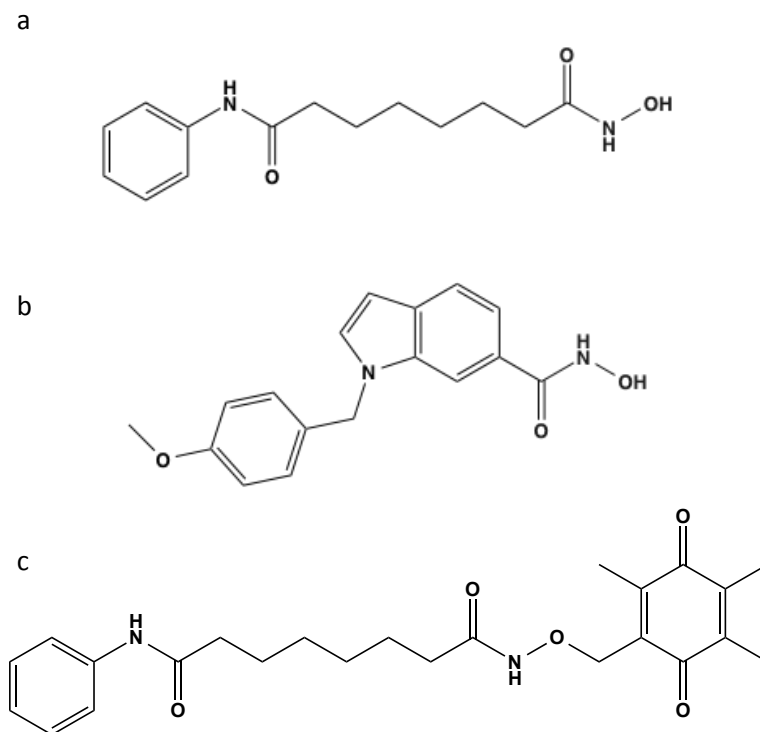
Figure 6.2: HDACi structures

A comparison of (A) the pan-HDAC inhibitor SAHA, (B) the HDAC8-specific inhibitor PCI-34051, and (C) the prodrug SAHA-TAP.

Conclusion

In the five years that I've been working on HDACs, I have witnessed significant advancements in our understanding of the biological roles these enzymes play. Researchers continue to link misregulation of this PTM to disease phenotypes, like the Cornelia de Lange syndrome. As the biological importance of acetylation grows, we need to strengthen the biochemical foundation upon which our understanding of the function of these important enzymes is based. In the work presented here, we have made exciting discoveries, like the determination that HDAC8 catalyzes deacetylation of recombinantly expressed, singly acetylated IDH1. The methods and techniques described in this document will continue to be used as tools to study HDAC-catalysis.

Appendix 1

Table A1.1: chip round 1 HDAC8 hits

Protein	UNIPROT I.D.	Acetylated
RDH16	O75452	Yes
PPP1R12B	O60237	
RABL3	Q5HYI8	Yes
TCHHL1	Q5QJ38	Yes
CRIP1	P50238	Yes
XAGE2	Q96GT9	
ADD1	P35611	
FHL3	Q13643	
AKR1C2	P52895	Yes
FLAD1	Q8NFF5	
C1QTNF9B	B2RNN3	
BCAR1	P56945	Yes
HSPA1L	P34931	Yes
MLIP	Q5VWP3	
ZNF277	E7EW13	
RFK	Q969G6	Yes
PRKG2	Q13237	
AAMP	Q13685	
PPIL3	Q9H2H8	
LOC653486	Q8TD33	
IDH1	O75874	Yes
MS4A3	Q96HJ5	
PTEN	P60484	Yes
AKR1D1	P51857	Yes
KCNK10	P57789	
RPA3	P35244	

Table A1.2: chip round 2 HDAC8 hits identified in at least 2 of 3 analysis methods

Protein	UNIPROT I.D.	Acetylated
ZFYVE16	Q7Z3T8	
PFKP	Q01813	Yes
PRPF38A	Q8NAV1	Yes
RNF121	Q9H920	
BOLL	Q8N9W6	Yes
RPS19BP1	Q86WX3	
TTR	P02766	
EMD	P50402	
APPL2	Q8NEU8	
ASAP2	O43150	Yes
DTNBP1	Q96EV8	Yes
EIF4B	P23588	Yes
KLC2	Q9H0B6	Yes
MAGEA9	P43362	
P4HB	P07237	Yes
PRDX4	Q13162	Yes
PRMT2	P55345	
PSMC3	P17980	Yes
TCOF1	Q13428	Yes

Table A1.3: chip round 2 HDAC8 hits identified in 1 of 3 analysis methods

Protein	Accession Number
RSAD2	NM_080657.4
NME7	NM_197972.1
PLCD1	NM_006225.1
--	BC029877.1
PRKCDBP	BC011585.1
SHCBP1	NM_024745.2
LOC400201	XM_378449.1
RFX4	NM_032491.3
GPATCH3	BC007767.2
PLEKHG5	BC015231.1
VWA8	NM_001009814.1
TPD52L3	NM_033516.4
TSPAN4	NM_001025239.1
QARS	NM_005051.1
PEPD	BC028295.1
BZW1	BC026303.1
PPM1D	NM_003620.2
MYOC	NM_000261.1
DCD	NM_053283.2
API5	BC017709

GALNT3	BC056246.1
SAV1	NM_021818.2
ECHDC1	BC003549.1
CCDC53	NM_016053.1
FGD2	NM_173558.2
NOS1AP	NM_014697.1
ITIH3	NM_002217.3
IGKC	BC029444.1
Sim1	Sim1
THEMIS2	BC081568.1
SYN3	BC075065.2
HSPA13	NM_006948.4
PLEKHA8	BC053990.1
SMYD5	NM_006062.1
APIP	BC017594.2
BBX	NM_020235.2
BLVRA	NM_000712.3
C11orf16	BC027865.1
C16orf70	NM_025187.3
CTSS	BC002642.2
DDHD1	NM_030637.1
DKK1	NM_012242.2
ERP27	NM_152321.1

ESM1	NM_007036.3
FAM9C	NM_174901.3
GABPB2	NM_144618.1
GAGE8	NM_012196.1
IFIT5	NM_012420.1
ISCA2	NM_194279.1
ITFG2	BC013399.2
KRTAP19-5	NM_181611.1
LCN8	NM_178469.3
LETM2	BC029541.1
ND	BC024211.2
ND	NM_022406.1
ND	NM_003363.2
ND	BC021720.2
ND	NM_018025.2
ND	NM_024726.3
NUAK2	NM_030952.1
PCLO	BC001304.1
POMK	NM_032237.2
RASSF1	NM_170713.1
SCIN	NM_033128.1
SLC10A1	NM_003049.1
SLC39A6	BC039498.1

|	
SNAP47	BC018760.1
SSU72	NM_014188.2
STXBP2	BC002869.2
TAPBP	NM_172208.1
TSPAN4	NM_001025239.1
TXNDC8	NM_001003936.1
VSTM2L	BC033818.1
WDR34	BC011874.2
ZFP64	BC012759.2
ZFP92	ZFP92
ZIM2	NM_015363.3
ZNF641	BC018090.1

Table A1.4: chip round 2 HDAC11 hits

*This entry is for an uncharacterized gene product from brain tissue, and the supplied identification is the NCBI Accession Number.

Protein	UNIPROT I.D.	Acetylated
ZFYVE16	Q7Z3T8	
GPATCH1	Q9BRR8	Yes
CCDC6	Q16204	
IGFLR1	Q9H665	
UBE3A	Q96GR7	
INO80E	Q8NBZ0	
NIF3L1	Q9GZT8	Yes
C11orf57	Q6ZUT1	
ZNF641	Q96N77	Yes
UIMC1	Q96RL1	Yes
CHIC2	Q9UKJ5	
TCAP	O15273	
ZNF175	Q9Y473	
GOT1	P17174	Yes
INTU	Q9ULD6	Yes
LUC7L	Q9NQ29	Yes
--	BC029877.1*	
NEK4	P51957	Yes

ZBTB21	Q9ULJ3	Yes
EIF5	P55010	Yes
AP3M2	P53677	Yes
CNP	P09543	Yes
CEBPZ	Q03701	Yes
DNAJB2	P25686	
C2orf47	Q8WWC4	Yes

Appendix 2

General Experimental Details: All chemicals were purchased from commercial suppliers (Sigma-Aldrich, Acros Organics, TCI America, Fisher Scientific) and were used without further purification. All reactions were carried out under N_2 in oven-dried glassware. E. Merck silica gel (60, particle size 0.040-0.063 mm) was used for flash chromatography, which was performed using a CombiFlash *Rf* 200 automated system from TeledyneISCO (Lincoln, NE, USA). NMR spectra were recorded on a Varian FT 400 MHz NMR instrument. Small molecule mass spectrometry (MS) was performed at the Molecular Mass Spectrometry Facility (MMSF) in the Department of Chemistry and Biochemistry at the University of California, San Diego.
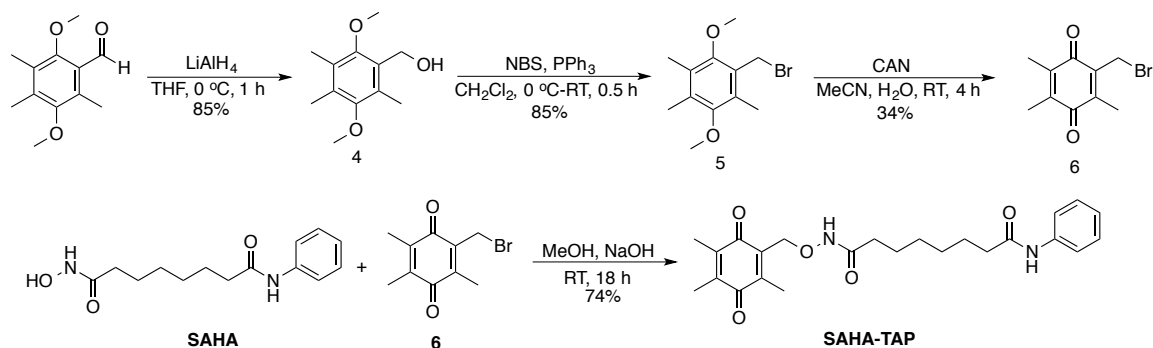
(2,5-Dimethoxy-3,4,6-trimethylphenyl)methanol (4). 2,5-Dimethoxy-3,4,6-trimethylbenzaldehyde[2] (1.28 g, 6.2 mmol) was dissolved in anhydrous DMF (10 mL). A separate solution of LiAlH$_4$ (0.35 g, 9.23 mmol) in anhydrous DMF (40 mL) was prepared. The first suspension was added to the LiAlH$_4$ suspension slowly over ice, and the reaction was held at 0 °C for 1 h. The reaction was quenched by the addition of MeOH (10 mL) followed by water
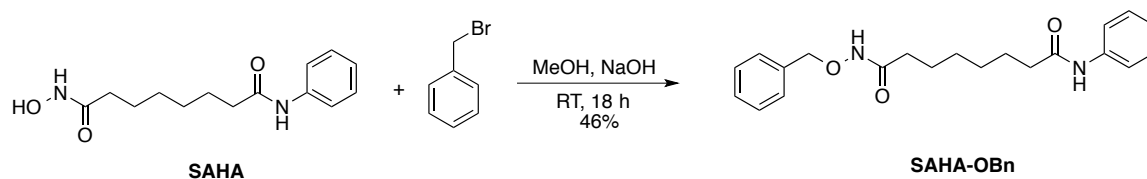
(15 mL).   The solvent was removed via rotary evaporation, and the resulting residue was dissolved in CH_2Cl_2 (100 mL) and washed with 1 M HCl (2×100 mL).   The organic layer was collected, dried over $MgSO_4$, filtered, and concentrated via rotary evaporation.   The resulting crude product was purified by silica gel chromatography eluting 30-50% EtOAc in hexanes to afford **4** in 85% yield (1.10 g, 5.2 mmol).   ^{1}H NMR (400 MHz, CDCl$_3$) $δ$ 4.73 (d, J = 6.0 Hz, 2H), 3.74 (s, 3H), 3.65 (s, 3H), 2.32 (s, 3H), 2.20 (s, 3H), 2.18 (s, 3H), 2.04 (t, J = 6.0 Hz, 1H).

1-(Bromomethyl)-2,5-dimethoxy-3,4,6-trimethylbenzene (5).   **4** (0.50 g, 2.4 mmol) was dissolved in CH_2Cl_2 (25 mL) and cooled on ice before the addition of PPh$_3$ (0.81 g, 3.1 mmol) and NBS (0.55 g, 3.1 mmol).   After 0.5 h, the solvent was removed via rotary evaporation, and the product was purified by silica gel chromatography eluting 5% EtOAc in hexanes to afford **5** in 85% yield (0.55 g, 2.0 mmol).   ^{1}H NMR (400 MHz, CDCl$_3$) $δ$ 4.65 (s, 2H), 3.82 (s, 3H), 3.65 (s, 3H), 2.32 (s, 3H), 2.20 (s, 3H), 2.18 (s, 3H).

2-(Bromomethyl)-3,5,6-trimethylcyclohexa-2,5-diene-1,4-dione (6).   **5** (0.30 g, 1.1 mmol) was dissolved in MeCN (6 mL).   A separate solution of ceric ammonium nitrate (CAN) (1.57 g, 2.9 mmol) dissolved in H_2O (4 mL) was prepared.   This solution was added to the first solution slowly.   After 4 h, water (20 mL) was added to the solution and an extraction with CH_2Cl_2 (3×30 mL) was preformed.   The organic layer was collected, dried over $MgSO_4$, and concentrated by rotary evaporation.   The resulting crude product was purified by silica gel chromatography eluting 2% EtOAc in hexanes to afford **6** in 34% yield (0.09 g, 0.4 mmol).   ^{1}H NMR (400 MHz, CDCl$_3$) $δ$ 4.32 (s, 2H), 2.09 (s, 3 H), 2.03-2.02 (m, 6H).

***N*[1]-Phenyl-*N*[8]-((2,4,5-trimethyl-3,6-dioxocyclohexa-1,4-dien-1-yl)methoxy)octanediamide (SAHA-TAP).** SAHA (0.06 g, 0.2 mmol) was dissolved in MeOH (2 mL). To this was added **6** (0.07 g, 0.3 mmol) followed by 40% (w/v) NaOH (0.02 mL) dropwise. The reaction was held at RT for 18 h. The solvent was then removed via rotary evaporation. The resulting residue was dissolved in H_2O (1 mL) and acidified to pH 1 dropwise with 1 M HCl. An extraction was then

preformed with EtOAc (3×15 mL). The organic layer was collected, dried over MgSO$_4$, filtered, and concentrated by rotary evaporation. The resulting crude product was purified by silica gel chromatography eluting 50% EtOAc in hexanes to afford SAHA-TAP in 74% yield (0.08 g, 0.2 mmol). ^{1}H NMR (400 MHz, CDCl$_3$) δ (br, 1H, N*H*), 8.17 (br, 1H, N*H*), 7.52 (d, *J* = 7.6 Hz, 2H), 7.25 (t, *J* = 7.6 Hz, 2H), 7.04 (t, *J* = 7.2 Hz, 1 H), 4.83 (s, 2H), 2.29 (t, *J* = 6.8 Hz, 2H), 2.15 (s, 3H), 2.04-2.03 (m, 2H), 1.96 (s, 6 H), 1.66-1.58 (m, 4H), 1.31-1.29 (m, 4H). ^{13}C NMR (100 MHz, CDCl$_3$) δ 187.72, 186.43, 172.21, 171.61, 146.04, 141.27, 140.87, 138.41, 136.12, 129.08, 124.29, 120.09, 68,78. 37.46, 33.04, 33.04, 28.76, 28.68, 25.53, 25.23, 12.89, 12.69, 12.60. HRMS (ESI) calcd for [C$_{24}$H$_{30}$N$_2$O$_5$Na]$^+$: 449.2047; Found: 449.2049.

SAHA   +   (MeOH, NaOH / RT, 18 h / 46%) → SAHA-OBn

***N*^{1}-(Benzyloxy)-*N*^{8}-phenyloctanediamide (SAHA-OBn)**.   SAHA (0.05 g, 0.2 mmol) was dissolved in MeOH (2 mL). To this was added benzyl bromide (0.03 mL, 0.3 mmol) followed by 40% (w/v) NaOH (0.04 mL) dropwise. The reaction was held at RT for 18 h. The solvent was then removed via rotary evaporation. The resulting residue was dissolved in H$_2$O (3 mL) and acidified to pH 1 dropwise with 1 M HCl. An extraction was then preformed with EtOAc (3×15 mL). The organic layer was collected, dried over MgSO$_4$, filtered, and concentrated by rotary evaporation. The resulting crude product was purified by silica gel chromatography eluting 50-75% EtOAc in hexanes to afford SAHA-OBn in 46% yield (0.03 g, 0.09 mmol). ^{1}H NMR (400 MHz, CD$_3$OD) δ 7.53 (d, *J* = 8.4 Hz, 2H), 7.41-7.32 (m, 5H), 7.29 (t, *J* = 7.2 Hz, 1H), 7.07 (td, *J*$_1$ = 7.6 Hz, *J*$_2$ = 1.2 Hz), 4.83 (s, 2H), 2.35 (t, *J* = 7.6 Hz, 2H), 2.05 (t, *J* = 7.6 Hz, 2H), 1.68 (p, *J* = 7.2 Hz, 2H), 1.59 (p, *J* = 7.2 Hz, 2H), 1.41-1.29 (m, 4H).   HRMS (ESI) calcd for [C$_{21}$H$_{26}$N$_2$O$_3$Na]$^+$: 377.1834; Found: 377.1836.

	SAHA	SAHA-TAP	SAHA-OBn
HDAC-1	34	371	>10,000
HDAC-2	5	255	>10,000
HDAC-3	40	149	>10,000
HDAC-6	11	23	>10,000
HDAC-8	1337	3842	>10,000

Table A2.1: Supplementary Table 1.

Apparent IC_{50} values (nM) of SAHA, SAHA-TAP, and SAHA-OBn against several HDAC isoforms as determined using an in vitro fluorescence based assay.

		WT Protein	**SAHA-TAP Treated**
y ion #	Residue	Mass	Mass
18	D	2012.95373	2118.05373
17	E	1897.92679	2003.02679
16	A	1768.88419	1873.98419
15	S	1697.84708	1802.94708
14	G	1610.81505	1715.91505
13	F	1553.79359	1658.89359
12	**C**	**1406.72517**	**1511.82517**
11	Y	1246.71599	1246.71599
10	L	1083.65266	1083.65266
9	N	970.56860	970.56860
8	D	856.52567	856.52567
7	A	741.49873	741.49873
6	V	670.46161	670.46161
5	L	571.39320	571.39320
4	G	458.30914	458.30914
3	I	401.28767	401.28767
2	L	288.20361	288.20361
1	R	175.11955	175.11955

N Terminus

C Terminus

Table A2.2: Supplementary Table 2.

Fragment Ion Table (*y* ion series) of the monoisotopic mass for the tryptic fragment (DEASGFCYLNDAVLGILR) of HDAC-8 (WT and treated). The expected mass *y* ions 12-20 are highlighted in yellow, indicative of a covalent modification of Cys153 with the SAHA-TAP promoiety.

Figure A2.1: Supplementary Figure 1.

Amino acid sequence alignment of human HDAC enzymes. Conserved residues amongst all isoforms are highlighted in yellow, and the only Cys conserved in all isoforms is highlighted in green. Amino acids involved in the formation of the active site pocket are indicated by the orange bar. Adapted from Furumai, et al.[1]
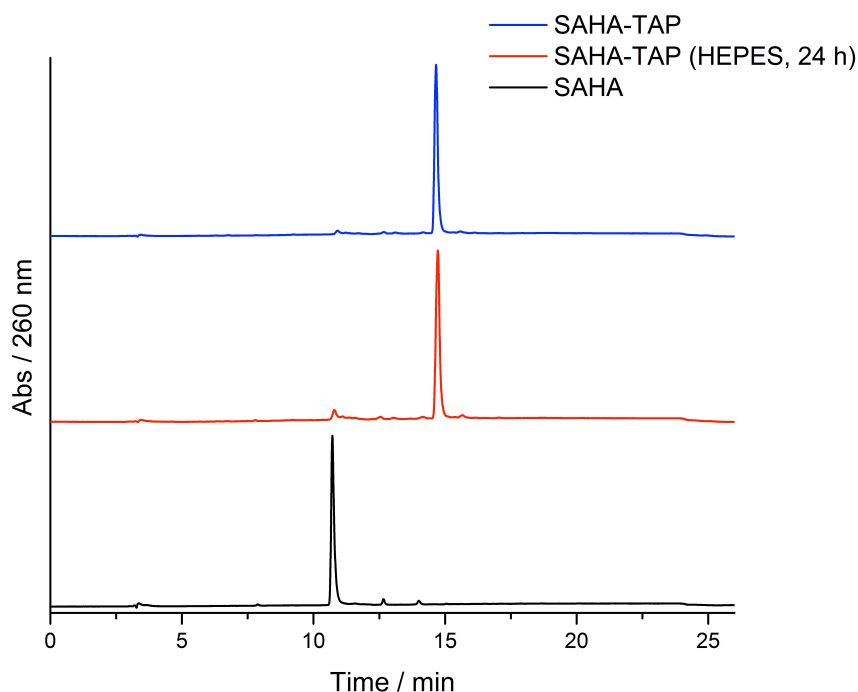
Figure A2.2: Supplementary Figure 2.

HPLC trace of SAHA (black), SAHA-TAP (blue), and SAHA-TAP after incubation in HEPES (50 mM, pH 7.4) for 24 h at 37 °C (red). Retention times are 10.7 min for SAHA and 14.7 min for SAHA-TAP.
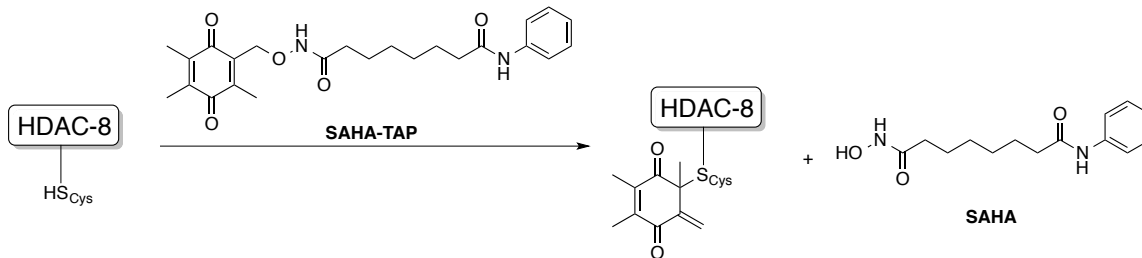
Figure A2.3 Supplementary Figure 3.

Activation of SAHA-TAP by Cys153 in HDAC-8. Cys153 can be covalently modified, leading to release of SAHA.
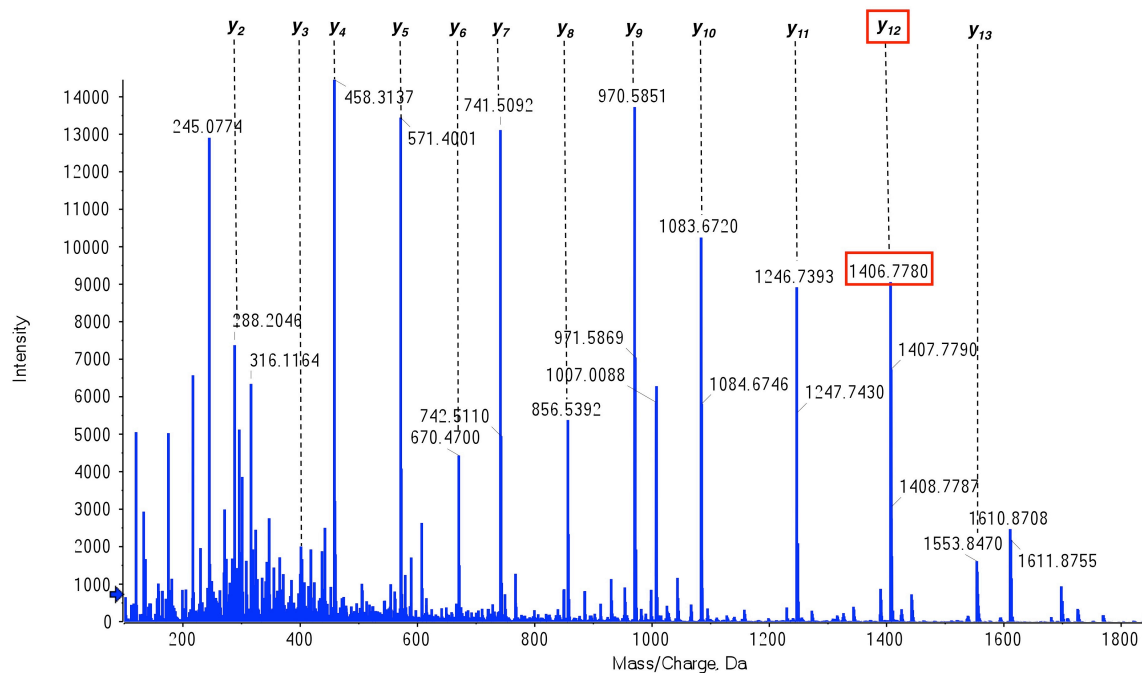
Figure A2.4: Supplementary Figure 4.

MS/MS fragmentation spectrum for the WT HDAC-8 tryptic fragment, DEASGFCYLNDAVLGILR. The *y* series ions detected are indicated by dashed lines.
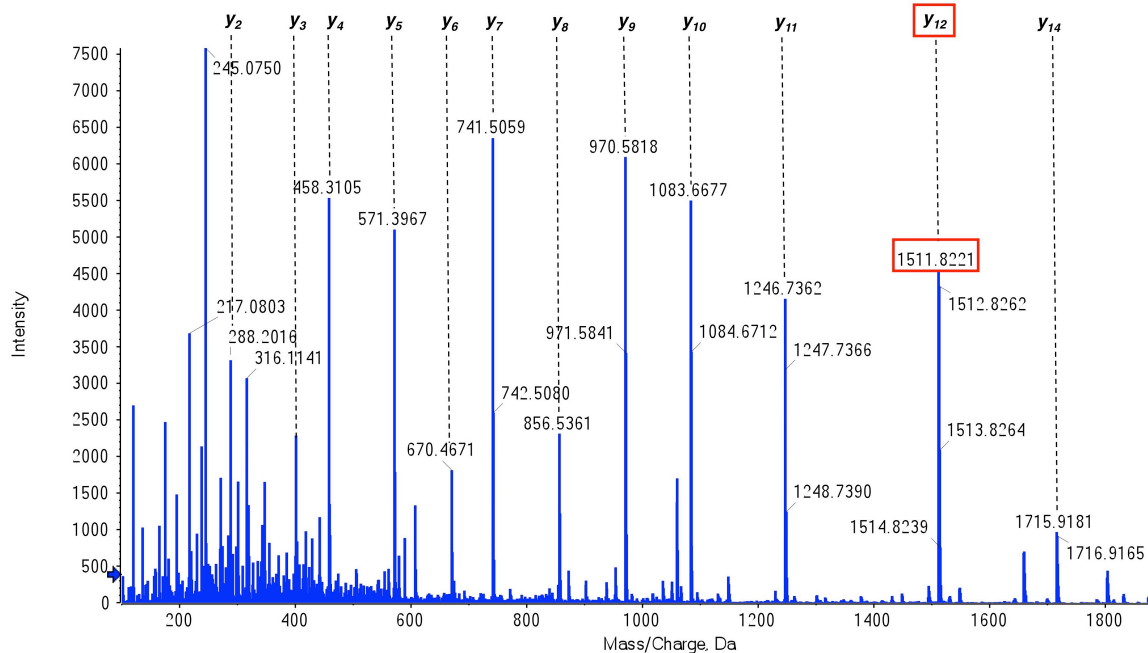
Figure A2.5: Supplementary Figure 5.

MS/MS fragmentation spectrum for the SAHA-TAP treated HDAC-8 tryptic fragment, DEASGFCYLNDAVLGILR. The *y* series ions detected are indicated by dashed lines. The y_{12} ion shows the mass increase expected for covalent attachment of the SAHA-TAP promoiety.
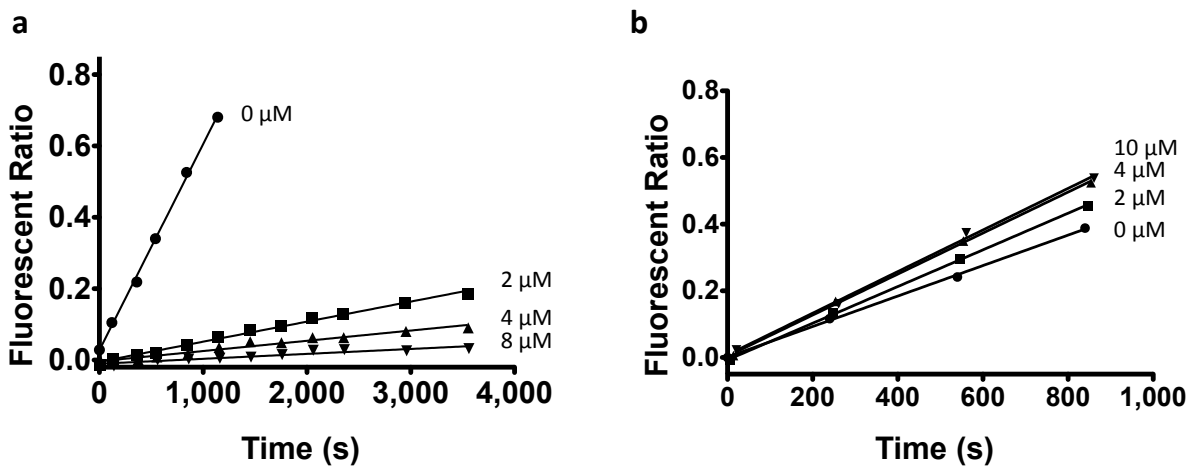
Figure A2.6: Supplementary Figure 6.

WT HDAC8 progress curves at varying concentrations of (**a**) SAHA (0-8 μM) and (**b**) SAHA-OBn (0-10 μM).
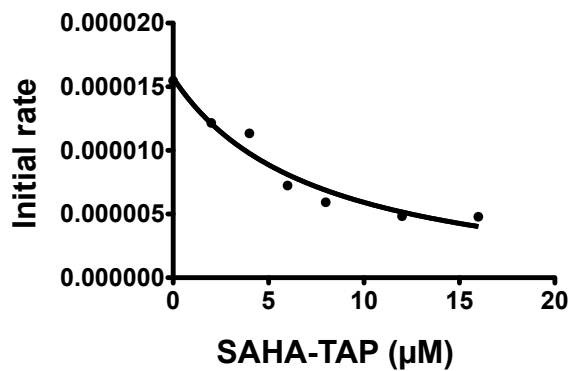
Figure A2.7: Supplementary Figure 7.

Dependence of the Cys153Ala HDAC8 (2 μM) initial rate on the concentration (0-16 μM) of SAHA-TAP.
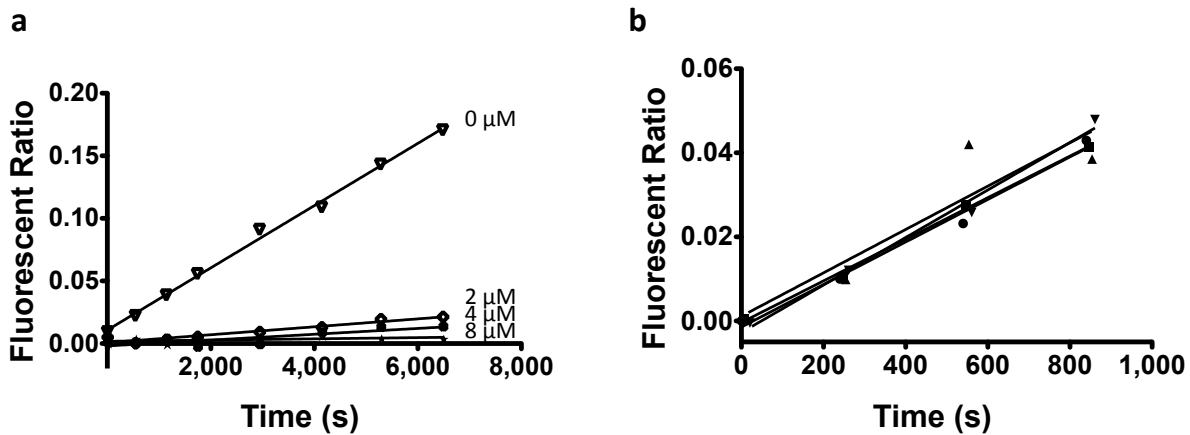
Figure A2.8: Supplementary Figure 8.

Cys153Ala HDAC8 progress curves at varying concentrations of (**a**) SAHA (0-8 μM) and (**b**) 0 (◆), 2 (■), 4 (▲), or 10 (▼) μM SAHA-OBn.

206
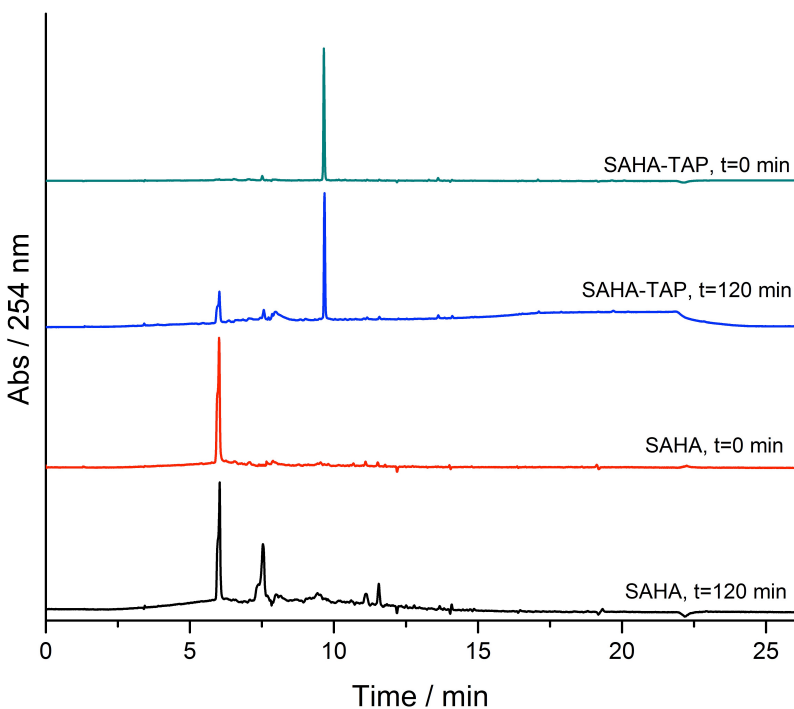
Figure A2.9: Supplementary Figure 9.

HPLC trace of SAHA-TAP after incubation in human plasma at 37 °C at 0 min (green) and 120 min (blue). HPLC trace of SAHA after incubation in human plasma at 37 °C at 0 min (red) and 120 min (black).

References

1   Furumai, R. *et al.* FK228 (depsipeptide) as a natural prodrug that inhibits class I histone deacetylases. *Cancer Res* **62**, 4916-4921 (2002).

2   Huang, S. T., Ting, K. N. & Wang, K. L. Development of a long-wavelength fluorescent probe based on quinone-methide-type reaction to detect physiologically significant thiols. *Anal Chim Acta* **620**, 120-126, doi:Doi 10.1016/J.Aca.2008.05.006 (2008).

Bibliography

1.   Parbin, S., Kar, S., Shilpi, A., Sengupta, D., Deb, M., Rath, S. K., and Patra, S. K. (2014) Histone deacetylases: a saga of perturbed acetylation homeostasis in cancer., *J. Histochem. Cytochem. 62*, 11–33.

2.   Verdin, E., and Ott, M. (2015) 50 years of protein acetylation: from gene regulation to epigenetics, metabolism and beyond., *Nat. Rev. Mol. Cell Biol. 16*, 258–64.

3.   Caron, C., Boyault, C., and Khochbin, S. (2005) Regulatory cross-talk between lysine acetylation and ubiquitination: role in the control of protein stability., *Bioessays 27*, 408–15.

4.   Glozak, M. A., Sengupta, N., Zhang, X., and Seto, E. (2005) Acetylation and deacetylation of non-histone proteins., *Gene 363*, 15–23.

5.   Khoury, G. A., Baliban, R. C., and Floudas, C. A. (2011) Proteome-wide post-translational modification statistics: frequency analysis and curation of the swiss-prot database., *Sci Rep 1*.

6.   Hornbeck, P. V., Zhang, B., Murray, B., Kornhauser, J. M., Latham, V., and Skrzypek, E. (2015) PhosphoSitePlus, 2014: mutations, PTMs and recalibrations., *Nucleic Acids Res. 43*, D512–20.

7.   Halkidou, K., Gaughan, L., Cook, S., Leung, H. Y., Neal, D. E., and Robson, C. N. (2004) Upregulation and nuclear recruitment of HDAC1 in hormone refractory prostate cancer., *Prostate 59*, 177–89.

8.   Zhang, Z., Yamashita, H., Toyama, T., Sugiura, H., Omoto, Y., Ando, Y., Mita, K.,

Hamaguchi, M., Hayashi, S.-I., and Iwase, H. (2004) HDAC6 expression is correlated with better survival in breast cancer., *Clin. Cancer Res. 10*, 6962–8.

9.   Wilson, A. J., Byun, D.-S. S., Popova, N., Murray, L. B., L'Italien, K., Sowa, Y., Arango, D., Velcich, A., Augenlicht, L. H., and Mariadason, J. M. (2006) Histone deacetylase 3 (HDAC3) and other class I HDACs regulate colon cell maturation and p21 expression and are deregulated in human colon cancer., *J. Biol. Chem. 281*, 13548–58.

10.   Deardorff, M. A., Bando, M., Nakato, R., Watrin, E., Itoh, T., Minamino, M., Saitoh, K., Komata, M., Katou, Y., Clark, D., Cole, K. E., De Baere, E., Decroos, C., Di Donato, N., Ernst, S., Francey, L. J., Gyftodimou, Y., Hirashima, K., Hullings, M., Ishikawa, Y., Jaulin, C., Kaur, M., Kiyono, T., Lombardi, P. M., Magnaghi-Jaulin, L., Mortier, G. R., Nozaki, N., Petersen, M. B., Seimiya, H., Siu, V. M., Suzuki, Y., Takagaki, K., Wilde, J. J., Willems, P. J., Prigent, C., Gillessen-Kaesbach, G., Christianson, D. W., Kaiser, F. J., Jackson, L. G., Hirota, T., Krantz, I. D., and Shirahige, K. (2012) HDAC8 mutations in Cornelia de Lange syndrome affect the cohesin acetylation cycle., *Nature 489*, 313–7.

11.   Jia, H., Morris, C. D., Williams, R. M., Loring, J. F., and Thomas, E. A. (2015) HDAC inhibition imparts beneficial transgenerational effects in Huntington's disease mice via altered DNA and histone methylation., *Proc. Natl. Acad. Sci. U.S.A. 112*, E56–64.

12.   Khan, A. N., Magner, W. J., and Tomasi, T. B. (2004) An epigenetically altered tumor cell vaccine., *Cancer Immunol. Immunother. 53*, 748–54.

13.   Gallagher, S. J., Tiffen, J. C., and Hersey, P. (2015) Histone Modifications, Modifiers and Readers in Melanoma Resistance to Targeted and Immune Therapy., *Cancers (Basel) 7*, 1959–82.

14.   Mottamal, M., Zheng, S., Huang, T. L., and Wang, G. (2015) Histone deacetylase

inhibitors in clinical studies as templates for new anticancer agents., *Molecules 20*, 3898–941.

15.   Poole, R. M. (2014) Belinostat: first global approval., *Drugs 74*, 1543–54.

16.   Fenichel, M. P. (2015) FDA approves new agent for multiple myeloma., *J. Natl. Cancer Inst. 107*, djv165.

17.   Cao, K., Wang, G., Li, W., Zhang, L., Wang, R., Huang, Y., Du, L., Jiang, J., Wu, C., He, X., Roberts, A. I., Li, F., Rabson, A. B., Wang, Y., and Shi, Y. (2015) Histone deacetylase inhibitors prevent activation-induced cell death and promote anti-tumor immunity., *Oncogene 34*, 5960–70.

18.   Khan, A. N., Magner, W. J., and Tomasi, T. B. (2007) An epigenetic vaccine model active in the prevention and treatment of melanoma., *J Transl Med 5*, 64.

19.   Haberland, M., Montgomery, R. L., and Olson, E. N. (2009) The many roles of histone deacetylases in development and physiology: implications for disease and therapy., *Nat. Rev. Genet. 10*, 32–42.

20.   Gantt, S. M., Decroos, C., Lee, M. S., Gullett, L. E., Bowman, C. M., Christianson, D. W., and Fierke, C. A. (2016) General Base-General Acid Catalysis in Human Histone Deacetylase 8., *Biochemistry 55*, 820–32.

21.   Gantt, S. L., Joseph, C. G., and Fierke, C. A. (2010) Activation and inhibition of histone deacetylase 8 by monovalent cations., *J. Biol. Chem. 285*, 6036–43.

22.   Smith, B. C., and Denu, J. M. (2009) Chemical mechanisms of histone lysine and arginine modifications., *Biochim. Biophys. Acta 1789*, 45–57.

23.   Waltregny, D., Glénisson, W., Tran, S. L., North, B. J., Verdin, E., Colige, A., and Castronovo, V. (2005) Histone deacetylase HDAC8 associates with smooth muscle alpha-actin and is essential for smooth muscle cell contractility., *FASEB J. 19*, 966–8.

24. Gao, L., Cueto, M., Asselbergs, F., and Atadja, P. (2002) Cloning and Functional Characterization of HDAC11, a Novel Member of the Human Histone Deacetylase Family, *Journal of Biological Chemistry 277*, 25748–25755.

25. Millard, C. J., Watson, P. J., Celardo, I., Gordiyenko, Y., Cowley, S. M., Robinson, C. V., Fairall, L., and Schwabe, J. W. (2013) Class I HDACs share a common mechanism of regulation by inositol phosphates., *Mol. Cell 51*, 57–67.

26. Bressi, J. C., Jennings, A. J., Skene, R., Wu, Y., Melkus, R., De Jong, R., O'Connell, S., Grimshaw, C. E., Navre, M., and Gangloff, A. R. (2010) Exploration of the HDAC2 foot pocket: Synthesis and SAR of substituted N-(2-aminophenyl)benzamides., *Bioorg. Med. Chem. Lett. 20*, 3142–5.

27. Watson, P. J., Fairall, L., Santos, G. M., and Schwabe, J. W. (2012) Structure of HDAC3 bound to co-repressor and inositol tetraphosphate., *Nature 481*, 335–40.

28. Bottomley, M. J., Lo Surdo, P., Di Giovine, P., Cirillo, A., Scarpelli, R., Ferrigno, F., Jones, P., Neddermann, P., De Francesco, R., Steinkühler, C., Gallinari, P., and Carfí, A. (2008) Structural and functional analysis of the human HDAC4 catalytic domain reveals a regulatory structural zinc-binding domain., *J. Biol. Chem. 283*, 26694–704.

29. Ouyang, H., Ali, Y. O., Ravichandran, M., Dong, A., Qiu, W., MacKenzie, F., Dhe-Paganon, S., Arrowsmith, C. H., and Zhai, R. G. (2012) Protein aggregates are recruited to aggresome by histone deacetylase 6 via unanchored ubiquitin C termini., *J. Biol. Chem. 287*, 2317–27.

30. Hai, Y., and Christianson, D. W. (2016) Histone deacetylase 6 structure and molecular basis of catalysis and inhibition., *Nat. Chem. Biol.*

31. Schuetz, A., Min, J., Allali-Hassani, A., Schapira, M., Shuen, M., Loppnau, P.,

Mazitschek, R., Kwiatkowski, N. P., Lewis, T. A., Maglathin, R. L., McLean, T. H., Bochkarev, A., Plotnikov, A. N., Vedadi, M., and Arrowsmith, C. H. (2008) Human HDAC7 harbors a class IIa histone deacetylase-specific zinc binding motif and cryptic deacetylase activity., *J. Biol. Chem. 283*, 11355–63.

32.   Vannini, A., Volpari, C., Gallinari, P., Jones, P., Mattu, M., Carfí, A., De Francesco, R., Steinkühler, C., and Di Marco, S. (2007) Substrate binding to histone deacetylases as shown by the crystal structure of the HDAC8-substrate complex., *EMBO Rep. 8*, 879–84.

33.   Han, A., He, J., Wu, Y., Liu, J. O., and Chen, L. (2005) Mechanism of recruitment of class II histone deacetylases by myocyte enhancer factor-2., *J. Mol. Biol. 345*, 91–102.

34.   Spiegel, S., Milstien, S., and Grant, S. (2012) Endogenous modulators and pharmacological inhibitors of histone deacetylases in cancer therapy., *Oncogene 31*, 537–51.

35.   Balasubramanian, S., Ramos, J., Luo, W., Sirisawad, M., Verner, E., and Buggy, J. J. (2008) A novel histone deacetylase 8 (HDAC8)-specific inhibitor PCI-34051 induces apoptosis in T-cell lymphomas., *Leukemia 22*, 1026–34.

36.   Adams, H., Fritzsche, F. R., Dirnhofer, S., Kristiansen, G., and Tzankov, A. (2010) Class I histone deacetylases 1, 2 and 3 are highly expressed in classical Hodgkin's lymphoma., *Expert Opin. Ther. Targets 14*, 577–84.

37.   Gao, L., and Alumkal, J. (2010) Epigenetic regulation of androgen receptor signaling in prostate cancer., *Epigenetics 5*, 100–4.

38.   Senese, S., Zaragoza, K., Minardi, S., Muradore, I., Ronzoni, S., Passafaro, A., Bernard, L., Draetta, G. F., Alcalay, M., Seiser, C., and Chiocca, S. (2007) Role for histone deacetylase 1 in human tumor cell proliferation., *Mol. Cell. Biol. 27*, 4784–95.

39.   Pulukuri, S. M., Gorantla, B., and Rao, J. S. (2007) Inhibition of histone deacetylase

activity promotes invasion of human cancer cells through activation of urokinase plasminogen activator., *J. Biol. Chem. 282*, 35594–603.

40.	Joshi, P., Greco, T. M., Guise, A. J., Luo, Y., Yu, F., Nesvizhskii, A. I., and Cristea, I. M. (2013) The functional interactome landscape of the human histone deacetylase family., *Mol. Syst. Biol. 9*, 672.

41.	Santoro, F., Botrugno, O. A., Dal Zuffo, R., Pallavicini, I., Matthews, G. M., Cluse, L., Barozzi, I., Senese, S., Fornasari, L., Moretti, S., Altucci, L., Pelicci, P. G., Chiocca, S., Johnstone, R. W., and Minucci, S. (2013) A dual role for Hdac1: oncosuppressor in tumorigenesis, oncogene in tumor maintenance., *Blood 121*, 3459–68.

42.	Lagger, S., Meunier, D., Mikula, M., Brunmeir, R., Schlederer, M., Artaker, M., Pusch, O., Egger, G., Hagelkruys, A., Mikulits, W., Weitzer, G., Muellner, E. W., Susani, M., Kenner, L., and Seiser, C. (2010) Crucial function of histone deacetylase 1 for differentiation of teratomas in mice and humans., *EMBO J. 29*, 3992–4007.

43.	Dovey, O. M., Foster, C. T., Conte, N., Edwards, S. A., Edwards, J. M., Singh, R., Vassiliou, G., Bradley, A., and Cowley, S. M. (2013) Histone deacetylase 1 and 2 are essential for normal T-cell development and genomic stability in mice., *Blood 121*, 1335–44.

44.	Heideman, M. R., Wilting, R. H., Yanover, E., Velds, A., de Jong, J., Kerkhoven, R. M., Jacobs, H., Wessels, L. F., and Dannenberg, J.-H. H. (2013) Dosage-dependent tumor suppression by histone deacetylases 1 and 2 through regulation of c-Myc collaborating genes and p53 function., *Blood 121*, 2038–50.

45.	Yao, Y.-L. L., and Yang, W.-M. M. (2003) The metastasis-associated proteins 1 and 2 form distinct protein complexes with histone deacetylase activity., *J. Biol. Chem. 278*, 42560–8.

46.	Krusche, C. A., Wülfing, P., Kersting, C., Vloet, A., Böcker, W., Kiesel, L., Beier, H. M.,

and Alfer, J. (2005) Histone deacetylase-1 and -3 protein expression in human breast cancer: a tissue microarray analysis., *Breast Cancer Res. Treat. 90*, 15–23.

47.   Jung, K. H., Noh, J. H., Kim, J. K., Eun, J. W., Bae, H. J., Xie, H. J., Chang, Y. G., Kim, M. G., Park, H., Lee, J. Y., and Nam, S. W. (2012) HDAC2 overexpression confers oncogenic potential to human lung cancer cells by deregulating expression of apoptosis and cell cycle proteins., *J. Cell. Biochem. 113*, 2167–77.

48.   Ropero, S., Fraga, M. F., Ballestar, E., Hamelin, R., Yamamoto, H., Boix-Chornet, M., Caballero, R., Alaminos, M., Setien, F., Paz, M. F., Herranz, M., Palacios, J., Arango, D., Orntoft, T. F., Aaltonen, L. A., Schwartz, S., and Esteller, M. (2006) A truncating mutation of HDAC2 in human cancers confers resistance to histone deacetylase inhibition., *Nat. Genet. 38*, 566–9.

49.   Inoue, S., Mai, A., Dyer, M. J., and Cohen, G. M. (2006) Inhibition of histone deacetylase class I but not class II is critical for the sensitization of leukemic cells to tumor necrosis factor-related apoptosis-inducing ligand-induced apoptosis., *Cancer Res. 66*, 6785–92.

50.   Kwon, K.-D. D., Choi, M. J., Park, J.-M. M., Song, K.-M. M., Kwon, M.-H. H., Batbold, D., Yin, G. N., Kim, W. J., Ryu, J.-K. K., and Suh, J.-K. K. (2014) Silencing histone deacetylase 2 using small hairpin RNA induces regression of fibrotic plaque in a rat model of Peyronie's disease., *BJU Int. 114*, 926–36.

51.   Ryu, J.-K. K., Kim, W.-J. J., Choi, M.-J. J., Park, J.-M. M., Song, K.-M. M., Kwon, M.-H. H., Das, N.-D. D., Kwon, K.-D. D., Batbold, D., Yin, G.-N. N., and Suh, J.-K. K. (2013) Inhibition of histone deacetylase 2 mitigates profibrotic TGF-β1 responses in fibroblasts derived from Peyronie's plaque., *Asian J. Androl. 15*, 640–5.

52.   Zimmermann, S., Kiefer, F., Prudenziati, M., Spiller, C., Hansen, J., Floss, T., Wurst, W.,

Minucci, S., and Göttlicher, M. (2007) Reduced body size and decreased intestinal tumor rates in HDAC2-mutant mice., *Cancer Res. 67*, 9047–54.

53.   Fritzsche, F. R., Weichert, W., Röske, A., Gekeler, V., Beckers, T., Stephan, C., Jung, K., Scholman, K., Denkert, C., Dietel, M., and Kristiansen, G. (2008) Class I histone deacetylases 1, 2 and 3 are highly expressed in renal cell cancer., *BMC Cancer 8*, 381.

54.   Jiao, F., Hu, H., Yuan, C., Jin, Z., Guo, Z., Wang, L., and Wang, L. (2014) Histone deacetylase 3 promotes pancreatic cancer cell proliferation, invasion and increases drug-resistance through histone modification of P27, P53 and Bax., *Int. J. Oncol. 45*, 1523–30.

55.   Atsumi, A., Tomita, A., Kiyoi, H., and Naoe, T. (2006) Histone deacetylase 3 (HDAC3) is recruited to target promoters by PML-RARalpha as a component of the N-CoR co-repressor complex to repress transcription in vivo., *Biochem. Biophys. Res. Commun. 345*, 1471–80.

56.   Sun, Z., Feng, D., Fang, B., Mullican, S. E., You, S.-H. H., Lim, H.-W. W., Everett, L. J., Nabel, C. S., Li, Y., Selvakumaran, V., Won, K.-J. J., and Lazar, M. A. (2013) Deacetylase-independent function of HDAC3 in transcription and metabolism requires nuclear receptor corepressor., *Mol. Cell 52*, 769–82.

57.   Gantt, S. L., Gattis, S. G., and Fierke, C. A. (2006) Catalytic activity and inhibition of human histone deacetylase 8 is dependent on the identity of the active site metal ion., *Biochemistry 45*, 6170–8.

58.   Dowling, D., Gattis, S., Fierke, C., and Christianson, D. (2010) Structures of metal-substituted human histone deacetylase 8 provide mechanistic inferences on biological function ., *Biochemistry 49*, 5048–56.

59.   Yang, X.-J. J., and Seto, E. (2008) The Rpd3/Hda1 family of lysine deacetylases: from bacteria and yeast to mice and men., *Nat. Rev. Mol. Cell Biol. 9*, 206–18.

60.   Oehme, I., Deubzer, H. E., Wegener, D., Pickert, D., Linke, J.-P. P., Hero, B., Kopp-Schneider, A., Westermann, F., Ulrich, S. M., von Deimling, A., Fischer, M., and Witt, O. (2009) Histone deacetylase 8 in neuroblastoma tumorigenesis., *Clin. Cancer Res. 15*, 91–9.

61.   Olson, D. E., Udeshi, N. D., Wolfson, N. A., Pitcairn, C. A., Sullivan, E. D., Jaffe, J. D., Svinkina, T., Natoli, T., Lu, X., Paulk, J., McCarren, P., Wagner, F. F., Barker, D., Howe, E., Lazzaro, F., Gale, J. P., Zhang, Y.-L. L., Subramanian, A., Fierke, C. A., Carr, S. A., and Holson, E. B. (2014) An unbiased approach to identify endogenous substrates of "histone" deacetylase 8., *ACS Chem. Biol. 9*, 2210–6.

62.   Rettig, I., Koeneke, E., Trippel, F., Mueller, W. C., Burhenne, J., Kopp-Schneider, A., Fabian, J., Schober, A., Fernekorn, U., von Deimling, A., Deubzer, H. E., Milde, T., Witt, O., and Oehme, I. (2015) Selective inhibition of HDAC8 decreases neuroblastoma growth in vitro and in vivo and enhances retinoic acid-mediated differentiation., *Cell Death Dis 6*, e1657.

63.   Grozinger, C. M., Hassig, C. A., and Schreiber, S. L. (1999) Three proteins define a class of human histone deacetylases related to yeast Hda1p., *Proc. Natl. Acad. Sci. U.S.A. 96*, 4868–73.

64.   Dequiedt, F., Kasler, H., Fischle, W., Kiermer, V., Weinstein, M., Herndier, B. G., and Verdin, E. (2003) HDAC7, a thymus-specific class II histone deacetylase, regulates Nur77 transcription and TCR-mediated apoptosis., *Immunity 18*, 687–98.

65.   Mahlknecht, U., Schnittger, S., Ottmann, O. G., Schoch, C., Mosebach, M., Hiddemann, W., and Hoelzer, D. (2000) Chromosomal organization and localization of the human histone deacetylase 5 gene (HDAC5)., *Biochim. Biophys. Acta 1493*, 342–8.

66.   Morin, R. D., Mendez-Lago, M., Mungall, A. J., Goya, R., Mungall, K. L., Corbett, R. D., Johnson, N. A., Severson, T. M., Chiu, R., Field, M., Jackman, S., Krzywinski, M., Scott, D.

W., Trinh, D. L., Tamura-Wells, J., Li, S., Firme, M. R., Rogic, S., Griffith, M., Chan, S., Yakovenko, O., Meyer, I. M., Zhao, E. Y., Smailus, D., Moksa, M., Chittaranjan, S., Rimsza, L., Brooks-Wilson, A., Spinelli, J. J., Ben-Neriah, S., Meissner, B., Woolcock, B., Boyle, M., McDonald, H., Tam, A., Zhao, Y., Delaney, A., Zeng, T., Tse, K., Butterfield, Y., Birol, I., Holt, R., Schein, J., Horsman, D. E., Moore, R., Jones, S. J., Connors, J. M., Hirst, M., Gascoyne, R. D., and Marra, M. A. (2011) Frequent mutation of histone-modifying genes in non-Hodgkin lymphoma., *Nature 476*, 298–303.

67.   Liu, H., Hu, Q., Kaufman, A., D'Ercole, A. J., and Ye, P. (2008) Developmental expression of histone deacetylase 11 in the murine brain., *J. Neurosci. Res. 86*, 537–43.

68.   Villagra, A., Cheng, F., Wang, H.-W., Suarez, I., Glozak, M., Maurin, M., Nguyen, D., Wright, K., Atadja, P., Bhalla, K., Pinilla-Ibarz, J., Seto, E., and Sotomayor, E. (2009) The histone deacetylase HDAC11 regulates the expression of interleukin 10 and immune tolerance, *Nature Immunology 10*, 92–100.

69.   Deubzer, H. E., Schier, M. C., Oehme, I., Lodrini, M., Haendler, B., Sommer, A., and Witt, O. (2013) HDAC11 is a novel drug target in carcinomas., *Int. J. Cancer 132*, 2200–8.

70.   Wong, P. G., Glozak, M. A., Cao, T. V., Vaziri, C., Seto, E., and Alexandrow, M. (2010) Chromatin unfolding by Cdt1 regulates MCM loading via opposing functions of HBO1 and HDAC11-geminin., *Cell Cycle 9*, 4351–63.

71.   Glozak, M. A., and Seto, E. (2009) Acetylation/deacetylation modulates the stability of DNA replication licensing factor Cdt1., *J. Biol. Chem. 284*, 11446–53.

72.   Woods, D., Woan, K., Wang, D., Yu, Y., Powers, J., Sahakian, E., Cheng, F., Wang, H., Rock-Klotz, J., and Villagra, A. (2013) Histone deacetylase 11 is an epigenetic regulator of cytotoxic T-lymphocyte effector function and memory formation (P1404), *The Journal of*

Immunology, Am Assoc Immnol *190*, 117.2–117.2.

73.   Gregoretti, I., Lee, Y.-M., and Goodson, H. (2004) Molecular Evolution of the Histone Deacetylase Family: Functional Implications of Phylogenetic Analysis, *Journal of Molecular Biology 338*, 1731.

74.   Dowling, D., Gantt, S., Gattis, S., Fierke, C., and Christianson, D. (2008) Structural studies of human histone deacetylase 8 and its site-specific variants complexed with substrate and inhibitors., *Biochemistry 47*, 13554–63.

75.   Fournel, M., Bonfils, C., Hou, Y., Yan, P. T., Trachy-Bourget, M.-C. C., Kalita, A., Liu, J., Lu, A.-H. H., Zhou, N. Z., Robert, M.-F. F., Gillespie, J., Wang, J. J., Ste-Croix, H., Rahil, J., Lefebvre, S., Moradei, O., Delorme, D., Macleod, A. R., Besterman, J. M., and Li, Z. (2008) MGCD0103, a novel isotype-selective histone deacetylase inhibitor, has broad spectrum antitumor activity in vitro and in vivo., *Mol. Cancer Ther. 7*, 759–68.

76.   Wolfson, N. A., Pitcairn, C. A., Sullivan, E. D., Joseph, C. G., and Fierke, C. A. (2014) An enzyme-coupled assay measuring acetate production for profiling histone deacetylase specificity., *Anal. Biochem. 456*, 61–9.

77.   Zhang, J., Shi, X., Li, Y., Kim, B.-J. J., Jia, J., Huang, Z., Yang, T., Fu, X., Jung, S. Y., Wang, Y., Zhang, P., Kim, S.-T. T., Pan, X., and Qin, J. (2008) Acetylation of Smc3 by Eco1 is required for S phase sister chromatid cohesion in both human and yeast., *Mol. Cell 31*, 143–51.

78.   Beckouët, F., Hu, B., Roig, M. B., Sutani, T., Komata, M., Uluocak, P., Katis, V. L., Shirahige, K., and Nasmyth, K. (2010) An Smc3 acetylation cycle is essential for establishment of sister chromatid cohesion., *Mol. Cell 39*, 689–99.

79.   Wrighton, K. H. (2010) Cell cycle: cycling through acetylation., *Nat. Rev. Mol. Cell Biol. 11*, 755.

80.   Wilson, B. J., Tremblay, A. M., Deblois, G., Sylvain-Drolet, G., and Giguère, V. (2010) An acetylation switch modulates the transcriptional activity of estrogen-related receptor alpha., *Mol. Endocrinol. 24*, 1349–58.

81.   Lu, Q., Hutchins, A. E., Doyle, C. M., Lundblad, J. R., and Kwok, R. P. (2003) Acetylation of cAMP-responsive element-binding protein (CREB) by CREB-binding protein enhances CREB-dependent transcription., *J. Biol. Chem. 278*, 15727–34.

82.   Gao, J., Siddoway, B., Huang, Q., and Xia, H. (2009) Inactivation of CREB mediated gene transcription by HDAC8 bound protein phosphatase., *Biochem. Biophys. Res. Commun. 379*, 1–5.

83.   Villena, J. A., and Kralli, A. (2008) ERRalpha: a metabolic function for the oldest orphan., *Trends Endocrinol. Metab. 19*, 269–76.

84.   Shen, S., Li, J., and Casaccia-Bonnefil, P. (2005) Histone modifications affect timing of oligodendrocyte progenitor differentiation in the developing rat brain, *The Journal of Cell Biology 169*.

85.   Buglio, D., Khaskhely, N. M., Voo, K. S., Martinez-Valdez, H., Liu, Y.-J. J., and Younes, A. (2011) HDAC11 plays an essential role in regulating OX40 ligand expression in Hodgkin lymphoma., *Blood 117*, 2910–7.

86.   Choudhary, C., Kumar, C., Gnad, F., Nielsen, M. L., Rehman, M., Walther, T. C., Olsen, J. V., and Mann, M. (2009) Lysine acetylation targets protein complexes and co-regulates major cellular functions., *Science 325*, 834–40.

87.   Wegener, D., Wirsching, F., Riester, D., and Schwienhorst, A. (2003) A fluorogenic histone deacetylase assay well suited for high-throughput activity screening., *Chem. Biol. 10*, 61–8.

88.   Gill, S. C., and von Hippel, P. H. (1989) Calculation of protein extinction coefficients from amino acid sequence data., *Anal. Biochem. 182*, 319–26.

89.   Alam, N., Zimmerman, L., Wolfson, N. A., Joseph, C. G., Fierke, C. A., and Schueler-Furman, O. (2016) Structure-Based Identification of HDAC8 Non-histone Substrates., *Structure 24*, 458–68.

90.   Zhao, S., Xu, W., Jiang, W., Yu, W., Lin, Y., Zhang, T., Yao, J., Zhou, L., Zeng, Y., Li, H., Li, Y., Shi, J., An, W., Hancock, S., He, F., Qin, L., Chin, J., Yang, P., Chen, X., Lei, Q., Xiong, Y., and Guan, K.-L. (2010) Regulation of Cellular Metabolism by Protein Lysine Acetylation, *Science 327*, 1000–1004.

91.   Yang, X.-J., and Seto, E. (2008) Lysine Acetylation: Codified Crosstalk with Other Posttranslational Modifications, *Molecular Cell 31*.

92.   Pedersen, S., Bloch, P., Reeh, S., and Neidhardt, F. (1978) Patterns of protein synthesis in E. coli: a catalog of the amount of 140 individual proteins at different growth rates, *Cell 14*, 179–190.

93.   Robichon, C., Luo, J., Causey, T. B., Benner, J. S., and Samuelson, J. C. (2011) Engineering Escherichia coli BL21(DE3) derivative strains to minimize E. coli protein contamination after purification by immobilized metal affinity chromatography., *Appl. Environ. Microbiol. 77*, 4634–46.

94.   Craig, E. A., Eisenman, H. C., and Hundley, H. A. (2003) Ribosome-tethered molecular chaperones: the first line of defense against protein misfolding?, *Curr. Opin. Microbiol. 6*, 157–62.

95.   Hoffmann, A., Bukau, B., and Kramer, G. (2010) Structure and function of the molecular chaperone Trigger Factor., *Biochim. Biophys. Acta 1803*, 650–61.

96.   Thangapandian, S., John, S., Lee, Y., Arulalapperumal, V., and Lee, K. W. (2012) Molecular modeling study on tunnel behavior in different histone deacetylase isoforms., *PLoS ONE 7*, e49327.

97.   Grunstein, M. (1997) Histone acetylation in chromatin structure and transcription, *Nature 389*, 349–352.

98.   Peng, L., and Seto, E. (2011) Deacetylation of nonhistone proteins by HDACs and the implications in cancer., *Handbook of experimental pharmacology*, pp 39–56.

99.   Juan, L. J., Shia, W. J., Chen, M. H., Yang, W. M., Seto, E., Lin, Y. S., and Wu, C. W. (2000) Histone deacetylases specifically down-regulate p53-dependent gene activation., *J. Biol. Chem. 275*, 20436–43.

100.   Jeong, J., Jiang, L., Albino, E., Marrero, J., Rho, H., Hu, J., Hu, S., Vera, C., Bayron-Poueymiroy, D., Rivera-Pacheco, Z., Ramos, L., Torres-Castro, C., Qian, J., Bonaventura, J., Boeke, J., Yap, W., Pino, I., Eichinger, D., Zhu, H., and Blackshaw, S. (2012) Rapid Identification of Monospecific Monoclonal Antibodies Using a Human Proteome Microarray, *Molecular & Cellular Proteomics 11*, O111.016253.

101.   Thompson, P. R., Wang, D., Wang, L., Fulco, M., Pediconi, N., Zhang, D., An, W., Ge, Q., Roeder, R. G., Wong, J., Levrero, M., Sartorelli, V., Cotter, R. J., and Cole, P. A. (2004) Regulation of the p300 HAT domain via a novel activation loop., *Nat. Struct. Mol. Biol. 11*, 308–15.

102.   Wu, B., Wang, Z., Huang, Y., and Liu, W. R. (2012) Catalyst-free and site-specific one-pot dual-labeling of a protein directed by two genetically incorporated noncanonical amino acids., *Chembiochem 13*, 1405–8.

103.   Lee, Y.-J. J., Wu, B., Raymond, J. E., Zeng, Y., Fang, X., Wooley, K. L., and Liu, W. R.

(2013) A genetically encoded acrylamide functionality., *ACS Chem. Biol. 8*, 1664–70.

104.   Dang, L., White, D. W., Gross, S., Bennett, B. D., Bittinger, M. A., Driggers, E. M., Fantin, V. R., Jang, H. G., Jin, S., Keenan, M. C., Marks, K. M., Prins, R. M., Ward, P. S., Yen, K. E., Liau, L. M., Rabinowitz, J. D., Cantley, L. C., Thompson, C. B., Vander Heiden, M. G., and Su, S. M. (2009) Cancer-associated IDH1 mutations produce 2-hydroxyglutarate., *Nature 462*, 739–44.

105.   Geisbrecht, B. V., and Gould, S. J. (1999) The human PICD gene encodes a cytoplasmic and peroxisomal NADP(+)-dependent isocitrate dehydrogenase., *J. Biol. Chem. 274*, 30527–33.

106.   Stein, E. (2015) IDH2 inhibition in AML: Finally progress?, *Best Practice & Research Clinical Haematology 28*, 112–115.

107.   Balss, J., Meyer, J., Mueller, W., Korshunov, A., Hartmann, C., and von Deimling, A. (2008) Analysis of the IDH1 codon 132 mutation in brain tumors., *Acta Neuropathol. 116*, 597–602.

108.   Yu, W., Dittenhafer-Reed, K. E., and Denu, J. M. (2012) SIRT3 protein deacetylates isocitrate dehydrogenase 2 (IDH2) and regulates mitochondrial redox status., *J. Biol. Chem. 287*, 14078–86.

109.   Hughes, C. A., and Bennett, V. (1995) Adducin: a physical model with implications for function in assembly of spectrin-actin complexes., *J. Biol. Chem. 270*, 18990–6.

110.   Guelman, S., Kozuka, K., Mao, Y., Pham, V., Solloway, M. J., Wang, J., Wu, J., Lill, J. R., and Zha, J. (2009) The double-histone-acetyltransferase complex ATAC is essential for mammalian development., *Mol. Cell. Biol. 29*, 1176–88.

111.   Isaac, C., Marsh, K. L., Paznekas, W. A., Dixon, J., Dixon, M. J., Jabs, E. W., and Meier, U. T. (2000) Characterization of the nucleolar gene product, treacle, in Treacher Collins

syndrome., *Mol. Biol. Cell 11*, 3061–71.

112.   Sakai, D., and Trainor, P. A. (2009) Treacher Collins syndrome: unmasking the role of

Tcof1/treacle., *Int. J. Biochem. Cell Biol. 41*, 1229–32.

113.   Lum, L. S., Sultzman, L. A., Kaufman, R. J., Linzer, D. I., and Wu, B. J. (1990) A cloned

human CCAAT-box-binding factor stimulates transcription from the human hsp70 promoter.,

Mol. Cell. Biol. 10, 6709–17.

114.   Wu, Q., Cheng, Z., Zhu, J., Xu, W., Peng, X., Chen, C., Li, W., Wang, F., Cao, L., Yi,

X., Wu, Z., Li, J., and Fan, P. (2015) Suberoylanilide hydroxamic acid treatment reveals

crosstalks among proteome, ubiquitylome and acetylome in non-small cell lung cancer A549 cell

line., *Sci Rep 5*, 9520.

115.   Keedy, K. S., Archin, N. M., Gates, A. T., Espeseth, A., Hazuda, D. J., and Margolis, D.

M. (2009) A limited group of class I histone deacetylases acts to repress human

immunodeficiency virus type 1 expression., *J. Virol. 83*, 4749–56.

116.   De Ruijter, A. J., van Gennip, A. H., Caron, H. N., Kemp, S., and van Kuilenburg, A. B.

B. (2003) Histone deacetylases (HDACs): characterization of the classical HDAC family.,

Biochem. J. 370, 737–49.

117.   Marks, P., Rifkind, R., Richon, V., Breslow, R., Miller, T., and Kelly, W. (2001) Histone

deacetylases and cancer: causes and therapies, *Nature Reviews Cancer 1*, 194–202.

118.   Johnstone, R. W. (2002) Histone-deacetylase inhibitors: novel drugs for the treatment of

cancer., *Nat Rev Drug Discov 1*, 287–99.

119.   Agalioti, T., Chen, G., and Thanos, D. (2002) Deciphering the transcriptional histone

acetylation code for a human gene., *Cell 111*, 381–92.

120.   Matangkasombut, O., and Buratowski, S. (2003) Different sensitivities of bromodomain

factors 1 and 2 to histone H4 acetylation., *Mol. Cell 11*, 353–63.

121.   Gryder, B. E., Sodji, Q. H., and Oyelere, A. K. (2012) Targeted cancer therapy: giving

histone deacetylase inhibitors all they need to succeed., *Future Med Chem 4*, 505–24.

122.   Dokmanovic, M., Clarke, C., and Marks, P. A. (2007) Histone deacetylase inhibitors:

overview and perspectives., *Mol. Cancer Res. 5*, 981–9.

123.   Kantharaj, E., and Jayaraman, R. (2011) Histone deacetylase inhibitors as therapeutic

agents for cancer therapy: drug metabolism and pharmacokinetic properties, INTECH Open

Access Publisher.

124.   Marks, P. A., and Breslow, R. (2007) Dimethyl sulfoxide to vorinostat: development of

this histone deacetylase inhibitor as an anticancer drug., *Nat. Biotechnol. 25*, 84–90.

125.   U.S. Food and Drug Administration. (2015) FDA approves Farydak for treatment of

multiple myeloma, Silver Spring, MD.

126.   U.S. Food and Drug Administration. (2014) Belinostat, Silver Spring, MD.

127.   Rubin, E. H., Agrawal, N. G., Friedman, E. J., Scott, P., Mazina, K. E., Sun, L., Du, L.,

Ricker, J. L., Frankel, S. R., Gottesdiener, K. M., Wagner, J. A., and Iwamoto, M. (2006) A

study to determine the effects of food and multiple dosing on the pharmacokinetics of vorinostat

given orally to patients with advanced cancer., *Clin. Cancer Res. 12*, 7039–45.

128.   Flipo, M., Charton, J., Hocine, A., Dassonneville, S., Deprez, B., and Deprez-Poulain, R.

(2009) Hydroxamates: relationships between structure and plasma stability., *J. Med. Chem. 52*,

6790–802.

129.   Andreu-Vieyra, C. V., and Berenson, J. R. (2014) The potential of panobinostat as a

treatment option in patients with relapsed and refractory multiple myeloma., *Ther Adv Hematol

5*, 197–210.

130. Rautio, J., Kumpulainen, H., Heimbach, T., Oliyai, R., Oh, D., Järvinen, T., and Savolainen, J. (2008) Prodrugs: design and clinical applications., *Nat Rev Drug Discov 7*, 255–70.

131. Huttunen, K. M., Raunio, H., and Rautio, J. (2011) Prodrugs--from serendipity to rational design., *Pharmacol. Rev. 63*, 750–71.

132. Miller, T. A. (2005, April 2) Histone deacetylase inhibitor prodrugs.

133. Schlimme, S., Hauser, A.-T. T., Carafa, V., Heinke, R., Kannan, S., Stolfa, D. A., Cellamare, S., Carotti, A., Altucci, L., Jung, M., and Sippl, W. (2011) Carbamate prodrug concept for hydroxamate HDAC inhibitors., *ChemMedChem 6*, 1193–8.

134. Estrela, J. M. M., Ortega, A., and Obrador, E. (2006) Glutathione in cancer biology and therapy., *Crit Rev Clin Lab Sci 43*, 143–81.

135. Huang, S.-T. T., Ting, K.-N. N., and Wang, K.-L. L. (2008) Development of a long-wavelength fluorescent probe based on quinone-methide-type reaction to detect physiologically significant thiols., *Anal. Chim. Acta 620*, 120–6.

136. Thomas, M., Rivault, F., Tranoy-Opalinski, I., Roche, J., Gesson, J.-P. P., and Papot, S. (2007) Synthesis and biological evaluation of the suberoylanilide hydroxamic acid (SAHA) beta-glucuronide and beta-galactoside for application in selective prodrug chemotherapy., *Bioorg. Med. Chem. Lett. 17*, 983–6.

137. Kelly, W. K., Richon, V. M., O'Connor, O., Curley, T., MacGregor-Curtelli, B., Tong, W., Klang, M., Schwartz, L., Richardson, S., Rosa, E., Drobnjak, M., Cordon-Cordo, C., Chiao, J. H., Rifkind, R., Marks, P. A., and Scher, H. (2003) Phase I clinical trial of histone deacetylase inhibitor: suberoylanilide hydroxamic acid administered intravenously., *Clin. Cancer Res. 9*, 3578–88.

138.   Furumai, R., Matsuyama, A., Kobashi, N., Lee, K.-H. H., Nishiyama, M., Nakajima, H., Tanaka, A., Komatsu, Y., Nishino, N., Yoshida, M., and Horinouchi, S. (2002) FK228 (depsipeptide) as a natural prodrug that inhibits class I histone deacetylases., *Cancer Res. 62*, 4916–21.

139.   Kim, B., Pithadia, A. S., and Fierke, C. A. (2015) Kinetics and thermodynamics of metal-binding to histone deacetylase 8., *Protein Sci. 24*, 354–65.

140.   McLafferty, F. W. (1981) Tandem mass spectrometry., *Science 214*, 280–7.

141.   McClerren, A. L., Endsley, S., Bowman, J. L., Andersen, N. H., Guan, Z., Rudolph, J., and Raetz, C. R. (2005) A slow, tight-binding inhibitor of the zinc-dependent deacetylase LpxC of lipid A biosynthesis with antibiotic activity comparable to ciprofloxacin., *Biochemistry 44*, 16574–83.

142.   Sculley, M. J., Morrison, J. F., and Cleland, W. W. (1996) Slow-binding inhibition: the general case., *Biochim. Biophys. Acta 1298*, 78–86.

143.   Teitelbaum, A. M., Meissner, A., Harding, R. A., Wong, C. A., Aldrich, C. C., and Remmel, R. P. (2013) Synthesis, pH-dependent, and plasma stability of meropenem prodrugs for potential use against drug-resistant tuberculosis., *Bioorg. Med. Chem. 21*, 5605–17.

144.   Zhang, C., Richon, V., Ni, X., Talpur, R., and Duvic, M. (2005) Selective induction of apoptosis by histone deacetylase inhibitor SAHA in cutaneous T-cell lymphoma cells: relevance to mechanism of therapeutic action., *J. Invest. Dermatol. 125*, 1045–52.

145.   Sodji, Q. H., Patil, V., Kornacki, J. R., Mrksich, M., and Oyelere, A. K. (2013) Synthesis and structure-activity relationship of 3-hydroxypyridine-2-thione-based histone deacetylase inhibitors., *J. Med. Chem. 56*, 9969–81.

146.   Zhang, Y., Li, N., Caron, C., Matthias, G., Hess, D., Khochbin, S., and Matthias, P.

(2003) HDAC-6 interacts with and deacetylates tubulin and microtubules in vivo., *EMBO J. 22*, 1168–79.

147.   Bantscheff, M., Hopf, C., Savitski, M. M., Dittmann, A., Grandi, P., Michon, A.-M., Schlegl, J., Abraham, Y., Becher, I., and Bergamini, G. (2011) Chemoproteomics profiling of HDAC inhibitors reveals selective targeting of HDAC complexes, *Nature biotechnology*, Nature Publishing Group *29*, 255–265.

148.   Gryder, BE, Akbashev, MJ, and Rood, MK. (2013) Selectively targeting prostate cancer with antiandrogen equipped histone deacetylase inhibitors, *ACS chemical …*.

149.   PHILLIPS, D. M. (1963) The presence of acetyl groups of histones., *Biochem. J. 87*, 258–63.

150.   ALLFREY, V. G., FAULKNER, R., and MIRSKY, A. E. (1964) ACETYLATION AND METHYLATION OF HISTONES AND THEIR POSSIBLE ROLE IN THE REGULATION OF RNA SYNTHESIS., *Proc. Natl. Acad. Sci. U.S.A. 51*, 786–94.

151.   Taunton, J., Hassig, C. A., and Schreiber, S. L. (1996) A mammalian histone deacetylase related to the yeast transcriptional regulator Rpd3p., *Science 272*, 408–11.

152.   Gurard-Levin, Z., Kim, J., and Mrksich, M. (2009) Combining Mass Spectrometry and Peptide Arrays to Profile the Specificities of Histone Deacetylases, *ChemBioChem 10*, 2159–2161.

153.   Rathert, P., Dhayalan, A., Murakami, M., Zhang, X., Tamas, R., Jurkowska, R., Komatsu, Y., Shinkai, Y., Cheng, X., and Jeltsch, A. (2008) Protein lysine methyltransferase G9a acts on non-histone targets., *Nat. Chem. Biol. 4*, 344–6.